



KIT SCIENTIFIC REPORTS 7725

# Annual Report 2015

Institute for Nuclear Waste Disposal  
Institut für Nukleare Entsorgung

H. Geckeis, M. Altmaier, S. Fanghänel (eds.)



H. Geckeis, M. Altmaier, S. Fanghänel (eds.)

**Annual Report 2015**

Institute for Nuclear Waste Disposal  
Institut für Nukleare Entsorgung

**Karlsruhe Institute of Technology**  
**KIT SCIENTIFIC REPORTS 7725**

# Annual Report 2015

Institute for Nuclear Waste Disposal  
Institut für Nukleare Entsorgung

by

H. Geckeis, M. Altmaier, S. Fanghänel (eds.)

The Institute for Nuclear Waste Disposal, INE, (Institut für Nukleare Entsorgung) belongs to the KIT Energy Center. The KIT Energy Center with its 1100 employees is one of the largest energy research centers in Europe. It bundles the energy research activities of the KIT, the merger of the former Forschungszentrum Karlsruhe and Universität Karlsruhe and reknown cooperation partners. By this, it crosses the lines between disciplines and combines fundamental and applied research in all relevant energies for industry, household, service and mobility. The involved institutes and research groups conduct the research work on their own authority. The joining of subjects, the interdisciplinary collaboration of scientists, and the common use of high-end devices and installations, develops a new quality of research and teaching. The KIT Energy Center develops solutions in energy technology from a single source and acts as a highly valuable consultancy institution for politics, business, and society in all questions of energy. (<http://www.energy.kit.edu/>)

## Impressum



Karlsruher Institut für Technologie (KIT)  
KIT Scientific Publishing  
Straße am Forum 2  
D-76131 Karlsruhe

KIT Scientific Publishing is a registered trademark of Karlsruhe  
Institute of Technology. Reprint using the book cover is not allowed.

[www.ksp.kit.edu](http://www.ksp.kit.edu)



*This document – excluding the cover, pictures and graphs – is licensed  
under the Creative Commons Attribution-Share Alike 3.0 DE License  
(CC BY-SA 3.0 DE): <http://creativecommons.org/licenses/by-sa/3.0/de/>*



*The cover page is licensed under the Creative Commons  
Attribution-No Derivatives 3.0 DE License (CC BY-ND 3.0 DE):  
<http://creativecommons.org/licenses/by-nd/3.0/de/>*

Print on Demand 2017

ISSN 1869-9669

DOI: 10.5445/KSP/1000061835

# Foreword

## Prof. Dr. Horst Geckeis

*Director of the Institute for Nuclear Waste Disposal*

Within the Helmholtz Association of German Research Centers (HGF) the third period of Program oriented funding (POFIII) started in January 2015 and the respective proposal for the NUSAFE (Nuclear waste management, safety and radiation research) program defines KIT-INE's research roadmap for the next years. The new president of the Helmholtz association, Prof. Wiestler, has clearly emphasized that the grand societal challenges related to the decommissioning of nuclear facilities and the disposal of radioactive waste will be a constituent of the strategic future concept of the HGF. The safe phase-out of nuclear energy represents an important component of the German "Energiewende" process and, thus, calls for provident research in this respect as well as education and training of young scientists. The fact that scientific expertise and know-how in the field of nuclear waste management will be definitely required for the next decades is also politically recognized. During their visits of INE laboratories in 2015, Helmfried Meinel, ministerial director and Gerrit Niehaus, head of the nuclear energy oversight and radiation protection section, both at the Ministry for Environment, Climate and Energy Economy of the Federal State of Baden-Württemberg, as well as Rita Schwarzelühr-Sutter, Parliamentary State Secretary at the German Federal Ministry for the Environment, Nature Conservation, Building and Nuclear Safety (BMUB) emphasized the need for respective efforts. We can take these statements as a strong motivation for shaping INE research for the coming years!

2015 represents an interesting and successful year for INE: 10 PhD students defended their theses very successfully which reflects the strong interest of young scientists in nuclear waste disposal topics and which demonstrates the attractive research profile and leading edge research opportunities at INE. Research topics covered by those theses ranged from radionuclide release behavior from high active waste forms through actinide and long-lived fission product aquatic chemistry topics, geochemical aspects of radionuclide migration and coupled reactive transport phenomena up to actinide coordination chemistry with organic ligands of different origin and the development of novel highly sensitive analytical and spectroscopic methods for radionuclide speciation characterization. I would like to take the opportunity to congratulate to all young scientists for their excellent work, which partly is described in the report in hand!

Furthermore, the positive evolution of publication record during 2015 together with the very successful acquisition of quite a number of third party funded projects (EU, BMBF, BMWi, BfS, etc.) document *inter alia* the strong accomplishments of INE scientists. Without their commitment and motivation, INE would not be able to keep its international reputation. INE scientists were strongly involved in the organization of international conferences and workshops such as the XAFS16 conference in Karlsruhe with more than 550 participants, the 15<sup>th</sup> International Conference on the Chemistry and Migration Behavior of Actinides and Fission Products in the Geosphere (MIGRATION 2015) in Santa Fe, USA, with more than 250 participants, the international workshop on ABC salt (actinide brine chemistry) and HITAC (High Temperature Actinide Chemistry) together with the university of Heidelberg and the GENTLE (Graduate and Executive Nuclear Training and Lifelong Education) intersemester course funded by the European Commission.

Dr. Bernhard Kienzler finally stepped down from his position as the head of the INE department *Safety of Nuclear Waste Disposal* entering his regular retirement age and Dr. Volker Metz became his successor. Bernhard Kienzler has always been a continuously driving force for initiating and coordinating very successfully new projects on a national and international level. INE owes a lot to him! We are glad, that he agreed to stay for a while as an excellent expert on the scene transferring his advice, experience and knowledge.

Finally, I would like to express my gratitude to our numerous partners, visitors and collaborators. Last, but not least, I extend a sincere thank you to the entire staff of INE for their dedication in both scientific activities and in administrative and technical support.



## Table of contents

<b>1</b>	<b>Introduction to the Institute for Nuclear Waste Disposal (INE)</b> .....	<b>1</b>
<b>2</b>	<b>Education and training</b> .....	<b>5</b>
<b>3</b>	<b>National and international cooperation, conferences and workshops</b> .....	<b>7</b>
3.1	General overview .....	7
3.2	Contribution of INE to the FP7 TALISMAN project .....	12
3.3	XAFS16 conference.....	14
3.4	CMS Euroclay 2015.....	15
<b>4</b>	<b>Fundamental studies: Process understanding on a molecular scale</b> .....	<b>17</b>
4.1	Chemistry and thermodynamics of actinides and fission products in aqueous solution .....	17
4.2	Sorption on mineral surfaces.....	24
4.3	Retention of radionuclides by secondary phase formation .....	31
4.4	Effect of pore-scale mineral precipitation on transport parameters in diffusion controlled systems .....	37
<b>5</b>	<b>Applied studies: Radionuclide retention in the multi-barrier system</b> .....	<b>41</b>
5.1	Highly radioactive waste forms .....	41
5.2	Non-heat producing waste forms and barrier materials .....	45
5.3	Colloid impact on radionuclide migration .....	49
5.4	Reactive transport modelling .....	53
<b>6</b>	<b>Separation of long-lived minor actinides</b> .....	<b>57</b>
6.1	Water soluble complexing agents for actinides(III).....	57
6.2	Dissolution of PuO <sub>2</sub> -Mo CerMet pellets .....	59
6.3	REE separation.....	60
<b>7</b>	<b>Decommissioning of nuclear facilities</b> .....	<b>63</b>
<b>8</b>	<b>Development of radionuclide speciation methods</b> .....	<b>67</b>
8.1	R&D projects conducted at the INE and CAT-ACT beamline at ANKA and at external SR sources.....	67
8.2	Laser spectroscopy.....	72
8.3	Microscopy and Surface Analytics .....	75
8.4	Investigations into structure and bonding by NMR spectroscopy .....	78
8.5	Accelerator mass spectrometry .....	81
8.6	Computational chemistry .....	83
<b>9</b>	<b>(Radio-)chemical analysis</b> .....	<b>89</b>
<b>10</b>	<b>Radiation protection research</b> .....	<b>93</b>
10.1	Modeling of individual dosimetry for working scenarios with respect to emplacement of spent nuclear fuel canister in a rock salt repository .....	93
10.2	A novel radiation detector for deconstruction and decommissioning of nuclear buildings .....	96
10.3	Stochastic chemistry for human-cell equivalent systems.....	98
<b>11</b>	<b>Geoenergy</b> .....	<b>99</b>
<b>12</b>	<b>Publications</b> .....	<b>103</b>



# 1 Introduction to the Institute for Nuclear Waste Disposal (INE)

The **Institute for Nuclear Waste Disposal (INE)**, at the Karlsruhe Institute of Technology **KIT** performs R&D focusing on

- (i) **Long-term safety research for nuclear waste disposal (key focus of INE research),**
- (ii) **Immobilization of high level radioactive waste (HLW),**
- (iii) **Radiation protection**
- (iv) **Decommissioning of nuclear facilities**
- (v) **Geoenergy.**

All R&D activities of KIT-INE are integrated into the program Nuclear Safety Research within the KIT-Energy Centre and the program Nuclear Waste Management, Safety and Radiation Research (NUSAFE) within the Helmholtz Association. INE contributes to German provident research for the safety of nuclear waste disposal, which is the responsibility of the Federal Government.

Following the decision taken by Germany to phase out the use of nuclear energy, the safe disposal of long-lived nuclear waste remains as a key topic of highest priority. Projections based on scheduled operation times for nuclear power plants in Germany (Amendment to German Atomic Energy Act, August 2011) indicate that about a total of 17,770 tons of spent nuclear fuel will be generated. About 6,670 tons have been shipped to France and the UK until 2005 for reprocessing, to recover plutonium and uranium. Consequently, two types of high level, heat producing radioactive waste have to be disposed of safely: spent nuclear fuel and vitrified high level waste from reprocessing (HLW glass). The disposal of low- and intermediate level waste present in much larger quantities likewise needs to be addressed.

Over the last decades, a consensus within the international scientific/technical community was established, clearly emphasizing that emplacement in deep geological formations is the safest way to dispose of high level, heat producing radioactive waste. Disposal concepts with strong inherent passive safety features ensure the effective protection of the population and the biosphere against radiation exposure over very long periods of time. The isolation and immobilization of nuclear waste in a repository is ensured by the appropriate combination of redundant barriers (multi-barrier system).

**Long term safety research for nuclear waste disposal** at KIT-INE establishes geochemical expertise and models to be used in the disposal Safety Case, focusing primarily on the detailed scientific description of aquatic radionuclide chemistry in the geochemical environment of a repository. Work concentrates on the disposal of spent nuclear fuel and HLW-glass in the relevant potential host rock

formations currently considered: rock salt, clay and crystalline rock formations. Actinides and long-lived fission products and long-lived activation products play a central role, as they dominate HLW radiotoxicity over long periods of time. Long-lived anionic fission/activation products are likewise investigated as significant contributors to the maximum radiation dose projected for relevant scenarios.

Relevant long-term scenarios for nuclear repositories in deep geological formations have to take into account possible radionuclide transport via the groundwater pathway. Thermomechanical studies are performed at INE, in order to describe the evolution of the constructed repository after closure. Possible groundwater intrusion into emplacement caverns is assumed to cause waste form corrosion and eventually radionuclide release. Radionuclide mobility is then determined by the various geochemical reactions in complex aquatic systems: i.e. dissolution of the nuclear waste form (HLW glass, spent nuclear fuel), radiolysis phenomena, redox reactions, complexation with inorganic and organic ligands, colloid formation, surface reactions at mineral surfaces, precipitation of solid phases and solid solutions.

Prediction and quantification of all these processes require fundamental thermodynamic data and comprehensive process understanding at the molecular scale. Radionuclide concentrations in relevant aqueous systems typically lie in the nano-molar range, which is exceedingly small in relation to main groundwater components. Quantification of chemical reactions occurring in these systems require the application and development of advanced sophisticated methods and experimental approaches, to provide insight into the chemical speciation of radionuclides at trace concentrations. Innovative laser and X-ray spectroscopic techniques are continuously developed and applied to this end. A specialized working group performing state-of-art theoretical quantum chemical calculations for actinide chemistry support both interpretation of experimental results and optimized experiment design.

The long-term safety of a nuclear waste repository must be demonstrated by application of modelling tools on real natural systems over geological time scales. Geochemical models and thermodynamic databases are developed at INE as basis for the description of radionuclide geochemical behavior in complex natural aquatic systems. The prediction of radionuclide migration in the geosphere necessitates coupled modelling of geochemistry and transport. Transferability and applicability of model predictions are examined by designing dedicated laboratory experiments, field studies in underground laboratories and by studying natural analog systems. This strategy allows to identify and ana-

lyze key uncertainties and continuously optimize the developed models.

Within the R&D topic **immobilization of high-level radioactive waste**, INE contributes to the decommissioning of nuclear facilities. The core process technology for the Vitrification Plant (VEK) on the site of the former Karlsruhe Reprocessing Plant (WAK; located at KIT Campus North) has been developed by INE. INE was involved in functional testing of process systems, as well as in the performance of the cold test operation and played a leading role in the highly successful hot operation of the VEK plant. The vitrification technology developed at INE is highly competitive on an international level. This is evidenced by the strong interest of countries like China in establishing technology transfer.

The R&D topic **radiation protection** at INE focuses on the assessment of radiation exposures on man by estimating doses either from external radiation fields or from incorporation of radionuclides. The strategy driving this work is to provide techniques and models for an individualized dosimetry, which goes beyond the current approach of applying reference models in dose assessments. Both the specific anatomical and physiological features of the exposed individual and the specific effective radiation fields are considered in the frame of an individualized dosimetry. Work is performed in close cooperation with the KIT safety management SUM.

The R&D topic **decommissioning of nuclear and conventional facilities** was set up at INE in 2015 expanding the existing activities at the Institute of Technology and Management in Construction (TMB) of the KIT. Research in this field is focusing on a better understanding of the complete decommissioning process in Germany as well as on a global level.

In 2014 a working group concerning **geoenergy** was set up at INE. The main focus of this topic is geothermal energy research in fractured reservoir systems with special focus on Enhanced Geothermal Systems (EGS)

**INE laboratories** are equipped with all necessary infrastructures to perform radionuclide/actinide research, including hot cells, alpha glove boxes, inert gas alpha glove boxes and radionuclide laboratories. State-of-the-art analytical instruments and methods are applied for analysis and speciation of radionuclides and radioactive materials. Advanced spectroscopic tools exist for the sensitive detection and analysis of radionuclides. Trace element and isotope analysis is made by instrumental analytical techniques such as atomic absorption spectroscopy (AAS), ICP-atomic emission spec-

troscopy (ICP-AES) and ICP-mass spectrometry (Quadrupole-ICP-MS and high resolution ICP-MS). Methods available for surface sensitive analysis and characterization of solid samples include X-ray diffraction (XRD), atomic force microscopy (AFM) and laser-ablation coupled with ICP-MS. A modern X-ray photoelectron spectrometer (XPS) and an environmental scanning electron microscope (ESEM) are installed. INE has direct access to a TEM instrument on the KIT Campus North site (Institute for Applied Materials, IAM). Laser spectroscopic techniques are developed and applied for sensitive actinide and fission product speciation such as time-resolved laser fluorescence spectroscopy (TRLFS), laser photo acoustic spectroscopy (LPAS), laser-induced breakdown spectroscopy (LIBS) and Raman spectroscopy. Insight into structural and electronic properties of radionuclide species is obtained by X-ray absorption fine structure (XAFS) spectroscopy at the INE-Beamline at the KIT synchrotron source ANKA. The INE-Beamline, in close proximity to INE controlled area laboratories, represents in combination with the other analytical methods a unique experimental infrastructure, which both profits from and contributes to INE's leading expertise in the field of actinide chemistry and spectroscopy. INE's synchrotron-based instrumentation is currently augmented by installing the CAT-ACT beamline at ANKA, a state-of-the-art X-ray absorption spectroscopy beamline jointly funded, constructed, and operated by KIT institutes IKFT/ITCP for CATalysis research and INE for ACTinide/radionuclide research. The CAT-ACT beamline is foreseen to become fully operational towards the end of 2016. Quantum chemical calculations are performed on INE's computing cluster, which is equipped with 17 nodes and 76 processors. A 400 MHz-NMR spectrometer adapted to measuring radioactive liquid samples adds to the analytical and speciation portfolio of INE. The INE CAD workstations enable construction and planning of hardware components, process layout and flow sheets. The institute workshop is equipped with modern machine tools to manufacture components for specific experimental and analytical devices in hot laboratories.

In 2015 the **Institute for Nuclear Waste Disposal** had **110 employees** working in the seven departments, which reflect the R&D and organizational tasks of the institute (Fig. 1): (i) scientific/technical coordination and analytical chemistry, (ii) safety of nuclear waste disposal, (iii) radiochemistry, (iv) radionuclide speciation, (v) vitrification of high level waste, (vi) geochemistry and (vii) decommissioning of nuclear and conventional facilities.

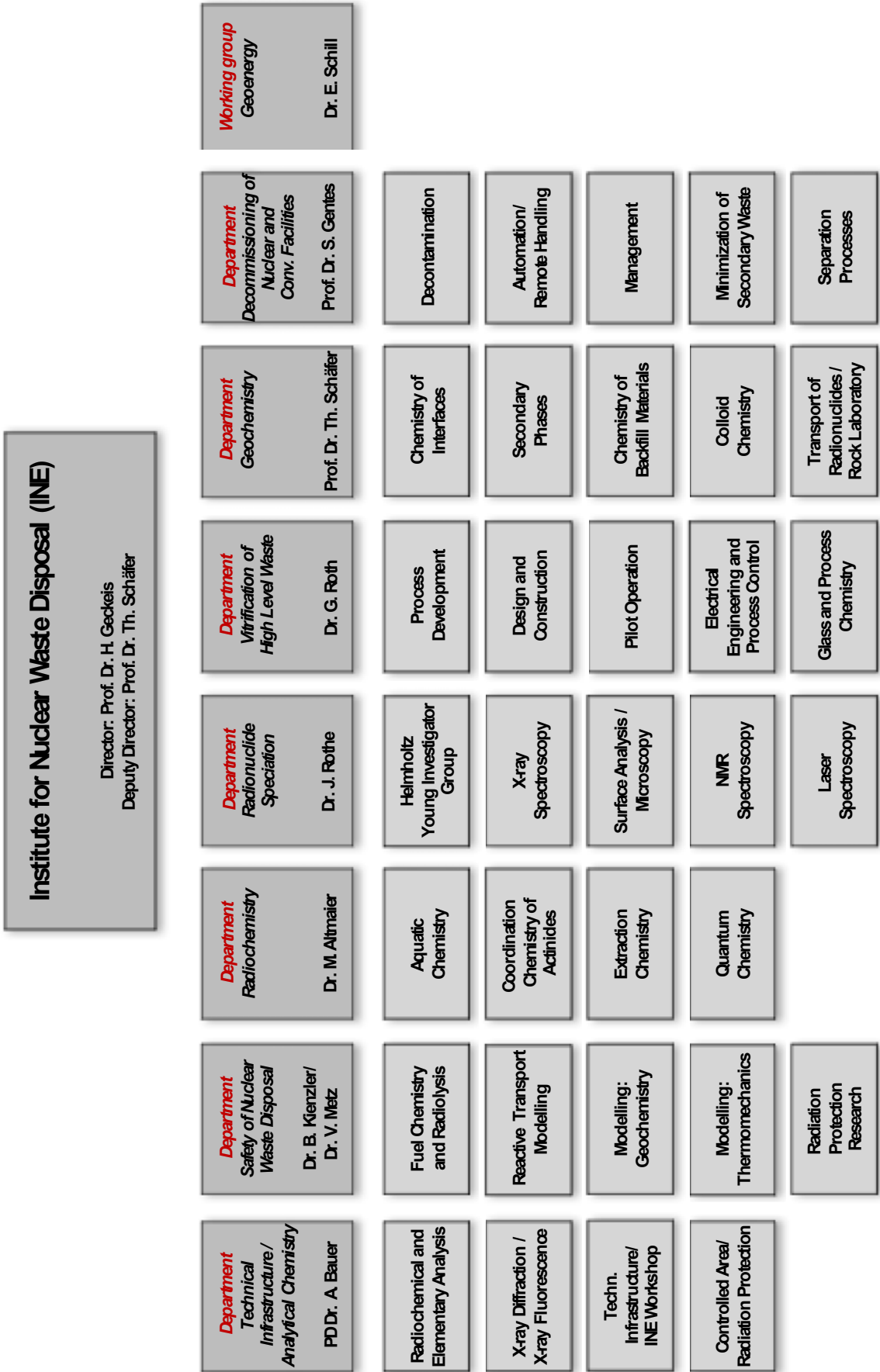


Fig. 1: Organizational chart of the Institute for Nuclear Waste Disposal (INE)



## 2 Education and training

Teaching of students and promotion of young scientists is of fundamental importance to ensure high-level competence and to maintain a leading international position in the fields of nuclear and radiochemistry. INE scientists are strongly involved in teaching at KIT Campus South and the Universities of Heidelberg, Berlin, Jena and Strasbourg as well as the Baden-Wuerttemberg Cooperative State University.

Prof. Dr. **Horst Geckeis**, director of INE, holds a professorship for radiochemistry at KIT Campus South, Department of Chemistry and Biosciences. He teaches fundamental and applied radiochemistry for chemistry students in bachelor and master courses. A radiochemistry module consisting of basic and advanced lectures on nuclear chemistry topics and laboratory courses has been set up for master students in Karlsruhe. In addition, Dr. **Marcus Altmaier**, head of the department radiochemistry, gives a lecture concerning the chemistry of f-elements.

Prof. Dr. **Sascha Gentes** head of the department decommissioning of nuclear and conventional facilities holds a professorship at the Institute for Technology and Management in Construction at the KIT-Department of Civil Engineering, Geo and Environmental Sciences and gives lectures in the field of decommissioning of nuclear facilities, environmentally-friendly Recycling and Disassembly of Buildings, Machinery and Process Engineering as well as construction technology.

Prof. Dr. **Petra Panak**, heading a working group on actinide speciation at INE, holds a professorship of radiochemistry at the University of Heidelberg. A basic course in radiochemistry is offered for bachelor and/or master students. An advanced course comprised of the chemistry of f-elements and medical applications of radionuclides is also offered. The advanced radiochemistry lectures are supplemented by scientific internships at the INE radioactive laboratories.

Nearly 40 students from Karlsruhe and Heidelberg participated in two 3-week radiochemistry laboratory courses in 2015 held at KIT Campus North in the FTU radiochemistry and hot laboratories at INE. Some students are intensifying their knowledge in nuclear/radiochemistry topics during scientific internships at INE. Obviously students are very interested in nuclear chemistry topics and appreciate the various semester courses.

In 2015 Dr. **Tonya Vitova** gave lectures at the KIT Campus South, Department of Chemistry and Biosciences, in the field of instrumental analytics and Dr. **Eva Schill** and Dr. **Marika Vespa** at the Department of Civil Engineering, Geo and Environmental Sciences in the field of geophysics, general geology and analytical methods in applied mineralogy. Dr. **Volker Metz** gave lectures at the Department of Mechanical Engineering and Department of Civil Engineering,

Geo and Environmental Sciences in the field of radioactivity and radioactive waste research.

Lectures and practical units taught by Prof. Dr. **Thorsten Schäfer**, Deputy Director of INE; at the Freie Universität Berlin, Institute of Geological Sciences, Department of Earth Sciences, focused in 2015 on a master degree course on laboratory and field methods in hydrogeology, including performance and analysis of tracer tests using conservative, weakly sorbing tracers and colloids, pumping tests and determination of hydraulic parameters (Applied Hydrogeology III). Moreover, Prof. Dr. Schäfer set up a new lecture concerning the environmental geology: radio- & chemotoxic elements at KIT Campus South, Department of Civil Engineering, Geo and Environmental Sciences.

Dr. **Andreas Bauer** is lecturing Clay Mineralogy at the University of Jena. His lecture deals with the mineralogical characterization of these fine materials and the importance of quantifying surface reactions. In the second part of the lectures sound, practical advice on powder X-ray diffraction in general is provided, as well as a useful set of step-by step instructions for the novice.

Dr. **Andreas Geist** gave lectures at the École européenne de chimie, polymères et matériaux in Strasbourg concerning the Solvent Extraction of Metal Ions.

Dr. **Frank Becker** gave lectures at the Baden-Wuerttemberg Cooperative State University (DHBW). The lectures comprised principles of statistics and measurements, atomic physics and nuclear physics.

Moreover, INE was involved in many schools and workshops concerning the education and teaching of students and young scientists:

- Second Joint Student Workshop on f-Element Chemistry, June 9-10, 2015
- GENTLE Intersemester course: Nuclear waste management, June 28 – July 3, 2015
- Thul Autumn School 2015, September 28 – October 2, 2015
- CP BELBaR Clay Training Course, October 14-16, 2015
- 4th JRC-KIT Research Fellow Day, October 13-14, 2015

Through this close cooperation with universities, students are educated in the field of nuclear and actinide chemistry, which most universities can no longer offer. Hence, INE makes a vital contribution to the intermediate and long perspective of maintaining nuclear science competence. Moreover, INE is involved in the education of trainees (chemical technicians, industrial mechanics and product designers) as well as student internships like BORS and BOGY.

## PhD students

In 2015 24 PhD students worked at INE on their doctoral dissertations; 10 of them were awarded their doctorate. Topics of the theses are:

- Experimental and modelling studies of cement/clay interface process
- Advanced spectroscopic and microscopic structural investigations of nuclear waste glass forms
- Technetium interaction with inorganic ligands and retention processes in the sulfide system
- Release and speciation of actinides by the fabrication and dissolution of Mo- and Zr-based nuclear fuel oxides
- Solubility, speciation and thermodynamics of tetravalent and hexavalent Uranium
- Characterization of structural properties of U and Pu in model systems by advanced synchrotron based X-ray spectroscopy
- Bentonite erosion and colloid mediated radionuclide transport in advection controlled systems
- Development of methods for the individual dosimetry of the staff in disposal facilities
- Investigation of solubility and complexation of Plutonium and Neptunium in highly reducing aquatic systems
- Impact of the flow channel geometry on the agglomeration of colloids and the reduction of permeability in altered granites of potential geothermic reservoir rocks
- Redox behavior, solubility and sorption of Pu(III/IV) in the presence of ISA
- Spectroscopic and thermodynamic investigations of the complexation of An(III) and Ln(III) with hydrophilic Bis-triazinylpyridines
- Investigation of the retention of actinides, lanthanides and long-lived fission products on stable solid phases within the system  $Mg - Na \pm Cl \pm CO_2 - H_2O$
- The influence of repository relevant electrolytes on the interaction of trivalent lanthanides and actinides with calcite
- Interaction of Ln(III) and An(III)/IV/V/VI with borate in dilute to concentrated NaCl, CaCl<sub>2</sub> and MgCl<sub>2</sub> solutions
- Tc-migration in advection/diffusion controlled natural systems: Influence of ferrous iron pool
- Investigation of the sorption of radionuclides on clay mineral surfaces at high ionic strengths
- Redox speciation of repository relevant elements with separation methods coupled to mass spectrometry with inductively coupled plasma
- Study on the effect of speciation on radionuclide mobilization - C-14 speciation in irradiated Zircaloy-4 cladding and nitrate/chloride interaction with An(III)/Ln(III)
- The fate of Eu(III)/Cm(III) during the nucleation and growth of celestite (SrSO<sub>4</sub>) and strontianite (SrCO<sub>3</sub>)
- Characterization of partitioning relevant lanthanide and actinide complexes with NMR spectroscopy
- Characterization of bonding differences by advanced synchrotron based X-ray spectroscopy
- Investigation of the interaction of trivalent actinide and lanthanide ions with human serum transferrin with TRLFS
- Redox, solubility and sorption chemistry of technetium in dilute to concentrated saline systems

## 3 National and international cooperation, conferences and workshops

### 3.1 General overview

INE R&D involves numerous national and international collaborations and projects. These are described in the following.

#### National

INE is involved in various bi- and multilateral collaborations with national research centers, universities and industrial partners on different topics. The projects are partly supported by the German Federal Ministry for Economics and Technology (BMWt), the Federal Ministry for Education and Research (BMBWF), the Federal Ministry for the Environment, Nature Conservation, Building and Nuclear Safety (BMUB), the German Research Foundation (DFG) and the Helmholtz Association of German Research Centers (HGF).

The **ThermAc** project aims at extending the chemical understanding and available thermodynamic database for actinides, long-lived fission products and relevant matrix elements in aquatic systems at elevated temperatures. To this end, a systematic use of estimation methods, new experimental investigations and quantum-chemistry-based information is intended. ThermAc has started in March 2015 and is projected for three years. The project is funded by the German Federal Ministry for Education and Research (BMBWF) and is coordinated by KIT-INE. The ThermAc project is developed in order to improve the scientific basis for assessing nuclear waste disposal scenarios at elevated temperature conditions. In the case of disposal of highly active heat producing waste, the repository system is expected to feature elevated temperature conditions over a significant period of time at an early stage of repository operation. If early canister failure occurs, radionuclides therefore may contact aquatic systems at higher temperature conditions. Adequate scientific tools must be available to assess the related chemical effects and their impact upon safety. A clear focus of ThermAc is on long-lived actinides in oxidation states III, V and VI, with selected fission products and important redox controlling matrix elements like Fe also receiving attention. An(IV) and detailed investigations of redox processes are excluded from the current ThermAc work program. ThermAc addresses the temperature range from  $\sim 5^{\circ}\text{C}$  up to  $\sim 90^{\circ}\text{C}$ , focusing on systems at low or intermediate ionic strength. Only for selected cases with specific relevance or scientific interest, higher temperatures up to  $200^{\circ}\text{C}$  or salt brine solutions are investigated.

Within the **THEREDA** project (launched 2005), INE generates and evaluates thermodynamic data – complex formation constants, solubility data – for selected radionuclides from experiments and literature

data that are incorporated into a centrally managed and administered database of evaluated thermodynamic parameters. Thermodynamic data are required for environmental applications in general and radiochemical issues in particular. This database is developed to a national (reference) standard and will be the basis for performance assessment calculations for a national nuclear waste repository. The database is established by KIT-INE, Gesellschaft für Anlagen- und Reaktorsicherheit (GRS), Helmholtz-Zentrum Dresden-Rossendorf (HZDR), TU Bergakademie Freiberg, and AF-Consult Switzerland Ltd. AF-Consult was replaced by Paul-Scherrer-Institut (PSI, Switzerland) in May 2015. More information about this project can be obtained from the web page: [www.thereda.de](http://www.thereda.de).

The **GRaZ** project (**G**eochemische **R**adionuklidrückhaltung und **Z**ementalterationsphasen) started in September 2015 and is funded by BMWt for three years. GRaZ is a collaborative project. The partners are KIT, HZDR, the Universities of Heidelberg, Mainz, Potsdam, and Saarland as well as the Technical Universities of Dresden and Munich. The project deals with the migration of radionuclides in the near field of a repository for radioactive waste in clay formations with focus on the hyper-alkaline water-cement-system. KIT-INE investigates the retention of actinides and lanthanides by clay minerals in presence of carbonate and silicate, cement phases and cement alteration phases. Furthermore, the influence of cement additives (e.g. plasticizer and superplasticizers) on the sorption of actinides is studied at high pH values. One important issue of the project is the thermodynamic modelling of experimental solubility, complexation, and sorption data. The project provides basic knowledge and thermodynamic data needed in the frame of a long-term safety analysis of different repository concepts.

The disassembly of the reactor pressure vessel and internals poses one of the most demanding challenges in the decommissioning of a nuclear power plant. For this purpose, a waterjet cutting technique (German: Wasser - Abrasiv - Suspensions - Schneidverfahren, WASS) is used, employing a high-pressure water jet and a sharp-edged abrasive medium directed to the cutting material. Advantages of WASS among other, conventional cutting techniques are in the compact design of the setup, the ease of remote manipulation (also at difficult positions) and the “cold” operation under water, which also serves as shielding. However, this technique produces a considerable amount of expensive secondary waste, a water suspension containing small-grained radioactive metal cuttings and abrasive grains. The joint **MASK** (Magnet-Separation von Korngemischen zur Minimierung von

Sekundärabfällen im Rückbau kerntechnischer Anlagen) project between KIT-TMB and KIT-INE is initialized to overcome this limitation. Metal cuttings are separated by a magnetic filter in order to substantially minimize the radioactive secondary waste. INE performs laboratory experiments to analyze in detail the separated fractions and to determine the residual activities. At TMB, the separation process is numerically simulated in order to reveal the key parameters for further optimization of the separation technique. A bench-scale unit is assembled to validate the results of the numerical and experimental investigations.

The bilateral GRS-INE project **KOLLORADO-e** started in March 2013 with a duration of three years as a successor of the KOLLORADO-2 project, focusing on the erosion stability of compacted bentonite (geotechnical barrier) as a function of the contact water chemistry/ hydraulics and the formation of near-field colloids/ nanoparticles as potential carriers for actinides/radionuclides. Both, a detailed experimental program quantifying the bentonite erosion and investigating the influence of surface roughness/ charge heterogeneity on nanoparticle mobility and actinide bentonite nanoparticle sorption reversibility, as well as approaches to implement the acquired process understanding in reactive transport modeling codes comprise the project activities.

The BMWi funded joint research project **Comparison of Constitutive Models for the Thermomechanical Behavior of Rock Salt III** deals with the ability of numerical models to describe adequately relevant deformation phenomena in rock salt under various influences. Modelling approaches to simulate the thermo-mechanical behavior of rock salt are compared and tested by back-calculating previous series of laboratory experiments and in-situ arrangements in underground research laboratories.

The BMBF funded joint research project **ImmoRad** (fundamental investigations for the immobilization of long-lived radionuclides through interaction with secondary mineral phases in deep geological nuclear waste repositories) started in February, 2012 and ended in September 2015. ImmoRad concentrated on application-based fundamental research on retention processes in deep geological environments. Within this project, structural incorporation/ entrapment or formation of solid solutions of radionuclides into secondary phases or rock forming minerals in aquatic environments were studied. National (KIT-INE, HZDR, FZJ, University Frankfurt, University of Bonn) and international partners (PSI-LES; Switzerland and University Oviedo; Spain) collaborated within this project. A proposal for continuation of the ImmoRad project has been submitted and is currently under scientific evaluation.

The project **“Untersuchungen zum grundlegenden Verständnis der selektiven Komplexierung von f-Elementen (f-Kom)”** funded by the German Federal Ministry of Research and Education in the field of Basic Energy Research 2020+ aims at establishing a fundamental understanding of the separation of actinides from nuclear waste. The participating project

partners from KIT-INE, KIT-CS, Universität Erlangen, Universität Heidelberg and Forschungszentrum Jülich are combining their expertise and activities in synthesis, spectroscopy, technology and theory, in order to be able to describe and ultimately predict and optimize liquid-liquid extraction separation processes for actinides at the molecular scale. The project includes a strong component of education and training of young scientists in research topics related to nuclear waste disposal and promotes their networking in the European research landscape.

Within the BMBF funded joint project **Disposal Options for Radioactive Residues: Interdisciplinary Analyses and Development of Evaluation Principles (ENTRIA)** various evaluation principles for three options for management of heat generating nuclear residues are developed: prolonged surface storage, emplacement in deep geological formations without retrievability measures and with monitoring retrievability measures, respectively. Besides disciplinary activities, the projects aim on education of young scientists and interdisciplinary co-operation in the field of radioactive waste management. Scientists of KIT and five other German universities as well as a Swiss partner participate in ENTRIA. They represent disciplines of natural sciences, civil engineering, philosophy, law, and social sciences. Within the project, KIT-INE develops radionuclide source terms and individual dosimetry for personnel with respect to the three options. Moreover, KIT-INE contributes to publications and workshops with respect to interdisciplinary studies on long-term management of nuclear residues.

The collaborative project **EDUKEM**, aiming at an improved understanding of uranium chemistry in saline systems and establishing targeted experimental techniques, was started in December 2014 with a projected 3-year duration. Work of KIT-INE within EUDKEM focusses on the aquatic chemistry and thermodynamics of hexavalent and tetravalent uranium in relevant saline solutions. Based upon new solubility studies, spectroscopic evidence and literature, a comprehensive description of U(IV) and U(VI) solubility and speciation in key saline systems relevant for nuclear waste disposal in salt-based repositories will be established.

The Helmholtz young investigators group (HYIG) **“Advanced synchrotron-based systematic investigations of actinide (An) and lanthanide (Ln) systems to understand and predict their reactivity”** started in July 2011 and systematically investigates the electronic and coordination structure of actinides and chemical homologue lanthanide systems with novel synchrotron-based high-resolution X-ray emission/inelastic scattering techniques (XES/RIXS). Using advanced spectroscopic methods to secure the knowledge of actinide redox speciation and the electronic structure can improve predicting actinide environmental behavior and provide benchmark data for the improvement of quantum chemical codes. The utility of high-energy resolution X-ray absorption near edge structure (HR-XANES) studies in studies of

actinide elements was the motivator for installing and commissioning a multi-analyzer Johann type XES spectrometer (MAC-spectrometer) at the INE-Beamline for actinide research at the ANKA synchrotron radiation facility, Karlsruhe, Germany. A number of systems for the determination of actinide redox states in liquids and solid crystalline and amorphous systems were investigated. For example, it was unambiguously demonstrated that U(V) can be stable incorporated in the magnetite structure. Results from characterization of U and Pu oxidation states in spent nuclear fuel were obtained too. In 2015 the interim evaluation of the HYIG was completed by an independent external review committee and the KIT Council for Research and Promotion of Young Scientist (KIT-CRYS). The achievements of the group were highly recognized and designated “mit sehr gutem Erfolg”. The HYIG project was granted one additional year funded with 250 k€.

In the framework of measures for retrieval of radioactive waste and decommissioning of the **Asse II salt mine**, provisions for emergency preparedness are taken. Therefore, the operator of Asse II, the Federal Office for Radiation Protection (BfS), sank an exploration drilling in the overlaying sedimentary rocks of the salt diapir and coordinates studies with respect to the near-field of the radioactive waste. KIT-INE contributes both to the studies on samples of the overlaying sediments as well as to studies on geo-engineered barriers in the near field of the radioactive waste. Drill cores and pore water samples of the exploration borehole, comprising Triassic shell limestone (Muschelkalk), Bunter sandstone (Buntsandstein) and sulfate-rich cap rock samples, are geochemically and mineralogically characterized. The sample characterization data provide a basis for interpretation for forthcoming radionuclide sorption studies with selected drill core samples and pore water simulates. With respect to the near field KIT-INE compiles the present state of knowledge on geochemical processes in the waste emplacement rooms.

### International

The international Colloid Formation and Migration (CFM) project focuses on the stability of the bentonite buffer/backfill in contact with water conducting features and the influence of colloids on radionuclide migration in crystalline host rocks coordinated by NAGRA (National Cooperative for the Disposal of Radioactive Waste, Switzerland). The project uses the experimental set-up in the controlled zone at the Grimsel Test Site (Switzerland). Additional partners involved are from Japan (JAEA, AIST, CRIEPI), South Korea (KAERI), Finland (POSIVA Oy and Helsinki University), Switzerland (NAGRA, PSI-LES), Spain (CIEMAT), Sweden (SKB, KTH), United Kingdom (NDA RWMD) and United States (LANL). INE plays a decisive role in the laboratory program and is also mainly carrying out the field activities.

Within the framework of the strategy of the German Federal Government for the internationalization of science and research to foster the bilateral cooperation

with Korea in the area of science and technology (WTZ) KIT-INE has started a two year project from 1.10.2014 entitled “Molecular-scale investigation of interaction mechanisms between uranium and iron-bearing minerals under diverse geochemical conditions of groundwater (**BioFeRad**)” with KAIST (Korean Advanced Institute of Science and Technology), group of Prof. Woojin Lee including student exchange and two bilateral workshops. In parallel, an Alexander von Humboldt (AvH) Fellowship of Dr. Sungjun Bae from KAIST was granted and started in May 2015 focusing on the iron corrosion product interaction with uranium.

### EURATOM FP7 and Horizon 2020

**ASGARD** (Advanced fuelS for Generation IV reActors: Reprocessing and Dissolution; 1/2012–6/2016) is a EURATOM FP7 Large Scale Integrated Project focusing on advanced/novel nuclear fuels fabrication and their respective reprocessing issues. ASGARD seeks integration between reactor, fuel and recycling communities, which today is lacking. In some cases, this results in discrepancies between the reactor design on one hand, and the technological feasibility of fabricating, dissolving and reprocessing the selected fuel on the other hand. ASGARD is an integrated effort of 16 institutions from 9 European countries. It is coordinated by Chalmers Technical University.

**SACSESS** (Safety of ACTinide SEparation proceSSes; 3/2013–6/2016) is a EURATOM FP7 Collaborative Project dealing with safety aspects of hydrometallurgical and pyrometallurgical actinide separation processes developed in previous EURATOM projects. SACSESS provides a structured framework to enhance the fuel cycle safety associated to P&T. In addition, safety studies are performed to identify weak points to be further studied. These data are used to optimize flow sheets and process operation conditions. 26 Partners from 10 countries (plus JRC-ITU and Japan) contribute to SACSESS. The project is coordinated by CEA; KIT is in charge of the hydrometallurgy domain.

The separation of rare earth elements (REE) from secondary sources such as mine tailings is studied in the ERA-MIN project **ENVIREE** (environmentally friendly and efficient methods for extraction of rare earth elements from secondary sources; 3/2015–2/2018). The project is coordinated by CHALMERS (Sweden). Eleven partners from eight countries contribute to the following areas: assessment of sources, development of innovative, efficient and environmentally benign leaching and separation methods, life cycle assessment and economic feasibility studies.

Recent safety assessments of nuclear waste repositories in crystalline formations have shown that the formation and stability of colloids may have a direct impact on the overall performance of the repository. The main aim of the 7<sup>th</sup> framework collaborative project **BELBaR** is to increase the mechanistic understanding of the processes that control bentonite erosion, clay colloid stability, and ability to transport radionuclides. The final outcome is to examine how

colloids and related phenomena can be considered in the long-term safety case and to make recommendations on the quantitative and qualitative approaches that a safety case could pursue to adequately address this potentially very significant issue. BELBaR coordinated by SKB consists of a consortium of 14 partners from Sweden, Finland, Spain, Czech Republic, Great Britain, Russia and Germany with KIT-INE leading WP3 on “Colloid radionuclide & host rock interaction”.

The Collaborative Project **CArbon-14 Source Term (CAST)** was started in October 2013 with a duration of four years. The project aims to develop understanding of the generation and release of C-14 from radioactive waste materials under conditions of underground geological repositories. KIT-INE contributes with experimental studies to work packages “Irradiated Steel” and “Irradiated Zircaloy” as well as to the work package “Dissemination of Knowledge”. Within the two experimental work packages KIT-INE conducted studies with highly-active stainless steel and Zircaloy-4 samples in the shielded box-line of KIT-INE. Liquid and gaseous samples are chemically treated in a specifically designed glove box. In the experiments C-14 is separated from other radionuclides aliquots and the distribution of inorganic and organic C-14 fractions are determined.

KIT-INE contributes actively to international organizations, such as the Thermodynamic Database Project of the Nuclear Energy Agency (NEA).

**Cebama** is a collaborative project investigating cement-based materials, properties, evolution and barrier functions within the European Commission Horizon 2020 frame. The 4-year project, started 1<sup>st</sup> of June 2015, is carried out by a consortium of 27 partners consisting of large Research Institutions, Universities, one TSO (Technical and Scientific Support Organizations), and one SME (small medium enterprise) from 9 EURATOM Signatory States, Switzerland and Japan. National Waste Management Organizations support Cebama by co-developing the work plan, participating in the End-User Group, granting co-funding to some beneficiaries, and providing for knowledge and information transfer. Cebama is coordinated by KIT-INE. The overall strategic objective of Cebama is to support the implementation of geological disposal by significantly improving the knowledge base for the Safety Case for European repository concepts. Scientific/technical research in Cebama is largely independent of specific disposal concepts and addresses different types of host rocks, as well as bentonite. Cebama is not focusing on one specific cementitious material, but aims at studying a variety of important cement-based materials in order to provide insight on general processes and phenomena which can later be transferred to different applications and projects. Main objectives of Cebama are:

- Perform experimental studies to understand the interface processes between cement-based materials and the host rocks (crystalline rock, Boom Clay, Opalinus Clay (OPA), Callovo-Oxfordian (COX), Toarcian mudstone) or bentonite back-

fill and assess the impact on physical (transport) properties.

- Study radionuclide retention processes in high pH concrete environments. Radionuclides which have high priority from the scientific and applied perspective are selected.
- Improve validity of numerical models to predict changes in transport processes as a result of chemical degradation. Support advanced data interpretation and process modelling, covering mainly issues responsible for changes in transport properties.

Further information on Cebama and on upcoming Cebama project events is available at the project website [www.cebama.eu](http://www.cebama.eu).

The Coordination and Support Action **Graduate and Executive Nuclear Training and Lifelong Education (GENTLE)** focuses on education of undergraduate and graduate students of European academic institutions by means of student research experiences in nuclear laboratories and intersemester courses. Scientists of universities and major research institutions of ten European countries participate in this Education and Training action, which started in January 2013 with a duration of four years. Within GENTLE, KIT-INE supervised students of European universities, who conducted research projects at the KIT-INE laboratories. In July 2015 an intersemester course on Nuclear Waste Management was organized by KIT-INE. The course provided advanced level understanding of different waste streams, their origins, radiological and chemical properties of nuclear wastes, and the hazards they represent. Moreover, it covered waste management of decommissioning wastes, irradiated materials, spent nuclear fuel and nuclear materials.

The H2020 project "Deployment of deep enhanced geothermal systems for sustainable energy business **DEEPEGS**" started in December 2015. The project focusses on the demonstration of the feasibility of enhanced geothermal systems (EGS) for delivering energy from renewable resources in Europe. Testing of stimulating technologies for EGS in deep wells in different geological environments, will deliver new innovative solutions and models for wider deployments of EGS reservoirs with sufficient permeability. INE is involved mainly in the evaluation of hydraulic stimulation techniques and monitoring of their application at the Reykjanes geothermal field. There, the consortium aims at demonstrating EGS for widespread exploitation of high enthalpy heat beneath the existing volcanic-hydrothermal field at Reykjanes with a temperature up to 550°C. INE is also partly involved in exploration of very deep, sedimentary, hydrothermal reservoirs at Vistrenque (France) with temperatures up to 220°C. The consortium includes seven industrial companies from Iceland, France, Norway, Germany and Italy with HS Orka HF as coordinator, and two scientific institutions (BRGM, France, and KIT, Germany).

### Conferences and workshops

INE has organized a series of workshops and conferences or has contributed significantly to the organization:

- Workshop on Actinide-Brine-Chemistry (ABC-Salt IV), Heidelberg, Germany, April 14-15, 2015
- Workshop on High Temperature Aqueous Chemistry (HiTAC II), Heidelberg, Germany, April 16, 2015
- Cebama Kick-Off Meeting, July 1<sup>st</sup> 2<sup>nd</sup>, 2015, Brussels, Belgium.
- Geothermal workshop at the Äspö Hard Rock Laboratory (Äspö HRL), Äspö HRL, Oskarhamn, Sweden November 4-5, 2015
- XAFS16, Karlsruhe, Germany, August 23-18, 2015
- Migration, Santa Fe, USA, September 13-18, 2015
- NEA-OECD “ClayClub” Workshop entitled “Filling the gaps – from microscopic pore structures to transport properties in shales” held in conjunction with the EUROCLAY 2015 conference in Edinburgh, UK, July 5, 2015. The outcome of this workshop will be published in a CMS Workshop Lecture Series (WLS) volume.
- INE initiated a DFG round table discussion on the topic “Coupled processes in tight formations (clays and claystones)”, Karlsruhe, Germany, May 19, 2015
- 7th EC FP – CP BELBaR 4<sup>th</sup> Annual Meeting and Training Course “Swelling clays: From compacted bentonite to clay colloids in the context of nuclear waste disposal”, Karlsruhe, Germany, October 12-16, 2015

## 3.2 Contribution of INE to the FP7 TALISMAN project

Over the last decades, the scientific understanding of radionuclide mobilization and retention processes was significantly improved, largely owing to the use of advanced spectroscopic and analytical techniques. The use of innovative technical tools allows researchers to derive the required process understanding at the molecular level which is at the very core of reliable and robust geochemical predictions. Research on radioactive substances furthermore requires dedicated facilities which are properly licensed and equipped to handle the potentially highly hazardous materials.

The need of ensuring access for a wide user and research community to selected large experimental infrastructures equipped with state-of-art analytical equipment dedicated to working with radionuclides was identified previously. Consequently, a series of projects were developed on an international level, namely the ACTINET projects and the recently finalized TALISMAN project. All these projects received funding from the European Commission. As these projects were not entirely restricted to studies pertaining to the Nuclear Waste Disposal Safety Case, a significant portion of the activities were clearly related to this topic.

The 36 months TALISMAN project (start January 2013, end December 2015) was built on the positive experiences gained in the previous ACTINET projects. TALISMAN featured a proposal system to fund

and grant access of researchers via Joint Research Projects (JRP) to work at the 9 international TALISMAN Pooled Facilities, INE-Radlabs and INE-Beamline being two of them. R&D at the Pooled Facilities was mainly addressed within three different topical scopes,

- Actinide separation chemistry,
- Actinides in the geological environment,
- Actinide materials.

In addition to the Joint Research Projects in which the main experimental research was performed and which were usually developed bilaterally between the visiting scientists and the collaborating Pooled Facility experts, a series of summer-schools and workshops were organized in TALISMAN with a strong focus on dissemination, training and education.

The TALISMAN project features a dedicated website (Fig.1), on which important project related information is made available. For example, information on experimental tools and technical infrastructures available at the Pooled Facilities (see Fig. 2), the seven TALISMAN newsletters and an impressive total of 94 end-of-stay reports related to the JRPs performed at the different Pooled Facilities is given.

The experience gained by KIT-INE in the TALISMAN and ACTINET projects and especially during the many Joint Research Projects realized with external partners at KIT-INE is very positive, both from a genuine scientific perspective and in view of promoting increased networking, exchange and productive synergies on a European level. JRP activities at KIT-INE were using the radiochemical laboratories of KIT-INE equipped with spectroscopic and analytical tools and the INE-Beamline for Actinide Research at ANKA with a unique technical infrastructure.

Within TALISMAN, 21 JRPs were selected and funded to perform experimental investigations at KIT-INE. Several research projects have explicitly profited from the close connection of KIT rad-labs and the INE-Beamline for Actinide Research at ANKA. The total quantity of access provided by KIT-INE was 596 days in the 21 JRPs. Within these activities, 50 users from 6 external universities and 8 research institutions were visiting, with a total of 15 students participating. Activities at KIT-INE were well distributed over the three topical scopes in TALISMAN. There were 5 JRPs with 8 users and 205 access units provided in Scope 1 (actinide separation chemistry), 8 JRPs with 11 users and 255 access units provided in Scope 2 (actinides in the geological environment), and 8 JRPs with 29 users and 97 access units provided in Scope 3 (actinide materials). Topics covered in the nuclear waste disposal context include fundamental actinide chemistry relevant to assess radionuclide source terms, XAS studies at ANKA on repository relevant systems,



Fig. 1: Talisman website at [www.talisman-project.eu](http://www.talisman-project.eu).

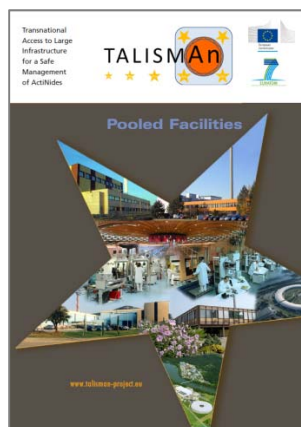


Fig. 2: Talisman Pooled Facility brochure describing the available technical infrastructure (download at TALISMAN website).



**Fig. 3:** “ThUL School 2014 in Actinide Chemistry”, hosted and organised by KIT-INE in Karlsruhe.

use of analytical tools to investigate radionuclide chemistry in real systems, and a study performed in the context of decommissioning nuclear facilities.

The JRPs performed in cooperation with KIT-INE were successfully disseminated and presented at more than 45 national and international scientific conferences as of December 2015. In addition, about 25 peer-reviewed publications related to the JRPS at KIT-INE were published or ready to be submitted.

Further activities at KIT-INE within TALISMAN were focusing on computational actinide chemistry with the aim of strengthening links and synergies between theory and experimental studies. To this end, a series of ThUL schools were organized by KIT-INE in continuation of activities related to the Theoretical UserLab (ThUL) established in ACTINET-I3 which was successfully fostering the interaction between experimental and computational actinide chemistry and physics.

The main lesson learnt from the participation of KIT-INE in the TALISMAN and previous ACTINET projects is, that there is definitely a strong need of

both the national and international research communities to have advanced and technically innovative experimental tools and infrastructures available, allowing dedicated research in support of the Nuclear Waste Disposal Safety Case. In the specific applied context of the German “Energiewende” this demand is further accentuated by the need to establish scientifically justified options for the safe disposal of nuclear waste and support the development of optimized decommissioning technologies, i.e. targeting waste volume reduction.

Three main conclusions are:

- It is mandatory that large innovative experimental infrastructures and advanced radiochemical laboratories are maintained and further developed on a national level. This is a key component in support of the Nuclear Waste Disposal Safety Case, largely independent of the potential host rock formations and repository concepts.
- An excellent tool to support young researchers during PhD work or early Postdoc careers is offering access to advanced experimental research infrastructures. This is valuable both in view of extending the range of available scientific methods, and in the broader context of knowledge maintenance and promoting young talent.
- The EC funded TALISMAN and ACTINET projects highlight the significant scientific and technical synergies gained from improved networking on an international, i.e. European, level. Based upon the sharing of resources, expertise and experience within the frame of collaborative R&D actions, there is a clear added value and positive feedback meeting the specific requirements of national programs.

### 3.3 XAFS16 conference

Following previous conferences in Beijing (2012), Camerino (2009) and Stanford (2006), the sixteenth international conference on X-ray Absorption Fine Structure - XAFS16 ([www.xafs16.org](http://www.xafs16.org)) - was held between 23<sup>rd</sup> and 28<sup>th</sup> August 2015 at KIT Campus South. Jointly organized by KIT, DESY (Hamburg), HZB (Berlin) and the European XFEL (Hamburg) under the auspices of the International X-ray Absorption Society (IXAS), the conference hosted over 550 participants from 37 different countries, establishing a new record for the number of participants. The local organization was provided by the KIT institutes INE, IKFT and ITCP and the ANKA synchrotron facility. The triennial XAFS meeting brings together X-ray spectroscopy experts to discuss the latest developments in instrumentation and theoretical modelling of

inner-shell excitation spectra and to present XAFS applications in various fields of natural sciences and cultural heritage. XAFS16 witnessed a very dynamic community that embraces new techniques and applies them to solve problems in very diverse fields. Examples are micro-spectroscopy in environmental sciences and cultural heritage, X-ray dichroism for magnetic materials, extreme conditions in materials and earth science and X-ray emission spectroscopy in catalysis, biology and radionuclide research. The field of transient spectroscopy is growing with quick-scanning monochromators, modulation-enhanced detection and pump-and-probe techniques. A special symposium dedicated to applications of XAS in industrial research was organized for the first time at a XAFS conference.



*Fig. 1: The official XAFS16 conference photo with the conference logo designed by Wilfrid Schroeder, KIT († 2015).*

#### **Reference:**

J.-D. Grunwaldt, M. Hagelstein and J. Rothe (Eds.), 16th International Conference on X-ray Absorption Fine Structure (XAFS16), IOP Publishing, Journal of Physics: Conference Series, 712 (2016) 011001

### 3.4 CMS Euroclay 2015

INE organized together with BGR and the Durham University a workshop entitled “*Filling the gaps – from microscopic pore structures to transport properties in shales*”. This workshop was initiated by the NEA-OECD “ClayClub”, the Clay Minerals Society, and the Euroclay conference series. The aim of the workshop was to give a current state-of-the-art of different spectroscopy and microscopy methods to better understand microscopic pore structures and transport properties in shales. The full-day workshop was held in conjunction with the EUROCLAY 2015 conference in Edinburgh, UK on the 5th of July 2015. It addressed new developments in the field in order to address the above mentioned knowledge gaps in clay minerals and clay rich shales. This workshop was a continuation of the first workshop “*Clays under Nano- to Microscopic resolution*” which took place from 6<sup>th</sup>-8<sup>th</sup> September 2011 in Karlsruhe and documented the progress made over the past four years concerning research in low permeability, clay rich, geological formations [1]. The workshop also provided an excellent opportunity for exchange of knowledge

with research communities concerned with the safe long-term management of radioactive waste within argillaceous sediments, and the shale gas and oil exploration. The summary of this workshop including eighteen peer reviewed contributions will be published open access as Volume 21 of the CMS workshop lectures [2].

#### References:

- [1] NEA-CLAYCLUB (2013) Clay characterisation from nanoscopic to microscopic resolution. Workshop Proceedings (<http://www.oecd.org/officialdocuments/publicdisplaydocumentpdf/?cote=NEA/RWM/CLAYCLUB%282013%291&docLanguage=En>), Karlsruhe, Germany.
- [2] T. Schäfer, R. Dohrmann, H.C. Greenwell (eds.): “Filling the gaps – from microscopic pore structures to transport properties in shales”, The Clay Minerals Society Workshop Lectures Series, Vol. 21 (2016).



## 4 Fundamental studies: Process understanding on a molecular scale

In order to develop detailed scientific understanding on a molecular scale and ensure the reliable quantitative prediction of key processes in aquatic chemistry, fundamental studies on radionuclide chemistry and geochemistry are performed at KIT-INE. Aiming at a comprehensive assessment of radionuclide behavior and mobility in aquatic systems relevant for nuclear waste disposal, experimental studies with actinides and long-lived fission products are performed. The investigated aqueous systems cover from dilute solutions to highly saline salt brine systems and establish essential site-independent data and process understanding. Work is focusing both on detailed experimental investigations using the unique facilities available at KIT-INE, and subsequently developing reliable chemical models and consistent thermodynamic data. This combined approach allows a systematic and reliable evaluation of key processes such as radionuclide solubility, radionuclide speciation, radionuclide retention and transport processes in relevant near- and far-field scenarios.

The work summarized in this section is related to the (i) chemistry and thermodynamics of actinides and fission products in aqueous solution, (ii) radionuclide sorption on mineral phases, (iii) retention of radionuclides by secondary phase formation, and (iv) radionuclide diffusion. The studies aim at identifying relevant radionuclide retention/retardation mechanisms on a molecular level and their robust thermodynamic quantification in support of the Nuclear Waste Disposal Safety Case. The fundamental studies on aqueous radionuclide chemistry described in Chapter 4 are supporting the applied studies (see Chapter 5) performed at KIT-INE.

### 4.1 Chemistry and thermodynamics of actinides and fission products in aqueous solution

*M. Altmaier, N. L. Banik, A. Baumann, M. Böttle, N. Cevirim, K. Dardenne, F. Endrizzi, D. Fellhauer, D. R. Fröhlich, X. Gaona, P. Lindqvist-Reis, C. Marquardt, R. Marsac, P.J. Panak, Th. Rabung, J. Rothe, J. Schepperle, A. Skerencak-Frech, B. Schimmelpfennig, A. Tasi, E. Yalcintas*

In co-operation with:

*R. Belmecheri<sup>a</sup>, J. Bruno<sup>b</sup>, M. Denecke<sup>c</sup>, M. Grivé<sup>b</sup>, K., Källström<sup>d</sup>, F. Réal<sup>e</sup>, V. Vallet<sup>f</sup>, C. Walther<sup>f</sup>*

<sup>a</sup> Laboratoire de Thermodynamique et Modélisation Moléculaire, Faculté de Chimie, USTHB BP 32 El-Alia, 16111 Bab-Ezzouar, Algeria; <sup>b</sup> Amphos<sup>21</sup> Consulting S.L., Passeig Garcia i Faria, 49-51, 1-1a, 08019 Barcelona, Spain; <sup>c</sup> Dalton Nuclear Institute, The University of Manchester, Manchester, UK; <sup>d</sup> Svensk Kärnbränslehantering AB, Avd. Låg-och medelaktivt avfall, Box 250, 101 24 Stockholm, Sweden; <sup>e</sup> Laboratoire PhLAM, UMR-CNRS 8523, Université Lille 1 (Sciences et Technologies), F-59655 Villeneuve d'Ascq, France; <sup>f</sup> Institut für Radioökologie und Strahlenschutz, Leibniz Universität Hannover, Hannover, Germany

#### Introduction

The accurate knowledge of the aquatic chemistry and thermodynamics of actinides, fission and activation products is mandatory in the context of nuclear waste disposal. The availability of complete and correct chemical and thermodynamic models represents the fundamental basis for trustworthy, transparent and reliable geochemical model calculations and source-term estimations and, thus, for the safety assessment of repositories for nuclear waste disposal. The studies summarized in this section highlight the fundamental and applied research performed at KIT-INE in 2015 within this topic.

In addition to the experimental R&D activities, KIT-INE contributes to several national and international projects, e.g. with focus on the interdisciplinary analyses of disposal options for radioactive waste (ENTRIA, funded by BMBF), or the development of national (THEREDA) and international (NEA-TDB, funded by OECD) thermodynamic reference databases for actinides and fission products.

#### Redox chemistry of U(IV)/U(VI) under alkaline to hyperalkaline pH conditions

Uranium is the main element in the nuclear fuel cycle and, consequently, contributes with the largest inventory to the radioactive waste. U(VI) is the most stable oxidation state of uranium under anoxic and oxidizing conditions, whereas U(IV) prevails in strongly reducing environments. U(VI) shows an amphoteric behavior and precipitates as  $\text{UO}_3 \cdot 2\text{H}_2\text{O}(\text{cr})$  and  $\text{Na-U(VI)-OH}(\text{s})$  phases under acidic and alkaline NaCl solutions, respectively. U(IV) forms sparingly soluble  $\text{UO}_2(\text{am,hyd})$ , which defines  $[\text{U}] < 10^{-8}$  M above  $\text{pH} \approx 5$ . Due to the very different chemical behavior of U(IV) and U(VI), appropriate knowledge of the redox chemistry of uranium is mandatory for an accurate prediction of its behavior under repository-relevant conditions. This is especially challenging under hyperalkaline pH conditions, where U(IV) easily oxidizes to U(VI) and the formation of anionic U(IV) hydrolysis species has been also hypothesized in the literature [1].

In the frame of the BMWi funded project EDUKEM, the redox chemistry of uranium was investigated in 0.1 and 5.0 M NaCl–NaOH solutions at  $8 \leq \text{pH}_m \leq 14.7$ . All experiments were performed in Ar glove-boxes at  $T = 22 \pm 2$  °C. Strongly reducing conditions ( $\text{pH} + \text{pe} < 4$ ) were chemically set for each independent redox sample in the presence of several reducing systems ( $\text{Na}_2\text{S}_2\text{O}_4$ , Sn(II), Sn(II) + Fe(0), Sn(II) +  $\text{Fe}_3\text{O}_4$ , and Sn(II) +  $\text{TiO}_2$ ). U(VI) was added to these systems with  $3 \cdot 10^{-5} \text{ M} \leq [\text{U(VI)}]_0 \leq 4 \cdot 10^{-4} \text{ M}$ . Uranium concentration,  $\text{pH}_m$  and  $E_h$  values were monitored at regular time intervals and systematized on Pourbaix and solubility diagrams calculated using thermodynamic data reported elsewhere [2-4].

Figure 1 shows the experimental  $\text{pH}_m$  and  $E_h$  values (Sn(II), Sn(II) +  $\text{TiO}_2$  and  $\text{Na}_2\text{S}_2\text{O}_4$  systems) for  $t \leq 250$  days plotted in the Pourbaix diagram of U.  $E_h$  values for Sn(II) and  $\text{Na}_2\text{S}_2\text{O}_4$  systems are stable within this timeframe, and fall in the stability field of U(IV) according with the current NEA–TDB selection [2].

Concentrations of U measured in the investigated systems under equilibrium conditions (assumed by constant [U],  $\text{pH}_m$  and  $E_h$ ) are shown in Figure 2. Very low ( $< 10^{-8} \text{ M}$ ) and pH-independent values of [U] are observed within  $8 \leq \text{pH}_m \leq 14.7$ , clearly hinting towards the reduction of U(VI) to U(IV) and a solubility control by the chemical reaction  $\text{UO}_2(\text{am,hyd}) + 2\text{H}_2\text{O} \rightleftharpoons \text{U}(\text{OH})_4(\text{aq})$ . No indication of a solubility increase under hyperalkaline conditions is obtained for any of the investigated systems, thus disregarding the formation of anionic U(IV) species up to  $\text{pH}_m \approx 14.7$ .

Kinetics play an important role in the process of U(VI) reduction to U(IV). Depending upon the reducing system and  $[\text{U(VI)}]_0$ , equilibration times of

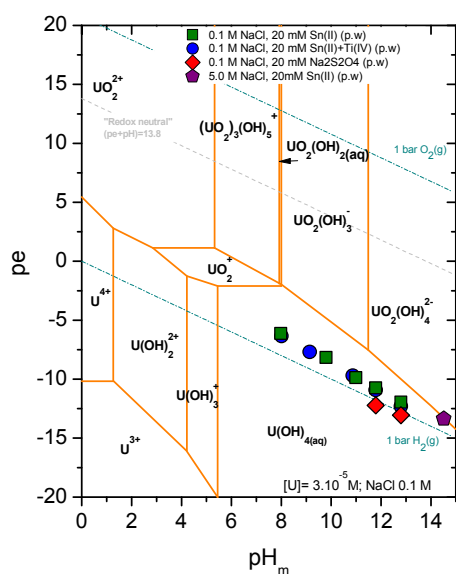


**Fig. 1:** Pourbaix diagram of U calculated for 0.1 M NaCl and  $[\text{U}] = 3 \cdot 10^{-5} \text{ M}$  using thermodynamic data reported in [2-4]. Symbols correspond to experimental  $\text{pH}_m$  and  $E_h$  values determined for Sn(II), Sn(II) +  $\text{TiO}_2$  and  $\text{Na}_2\text{S}_2\text{O}_4$  systems at  $t \leq 250$  days.

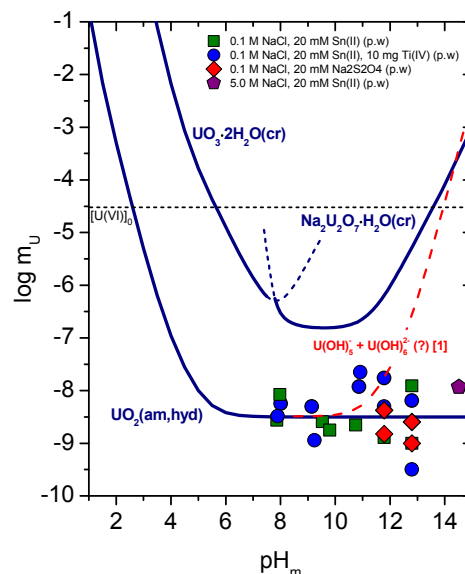


**Fig. 2:** U(IV) equilibrium concentration after quantitative reduction of initial  $[\text{U(VI)}]_0 = 3 \cdot 10^{-5} \text{ M}$  by Sn(II), Sn(II) +  $\text{TiO}_2$  and  $\text{Na}_2\text{S}_2\text{O}_4$  systems in 0.1 and 5.0 M NaCl solutions with  $8 \leq \text{pH}_m \leq 14.7$ . Solubility curves calculated using thermodynamic data reported in [2-4]. Dashed red line corresponding to the solubility of  $\text{UO}_2(\text{am,hyd})$  calculated considering the formation of  $\text{U}(\text{OH})_5^-$  and  $\text{U}(\text{OH})_6^{2-}$  as reported in [1].

100 days (or even longer) are needed to achieve a complete reduction of U(VI) to U(IV) and attain thermodynamic equilibrium.  $\text{TiO}_2$  acts as catalyzer and importantly accelerates the reduction of U(VI) to U(IV). These results indicate that insufficient equilibration time was allowed in previous studies where the formation of anionic U(IV) hydrolysis species was proposed [1].

Based on the outcome of this redox study, comprehensive undersaturation solubility experiments with  $\text{UO}_2(\text{am,hyd})$  are planned at KIT–INE in dilute to concentrated NaCl,  $\text{MgCl}_2$  and  $\text{CaCl}_2$  solutions. This study will provide complete chemical, thermodynamic and activity models for the solubility and hydrolysis of U(VI) from acidic to hyperalkaline pH conditions.

### Solubility of ternary M-Np(V)-OH solid phases in alkaline NaCl solutions

Within the series of possible main oxidation states of actinide elements in aqueous solutions, An(III)-An(VI), the pentavalent An(V) reveals the highest mobility in aqueous solutions due to its weak sorption properties and its high solubility. The latter is particularly true for amorphous  $\text{AnO}_2\text{OH}(\text{am})$  as solubility limiting solid phase. In the case of Np, which exists as Np(V) over a wide range of ( $\text{pH} + \text{pe}$ ) solutions conditions, we have recently demonstrated that  $\text{NpO}_2\text{OH}(\text{am})$  is only metastable in alkaline NaCl and  $\text{CaCl}_2$  solutions regarding transformation into higher hydroxide phases, M-Np(V)-OH(s) with M = Na and Ca [5-6]. In the present work, the solubility behavior and thermodynamic stability of ter-

nary M-Np(V)-OH solid phases (M = Na, Ca) is systematically investigated in alkaline NaCl solutions.

Ternary M-Np(V)-OH solids with M = Na and Ca were prepared by equilibration of binary (greenish)  $\text{NpO}_2\text{OH}(\text{am})$  in the respective alkaline NaCl and  $\text{CaCl}_2$  solutions for several months, as described in previous work [5-6]. The reddish transformation product obtained in  $\text{CaCl}_2$  solutions was analyzed by powder-XRD, SEM-EDX, and quantitative chemical analysis, and unambiguously identified as  $\text{Ca}_{0.5}\text{NpO}_2(\text{OH})_2(\text{s,hyd})$  reported in [6]. Analogous characterization of the purple transformation product in alkaline NaCl confirmed, that the targeted preparation of the Na-Np(V)-OH solid phase with the lowest ratio Na : Np described in [5] (determined in the present work as Na : Np  $\approx$  0.85 : 1) was successful. Both compounds show characteristic XRD patterns, platelet like morphology and are microcrystalline. The solubility behavior of the solids is investigated in alkaline 0.1 M and 5.0 M NaCl solutions (undersaturation approach with approximately 0.5 mg solid phase per sample). In the batch series with  $\text{Ca}_{0.5}\text{NpO}_2(\text{OH})_2(\text{s,hyd})$ , [Ca] was adjusted to 4 mM to ensure constant conditions of the background solutions.

The experimental solubility of both ternary phases is displayed in Figure 3 in comparison to published data for  $\text{NpO}_2\text{OH}(\text{am})$  [5, 7]. In pure 0.1 M (green symbols full) and 5.0 M NaCl (green symbols open) solutions with  $\text{pH}_m > 11$  and 10, respectively, measured Np(V) concentrations in equilibrium with Na-Np(V)-OH(s,hyd) are lower than the data for binary  $\text{NpO}_2\text{OH}(\text{am})$  (red symbols), *i.e.* the ternary phase is more stable in this region. As expected, Na-Np(V)-OH(s) solubility decreases with increasing NaCl concentrations.

In the corresponding NaCl solutions with additions

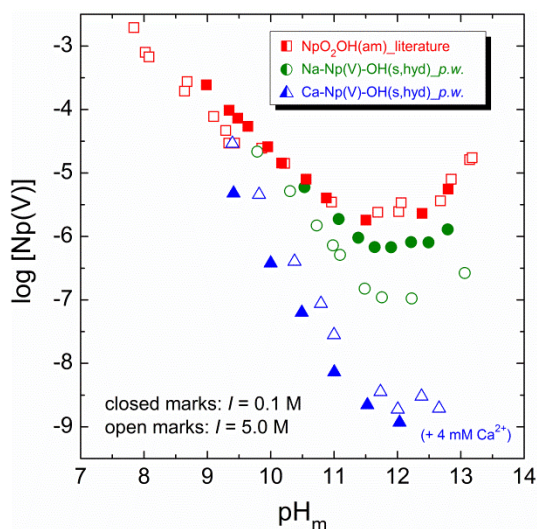


**Fig. 3:** Experimental solubility of binary  $\text{NpO}_2\text{OH}(\text{am})$  [5, 7] and ternary Na-Np(V)-OH(s,hyd) and Ca-Np(V)-OH(s,hyd) in 0.1 and 5.0 M NaCl solutions.

of 4 mM Ca (blue symbols), ternary Ca-Np(V)-OH(s,hyd) controls the Np(V) solubility over the entire  $\text{pH}_m$  range investigated although Ca is only present as trace element (ratio Na to Ca up to 1250 to 1). The great difference in [Np(V)] compared to binary  $\text{NpO}_2\text{OH}(\text{am})$  as well as ternary Na-Np(V)-OH(s,hyd) is especially apparent in hyperalkaline solutions ( $\text{pH}_m > 11$ ) where the solubility of Ca-Np(V)-OH(s,hyd) is up to 3 log-units lower. As [Ca] was kept constant in the batch series with Ca-Np(V)-OH(s,hyd), the systematically increasing Np(V) concentrations with ionic strength are a result of the changing activity in the systems, and agree well with the present activity model for  $\text{NpO}_2^+$  in chloride medium [8]. The pH dependence of the solubility curves is different for binary  $\text{NpO}_2\text{OH}(\text{am})$  and the ternary phases due to the greater hydroxide content of the latter: in the pH region, where hydrolyzed Np(V) is the predominant aqueous Np(V) species ( $\text{pH}_m < 11$ ), the slopes of the solubility curves are  $-2$  (Ca-phase),  $\approx -1.8$  (Na-phase in  $I = 5.0$  M), and  $-1$  (binary  $\text{NpO}_2\text{OH}(\text{am})$ ), respectively. The onset of hydrolysis leads to an increase of Np(V) solubility in more alkaline solutions ( $\text{pH}_m > 12$ ) for  $\text{NpO}_2\text{OH}(\text{am})$ , while this effect is less pronounced / absent for the ternary phases.

The results show that the concentration of Np(V) and, hence, its mobilization in alkaline solutions is significantly reduced due to the formation of ternary M-Np(V)-OH solid phases. The data are highly relevant for the assessment of more realistic solubility limits and source-terms for pentavalent actinides in a repository, where the formation and potential interaction of alkaline solutions with nuclear waste have to be considered due to a large inventory of cementitious material.

### Solubility behavior and carbonate complexation of Np(IV) and Pu(IV) in alkaline NaCl solutions

Carbonate minerals are ubiquitous in the natural environment and groundwater potentially contacting nuclear waste in a deep geological repository may contain dissolved carbonate as well. As a hard ligand in terms of the HSAB concept, carbonate forms stable complexes with tetravalent actinides and can lead to enhanced An(IV) solubility, *e.g.* as known from comprehensive solubility studies with  $\text{ThO}_2(\text{am,hyd})$  in NaCl-NaOH- $\text{Na}_2\text{CO}_3$  solutions [9-10]. In the present study, performed in the frame of the ENTRIA project, we have investigated the solubility of tetravalent  $\text{NpO}_2(\text{am,hyd})$  and  $\text{PuO}_2(\text{am,hyd})$  in carbonate bearing, dilute to concentrated NaCl-NaOH solutions.

All experiments were conducted inside an inert gas (Ar) glovebox. Batch experiments from undersaturation with  $\text{NpO}_2(\text{am,hyd})$  and  $\text{PuO}_2(\text{am,hyd})$  were performed as function of total carbonate (0.1 and 0.04 mol  $\text{kg}^{-1}$ ) and NaCl concentrations (0.5, 2.1 and 5.6 mol  $\text{kg}^{-1}$ ).  $\text{pH}_m$  ranged from 8 to 12. Reducing conditions were adjusted by additions of hydroqui-

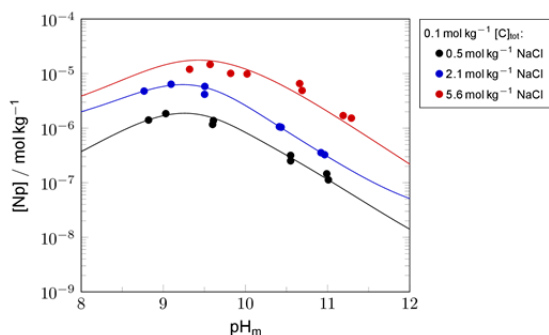


**Fig. 4:** Solubility of  $\text{NpO}_2(\text{am,hyd})$  in  $0.5\text{--}5.6 \text{ mol kg}^{-1}$  NaCl solutions with  $0.1 \text{ mol kg}^{-1}$  total carbonate content.

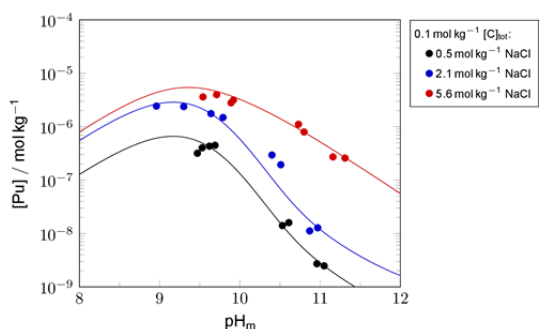


**Fig. 5:** Solubility of  $\text{PuO}_2(\text{am,hyd})$  in  $0.5\text{--}5.6 \text{ mol kg}^{-1}$  NaCl solutions with  $0.1 \text{ mol kg}^{-1}$  total carbonate content.

none (Pu) and Sn(II) (Np). The samples were analyzed for [An] and  $\text{pH}_m$  for up to 210 days.

The experimental solubility of  $\text{NpO}_2(\text{am,hyd})$  and  $\text{PuO}_2(\text{am,hyd})$  in the presence of  $0.1 \text{ mol kg}^{-1}$  carbonate and  $0.5\text{--}5.6 \text{ mol kg}^{-1}$  NaCl is shown in Figures 4 and 5, respectively.

Compared to  $\text{AnO}_2(\text{am,hyd})$  in carbonate-free NaCl solutions, where the pH and ionic strength independent solubility level is at  $\log [\text{An(IV)}] = -9 \pm 1$  (Np) and  $-10.8 \pm 0.7$  (Pu) for  $\text{pH}_m > 6$ , the An(IV) concentration is significantly enhanced for  $[\text{C}_{\text{tot}}] = 0.1 \text{ M}$ , and systematically increases with ionic strength, pointing to the presence of charged An(IV)-OH- $\text{CO}_3$  species.

Under the same solutions conditions, the solubility of  $\text{PuO}_2(\text{am,hyd})$  is lower by approximately 0.5 log-units compared to  $\text{NpO}_2(\text{am,hyd})$ .

The second series with  $[\text{C}_{\text{tot}}] = 0.04 \text{ mol kg}^{-1}$  shows consistently lower solubility than the analogous series with  $0.1 \text{ mol kg}^{-1}$  carbonate.

A preliminary chemical and thermodynamic model was derived (see Figures 4 and 5) based on the specific ion interaction theory (SIT) [2, 11-12]. The results show that a reasonable description of experimental Np(IV) and Pu(IV) data in the  $\text{pH}_m$  range 8 to 11 is possible with only two ternary species,  $\text{An}(\text{OH})(\text{CO}_3)_4^{5-}$  and  $\text{An}(\text{OH})_3(\text{CO}_3)_2^{3-}$ . Additional experiments are in progress to clarify if there is a contribution of a third ternary species at higher  $\text{pH}_m$  values.

The chemical and thermodynamics models derived in the present work provide an improved understand-

ing of the aqueous chemistry of Np(IV) and Pu(IV) in carbonate containing solutions, and help to better assess potential near- and far-field processes of tetravalent actinides in a repository.

### Solubility and redox behavior of Pu under alkaline, reducing conditions

Underground repositories are the internationally favored option for the disposal of long-lived radioactive waste. The development of strongly reducing conditions is expected in the post-closure period of these facilities due to the anoxic corrosion of steel. In the case of low- and intermediate-level radioactive waste, the preferred concept involves the use of cementitious materials for the stabilization of the waste and for construction purposes. The interaction of this material with groundwater buffers the pH in the alkaline to hyperalkaline range ( $10 \leq \text{pH} \leq 13.3$ ) over a very long time-scale. In the context of the safety assessment of nuclear waste disposal, plutonium is an element of highest relevance due to its abundance in the waste, high radiotoxicity, long half-life ( $t_{1/2}^{239}\text{Pu} = 2.41 \cdot 10^4 \text{ a}$ ) and challenging aqueous chemistry. Pu(III) and Pu(IV) are the most likely oxidation states under the reducing conditions predicted in underground repositories [13]. Relevant limitations and uncertainties affect the NEA-TDB thermodynamic selection for Pu(III) and Pu(IV) aqueous species and solid compounds [2]. This leads to a rather ill-defined Pu(IV) / Pu(III) redox border, which affects the correct assessment of the chemical behavior of Pu under these conditions. This study aims at investigating the solubility and redox behavior of Pu under alkaline reducing conditions as a first step towards the quantification of the impact of isosaccharinic acid on Pu solubility under conditions relevant for SFR, the Swedish repository for low- and intermediate-level waste.

All experiments were conducted at  $T = 22 \pm 2 \text{ }^\circ\text{C}$  in Ar gloveboxes. Undersaturation solubility experiments were performed using a well-characterized, aged  $^{242}\text{PuO}_2(\text{am,hyd})$  solid phase. Redox conditions were either buffered with 2 mM hydroquinone ( $\text{pe} + \text{pH}_m = 9.5 \pm 1$ ) or  $\text{SnCl}_2$  ( $\text{pe} + \text{pH}_m = 2 \pm 1$ ).  $\text{pH}_m$  was varied from 8 to 12.9 ( $I = 0.1 \text{ M NaCl-NaOH}$ ). The total concentration of Pu ( $[\text{Pu}]_{\text{tot}}$ ) was determined after ultracentrifugation by sector field (SF-)ICP-MS. A liquid-liquid extraction (L-L ext.) method [13] combined with LSC and capillary electrophoresis (CE) coupled to SF-ICP-MS, respectively, were used for the analysis of Pu-redox speciation in the aqueous phase. Pu solid phases were characterized by XRD, XPS, and synchrotron radiation in-situ XRD and XANES/EXAFS.

The redox state and nanocrystalline character of the initial  $\text{Pu(IV)O}_2(\text{am,hyd})$  solid phase was confirmed by XANES, XRD and XPS. The solubility product of this solid phase was experimentally determined using L-L extraction for the quantification of  $[\text{Pu(IV)}]_{\text{aq}}$  in weakly acidic conditions (Figure 6), where Pu(V) prevailed in the aqueous phase. The aqueous specia-

tion was further confirmed by CE-SF-ICP-MS. The solubility product determined in this work is in excellent agreement with  $\log_{10} *K_{s,0}$  currently selected in the NEA-TDB for  $\text{PuO}_2(\text{am,hyd})$  [2]. The solubility of Pu in hydroquinone-buffered systems at  $8 \leq \text{pH}_m \leq 12.9$ , is very low ( $\leq 10^{-10}$  m) and pH-independent (Figure 6), consistently with a solubility control by the equilibrium reaction  $\text{PuO}_2(\text{am,hyd}) + 2\text{H}_2\text{O} \Leftrightarrow \text{Pu}(\text{OH})_4(\text{aq})$ . Similar results are also obtained in Sn(II)-buffered systems. Considering the uncertainty associated with the corresponding thermodynamic calculations ( $\pm 1.5 \log_{10}$ -units for  $\log_{10} *K_{s,0}\{\text{Pu}(\text{OH})_3(\text{s})\}$ ), the latter results could be consistent both with a solubility control by  $\text{Pu}(\text{III})(\text{s}) \Leftrightarrow \text{Pu}(\text{III})(\text{aq})$  and with the reductive dissolution of  $\text{PuO}_2(\text{am,hyd}) \Leftrightarrow \text{Pu}(\text{III})(\text{aq})$  at  $\text{pe} + \text{pH}_m = 2$ .

Relevant differences are seen in the XANES spectra of Pu in hydroquinone and Sn(II) systems (Figure 7). The original  $\text{PuO}_2(\text{am,hyd})$  material remains the same in hydroquinone systems with  $\text{pH}_m = 9$  and 12, whereas a relevant fraction of Pu(III) ( $30 \pm 5\%$ ) is determined in Pu solids from Sn(II) buffered systems. Additional XANES measurements are planned at longer equilibration times (1–2 years) to assess whether the co-existence of Pu(III) and Pu(IV) solid phases under very reducing conditions corresponds to the thermodynamic equilibrium or rather to a transient state.

### First report on the structure of Pa(IV) in aqueous solution and the evidence of a curium break in the series of An(IV) aqua ions

The tetravalent actinide ions from Th(IV) to Pu(IV) are hard Lewis acids with high charge densities and thus they show a strong tendency to hydrolysis and condensation [16]. However, unlike its neighbor

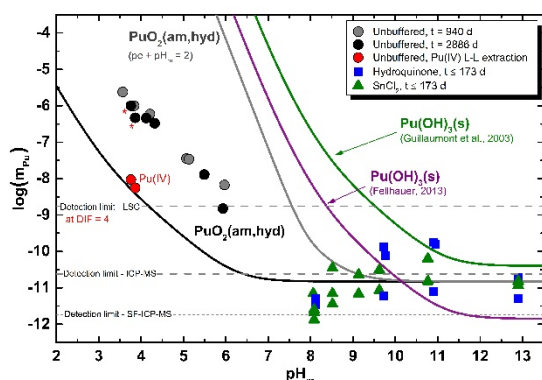


**Fig. 6:** Plutonium concentration in solution in equilibrium with  $\text{PuO}_2(\text{am,hyd})$  for unbuffered (○: 940 days, ●: 2886 days) and redox buffered systems (■: hydroquinone; ▲:  $\text{SnCl}_2$ ). Red points (●) show the concentration of Pu(IV) for selected unbuffered systems (\*) as quantified by L-L extraction. Solid lines correspond to the thermodynamically calculated solubility of  $\text{PuO}_2(\text{am,hyd})$  in equilibrium with  $\text{Pu}(\text{IV})_{\text{aq}}$  (black line) and for  $\text{pe} + \text{pH}_m = 2$  (grey line, predominance of  $\text{Pu}(\text{III})_{\text{aq}}$  below  $\text{pH}_m \approx 9$ ). Green and purple lines show the solubility of  $\text{Pu}(\text{OH})_3(\text{s})$  as calculated with  $\log_{10} *K_{s,0}$  values reported in Guillaumont et al., (2003) [2] and Fellhauer (2013) [14], respectively.

actinides the aqueous chemistry of Pa(IV) is rather unexplored [17]. This is partly due to the limited availability of the element and its radioactive nature, in addition to the instability of its tetravalent oxidation state: Pa(IV) is difficult to stabilize in water due to the low redox potential of the Pa(V)/Pa(IV) couple (-0.1 V/SHE) and the fact that it rapidly oxidizes to Pa(V) [17-18], while U(IV), Np(IV), and Pu(IV) are more stable. Up to recently [19], there were no experimental or theoretical studies published on the structure of  $\text{Pa}^{4+}$  in aqueous solution, while there are a number of EXAFS studies on the structures of the  $\text{Th}^{4+}$ ,  $\text{U}^{4+}$ ,  $\text{Np}^{4+}$ ,  $\text{Pu}^{4+}$ , and  $\text{Bk}^{4+}$  aqua ions [17, 20]. The coordination numbers of these ions are between eight and thirteen, showing large uncertainties in their determination. On the other hand, the An-O bond distances are obtained with higher precision and are therefore a better measure of the coordination number. This was discussed in our recent communication, where we also provided the first EXAFS data on Pa(IV) in aqueous solution and a method using Rongalite that enabled stabilization of Pa(IV) in aqueous solution over several days [19]. A summary of the Pa(IV) EXAFS results and a discussion about the hydration structure of the tetravalent actinide aqua ions from  $\text{Th}^{4+}$  to  $\text{Bk}^{4+}$  are given here.

Pa  $L_3$ -edge XAS spectra of a 0.3 mM Pa(IV) in 6 M HCl were collected at the INE beamline at ANKA. The mean Pa-O distance of the  $[\text{Pa}(\text{H}_2\text{O})_8\text{Cl}]^{3+}$  ion was determined to be  $2.43 \pm 0.02$  Å. This distance was considered to be virtually identical to the mean Pa-O distance of the  $[\text{Pa}(\text{H}_2\text{O})_9]^{4+}$  ion [19]. Fig. 1 plots the mean An-O bond distances of tetravalent actinide aqua ions versus their ionic radii [21]. A linear relationship with a slope of one (0.95) is apparent for the ions from  $\text{Th}^{4+}$  to  $\text{Pu}^{4+}$  while the mean Bk-O distance is below this line. No data exist for  $\text{Am}^{4+}$  and  $\text{Cm}^{4+}$ , which are unstable in aqueous solution without complexing anions. Be-

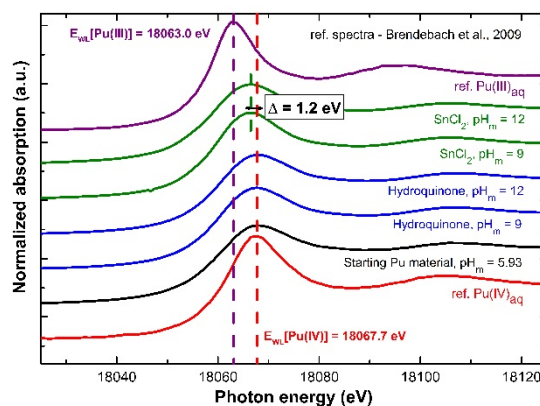


**Fig. 7:** Pu  $L_{III}$ -edge XANES spectra of solid phases recovered from hydroquinone and  $\text{SnCl}_2$  systems at  $\text{pH}_m = 9$  and 12. The spectra of the starting material used in this study and the given references for the aqueous species of Pu(III) (top) and Pu(IV) (bottom) reported in Brendebach et al., 2009 [15] are shown for comparison.

cause the An-O bond distance for the ions up to Pu<sup>4+</sup> follow closely this line and therefore the actinide contraction, we assume that there is no major change in these ions' hydration number, while a decrease in the hydration number, probably from nine to eight, is apparent to occur between Pu<sup>4+</sup> and Bk<sup>4+</sup>. Indeed, with supporting quantum chemical calculations we could show that there is a transition in the hydration number from nine to eight occurring near Cm<sup>4+</sup> [19]. Such a change has been much debated for the trivalent actinide (and lanthanide) ions, where the ions' hydration number has been reported to either change from nine to eight in the middle of the series or to remain nine across the series up to Cf<sup>3+</sup> [22]. Further evidence that the regression line in Figure 8 represents primarily nine-coordinated aqua ions comes from the fact that the mean Th-O bond distance of the Th<sup>4+</sup> aqua ion is ~ 0.05 Å shorter than the ten-coordinate [Th(H<sub>2</sub>O)<sub>10</sub>]Br<sub>4</sub> hydrate [23], indicating a nonahydrated ion or mixtures of nona- and decahydrated ions in aqueous solution.

In conclusion, aqueous Pa(IV) can be stabilized over a period of several days with rongalite. EXAFS data and supporting quantum chemical calculations (see ref. 19) showed that the An-O bonds of the Th<sup>4+</sup>-Bk<sup>4+</sup> aqua ions following the same monotonic decreasing trend as the An<sup>4+</sup> ionic radii and a decrease of the hydration number from nine to eight for the heaviest ions Cm<sup>4+</sup> and Bk<sup>4+</sup>. This is the first sound evidence of a "curium break" in the tetravalent actinide series.

### Complexation of Cm(III) with succinate

The complexation of the actinides with small and macromolecular (e.g. fulvic and humic acids) natural organic matter in natural waters is a relevant geochemical process with respect to the migration behavior of the actinides in a potential host rock formation for high-level nuclear waste. Up to now, the complexation behavior with various model compounds (e.g. salicylate, phthalate, succinate, etc.) has been investigated mainly at room-temperature to understand the interaction mechanisms with more complicated natural organics. For an improved un-

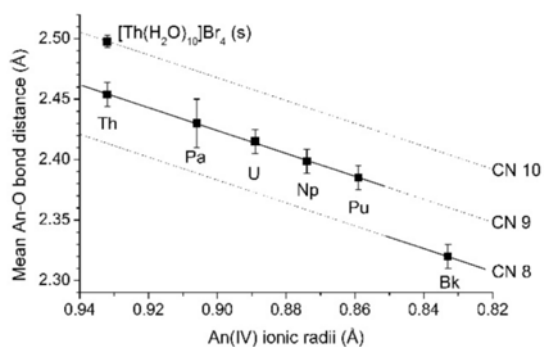


**Fig. 8:** Mean An-O bond distance vs. An(IV) ionic radii [6] for 8 and 9-coordinated An<sup>4+</sup> aqua ions from EXAFS data from ref. 19 and from earlier EXAFS studies. Note that for Pa<sup>4+</sup> the stoichiometry is that of Pa(H<sub>2</sub>O)<sub>8</sub>Cl<sup>3+</sup>. XRD data of [Th(H<sub>2</sub>O)<sub>10</sub>]Br<sub>4</sub>(s) is also shown [23].

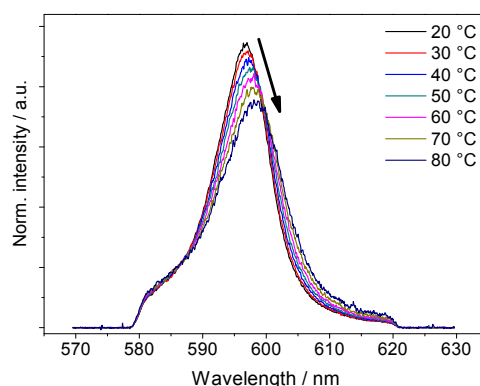


**Fig. 9:** Emission spectra of Cm(III) ( $5 \times 10^{-9}$  mol/kg) in the presence of  $10^{-2}$  mol/kg succinate in 0.5 mol/kg NaCl solution at varying temperature (20 - 80 °C).

derstanding of fundamental actinide-organics interaction processes over the extended temperature range potentially relevant in the context of HLW disposal, a reliable knowledge of the dominant species and their related thermodynamic properties is necessary.

In the present work, the complexation of Cm(III) with succinate has been investigated in the temperature range of 20 – 80 °C in order to determine the thermodynamic stability constants ( $\log K_n^0(T)$ ) for the formation of different Cm(III) succinate species.

As an example, Figure 9 shows the evolution of the fluorescence spectrum of Cm(III) in the presence of 0.01 mol/kg succinate with increasing temperature. The emission band is visibly shifted towards higher wavelength with increasing temperature. This is attributed to the successive shift of Cm(III) speciation towards complexed species. Several experimental series as a function of ionic strength, temperature, and ligand concentration were carried out and evaluated using the specific ion interaction theory (SIT) as performed for comparable ligand systems [24-27]. For the formation of [CmSuc<sub>n</sub>]<sup>3-2n</sup> ( $n = 1, 2$ ), the  $\log K_n^0(T)$  values were obtained in the entire temperature range.  $\log K_3^0(T)$  was determined for  $T = 50 - 80$  °C. All determined stability constants are shown in Figure 10.

Whereas  $\log K_1^0(T)$  is almost constant in the whole temperature range,  $\log K_2^0(T)$  increases with increasing temperature.  $K_1^0(T)$  and  $K_2^0(T)$  are higher by about 2 and 0.5-1.0 orders of magnitude, respectively, compared to monocarboxylic ligands [24-25]. The difference is attributed to a different interaction mechanism with succinate which is assumed to coordinate through both the carboxylic and  $\alpha$ -hydroxy function forming a chelate complex.

However, to fully comprehend the interaction mechanism further studies (e.g. EXAFS spectroscopic investigations) are required to resolve the molecular structure of the formed complex.

### References

- [1] Fujiwara, K., et al., *Radiochim. Acta*, **9**, 347-350, (2004).

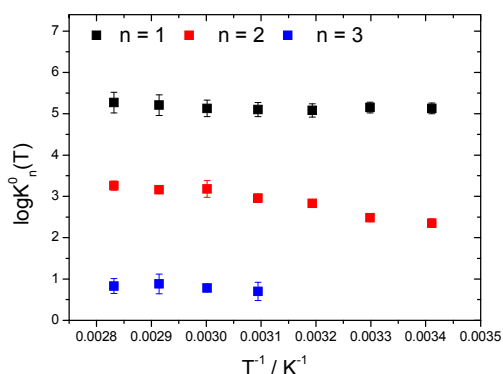


**Fig. 10:** Thermodynamic stability constants for the formation of  $[CmSuc_n]^{3-2n}$  ( $n = 1-3$ ) as a function of the reciprocal temperature.

- [3] Guillaumont, G., et al., *Chemical Thermodynamics Vol. 5*, Elsevier, Amsterdam, (2003).
- [4] Neck, V., et al., *Radiochim. Acta*, **89**, 1-16, (2001).
- [5] Altmaier, M., et al., Migration Conference, Gyeongju (Korea), (2003).
- [6] Petrov, V., et al., Migration Conference, Beijing, (China), (2011).
- [7] Fellhauer, D., et al., *Radiochim. Acta* (DOI 10.1515/ract-2015-2489), (2016).
- [8] Runde, W., et al., *Geochim. Cosmochim. Acta*, **60**, 2065–2073, (1996).
- [9] Neck, V., et al., *Radiochim. Acta*, **69**, 39–47, (1996).
- [10] Altmaier, M., et al., *Radiochim. Acta*, **93**, 83–92, (2005).
- [11] Altmaier, M., et al., *Radiochim. Acta*, **94**, 495–500, (2006).
- [12] Ciavatta, L., *Ann. Chim. (Rome)*, **70**, 551–567, (1980).
- [13] Lemire, R. J., et al, *Chemical Thermodynamics Vol. 4*, Elsevier, Amsterdam, (2001).
- [14] Neck, V., et al., *C. R. Chimie*, **10**, 959–977, (2007).
- [15] Fellhauer, D., PhD thesis, University of Heidelberg, (2013).
- [16] Brendebach, B., et al., *Radiochim. Acta*, **97**, 701–708, (2009).
- [17] a) Knope, K. E. et al. *Chem. Rev.*, **113**, 944 (2013); b) Walther, C. et al. *Chem. Rev.*, **113**, 995, (2013).
- [18] a) R. Wilson, *Nature Chem.*, **4**, 586 (2012); b) Marquardt, C. M. et al. *Radiochim. Acta*, **92**, 445 (2004); c) Mitsuji et al. T. *Bull. Chem. Soc. Jpn.*, **40**, 2091 (1967); d) Bagnall, K. W. et al. *Chem. Soc. A*, 275 (1967); e) Keller, C. *Angew. Chem. Int. Ed.*, **5**, 23 (1966); f) Brown, D. et al. *J. Chem. Soc.* 3804 (1961); g) Haïssinsky, M. et al. *Compt. Rend. Acad. Sci. Paris*, **226**, 573 (1948); h) Fried, S. et al. *J. Am. Chem. Soc.*, **76**, 4863 (1954).
- [19] R. Guillaumont, G. Ionova, J. C. Krupa, F. David, *Radiochim. Acta*, **75**, 97, (1996).
- [20] Banik, N. et al. *Dalton Trans.* **45**, 453 (2016)
- [21] a) Wilson, R. E. et al. *Angew. Chem., Int. Ed.*, **46**, 8043 (2007); b) Neck, V. et al. *Radiochim. Acta*, **90**, 485 (2002); c) Moll, H. Et al. *Inorg. Chem.* **38**, 1795 (1999); d) Torapava, N. et al. *Chem.*, **48**, 11712 (2009), e) Antonio, M.R. et al. *Radiochim. Acta.*, **90**, 851 (2002).
- [22] Choppin, G. R. et al. in *Handbook on the Physics and Chemistry of Rare Earths. Vol. 18: Lanthanides/Actinides: Chemistry*; Elsevier Science: Amsterdam, The Netherlands, 1994; Vol. 18, Ch. 128: pp 529.
- [23] a) Galbis, E. et al. *J. Chem. Phys.*, **140**, 214104 (2014); b) Galbis, E. et al. *Angew. Chem. Int. Ed.*, **49**, 3811 (2010); c) Lindqvist-Reis, P. et al. *J. Phys. Chem. B*, **109**, 3077 (2005); d) Lindqvist-Reis, P. et al. *Angew. Chem. Int. Ed.* **46**, 919 (2007); e) Apostolidis, C. et al. *Angew. Chem. Int. Ed.* **49**, 6343; 2010; f) D'Angelo, P. et al. *Inorg. Chem.*, **52**, 10318 (2013); g) D'Angelo, P. et al. *Chem. Eur. J.*, **18**, 11162 (2012).
- [24] Wilson, R. E. et al. *Angew. Chem., Int. Ed.*, **46**, 8043 (2007).
- [25] Skerencak, A. et al., *J. Solution Chem.*, **42**, 1-17, (2013).
- [26] Fröhlich, D.R. et al., *Dalton Trans.*, **43**, 3958-3965, (2014).
- [27] Fröhlich, D.R. et al., *Appl. Geochem.*, **61**, 1469-1474, (2015).
- [28] Skerencak-Frech, A. et al., *Inorg. Chem.*, **54**, 1860-1868, (2015).

## 4.2 Sorption on mineral surfaces

*N. L. Banik, K. Bender, A. Diascorn, H. Geckeis, J. Lützenkirchen, C. Marquardt, R. Marsac, T. Rabung, T. Schäfer, D. Schild, A. Schnurr*

### Introduction

Retention processes of radionuclides on mineral surfaces are key parameters in performance safety calculations for nuclear waste repositories. For a thorough estimation and quantification of these reactions a detailed mechanistic understanding is essential. This includes a profound knowledge of the mineral-water interfaces including a reliable thermodynamic description. Radionuclide sorption on different relevant solid phases needs to be studied by a large variation of experimental conditions as metal ion concentration, pH, composition of the electrolyte solution and competition with other sorbing radionuclides or other complexing aqueous ligands. The experimental studies take credit from a variety of very sensitive spectroscopic speciation techniques and subsequent description by using thermodynamic based surface complexation models and, therefore, provide substantial information to be used in performance assessment.

In the first part of the present annual report we want to focus on the work regarding to An/Ln retention onto clay minerals which are important as backfill and potential host rock materials in several repository concepts.

In the second part of the report the size-effect on the charge of small spherical particles is described as well as the slip-plane distance in zeta-potential simulation.

### Sorption and redox speciation of plutonium at the illite surface

Due to its high radiotoxicity and the very long half-lives of some isotopes, plutonium (Pu) is an important element in the context of nuclear waste disposal. Under environmentally relevant conditions, Pu can occur in the oxidation states +III, +IV, +V and +VI. As the geochemical behavior of Pu, such as solubility and mobility, strongly depends on its redox state [1,2] thermodynamic speciation calculations need to account for Pu redox speciation.

Several studies have shown that actinide redox chemistry is affected by interaction with mineral surfaces. The evaluation of Pu sorption data is particularly challenging as frequently a mixture of Pu redox states is found in solid/liquid systems (i.e. at the surface and/or in solution). In the presence of a mineral, rates for abiotic redox reactions range from a few hours to a few months and depend on the mineral type, pH, Pu concentration and initial Pu redox state, which further complicates data interpretation [3-6]. Generally, under ambient (air) atmosphere, when adding Pu(IV), Pu(V) or Pu(VI) to a mineral suspension (hematite, goethite, magnetite [5], quartz [6], montmorillonite, [3,4] kaolinite [7]) Pu(IV) is found at the mineral surface whereas very often Pu(V) prevails in

solution. Similar observations were made for neptunium (Np) and illite under slightly reducing conditions [8]. Pu sorption to minerals under reducing conditions, where Pu(III) should prevail, has been probed less frequently.

The present study is dedicated to Pu sorption and redox behavior to a purified clay mineral ("CatClay"-illite) under inert (Argon) atmosphere (< 1 ppm O<sub>2</sub>, absence of CO<sub>2</sub>). Classical batch experiments are performed in 0.1 M NaCl, 2 g/L of illite, at various pH (3-10), total Pu concentrations ( $[^{238}\text{Pu}]_{\text{tot}}=8\times 10^{-11}$  to  $3\times 10^{-8}$  M) and reaction times (1 week to 1 year). The <sup>238</sup>Pu stock solution contained 85% Pu(IV), 11% Pu(V) and 4% Pu(III). The pH/Eh measurements are monitored. Liquid-liquid extraction is applied to determine the Pu redox state at the illite surface. Finally, Pu sorption and redox speciation are described using surface complexation modelling. Thermodynamic constants from the NEA [9] are taken throughout this study using the specific ion interaction theory (SIT) [10]. PHREEQC [11] and PhreePlot [12] are applied for speciation calculations (including sorption) and constructing Pourbaix (pH-pe) diagrams, respectively.

The pH-pe data recorded after 1 week and 1-year equilibration time in the Pu-illite suspension in 0.1 M NaCl solution are plotted in Fig.1 together with the calculated predominance pH-pe diagram for dissolved Pu. The solid lines correspond to equal amounts of two Pu redox states. Large symbols indicate the samples where the supernatant was additionally analyzed by liquid-extraction ( $[\text{Pu}]_{\text{tot}} = 10^{-8}$  M). Data are compared to those reported for the Np-illite system [8] at similar metal ion concentration ( $3\times 10^{-8}$  M) and after contact times between 7 and 63 days. Between 1 week and 1 year, pH may slightly evolve due to further buffering of illite, since no additional pH-buffer was used. An increase in pe values is also observed for the batch series prepared to study the effect of pH ( $[\text{Pu}]_{\text{tot}}=8\times 10^{-11}$  M), which is potentially due to the presence of undetectable traces of O<sub>2</sub>(g) (i.e. < 1 ppm) during sample handling or storage over the one-year period. Significant amounts of Pu(III) are expected in the aqueous phase below pH  $\approx$  5 whereas Pu(IV) should prevail above pH  $\approx$  6 according to the calculations and taking pe data uncertainties into account. However, in sorption experiments ( $[\text{Pu}]_{\text{tot}} = 10^{-8}$  M) performed over a period of 1 week, we found at pH = 4.3 about 90% of the Pu in the supernatant aqueous phase being pentavalent. In analogy to the observed behavior of Np(V), the Pu(V) sorption to illite at pH = 4.3 is considered negligible and remains in solution. Pu(IV), like other tetravalent actinide ions, is expected to be almost completely sorbed.

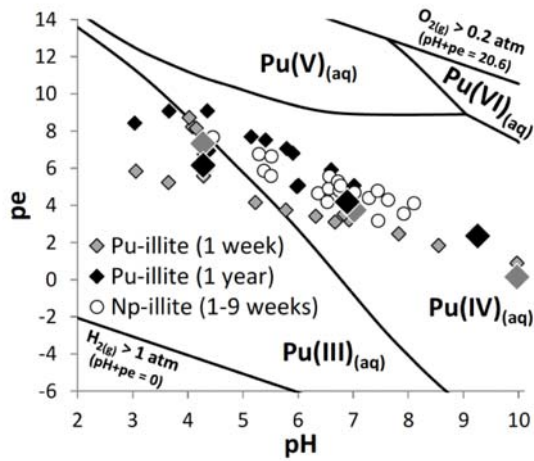


**Fig. 1:** pH-pe values measured in illite suspensions under anaerobic conditions. 1 week (gray diamonds) and 1-year equilibration time (black diamonds); Np-illite system [8]: white circles.

However, this has no impact on our conclusions, which are based on the finally established pe and pH values. Batch series conducted at  $\text{pH} \approx 4, 7$  and  $10$  ( $8 \times 10^{-11} < [\text{Pu}]_{\text{tot}} < 10^{-8}$  M) exhibit quite stable pe values with time, which suggests no significant  $\text{O}_2(\text{g})$  contamination or microbial activity over the one-year period.

As previously found for Np(V) interaction with illite and Pu sorption to kaolinite and hematite, the redox speciation of actinides is influenced by the formation of surface complexes. The following equation provides a simple approach to determine the stability field of Pu(IV) and Pu(III) at a mineral surface:

$$\begin{aligned} \{Pu(IV)/Pu(III)\}_{\text{surf}} &= \{Pu(IV)/Pu(III)\}_{\text{aq}} \\ &+ (\log R_d(Pu(III))) \\ &- \log R_d(Pu(IV)) \end{aligned}$$

$\{Pu(IV)/Pu(III)\}_{\text{aq}}$  can be calculated by the Nernst equation and the redox borderline in aqueous solution (Fig. 1 and 2a) denotes an equimolar Pu(III)/Pu(IV) ratio.  $\{Pu(IV)/Pu(III)\}_{\text{surf}}$  refers to the corresponding redox speciation at the illite surface.  $\log R_d(Pu(III))$  and  $\log R_d(Pu(IV))$  values in above eq. represent the respective individual uptake of the two Pu redox states under the same physico-chemical conditions and are expressed as distribution coefficients (denoted as Rd). As Rd values for Pu(III) and Pu(IV) are difficult to determine separately, we took in a first approach existing models for Eu(III) and Np(IV) to estimate sorption of Pu(III) and Pu(IV), respectively.

The resulting Pu(IV)/Pu(III) borderline is shown in Fig. 2a as a dashed bold red line. pH-edges for Eu(III) and Np(IV) sorption onto illite in 0.1 M NaCl calculated with the 2 SPNE SC/CE model are shown in Fig. 2b. For  $\text{pH} < 7$ , Eu(III) sorption to illite is weaker than

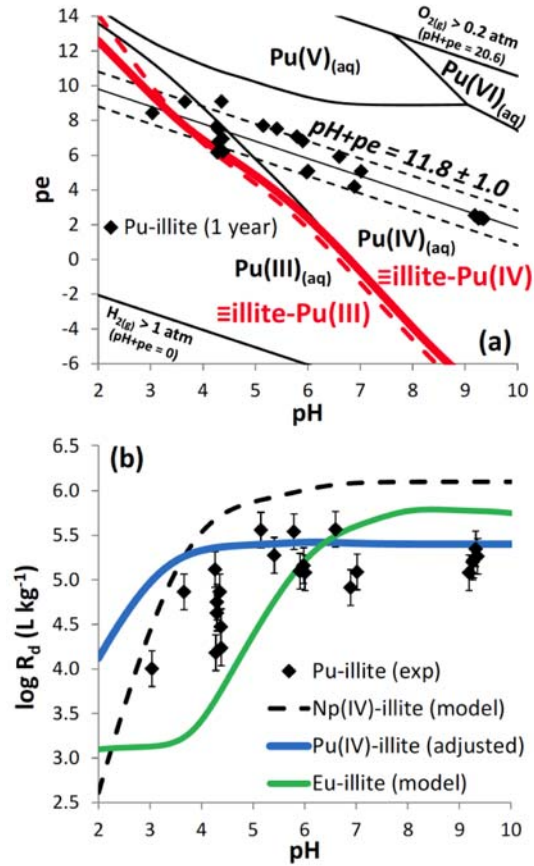


**Fig. 2:** ((a) Predominance pH-pe diagram for Pu in 0.1 M NaCl with pH-pe values measured in illite suspensions after 1-year equilibration time. The bold and dashed red lines show estimated borderlines for Pu(IV)/Pu(III) redox transition at the illite surface. Relevant redox conditions for this study ( $\text{pH} + \text{pe} = 11.8 \pm 1.0$ ) are shown as straight (solid and dashed) lines. (b) Data for Pu uptake onto illite ( $R_d$  in  $\text{L kg}^{-1}$ ) as a function of pH compared with model calculations for Eu(III) (green bold line), Np(IV) (dashed black line) and Pu(IV) (blue bold line) sorption based on the 2 SPNE SC/CE model.

that of Np(IV). At this low pH outer-sphere sorption (ion exchange) dominates for Eu(III).

Due to the higher thermodynamic stability of actinide(IV) surface complexes in this area, the predominance field of Pu(IV) is enlarged at the illite surface and overlaps with the stability field of Pu(III) in the aqueous phase. For  $\text{pH} > 7$ , Eu(III) and Np(IV) uptake are almost equal. As a consequence, the Pu(IV)/Pu(III) borderline at the illite surface coincides with that in solution ( $\{Pu(IV)/Pu(III)\}_{\text{surf}} \approx \{Pu(IV)/Pu(III)\}_{\text{aq}}$ ). The pH-pe values measured after 1 year in the Pu-illite suspensions are also plotted in Fig. 2a. According to these estimations, Pu(IV) is expected to prevail (or, at least, to be present in significant amounts) at the illite surface in all samples. For  $\text{pH} > 6$ , Pu(III) becomes negligible and Pu speciation in solution and at the illite surface is controlled by Pu(IV). For  $\text{pH} < 5$ , the overall Pu uptake by illite is predicted to lie between that of Eu(III) and Np(IV), which is indeed the case according to experimental data (Fig. 2b).

Using the 2 SPNE SC/CE model with the surface complexation constants [8] and taking into account the

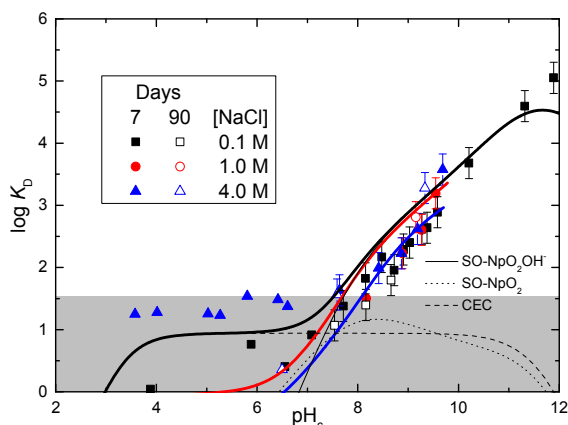


**Fig. 3:** *Np(V) sorption data ( $3.2E-6$  M) onto Na-IFM (2 g/L) in dependence on NaCl background electrolyte concentration after 2 different contact times. Modelling was done using the “SPNE SC/CE” model. The species distribution is shown for 0.1 M NaCl exemplarily. The grey area visualizes the range of the detection limit (very low sorption).*

range of measured redox conditions ( $pH + pe = 11.8 \pm 1.0$ ; Fig. 2a) allows for an excellent simulation of experimental Pu sorption data over the whole pH-range investigated. Decreasing Rd values at  $pH < 5$  are nicely reproduced as a consequence of progressing reduction of Pu(IV) to Pu(III) with decreasing pH. Variations in log Rd for  $pH = 4.3$  are assigned to the effect of pe rather than to a concentration effect. For  $6 < pe < 8.5$ , Pu(III) prevails in solution whereas Pu(IV) prevails at the illite surface. This explains why log Rd values lie between that of Pu(III) and Pu(IV), when they occur as single components.

A more accurate simulation of redox sensitive element behavior in near surface soil systems and deep geological formations becomes possible by implementing measured pe values of a given system into geochemical surface speciation calculations. Therefore, this study may allow a more accurate estimation of the Pu mobility in the geosphere.

### Experiment and modelling of U(VI) and Np(V) sorption onto synthetic montmorillonite, illite and kaolinite in saline solutions.

The present work is a continuation of earlier sorption investigations of trivalent europium (Eu) onto montmorillonite (SWy-2) and illite (Illite du Puy) under saline conditions (NaCl, CaCl<sub>2</sub>, MgCl<sub>2</sub>) [13, 14]. Such high ionic strength conditions are expected in the vicinity of salt deposits as e.g. in the Jurassic and lower Cretaceous clay rock in Northern Germany [15].

Batch sorption studies for Np(V) were carried out in pure NaCl solutions up to 4.0 M at  $1.6 E-8 - 3.2 E-6$  M Np(V), at a constant solid to liquid ratio (S:L = 2 g/L) of synthetic iron free montmorillonite (IFM) over a wide pH range (3-12) and excluding carbon dioxide. IFM was used to exclude potential surface reduction of Np(V) to Np(IV).

U(VI) sorption onto kaolinite was studied in pure NaCl solutions (0.1 – 4 M) at  $4 \cdot E-7$  M U(VI) and 2 g/L kaolinite (KGA-1, Georgia, USA).

For the U(VI) sorption study on Illite du Puy the identical U(VI) concentration and solid content were used. Background electrolyte concentrations were varied between 0.1 and 4 NaCl as well as between 0.06 and 2 M MgCl<sub>2</sub> and CaCl<sub>2</sub>.

The 2 site protolysis non-electrostatic surface complexation and cation exchange (2SPNE SC/CE) model [16] calibrated for “low” ionic strengths ( $[NaClO_4] = 0.1$  M), was applied to the data obtained in the saline systems.

In the Np(V)-IFM system there is no significant outer sphere sorption via cation exchange and only inner sphere sorption occurs. The sorption edge starts at  $pH_c > 8$ . Very high surface retention (> 90%) is observed at  $pH_c > 10$  and no Np(V) reduction is detected for the given experimental conditions (Fig. 3). The varying background salinities generally do not exhibit a quantitative effect on Np(V) retention. By using the 2SPNE SC/CE model the Np(V) retention data can be described accurately.

U(VI) sorption onto both kaolinite and illite in pure NaCl solution shows very comparable results up to  $pH_c 7$  (Fig. 4). No or very minor cation exchange reactions are observed only at low ionic strengths. In both cases pH edges start at  $\sim pH_c = 4$  and reach quasi quantitative retention (> 95%) with  $K_D \geq 5$  at  $pH_c > 7$ . At  $pH_c > 10$  U(VI) sorption decreases as consequence of the formation of negatively charged aqueous hydrolyzed species with a lower tendency to be bound to clay surfaces. As already observed for Np(V) also the U(VI) sorption onto the two different substrates is not significantly affected by a large variation of the background electrolyte concentration. For an adequate model description up to high pH values an additional inner-sphere sorption species with the stoichiometry  $SO-UO_2Cl(OH)_2^{2-}$  has to be introduced in the illite system. Although there is no clear spectroscopic indication for this surface sorbed species (Fig. 4) a chlorine containing U(VI) hydroxide solid phase and mixed U(VI) Cl-OH and Cl-CO<sub>3</sub> aqueous species are already described [14].



may affect uptake of solutes. In the previously published calculations on the effect of particles size Stern layers have been considered (see e.g. Abbas et al. [20]), but these authors were not involving ion-pairs. Their calculations showed a substantial effect of the size on the surface charge density, with smaller particles exhibiting higher charge densities. This agrees with independent calculations by the present author [21]. In other applications, the size effect on electrostatic terms is discussed and then discarded [22]. The implementation however, is based on the early work by Ohshima [17] and does not include the treatment of the Stern layer or a correction of the surface area that is relevant for the diffuse layer and in a three plane model also for the layer between the surface (0-plane) and the d-plane. In later work by the same authors, the effects are no longer mentioned [23], which is probably justified because of the platy morphology of the particles they deal with. Interestingly their experimental data show that the surface charge density decreases with the particle size [22]. In more recent work by others again the Stern layer has been omitted [24] but the calculation show the trend obtained by Abbas et al. [20]. The only relevant work, where all important aspects may have been considered is that by Hiemstra & van Riemsdijk [25]. However, it is not entirely clear how the charge balance was handled. The usual treatment involves surface charge density, which is inaccurate in the case of a spherical double layer as described by Ohshima [19].

Overall, both the theoretical treatment and the experimental data are inconclusive as to the existence and importance of a particle size effect. To shed some light on the issue, the present framework presents a simple and convenient way to calculate charging and uptake properties for spherical particles. The numerical procedure is fast and precise and numerically stable down to 1 nm sizes (radii).

Ohshima has provided a theoretical framework for including spherical geometry into site-binding models beyond pure diffuse layer electrostatics [19]. Here, his general treatment for a triple layer model is adopted to a Basic Stern model. A spherical polar coordinate is taken with its origin (O) at the center of a spherical particle of radius  $a$  (Fig. 7).

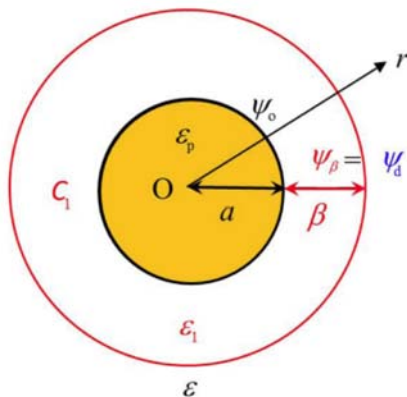


**Fig. 7:** Sketch of a spherical particle and the related geometrical variables and interfacial potentials.

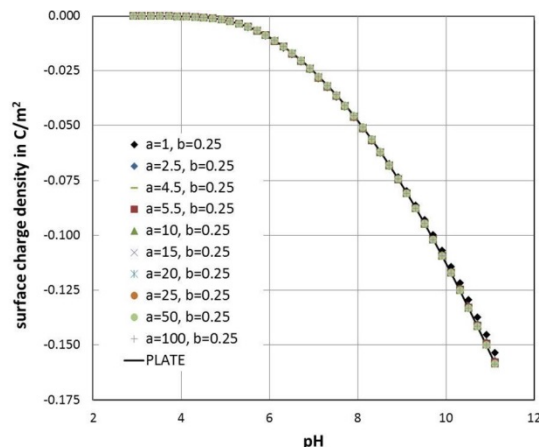


**Fig. 8:** Surface charge density for silica-like spherical particles as calculated by a Basic Stern model in 100 mM NaCl. The symbols  $a$  and  $b$  denote, respectively, the particle radius (ranging from 100 nm down to 1 nm) and the thickness of the Stern layer (constant at 0.25 nm). The drawn line is for the charging curve for the equivalent plate.

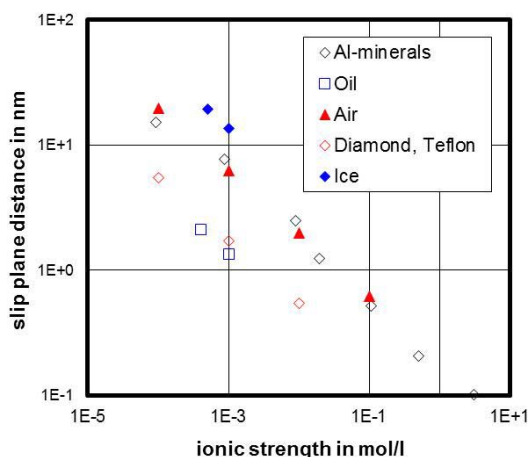
Implementation of the model according to Ohshima [19] and including the second order surface potential surface charge relationship for the diffuse layer into a general speciation code has been performed for the diffuse layer and the Basic Stern models.

Figure 8 shows that unlike for the pure diffuse layer model, there is no significant effect of size on the proton-surface charge down to very low particle sizes. All calculated curves down to 2.5 nm (radius) particles show the behaviour of the plate geometry in 100 mM salt, while Abbas et al. [20] obtain differences between plate and sphere at 10 nm (diameter) in 10 mM. Results with the present model in 10 mM do not show significant differences to the results shown on Figure 8.

The results suggest that compared to a model without an explicit Stern plane the size effect is more or less attenuated by the presence of the Stern plane and the association of counter-ions in the  $\beta$ -plane (Figure 7). While this conclusion agrees with that of Hiemstra & van Riemsdijk [25], it is not clear whether the treatment in the latter case was fully comprehensive. The code used for the present calculations will be extended to a three-plane-model and used for more extensive parameter studies including the variation of the Stern-layer thickness. To what extent the results in Figure 8 can be generalized is not clear, since the model calculations depend on the parameters used (thickness of the Stern layer) or on the ionic strength of the system. Also, experimental data show somewhat contradictory results.

### The slip-plane distance in zeta-potential simulation

Previous attempts to model the zeta-potential of particle surfaces and flat single crystals have typically involved a slip plane distance that is situated somewhere in the diffuse layer (c.f. Figure 7) [26-31]. The use of potentials at the head-end of the diffuse layer



**Fig. 9:** Slip plane distance as a function of ionic strength for a range of systems taken from the references given in the main text.

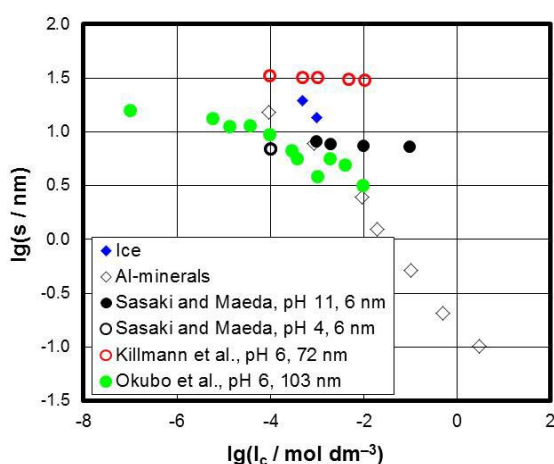


**Fig. 10:** Hydration layer thickness ( $s$ ) on silica particles as a function of salt concentration ( $I_c$  in NaCl) for various silica particle sizes (radii) and pH values compared to slip plane distances of "oxidic" equivalents.

were much higher than the measured data. Some of the results are given in Figure 9. While part of the problem may have been due to the presence of surface conductivity, which causes lower apparent zeta-potentials, and thus explain the issue, the slip plane distances at low salt levels become increasingly unrealistic. Therefore, they have been frequently considered as mere fitting-parameters. In turn the relationship between slip plane distance and ionic strength is intriguing. In principle, the slip-plane distance should correspond to the thickness of the hydration layer at such interfaces. In an electrokinetic experiment, the zeta-potential is measured at the shear-plane, where stagnant water meets mobile water. Thus measured hydrodynamic radii in relation to bare particle radii can indicate to what extent slip plane distances (from Figure 9) can be independently confirmed. The difference between the measured hydrodynamic radii and the respective bare (dry) radii of the same particles are

plotted in Figure 10 for three different silica samples from Killmann et al. [32], Sasaki and Maeda [33] and Okubo et al. [34].

A literature research has shown that measurements of the hydrodynamic diameter of monodisperse colloids as a function of salt level or pH yield similar relationships.

Clearly, Figure 10 shows that the two independent quantities are very similar in size and also show the same trend with salt content. The slip-plane distances do not include the Stern layer thickness. Unfortunately, the hydrodynamic radii may also result from the formation of gel layers. It has been mentioned in the discussion of the data by Killmann et al. [32] that the size dependence shown for silica in Figure 10 may have originated from "hairyness" and was not observed in the case of iron oxide particles. Yet, for silica particles the observation may remain relevant when zeta-potentials are to be interpreted.

For modelling adsorption processes the effect of geometry can now be investigated in some detail concerning the role of the different parameters, like thickness of the Stern layer or the adsorption of counterions. In the same line of reasoning the hydration layer thickness can be of importance since the chemistry in water layers close to mineral surfaces can be different from bulk water. In particular silica surfaces in many natural systems are relevant and they are related to clay systems. The behavior of sensitive probes like Curium could be systematically studied in such hydration layers with known and variable thickness.

## References

- [1] Altmaier et al., Chemical Reviews 2013, 113 (2), 901-943.
- [2] Geckeis et al., Chemical Reviews 113 (2), (2013) 1016-1062.
- [3] Begg et al., Environmental Science & Technology 47 (10) (2013), 5146-5153.
- [4] Zavarin et al., Environmental Science & Technology 46 (5) (2012), 2692-2698.
- [5] Tinnacher et al., Environmental Science & Technology 49 (5) (2015), 2776-2785.
- [6] Hixon et al., Journal of Colloid and Interface Science 403 (2013), 105-112.
- [7] Banik et al., Radiochimica Acta 95 (10) (2007), 569-575.
- [8] Marsac et al. Geochimica et Cosmochimica Acta 152 (2015), 39-51.
- [9] Guillaumont et al., Chemical Thermodynamics Vol. 5 (2003).
- [10] Ciavatta, Annali di, Chimica 70 (1980), 551-567.
- [11] Parkhurst and Appelo, User's guide to PHREEQC (Version 2) (1999).
- [12] Kinniburgh D.G. and Cooper D.M. (2009) <<http://www.phreeplot.org>>.
- [13] Schnurr A. et al., Geochim. Cosmochim. Acta 151, (2015), 192-202.
- [14] Schnurr A, PhD thesis, KIT, Karlsruhe, 2015

- [15] Brewitz, W.: Eignungsprüfung der Schachanlage Konrad für die Endlagerung radioaktiver Abfälle. GSF-T136, Neuherberg (1982).
- [16] Bradbury, M.H. and Baeyens, B., *Geochim. Cosmochim. Acta*, 73, 990-1003 (2009).
- [17] Ohshima H, Healy TW, White LR., *J Colloid Interf Sci.* 1982; 90: 17-26.
- [18] Loeb A.L. The electrical double layer around a spherical colloid particle: computation of the potential, charge density, and free energy of the electrical double layer around a spherical colloid particle: Massachusetts Institute of Technology; (1961).
- [19] Ohshima H., Chapter 3 Diffuse double layer equations for use in surface complexation models: approximations and limits. In: Johannes L, (editor). *Interface Science and Technology*. Vol. Volume 11: Elsevier; (2006), 67-87.
- [20] Abbas Z. et al., *The Journal of Physical Chemistry C.* (2008),112, 5715-23.
- [21] Lützenkirchen J., (2002),107; 631-710.
- [22] Ridley MK. et al., *Langmuir*, (2013), 29, 8572-83.
- [23] Ridley MK. Et al., *Langmuir*, (2015); 31, 703-13.
- [24] Barisik M. et al., *J Phys Chem C.* (2014), 118, 1836-42.
- [25] Hiemstra T., Van Riemsdijk WH., *Geochim Cosmochim Ac*, (2009), 73, 4423-36.
- [26] Bourikas K. et al., *Langmuir*, (2001); 17, 749-56.
- [27] Hiemstra T. et al., *Langmuir*. 1999; 15: 5942-55.
- [28] Heberling F. et al., *Colloid Interf Sci.* (2011), 354, 843-57.
- [29] Heberling F. et al., (vol 354, p. 843, 2011). *J Colloid Interf Sci.* (2013), 404, 230-.
- [30] Lützenkirchen J. et. al., *Phys Chem Chem Phys.* (2008), 10, 4946-55.
- [31] Lützenkirchen J. et al. *Faraday Discussions.* (2015)
- [32] Killmann E. et al., *Colloid Surface.* (1988) 31, 51-71.
- [33] Sasaki S., Maeda H., *J Colloid Interf Sci.* (1994),167, 146-9.
- [34] Okubo T. et al., *Colloid Polym Sci.* (1996), 274, 73-80.

## 4.3 Retention of radionuclides by secondary phase formation

N. Finck, F. Heberling, L. Paulig, Z. Nie, D. Schild

In co-operation with:

S. Nedel<sup>a</sup>, K. Dideriksen<sup>b</sup>, M. L. Schlegel<sup>c</sup>

<sup>a</sup> Haldor Topsøe A/S, Lyngby, Denmark; <sup>b</sup> Nano-Science Center, Department of Chemistry, University of Copenhagen, Denmark; <sup>c</sup> CEA, DEN/DPC/SEARS/LISL, Gif-sur-Yvette, France [29]

### Introduction

During the (geo)chemical evolution of deep repositories, ground water may migrate through the geological and geotechnical barriers of the multi-barrier system, and reach the intact or partly failed technical barrier initially encapsulating the high-level waste (HLW) matrix. In aqueous environments, various secondary phases may form as alteration or corrosion products of barrier materials. Regarding the examples presented here: steel canisters will corrode over extended periods of time in contact with ground water and various Fe-bearing secondary phases will form. Calcite on the other hand is expected to form as an alteration product of concrete based materials, and may be present as a constituent of possible host rock formations (e.g. argillites). Secondary phases have the potential to scavenge radionuclides (RNs) and to retard their release to the biosphere. Various molecular scale retention processes, from surface adsorption to structural incorporation have been reported. Especially structural incorporation, i.e. solid-solution formation, is argued to lead to sustainable retention of the radionuclides in the near field of a repository. However, despite the abundance of solid solutions in natural systems, reliable thermodynamic and kinetic models to predict their formation are hardly available. Such data can be obtained by combining information from specific lab experiments with molecular scale information from advanced spectroscopic and microscopic techniques and computational studies.

The group working on secondary phases at INE investigates the structural incorporation of RNs into secondary phases expected to form in deep geological repositories. Shown below are two examples: 1) investigations on An(III) uptake by iron phases as an example of a joint research proposal (JRP) performed within the European FP7 TALISMAN project at INE and 2) investigations on calcite recrystallization performed within a bachelor thesis (Leonie Paulig).

### Uptake of trivalent actinides by iron(hydro)oxides

In various countries, HLW will be confined in steel canisters which are foreseen to be surrounded by various barriers in deep disposal sites. However, geological (clay and crystalline formations) and engineered barriers (compacted bentonite) are expected to become water saturated over the geological time scales to be considered and the corrosion of the steel canister is to be expected. Long-term corrosion studies [1-3] have

shown that steel corrosion in the presence of clay pore water produces Fe(II)- bearing phases such as green rust (GR) or magnetite (Fe<sub>3</sub>O<sub>4</sub>).

The formation of magnetite during anaerobic steel corrosion at elevated temperatures follows a two-step process. The first step consists in the production of ferrous hydroxide and hydrogen by water reduction and iron oxidation. In the second step, Fe(OH)<sub>2</sub> is oxidized by water to form hydrogen and magnetite (Schikorr reaction). Partial Fe(OH)<sub>2</sub> oxidation can also form green rust, which belongs to the family of Fe(II)-Fe(III) layered double hydroxides [4] and which are known to be metastable reaction compounds between metallic iron and final corrosion products. Reducing conditions will develop as a consequence of the hydrogen evolution upon steel corrosion, thereby possibly reducing RN to lower oxidation state(s). Information on the immobilization of actinides by Fe(II)-bearing solids and the stable oxidation state under the established E<sub>H</sub>/pH- conditions could therefore be of importance for safety performance assessment of deep nuclear repositories. However, only few investigations on the retention of trivalent or tetravalent actinides by magnetite have been reported so far [5-8]. Magnetite and GR both have octahedral Fe(III) sites and thus homovalent substitution of trivalent actinides for octahedral Fe atoms can be expected. However, the substitution may be hindered due to the size mismatch between six-fold coordinated Fe(III) or Fe(II) ( $r^{\text{VI}}\text{Fe(III)} = 0.65 \text{ \AA}$ ;  $r^{\text{VI}}\text{Fe(II)} = 0.78 \text{ \AA}$ ) and trivalent actinides ( $r^{\text{VI}}\text{Pu(III)} = 1.00 \text{ \AA}$ ;  $r^{\text{VI}}\text{Am(III)} = 0.98 \text{ \AA}$ ;  $r^{\text{VI}}\text{Cm(III)} = 0.97 \text{ \AA}$ ) [9]. Yet, recent studies showed the possibility to incorporate some Am(III) at octahedral sites within brucite and sheet silicates [10] as well as in calcite [11], suggesting that incorporation within magnetite octahedral sites may be possible.

In this study we investigated the incorporation of Am(III), a typical trivalent actinide, in magnetite either by direct precipitation with aqueous Fe(II) and Fe(III) or by incorporation in a GR precursor followed by transformation of this solid.

**Sample preparation.** All samples were prepared and handled in an Ar glove box, and all measurements were performed under anoxic conditions. Fe(II) and Fe(III) sources were chloride salts and the Am(III) stock solution contained 15 mmol/L <sup>243</sup>Am in 1 mol/L HCl. pH was measured with a combined electrode and adjusted when necessary by using NaOH or HCl. E<sub>h</sub> values were measured using a Pt electrode. Suspensions were stirred during pH and E<sub>h</sub> measurements;

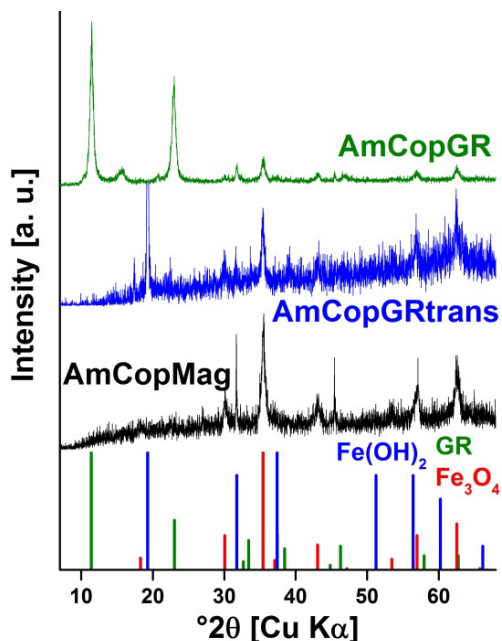


**Fig. 1:** Experimental X-ray diffractogram of samples AmCopGR, AmCopGRtrans and AmCopMag, and reference data from the PDF-2 database.

typical uncertainties on pH and  $E_h$  values are  $\pm 0.05$  and  $\pm 30$  mV, respectively.

Chloride GR formed in the presence of Am (sample AmCopGR) was prepared by addition of NaOH to a stirred solution containing Fe(II) and Fe(III) (Fe(II):Fe(III) molar ratio of  $\sim 7:1$ ) spiked with  $^{243}\text{Am}$  ( $[\text{Am(III)}] = 32 \mu\text{mol/L}$ ). pH and  $E_h$  were measured after two days (pH = 7.00;  $E_h = -333$  mV vs S.H.E.) and 10 mL of the suspension were centrifuged in the glove box for 10 minutes at 6500 rpm. The supernatant was removed and replaced by ultra-pure water ( $m/V = 2.1$  g/L) and the pH raised while stirring to induce transformation into magnetite (sample AmCopGRtrans). pH and  $E_h$  were measured after two days (pH = 11.00;  $E_h = -518$  mV vs S.H.E.). Separately, magnetite was prepared in the presence of  $^{243}\text{Am}$  similar to AmCopGR, but with Fe(II):Fe(III) = 1:2 and  $[\text{Am(III)}] = 33 \mu\text{mol/L}$ . After two days of reaction, the measured pH and  $E_h$  were 8.25 and -295 mV vs S.H.E., respectively. A portion of each suspension was also ultra-centrifuged for 1 hour at 694,000 g (Beckman XL-90) and the concentration of dissolved Am in the supernatant was determined by high resolution ICP-MS (Thermo Element XR). Two samples were used as model compounds for XAS: an  $^{243}\text{Am}$  stock solution in acidic medium and an  $\text{Am(OH)}_3(\text{s})$  precipitate formed by addition of NaOH to a stirred acidic Am(III) solution under air (sample AmHydrox).

**Solid phase characterization.** Solid phases were first characterized by XRD using an air-tight sample holder. Samples were prepared in the glove box and X-ray diffractograms were recorded on a D8 Advance (Cu  $K\alpha$  radiation) diffractometer (Bruker) equipped with an energy dispersive detector (Sol-X). Phases were identified by comparison with the PDF-2 database. Information on size and morphology was obtained by SEM with an environmental scanning electron micro-

scope (Quanta 650 FEG, FEI). Samples were prepared in the glovebox and quickly positioned in the microscope to minimize the air exposure time.

Information on the Am(III) local environment was provided by probing the  $L_3$ -edge by XAS at the INE-Beamline for actinide research at ANKA [12]. Energy calibration was done by assigning the first inflection point of the Zr  $K$ -edge of a Zr foil at 17998.0 eV, and this reference was measured in parallel with all samples. Data were collected in fluorescence mode using a 5-element solid state detector (Canberra-Eurisys). All Am-containing samples were mounted within a double container to meet safety regulations. Data were analyzed following standard procedures by using Athena and Artemis interfaces to the Iffeffit software [13]. EXAFS spectra were extracted from the raw data and Fourier transforms (FTs) were obtained from the  $k^3 \times \chi(k)$  functions. Data were fit in  $R$ -space using a combination of single scattering paths where phase and amplitude functions were calculated with feff8.4 [14].

**Results and interpretation.** X-ray diffractograms of all samples are presented in Figure 1 and scanning electron micrographs in Figure 2. Figure 1 indicates that sample AmCopGR consists mainly of GR, with minor amounts of magnetite, most likely due to partial GR oxidation during measurement. The SEM picture indicates that GR platelets have several hundreds of nanometers in size and that magnetite is of small size, scattered on the sample. Analysis of the supernatant indicates that more than 98 % of Am is associated with the solid. Sample AmCopGRtrans obtained by transformation of AmCopGR is composed of  $\text{Fe(OH)}_2$  intermixed with magnetite. SEM indicates that  $\text{Fe(OH)}_2$  platelets have several micrometers in size and that they are covered by fine grained magnetite. The concentration of dissolved Am in the supernatant ( $[\text{Am}] = 2.1 \times 10^{-9}$  mol/L) is low, indicating almost no release during phase transformation. Note that in that sample, Am can be bound to either one or two phases. The formation of  $\text{Fe(OH)}_2$  and  $\text{Fe}_3\text{O}_4$  by increasing the pH of a suspension containing chloride GR is in agreement with earlier findings of Jolivet et al. [15] for sulfate GR. Finally, only fine grained material could be detected in the magnetite directly precipitated in the presence of Am(III) and trace amounts of Am were found in the supernatant ( $[\text{Am}] = 3.0 \times 10^{-10}$  mol/L), indicating quantitative Am uptake by  $\text{Fe}_3\text{O}_4$ . XRD and SEM consistently show that the presence of Am(III) did not affect the syntheses of any Fe phase. The experimental and modeled EXAFS spectra of the samples and model compounds, with the corresponding Fourier transforms (FTs), are presented in Figure 3. The spectra of the model compounds differ from that of the Fe samples, especially at  $k > 7 \text{ \AA}^{-1}$ , implying that Am is connected to a solid Fe phase and that it did not precipitate as  $\text{Am(OH)}_3(\text{s})$ .

The EXAFS data of  $\text{Am(III)}_{\text{aq}}$  indicate the presence of only one ordered shell, and a good fit was obtained with one shell of 9.0(5) O atoms at  $d(\text{Am-O1}) = 2.47(2) \text{ \AA}$ , in agreement with earlier findings [10,16].

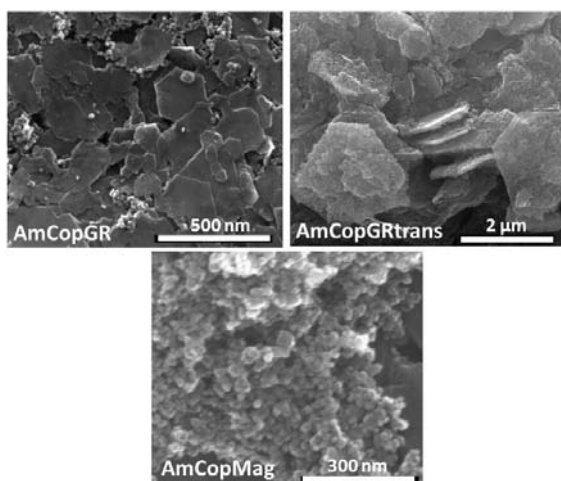


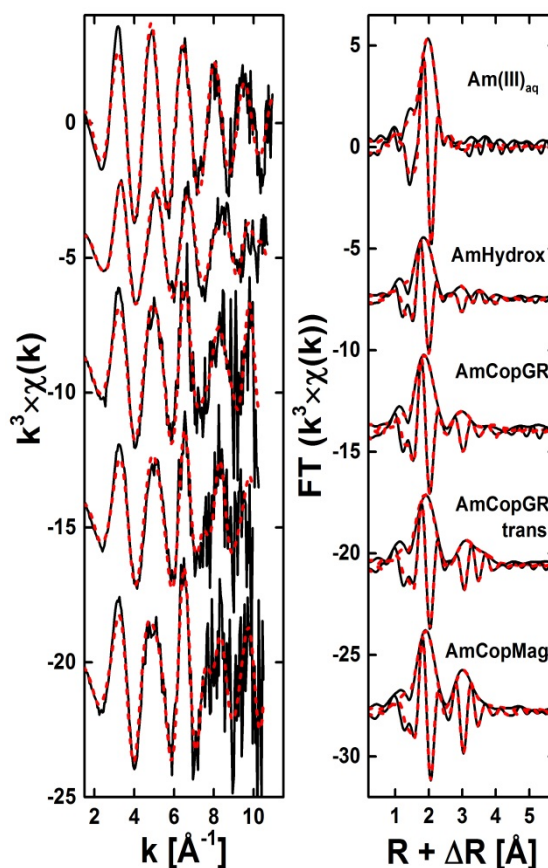
**Fig. 2:** Scanning electron micrographs of samples AmCopGR, AmCopGRtrans and AmCopMag.

The EXAFS spectrum of AmHydrox has lower wave amplitude maxima and frequency, hinting at a lower coordination number and interatomic distance to the first ligand shell. This is also evident from the position and amplitude of the first peak in the FT. Additional peaks of lower amplitude are also present at higher distances on the FT. A good fit to the data was obtained with 5.7(10) O atoms at 2.39(2) Å, as well as ~2 O atoms at 3.36(6) Å and ~2 Am atoms at ~3.76 Å. Unfortunately no published XAS data of Am(OH)<sub>3</sub> are available to compare with these values, but this compound is isostructural to Nd(OH)<sub>3</sub> and both have comparable unit cell parameters [17,18], suggesting that Nd(OH)<sub>3</sub> could be used as proxy for Am(OH)<sub>3</sub>. In Nd(OH)<sub>3</sub>, Nd is surrounded by two O subshells of 3 and 6 atoms at 2.50 and 2.52 Å, respectively, and two Nd atoms are located at 3.74 Å. AmHydrox is poorly crystalline and thus explains that the number of detected O atoms is lower compared to that found in the bulk structure. The detection of an Am shell at 3.76 Å compares more with the Nd-Nd distance in Nd(OH)<sub>3</sub>. The detection of an Am shell at similar distance in the Fe samples will thus inform on the presence of polymers/hydrous precipitate.

The spectra of AmCopGR and AmCopGRtrans are very similar in oscillation amplitude and frequency, hinting at very similar chemical environments (Figure 3). The FTs display peaks at  $R + \Delta R \sim 2$  and  $\sim 3$  Å, and a small additional contribution at  $\sim 3.5$  Å for AmCopGRtrans. For both samples, good fits were obtained with ~6 O atoms at  $d(\text{Am-O1}) = 2.43(2)$  Å, and with ~2 Fe atoms at  $\sim 3.45$  Å. This bond length is moderately larger than interatomic distances in sulfate GR (3.18 Å) [19] or in Fe(OH)<sub>2</sub> (3.25 Å) [20]. Furthermore, the increase in distance from  $d(\text{Fe-Fe})$  to  $d(\text{Am-Fe})$  (0.20 – 0.27) parallels the increase in ionic radius from Fe(II) or Fe(III) to Am(III) (0.20 – 0.33 Å), suggesting that the Fe shell at  $\sim 3.45$  Å may be attributed to neighboring octahedral Fe surrounding Am, which substitutes for Fe in GR (AmCopGR) or in Fe(OH)<sub>2</sub> (AmCopGRtrans). Some Am(III) may also be surface retained in these samples, thereby explaining the low number of detected Fe atoms and the number of O1

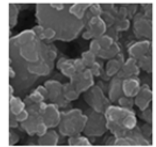
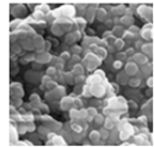
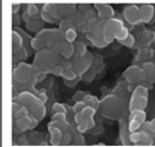
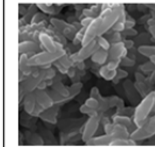
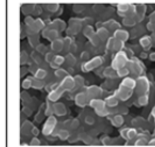
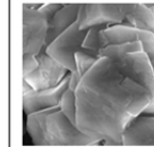
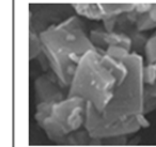
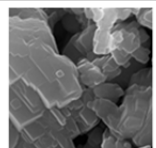
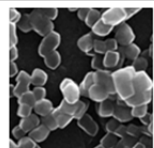
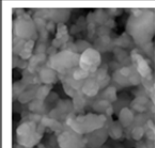
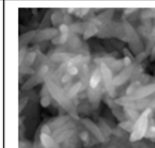
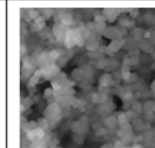
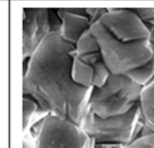
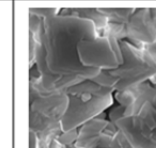
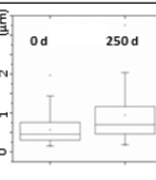
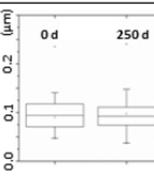
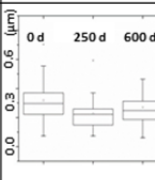
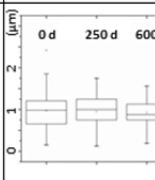
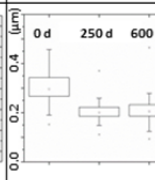
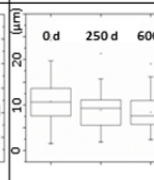
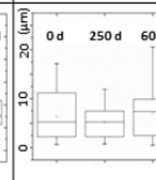
atoms slightly larger than six expected for Am located at octahedral site. No neighboring Am was detected, ruling out the presence of Am(OH)<sub>3</sub>(s) in the samples.

The spectrum of AmCopMag differs from that of the GR samples, mainly in amplitude of the oscillations and also in frequency at  $k > 7 \text{ \AA}^{-1}$ . Accordingly, the FT also differs, especially in the FT peak amplitude at  $\sim 3$  Å. A good fit to the data was provided considering a first O shell of 7.1(5) atoms at 2.44(2) Å, and higher distances shells of 3.3(8) Fe at  $d(\text{Am-Fe1}) = 3.45(4)$  Å and  $\sim 3$  Fe at  $\sim 4.00$  Å. The O1 and Fe1 shells are located at similar distances than in the GR samples, suggesting similar chemical environments. However, the O1 shell has a coordination number higher than expected for an octahedral environment, and the Fe1 shell is at significantly larger distance than for octahedral Fe in magnetite (2.97 Å), but close to the reported distance from octahedral Fe to tetrahedral Fe (3.48 Å) [21]. Within bulk magnetite, the substitution of Am(III) for Fe(III) would result in the actinide located at highly distorted sites, and thus the number of detected O atoms should be less than six because of damping out of EXAFS waves, in contrast to the observations. Compared to reported data for Am adsorbed onto preformed magnetite [7], the formation of surface complexes can be ruled out. Consequently, the data can best be explained by an uptake of Am(III) at Fe(III) sites at the surface, where the bonding envi-



**Fig. 3:** Experimental (solid black line) and modeled EXAFS spectra (left) with the corresponding Fourier transforms (right) of samples AmCopGR, AmCopGRtrans, AmCopMag, and of reference compounds.

**Table 1:** Characteristics of the Cc powders used in the recrystallization experiments (PCC stands for precipitated calcium carbonate). The first line indicates the label, the BET surface area, and the source of the Cc powders. SEM micrographs in the second and third line are taken before (2<sup>nd</sup> row) and after (3<sup>rd</sup> row) the experiments. Experiments ran for 250 days for Ground Cc and Fine PCC and for 600 days for the other powders. Particle sizes were analyzed before the experiment and after 250 and 600 days of recrystallization, respectively. The corresponding relative changes in particle size are indicated in the consecutive box-plots in the last row.

<b>Ground Cc</b> (3.9 m <sup>2</sup> /g) Icelandspar (5 x 5 μm <sup>2</sup> )*	<b>Fine PCC</b> (23.8 m <sup>2</sup> /g) Schäfer Kalk (1 x 1 μm <sup>2</sup> )*	<b>Prismatic PCC</b> (6.8 m <sup>2</sup> /g) Schäfer Kalk (4 x 4 μm <sup>2</sup> )*	<b>Scaleno-hedral PCC</b> (7.9 m <sup>2</sup> /g) Schäfer Kalk (4 x 4 μm <sup>2</sup> )*	<b>Rhombo-hedral PCC</b> (7.7 m <sup>2</sup> /g) Schäfer Kalk (4 x 4 μm <sup>2</sup> )*	<b>Coarse Cc (fresh)</b> (0.2 m <sup>2</sup> /g) Merck (40 x 40 μm <sup>2</sup> )*	<b>Coarse Cc (aged)</b> (0.6 m <sup>2</sup> /g) Merck (40 x 40 μm <sup>2</sup> )*
						
						
						

\*: area of SEM micrographs

ronment might be less constrained. This would be consistent with the rather high coordination number and interatomic distance of the O1 shell. In that configuration Am and Fe polyhedra may share corners in geometries ranging from bent ( $d(\text{Am-Fe1}) = 3.45(4)$  Å) to close to linear ( $d(\text{Am-Fe2}) \sim 4.00$  Å). The Am retention is also associated with high structural strain, as attested by the relatively high mean square displacement ( $\sigma^2 = 0.007$  Å<sup>2</sup>) of both Fe shells.

**Discussion.** In the GR experiment, the Am concentration is too low to have a significant influence on the sample preparation, but the increase in size from Fe(III) to Am(III) may strongly impact the local stability and thus the Am(III) retention mode. According to the synthesis pathway, Am(III) was first retained by a poorly ordered ferric phase and subsequently by GR. Structural data indicate that Am(III) can substitute for octahedral Fe(III) within GR structure, however, with a large distortion of the lattice site. The homovalent substitution seems to operate to a limited extent, certainly facilitated by the net charge balance. GR has a brucite-like structure made of stacked octahedral sheets which are likely to be able to accommodate the large actinide. This result corroborates recent findings on Am(III) substitution for octahedral Mg within brucite [10].

The transformation of GR into Fe(OH)<sub>2</sub> and magnetite by increasing the pH of the AmCopGR suspension agrees with earlier findings [15], and Am(III) had no detectable effect on the transformation pathway. No Am release from the bulk structure was detected and

the chemical environment hardly changed, suggesting that the actinide is still located at Fe octahedral sites. This is consistent with Am retained within Fe(OH)<sub>2</sub> rather than at magnetite octahedral sites, indicating that this formation pathway appears unfavorable to the incorporation of Am within magnetite.

The presence of Am(III) had also no detectable influence on the magnetite formation by direct precipitation and XAS data suggest that Am substitutes for Fe in AmCopMag at the surface. Furthermore, comparing the data of AmCopMag to that of AmCopGRtrans indicates that the magnetite fraction in that transformation sample does not contain significant amounts of Am(III), compared to that in the more abundant Fe(OH)<sub>2</sub> phase. This finding indicates that the synthesis pathway plays a critical role in the actinide incorporation within magnetite.

**Conclusion.** This study shows a possible retention of trivalent actinides within structures of Fe(II)-bearing solids or at their surfaces. Upon steel corrosion chemical conditions expected to develop in a repository near-field would favor the formation of corrosion products such as Fe(OH)<sub>2</sub>, GR and magnetite. Fe(OH)<sub>2</sub> and magnetite show high affinity for Am(III), indicating that at the early stage of canister corrosion, secondary phases could limit the Am(III) mobility. In the presence of Fe(II)<sub>aq</sub>, magnetite exhibits a high reactivity in suspension and thus the binding mode of trivalent actinides is likely to evolve. For example, trivalent actinides can form surface sorbed species together with Fe(II) species in equilibrium

with corrosion products and with time the solid recrystallization can lead to An(III) scavenged within the bulk structure. Magnetite thus appears as a potential sink for RN, attenuating their migration to the far field.

### Calcite recrystallization

Calcite (Cc) is expected to form as an alteration product of concrete based materials in the multi-barrier system around a potential deep geologic waste repository. It is also a major constituent of clay formations (argillites) and occurs as fracture filling material in crystalline rocks, both considered as potential host rocks for nuclear waste repositories in European countries. Numerous studies have shown that Cc effectively sequesters RNs upon precipitation or growth in the presence of RNs [22-25]. With the experiments presented here, we address questions of major importance regarding the relevance of previous results on RN-coprecipitation with Cc: In how far does Cc recrystallize spontaneously in aqueous environments, thereby opening a pathway to structural incorporation of RNs into pre-existing Cc minerals? What are the recrystallization rates? And finally, what drives Cc recrystallization in aqueous solutions that are nominally in equilibrium with Cc?

**Recrystallization experiments.** All experiments are carried out in Cc saturated solutions (CSS). These are prepared by adding an excess of Cc to ultrapure water (18.2 MΩ cm, < 4 ppb TOC) containing 100 mmol/L NaCl as background electrolyte. The resulting suspension is percolated with air (~390-500 ppm CO<sub>2</sub>) until the pH predicted by geochemical modelling (PhreeqC [26] and Nagra/PSI database [27]) is established. After equilibration, excess Cc is removed by filtration (Milipore 0.45 μm).

To start the experiments, we add 5 g/L Cc powder and a spike (116 Bq/mL) of <sup>45</sup>Ca to 40 mL CSS. Seven Cc powders with strongly differing characteristics are used in the recrystallization experiments (cf. Tab. 1). <sup>45</sup>Ca-activity data are displayed in Fig. 4. Uncertainties depict standard deviations of triplicate experiments. Reference experiments without added Cc exhibited no significant <sup>45</sup>Ca sorption to container walls.

**Results and Discussion.** All Cc powders show <sup>45</sup>Ca uptake, which strongly exceeds any uptake that might be explained by surface adsorption or surface ion-exchange. Correspondingly, we may conclude that <sup>45</sup>Ca is taken up into the bulk of the Cc minerals, most likely by dissolution- reprecipitation processes. The degree to which the Cc minerals recrystallize and take up <sup>45</sup>Ca may be estimated based on the homogeneous recrystallization model [28]. For the Cc powders in our study it varies from about 1 % for the coarse Cc powders to 100 % for the fine grained PCC. SEM images and a corresponding analysis of the particle size distributions indicate that an evolution from rounded irregular particle morphologies towards euhedral rhombohedral crystallites and a corresponding decrease of surface roughness is the main driving

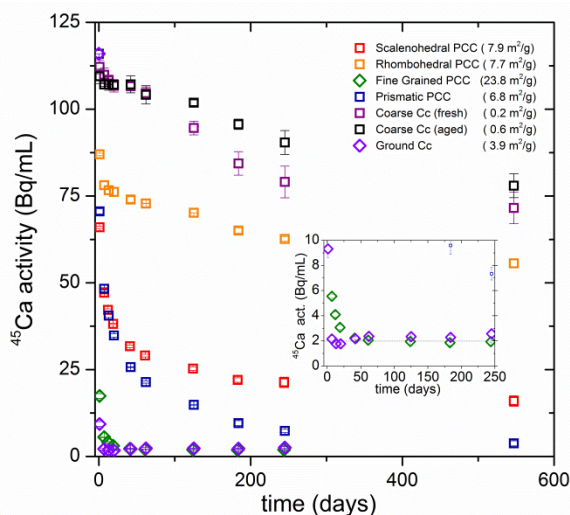


**Fig. 4:** Overview over decay corrected <sup>45</sup>Ca-activity data from Cc recrystallization experiments. Note that all experiments start at 116 Bq/mL. The insert highlights details of the experiments with Ground Cc and Fine Grained PCC that were stopped after 250 days. The thin dashed line indicates the equilibrium activity: 1.96 Bq/mL.

force for the recrystallization process. For the prismatic PCC a development from the metastable prismatic-, towards a stable rhombohedral morphology is observed. Interestingly this is not (or to a much lesser extent) the case for the scalenohedral PCC. Only the Ground Cc shows the expected trend in particle size evolution, i.e. smaller particles dissolve in favor of growth of larger particles. Most powders exhibit no significant change in particle size distribution. We interpret cases where an opposite evolution towards smaller particles is indicated (e.g. Rhombohedral PCC) as a de-agglomeration of particle aggregates.

Overall we conclude that Cc recrystallization is an Ostwald-ripening process. However, changes in particle sizes play a minor role and a classical treatment of interfacial free energy as presented e.g. by Schindler et al. [29] is not suitable to describe the driving forces of the process. More sophisticated expressions for interfacial free energy including energy contributions from particle morphology and roughness [30] need to be employed in order to capture the observations in this study. Quantification of the various contributions to interfacial free energy remains, however, a challenge.

With regard to applications we may conclude that:

- 1) General statements about the reactivity of Cc should be regarded with suspicion.
- 2) Specially designed freshly ground rough Cc powders may recrystallize to 100 % within days or weeks and may be highly effective scavengers for toxic substances in environmental remediation strategies.
- 3) On the other extreme, for natural Cc crystals whose surfaces have been equilibrated with the surrounding aqueous solution for millennia, recrystallization may be limited to some surface mono-layers even over geologic periods of time.

- 4) Experiments assessing the sorption capacity of natural Cc need to be performed with great care, as any disturbance of the Cc surfaces, e.g. by grinding, may strongly alter the reactivity.

Especially the last two points have to be considered in order to avoid an overestimation of the sorption capacity of Cc for RNs in host rock formations around potential nuclear waste repository sites.

## References

- [1] F. A. Martin et al., *J. Nucl. Mater.*, **379**, 80-90 (2008).
- [2] M. L. Schlegel et al., *Appl. Geochem.*, **51**, 1-14 (2014).
- [3] G. de Combarieu et al., *Appl. Geochem.*, **26**, 65-79 (2011).
- [4] P. H. Refait et al., *Corros. Sci.*, **40**, 1547-1560 (1998).
- [5] M. Tsukamoto et al., *Czech. J. Phys.*, **56**, D339-D348 (2006).
- [6] R. Kirsch et al., *ES&T*, **45**, 7267-7274 (2011).
- [7] N. Finck et al., *J. Phys. Conf Ser.*, Accepted manuscript (2015).
- [8] F. Seco et al., *ES&T*, **43**, 2825-2830 (2009).
- [9] R. D. Shannon, *Acta Crystallogr.*, **A32**, 751-767 (1976).
- [10] N. Finck et al., *Chem. Geol.*, **409**, 12-19 (2015).
- [11] T. Stumpf et al., *J. Colloids Interface Sci.*, **302**, 240-245 (2006).
- [12] J. Rothe et al., *Rev. Sci. Instrum.*, **83**, 043105 (2012).
- [13] B. Ravel and M. Newville, *J. Synchrotron Radiat.*, **12**, 537-541 (2005).
- [14] A. L. Ankudinov et al., *Phys. Rev.*, **B58**, 7565-7576 (1998).
- [15] J. P. Jolivet et al., *C. R. Geoscience*, **338**, 488-497 (2006).
- [16] A. Skerencak-Frech et al., *Inorg. Chem.*, **53**, 1062-1069 (2014).
- [17] W. O. Milligan et al., *Acta Crystallogr.*, **B24**, 979-980 (1968).
- [18] G. W. Beall et al., *Acta Crystallogr.*, **B32**, 2227-2229 (1976).
- [19] L. Simon et al., *Solid State Sci.*, **5**, 327-334 (2003).
- [20] G. Natta, *Gazz. Chim. Ital.*, **58**, 344-358 (1928).
- [21] M. E. Fleet, *J. Solid State Chem.*, **62**, 75-82 (1986).
- [22] F. Heberling et al. *ES&T* **42**, 471-476 (2008).
- [23] R. J. Reeder et al. *Geochim Cosmochim Acta.* **68**, 4799-4808 (2004).
- [24] M. Schmidt et al. *Angew Chem Int Edit.* **47**, 5846-5850 (2008).
- [25] G. Aurelio et al. *Chem Geol.* **270**, 249-256 (2010).
- [26] D.L. Parkhurst and C.A.J. Appelo *Water-Resources Investigations Report. Vol. 99*. US Geological Survey, Denver (1999).
- [27] W. Hummel et al. *Radiochim Acta.* **90**, 805-813 (2002).
- [28] E. Curti et al. *Geochim Cosmochim Acta.* **69**, 1721-1737 (2005).
- [29] P. Schindler et al. *Helvet. Chim. Acta.* **48**, 1204-1215 (1965).
- [30] B. Mutaftschiev. Springer Series in Materials Science. Vol. 43: Springer; 2001.

## 4.4 Effect of pore-scale mineral precipitation on transport parameters in diffusion controlled systems

A. Chagneau<sup>a</sup>, S. Heck, T. Kupcik, T. Schäfer

In co-operation with:

F. Claret<sup>b</sup>, C. Tournassat<sup>b</sup>, F. Enzmann<sup>c</sup>, M. Wolf<sup>c</sup>, M. Kersten<sup>c</sup>, B. Madé<sup>d</sup>, I. C. Bourg<sup>e</sup>, C. I. Steefel<sup>e</sup>

<sup>a</sup> Department of Geosciences, Freie Universität Berlin, Berlin, Germany; <sup>b</sup> Water and Environment division, French Geological Survey (BRGM), Orléans, France; <sup>c</sup> Department of Geosciences, Johannes Gutenberg University, Mainz, Germany; <sup>d</sup> French Agency for Nuclear Wastes Management (ANDRA), Châtenay-Malabry, France; <sup>e</sup> Earth Sciences Division, Lawrence Berkeley National Laboratory, Berkeley, USA

### Introduction

In geochemically perturbed systems due to pore water disequilibrium mineral precipitation/ dissolution might be induced which could possibly change the transport properties as porosity and pore diffusion coefficient. These reactions might alter the sealing capabilities of the rock by complete pore-scale precipitation (cementation) of the system or by opening new migration pathways through mineral dissolution. Furthermore, the formation of secondary phases might be an additional radionuclide retention pathway via incorporation in the newly formed phases [1]. In actual 1D continuum reactive transport codes the coupling of transport and porosity is generally accomplished through the empirical Archie law [2]. Experimental data on its general applicability for systems changing the porosity under well controlled conditions to constrain model input parameters to a maximum possible are rarely documented. In this study, celestite ( $\text{SrSO}_4$ ) was precipitated in the pore space of a compacted sand column under diffusion-controlled conditions and the effect on the fluid migration properties investigated by means of three complementary experimental approaches: (1) tritiated water (HTO) tracer through diffusion, (2) computed microtomography ( $\mu$ -CT) imaging and (3) post-mortem analysis of the precipitate (selective dissolution, SEM/ EDX). Details of this study can be found in [3].

Using a quite similar approach in clay based porous media the effect of pore scale celestite precipitation on anion exclusion; more specifically on  $\text{Cl}^-$  transport was investigated. Details to this work can be found in [4]. Both references [3, 4] are a summary of selected results from the PhD thesis of Aurélie Chagneau documenting a very fruitful and productive collaboration between BRGM and KIT-INE.

### Silica (sea sand) based porous media

The porous media transport parameters ( $D_e$  &  $\epsilon$ ) were very reproducible measured in separate column runs ( $n_{\text{tot}}=16$ ). The values determined are used as fixed input parameters for the 1D single continuum scale reactive transport model CrunchFlow [5]. The average parameter values determined were  $D_e$

$= (4.07 \pm 0.37)10^{-10} \text{ m}^2/\text{s}$ , a porosity  $\epsilon = 43.5 \pm 6.8\%$  and a cementation factor  $m = 1.99 \pm 0.33$  corresponding to a geometric factor  $G$  of  $2.24 \pm 0.24$ . Concerning the porosity determination, the  $\mu$ CT segmented porosity of  $40 \pm 3\%$  and the mercury intrusion porosimetry (MIP) of  $41.6 \pm 1.6\%$  matched quite well with the HTO through diffusion experimental data giving further confidence in the transport parameters chosen. As an impression of the porous media used in the experiments (sea sand) the 3D rendering of a typical reconstructed volume is presented in Fig. 1 given an impression of the pore morphology.

Pore scale precipitation of celestite was initiated by counter diffusion of 0.5M  $\text{SrCl}_2$  and 0.5M  $\text{Na}_2\text{SO}_4$  while continuously monitoring the HTO flux. The through-diffusion experiments reached steady state after 15 days, at which point celestite precipitation ceased and the non-reactive HTO flux became constant. The pore space in the precipitation zone remained fully connected under the  $6\mu\text{m}$   $\mu$ -CT spatial resolution with 25% porosity reduction in the approx. 0.35 mm thick dense precipitation zone (see Fig. 1). In none of the experiments full clogging was observed. The mass of  $\text{SrSO}_4$  precipitate estimated by  $\mu$ -CT with  $25 \pm 5 \text{ mg}$  and selective dissolution  $21.7 \pm 0.4 \text{ mg}$  were in good agreement, respectively. However, using the experimentally derived data as input parameters, the 1D continuum reactive transport model that assumed the direct linkage of porosity to the effective diffusivity via one cementation factor valid over the whole porosity variation range of the system investigated was not able to accurately reproduce both the celestite

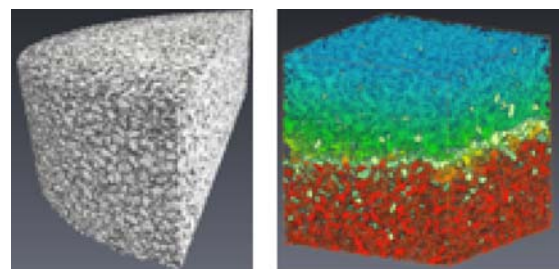


**Fig. 1:** (left) 3D pore scale reconstruction of the compacted sea sand of the diffusion cells used in [3]. (right) 3D representation of the Laplace field in the Z direction. The celestite grains appear in yellowish white. Figure modified after [3].

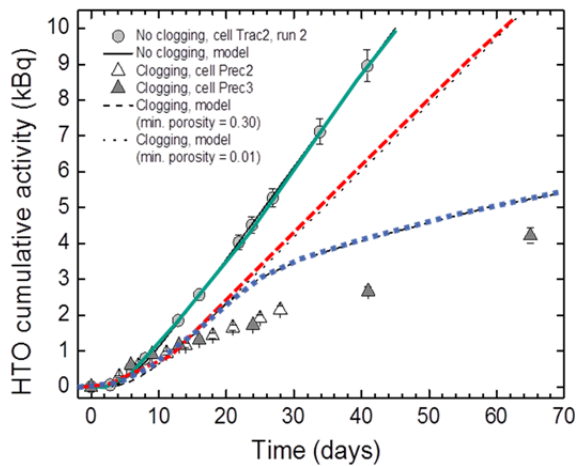


**Fig. 2:** HTO through-diffusion curves for diffusion experiments without pore space clogging (open circles), and two cells (open and full triangles, respectively) while porosity reduction by celestite precipitation. The full green line is the model without clogging (reduction). The dashed red and the dotted blue lines are obtained by running a reactive transport model taking into account the clogging (reduction), with a minimum porosity of 0.01 (best fit) and 0.30 (real CT determined porosity), respectively.

precipitation front and the remaining connected porosity.

The 1D continuous model either underestimated the remaining connected porosity in the precipitation zone, or overestimated the amount of precipitate to provide a best fit of the experimental data. These findings support the need to implement a modified, extended Archie's law to the reactive transport model and show that pore-scale precipitation transforms a system (following Archie's simple power law with only micropores present) towards a system similar to clays with micro- and nanoporosity.

Following our observations and analysis, our main conclusions are:

- (1) Celestite porosity reduction of sea sand was incomplete (the initial porosity was decreased by only 25%), as evidenced by the non-zero steady-state HTO flux at the end of all experiments and the fact that micro-CT mapping indicates an open and connected porosity of 0.30. The celestite precipitate was primarily localized in a  $\sim 0.35$  mm wide disk-shaped precipitation front surrounded by small areas of disperse precipitation in approximately the middle of the diffusion cell. The heterogeneity created by the precipitation front has a very strong influence on the transport parameters, despite the fact that the remaining porosity is fully connected. This phenomenon was evidenced by the strong effect of the porosity reduction on HTO flux and by the Laplace field calculation performed on the  $\mu$ -CT 3D volumes.
- (2) The 1D continuum reactive transport model successfully reproduced the experimental HTO through-diffusion data obtained prior to the sea

sand porosity reduction with an average porosity of 0.40. However, the same model failed to reproduce the HTO through-diffusion during celestite precipitation, indicating that a single continuum model is not capable of describing the system. When the minimum porosity of 0.30 determined with  $\mu$ -CT was used, the modelled tracer resembles more a homogeneously higher compacted system, which clearly contradicts the experimental observations. The best fit for the HTO through-diffusion flux curve was with a minimum porosity of 1%. However, the amount of precipitate obtained from this calculation was about 4.5 times greater than the experimental result.

From these observations we see that the system was well characterized, but that a simple 1D single continuum model cannot reproduce the clogging experiments satisfactorily. A more complex dual continuum 2D/3D pore-scale reactive transport model including a modified diffusivity/porosity relationship and possibly complex precipitation kinetics (e.g. heterogeneous nucleation and inhibition processes) may provide a better description. Indeed, the SEM observations seemed to indicate an intricate mix between heterogeneous nucleation and surface growth processes, as was shown by the wide range of shapes and sizes of precipitated celestite. The question of why no more precipitation seems to occur in the column after a very short time (less than 10 days) should also be addressed in terms of inhibition processes.

This more complex model is needed to firstly reproduce the experimental data presented here, and secondly predict transport behaviors in more complex, natural systems on long time scales, unreachable to the experimentalist (100, 1000, 10,000 years).

### Surface-charged porous media (compacted illite)

Clays are envisioned as efficient barriers for large scale confinement applications such as nuclear waste storage or  $\text{CO}_2$  geological sequestration. Their pores sizes and shapes hinder water flow and make diffusion the dominant solute transport mechanism. Most clay structures exhibit a negative charge that is balanced by an electrostatic diffuse layer at the surface-water interface, thereby retarding cations migration through adsorption processes, and decreasing anions accessible porosity and diffusion fluxes. Electrostatic interactions give also rise to semi-permeable properties inducing e.g. anomalously high fluid pressures in oil fields. Numerous models of membrane and diffusion properties differ in their representation of water, solutes and surface charge distributions in the clay pore network due to a lack of experimental constraints. Here we present an approach to evidence the total exclusion of anions from the smallest pore of a clay material. Two samples were prepared by compact-

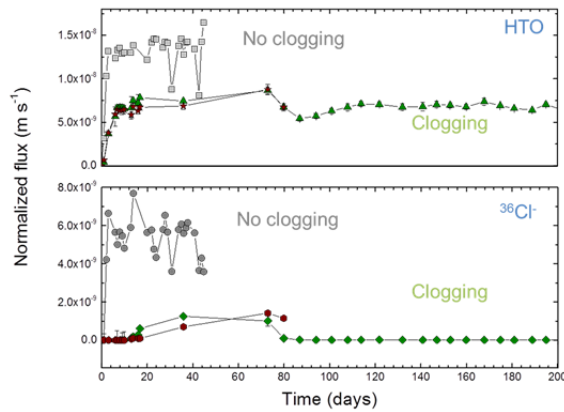


**Fig. 3:** Normalized HTO (squares) and  $^{36}\text{Cl}$  (circles) through-diffusion fluxes prior to (no clogging) and during porosity clogging by celestite precipitation in an illite sample. The drop of  $^{36}\text{Cl}$  flux to zero at day 80 evidences the selective disrupting of the pore network connectivity for  $^{36}\text{Cl}$  and not for HTO, thereby indicating that  $^{36}\text{Cl}$  is totally excluded from the pore throats.

ing 8.6 g of the illite in a half-open PEEK diffusion cell to a dry bulk density of  $1700 \text{ kg/m}^3$  corresponding to a total porosity of approx.  $\varepsilon = 0.40$ .

The porosity of compacted illite was clogged by celestite precipitation in the course of multi-tracers

diffusion experiments. While the water tracer diffusion flux decreased by a factor of two (see Fig. 3), chloride diffusion flux dropped to zero, thereby demonstrating the ideal membrane properties of the smallest pores and suggesting the necessity of considering a multi-porosity description of the pore network for accurate modelling predictions.

## References

- [1] Holliday, K.; Chagneau, A.; Schmidt, M.; Claret, F.; Schäfer, T.; Stumpf, T., *Dalton Transactions* 2012, 41(13), 3642-3647.
- [2] Archie (1942) *Petroleum Transactions of AIME*, 146, 54-62.
- [3] Chagneau, A.; Claret, F.; Enzmann, F.; Kersten, M.; Heck, S.; Madé, B.; Schäfer, T. *Geochem. Trans.* 2015, 16(13), 015-0027.
- [4] Chagneau, A.; Tournassat, C.; Steefel, C. I.; Bourg, I. C.; Gaboreau, S.; Esteve, I.; Kupcik, T.; Claret, F.; Schäfer, T., *ES&T Letters* 2015, 2(5), 139-143.
- [5] Steefel, C.I., Lasaga, A.C. (1994) *Am. J. Sci.* 294: 529–592.



## 5 Applied studies: Radionuclide retention in the multi-barrier system

Long-term safety of a deep geological repository for nuclear waste depends on a multi-barrier system which consists of technical and geo-technical barriers such as the waste form, the canister, backfilling and sealing of the mined openings as well as on the natural barrier function of the host rock. A series of applied studies on subsystems of various multi-barrier systems are performed, which cover a variety of components with specific characteristics and properties. Investigations presented in the first sub-chapter cover the quantification of radionuclides of irradiated cladding material of a spent nuclear fuel rod segment. In the following, we describe studies on the behavior of cemented waste forms, the characterization of solid, liquid and gaseous samples from rock formations overlaying the Asse II salt mine, and studies on the retention of actinides by  $Mg^{2+}/OH^-$  bearing materials, which are considered as geochemical buffer materials. These studies described in the second sub-chapter are related to the behavior of non-heat producing waste forms, the radionuclide release from these waste forms and the retention of radionuclides in geo-technical barriers and in the geological barrier, respectively. The third sub-chapter deals with the formation and deposition of bentonite colloids, the properties of di-octahedral smectites, which are the main constituents of bentonite, and the colloidal transport of radionuclides in bentonite backfilling / granite subsystems. In addition to these mainly experimental studies, modelling studies of multi-barrier systems are conducted, which are described in the final sub-chapter. Using reactive transport modelling, radionuclide release and retention processes in the near-field of spent nuclear fuel canister in a generic repository in claystone are simulated.

### 5.1 Highly radioactive waste forms

*E. Bohnert, M. Böttle, E. González-Robles, M. Herm, B. Kienzler, V. Metz, N. Müller*

In collaboration with:

*R. Dagan<sup>a</sup>, D. Papaioannou<sup>b</sup>*

<sup>a</sup> Karlsruhe Institute of Technology, Institute for Neutron Physics and Reactor Technology, Karlsruhe, Germany; <sup>b</sup> European Commission, Joint Research Centre, Institute for Transuranium Elements, Karlsruhe, Germany

#### Introduction

The long-lived activation product  $^{14}C$  is one of the crucial radionuclides with respect to estimated doses arising from the release in a deep geological repository for nuclear waste to the environment in a canister failure scenario due to its assumed mobility.

A scenario taken into account in long-term safety assessments of such facilities is corrosion of the fuel cladding upon contact with groundwater. This possibly leads to the formation of volatile and/or dissolved  $^{14}C$  bearing organic species. These compounds reveal a high mobility either in the aqueous or in the gaseous phase and, once released, are possibly transported into the biosphere, where  $^{14}C$  may be metabolized by any kind of organism. On the contrary, volatile/dissolved inorganic  $^{14}C$  bearing compounds are affected by various retention processes in the near field of a repository and the geosphere.

$UO_2$  or MOX (mixed oxide) fuel pellets used in light water moderated power reactors are usually inserted into fuel rods and sealed air-tight. In addition, the tubes are pressurized with helium to improve the conduction of heat from the fuel to the cladding. The fuel rods are bundled to fuel assemblies (e.g.  $15 \times 15$ ,  $17 \times 14$  lattice). These fuel assemblies are then used to build up the reactor core.

The cladding tube of fuel rods are made of Zircaloy, a zirconium based alloy, for nominal chemical composition see elsewhere [1-3]. Besides to its low neutron absorption, Zircaloy shows good mechanical properties and resistance to corrosion under reactor operation conditions [1]. Zircaloy-4 is used in many fuel assemblies for pressurized water reactors (PWR) whereas Zircaloy-2 is used in many assemblies for boiling water reactors (BWR). In contrast to Zircaloy-2, Zircaloy-4 does not contain nickel to reduce the absorption of hydrogen, which is more likely to occur in PWRs than in BWRs [2].

The principal source of  $^{14}C$  in Zircaloy is the activation by neutrons during reactor operation of: nitrogen-14 ( $^{14}N(n,p)^{14}C$ ), carbon-13 ( $^{13}C(n,\gamma)^{14}C$ ) and oxygen-17 ( $^{17}O(n,\alpha)^{14}C$ ).  $^{14}N$  is the main naturally occurring nitrogen isotope (99.6%), whereas  $^{13}C$  (1.1%) and  $^{17}O$  (0.038%) are low abundance naturally occurring carbon and oxygen isotopes, respectively [4].

Nitrogen and carbon are present as impurities in Zircaloy cladding and other reactor core structures. However,  $^{14}N$  is the main source of  $^{14}C$  due to its isotopic abundance and large thermal neutron capture cross-section (1.93 barn [4]). The content of  $^{14}N$  in Zircaloy is typically less than 80 ppm [1-3]. Gras estimated a general recommends an impurity level of about 40 ppm for Zircaloy-2 and Zircaloy-4 [5].

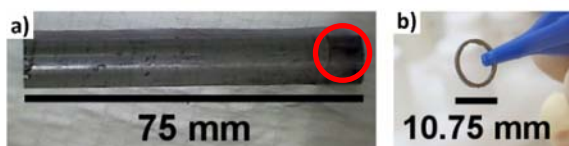


**Fig. 1:** Pictures of the irradiated plenum Zircaloy-4 cladding: (a) dimensions, the red circle indicates the welded end-plug; (b) subsample prepared for the dissolution experiments.

In the present study, focus is given to the determination of the inventory of  $^{14}\text{C}$  in an irradiated Zircaloy-4 cladding as well as the chemical form of  $^{14}\text{C}$  released from the material. Additionally, the inventories of other activation/fission products present in the Zircaloy cladding are determined. Finally, experimentally measured radionuclide contents are compared to theoretically predicted inventories of the irradiated Zircaloy-4, obtained by means of Monte Carlo N-Particle calculations (MCNP-X).

### Zircaloy-4 sample origin, irradiation characteristics and sample preparation

The studied Zircaloy-4 cladding was sampled from fuel rod segment N0204 of the fuel rod SBS1108, which was irradiated during four cycles in the PWR Gösigen (Switzerland). The fuel rod was finally discharged from the nuclear reactor in May 1989 after 1226 effective full power days and experienced an average burn-up of  $50.4 \text{ GWd/t}_{\text{HM}}$ .

In Fig. 1a the cut top of the fuel rod segment is shown. The so-called plenum region of a fuel rod contains beside the welded end-plug (Fig. 1a, last 12 mm on the right end side) a free volume. This free space accommodates thermal expansion of the pellets and further contains a stainless steel or Inconel<sup>®</sup> spring to compress the pellet stack and to minimize its movement.

The 16.618 g heavy plenum Zircaloy-4 cladding shown in figure 1a had a dose rate of  $\sim 20 \text{ mSv/h}$  in contact. Subsamples for dissolution experiments conducted in a glove-box were dry cut using an IsoMet<sup>®</sup> Low Speed Saw (11-1180, Buehler Ltd.) equipped with an IsoMet<sup>®</sup> diamond wafering blade (11-4254, Buehler Ltd.). In total six Zircaloy-4 specimens (see figure 1b) with masses ranging from  $119.7 \pm 0.2 \text{ mg}$  to  $189.0 \pm 0.2 \text{ mg}$  were prepared by remote handling in a hot cell. The mass and dose rate of each specimen was measured using an analytical balance (MS304S, Mettler-Toledo International Inc.) and a dose rate meter (6150AD6, automess – Automation und Messtechnik GmbH). Dose rate of the subsamples was typically less than  $0.3 \text{ mSv/h}$  in contact. This allowed us to remove the subsample from the hot cell and to perform dissolution experiments including the samples in a specifically manufactured glove box.

### Dissolution of irradiated Zircaloy-4 specimens

Two types of digestion experiments were conducted with the irradiated Zircaloy-4 specimens. The first approach, dissolution of Zircaloy specimens in a glass

reactor, gives insight into the  $^{14}\text{C}$  inventory and the partitioning between total inorganic and organic/ $\text{CO}$   $^{14}\text{C}$ , whereas no information about the distribution of  $^{14}\text{C}$  bearing compounds in the aqueous and gaseous phase is obtained. Therefore, dissolution of Zircaloy specimens in an autoclave were additionally performed. The partitioning of  $^{14}\text{C}$  between inorganic and organic/ $\text{CO}$  compounds and their distribution between the aqueous and gaseous phase is obtained by these autoclave experiments. However, the autoclave experiments are much more elaborate/costly and time-consuming.

Three cladding samples (denoted as #1, #2, #3)) were digested in 16%  $\text{H}_2\text{SO}_4$  + 3% HF in a flask of the  $^{14}\text{C}$  extraction apparatus set-up in a specifically manufactured glove box and two cladding sample (denoted as #4 and #6)) were digested using an autoclave equipped with a glass liner and a gas collecting cylinder with two valves mounted on top. Sample #5 was digested in a glass beaker and analyzed by  $\gamma$ -spectroscopy and LSC to check before working that the radioactive inventory of the samples is within the regulatory limits for working in a glove box.

### Carbon-14 extraction and separation technique

The  $^{14}\text{C}$  extraction and separation technique used in this work is based on a method developed for determining  $^{14}\text{C}$  in spent ion exchange resins and process water from nuclear reactors [6-8], and allows to determine at the same time the total inorganic and total organic  $^{14}\text{C}$  content and thus the  $^{14}\text{C}$  inventory. The method was adapted for highly activated materials and particularly for gaseous samples derived from dissolution experiments with irradiated Zircaloy-4 specimens using autoclaves. The total inorganic/organic  $^{14}\text{C}$  analysis in aqueous and gaseous samples and simultaneous distinction of  $^{14}\text{C}$  bearing inorganic/organic compounds in solution and gas phase is a novel procedure for irradiated Zircaloy-4 analysis, developed and applied in this work.

The separation procedure of  $^{14}\text{C}$  from other radionuclides in aqueous and gaseous aliquots by stepwise extraction of the inorganic and organic carbon fractions by conversion into  $\text{CO}_2$  is outlined in Fig. 2.

The experimental set-up, shown in figure 3, consists of a three-neck flask with gas-inlet, dropping funnel

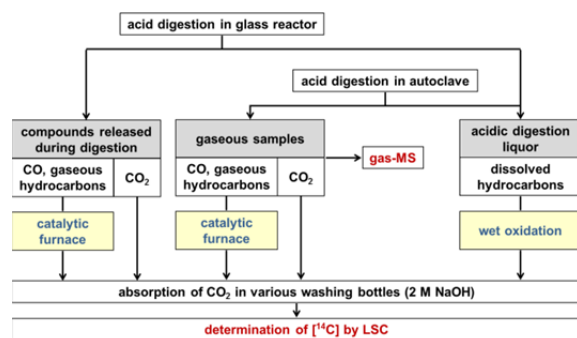


**Fig. 2:** Scheme of  $^{14}\text{C}$  extraction procedure for  $^{14}\text{C}$  bearing compounds released during digestion experiments performed in a glass reactor or autoclave.

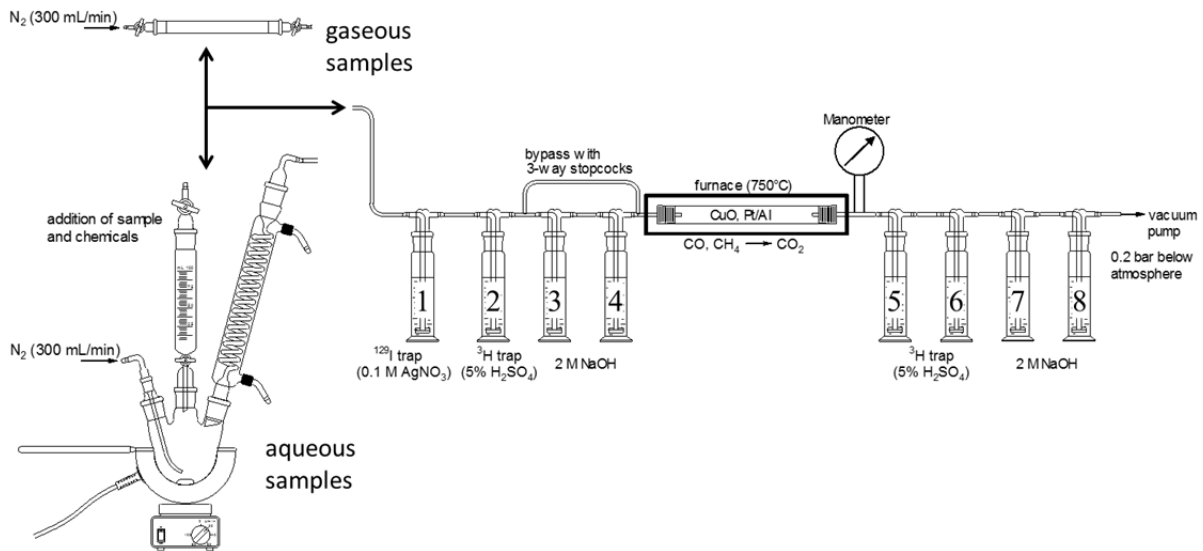


**Fig. 3:** Experimental design for  $^{14}\text{C}$  extraction from gaseous and aqueous aliquots obtained from dissolution experiments with irradiated Zircaloy-4.

and cooler or a gas collecting cylinder with two valves (SS-4CS-TW-50, Swagelok) connected to the  $\text{CO}_2$  extraction system.

The  $^{14}\text{C}$  extraction system consists of in total eight washing bottles. Four alkaline washing bottles for trapping  $\text{CO}_2/^{14}\text{CO}_2$ , three acidic and one silver nitrate washing bottles for tritium and iodine removal. A catalytic furnace between two sets of washing bottles ensures oxidation of reduced compounds (e.g.  $\text{CO}$ ,  $\text{CH}_4$ ).

Nitrogen is used as carrier gas and the system is operated under sub-atmospheric pressure to prevent the loss of any gases in the case of a leakage.

Finally, the content of  $^{14}\text{C}$  is analyzed by liquid scintillation counting.

### Activation calculation for Zircaloy-4 radionuclide inventory prediction

The activation of the Zircaloy-4 plenum cladding was calculated by means of the Monte Carlo N-particle code (version MCNP-X) with its burn-up and activation module CINDER [9]. The nuclear data library that was used was the ENDF/B-VII database [10]. The simulation is based on a fuel subassembly of the PWR Gösigen core in which the experimental fuel rod segment SBS1108-N0204 was inserted. Since the MCNP-X transport code evaluates the neutron flux of the subassembly, the input to the program includes geometrical shape and material composition of the fuel assembly, irradiation time, burn-up level, linear power rate to which the subassembly was exposed to. The obtained zone (material) and energy dependent fluxes are forwarded to the sub program CINDER within MCNP-X allowing for enhanced accuracy of the reaction rates evaluations upon which the activity of the relevant nuclides is determined. The properties of the plenum Zircaloy-4 (mass, density, dimension and stainless steel spring inside) were accounted for in

such a way that it will include as much as possible all heterogeneity effects around the fuel rod segment. Thereby, the local neutron flux within the plenum could be simulated more accurately.

Since the exact composition of the Zircaloy-4 cladding components used in the fuel rod segment about 25 years is not available, nominal chemical composition data were used for simulation of the neutron flux and consequently for the activation calculation.

### Results of experimental inventory analysis of irradiated Zircaloy-4 and chemical form of $^{14}\text{C}$ released from the studied material

Table 1 shows the results of the experimental inventory analysis obtained for each of the six Zircaloy-4 specimens. The experimentally determined activities of  $^{14}\text{C}$ ,  $^{55}\text{Fe}$  and  $^{125}\text{Sb}$  for each sample are in good agreement among themselves within the analytical. The results demonstrate the reliability of the  $^{14}\text{C}$  extraction and analysis method for both Zircaloy dissolution approaches (glass reactor/autoclave) used in this work.

Mean values of the experimentally determined inventories of  $^{14}\text{C}$ ,  $^{55}\text{Fe}$  and  $^{125}\text{Sb}$  are summarized in Table 2. These were further compared to the MCNP-X inventory calculations performed in the present study. Additionally, the  $^{14}\text{C}$  inventory was compared to Zircaloy-4 hull specimens of a similar PWR fuel rod studied by [11]. The experimental results obtained in this study for the inventory of  $^{14}\text{C}$ ,  $^{55}\text{Fe}$  and  $^{125}\text{Sb}$  are in very good agreement with the MCNP-X calculations within the uncertainties. The experimental  $^{14}\text{C}$  inventory exceeds the calculated value only by a factor of 1.2. In contrast, the experimental  $^{14}\text{C}$  inventory in irradiated stainless steel, recently assessed by [12], exceeds the calculated by a factor of four. Moreover, the  $^{14}\text{C}$  inventory is in good agreement with data of a similar PWR fuel rod hull specimen studied by [11].

**Tab. 1:** Results from LSC and  $\gamma$ -measurements obtained from the six Zircaloy-4 specimens.

sample no.	total $^{14}\text{C}$	$^{55}\text{Fe}$	$^{125}\text{Sb}$
	[Bq/g <sub>ZrV-4</sub> ]	[Bq/g <sub>ZrV-4</sub> ]	[Bq/g <sub>ZrV-4</sub> ]
#1	$3.9 (\pm 0.4) \times 10^4$	$1.3 (\pm 0.1) \times 10^5$	$2.6 (\pm 0.1) \times 10^5$
#2	$4.2 (\pm 0.4) \times 10^4$	ND	$2.4 (\pm 0.1) \times 10^5$
#3	$3.4 (\pm 0.3) \times 10^4$	ND	$2.5 (\pm 0.1) \times 10^5$
#4	$3.2 (\pm 0.3) \times 10^4$	ND	$2.3 (\pm 0.1) \times 10^5$
#5	ND	$1.7 (\pm 0.2) \times 10^5$	$2.5 (\pm 0.1) \times 10^5$
#6	$3.8 (\pm 0.4) \times 10^4$	ND	$2.2 (\pm 0.1) \times 10^5$

ND: not determined

**Tab. 2:** Mean values of the experimentally determined inventories of  $^{14}\text{C}$ ,  $^{55}\text{Fe}$  and  $^{125}\text{Sb}$  in comparison with results from the activation calculations performed in this study and experimentally measured  $^{14}\text{C}$  contents in a spent PWR Zircaloy-4 specimen with a similar burn-up [11].

Sample	segment SBS1108–N0204		fuel rod hull
BU (GWd/t <sub>HM</sub> )	50.4		47.9
Specific activity	measured	calculated	measured
$^{14}\text{C}$			
[Bq/g <sub>ZrV-4</sub> ]	$3.7 (\pm 0.4) \times 10^4$	$3.2 (\pm 0.3) \times 10^4$	$3.2 \times 10^4$
$^{55}\text{Fe}$			
[Bq/g <sub>ZrV-4</sub> ]	$1.5 (\pm 0.1) \times 10^5$	$1.3 (\pm 0.1) \times 10^5$	
$^{125}\text{Sb}$			
[Bq/g <sub>ZrV-4</sub> ]	$2.4 (\pm 0.1) \times 10^5$	$2.6 (\pm 0.1) \times 10^5$	

**Tab. 3:** Partitioning of  $^{14}\text{C}$  between total inorganic/organic fractions for each of the six samples.

sample no.	TIC-14	TOC-14
	[Bq/g <sub>ZrV-4</sub> ]	[Bq/g <sub>ZrV-4</sub> ]
#1	$9.5 (\pm 0.1) \times 10^1$	$3.9 (\pm 0.4) \times 10^4$
#2	$11.9 (\pm 0.1) \times 10^1$	$4.2 (\pm 0.4) \times 10^4$
#3	$11.8 (\pm 0.1) \times 10^1$	$3.4 (\pm 0.3) \times 10^4$
#4	$6.2 (\pm 0.1) \times 10^1$	$3.2 (\pm 0.3) \times 10^4$
#5	ND	ND
#6	$10.4 (\pm 0.1) \times 10^1$	$3.8 (\pm 0.4) \times 10^4$

Table 3 shows the partitioning between the total inorganic and organic  $^{14}\text{C}$  fractions for each of the six analyzed samples. Again, the results obtained for each sample are in good agreement among themselves within the analytical uncertainty, and virtually no differences are seen for the two Zircaloy dissolution approaches used in this study (glass reactor/autoclave). In all experiments, the vast majority of  $^{14}\text{C}$  is found in the organic/CO fraction, whereas almost no inorganic  $^{14}\text{C}$  is found.

Moreover, the autoclave experiments provide additional information about the distribution of the inorganic/organic  $^{14}\text{C}$  compounds released during the acid digestion into the aqueous and gaseous phases. The partitioning of  $^{14}\text{C}$  bearing compounds in inorganic and organic fractions and furthermore the distribution

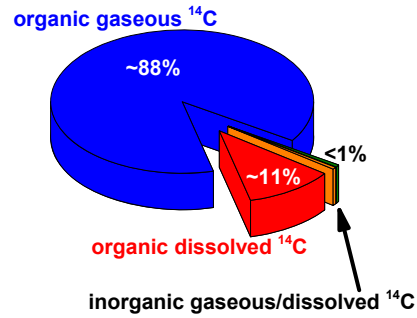


**Fig. 4:** Distribution of inorganic and organic  $^{14}\text{C}$  bearing compounds in the gaseous and aqueous phase

of these fractions in the gaseous and aqueous phase is provided in Fig. 4.

About  $88 \pm 10\%$  of the  $^{14}\text{C}$  inventory present in irradiated Zircaloy-4 is released as gaseous  $^{14}\text{C}$  bearing compounds during the dissolution into the gas phase. On the contrary, about  $11 \pm 10\%$  remains as dissolved organic compounds in the acidic digestion liquor. Almost no inorganic  $^{14}\text{C}$  bearing compounds ( $< 1\%$ ) are found in all experiments (glass reactor and autoclave) neither in the gaseous nor in the aqueous phase.

## References

- [1] Neeb, K.H. The radiochemistry of nuclear power plants with light water reactors. (de Gruyter, Berlin) (1997).
- [2] Bailly, H. et al. The nuclear fuel of pressurized water reactors and fast reactors: design and behaviour. (Lavoisier Publishing, Paris) (1999).
- [3] Rudling, P. et al., Advanced Nuclear Technology International (2007).
- [4] Magill, J. et al., Report EUR 22276 EN (2006).
- [5] Gras, J.-M. CAST-D3.1 deliverable (2014).
- [6] Magnusson, A., Stenstroem, K. LUNFD6/(NFFR-3097) (2005).
- [7] Magnusson, A., Ph.D. thesis, Lund University (2007).
- [8] Magnusson, A. et al., *Radioanal. Nucl. Ch.* **275**, 261-273 (2008).
- [9] MCNP-X. Los Alamos National Laboratory, LA-UR-11-1502 (2011).
- [10] ENDF/B-VII. Nucl. Data Sheets, 112, 2887-3152 (2011).
- [11] Yamaguchi, T. et al., Proceedings of the 7th International Conference on Environmental Remediation and Radioactive Waste Management - ICEM 1999, Nagoya, Japan (1999).
- [12] Schumann, D. et al., *Anal. Chem.* **86**, 5448-5454 (2014).

## Acknowledgement

The research was partially funded by the European Union's Seventh Framework Program for research, technological development and demonstration under grant agreement no. 604479, the CAST project.

## 5.2 Non-heat producing waste forms and barrier materials

*E. Bohnert, Ch. Borkel, B. Kienzler, V. Metz, N. Finck, Th. Rabung, M. Schlieker, M. Wiedemann*

### Introduction

Basic understanding of the long-term behavior of non-heat producing waste forms and barrier materials require the development and application of specific numerical tools. The reliability of such tools needs to be tested by comparison of modelling results with experimental findings. For this reason, efforts were made providing reasonable experimental databases for this kind of comparisons. The results presented in this chapter cover

- Long-term interactions of full-scale cemented waste simulates in salt brines.
- Characterization of solids, groundwater and gas sampled from rocks overlaying the Asse II salt mine.
- Actinide retention by solid phases in the system  $\text{Mg}^{2+}$ - $\text{Na}^+$ - $\text{Cl}^-$ - $\text{OH}^-$ - $(\pm\text{CO}_2)$ - $\text{H}_2\text{O}$ .

### Long-term interactions of full-scale cemented waste simulates in salt brines

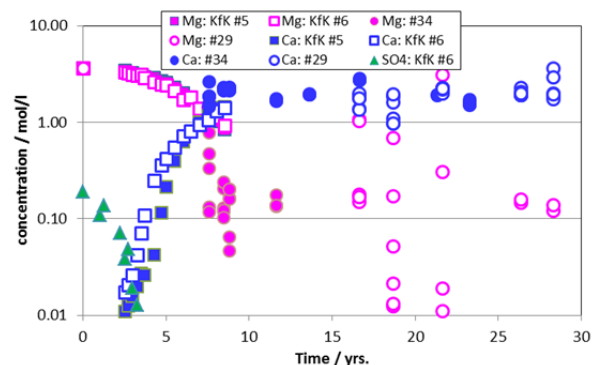
Between 1967 and 1978 low and intermediate level radioactive waste products were disposed of in the Asse II salt mine in Northern Germany. A significant part of these wastes originated from the pilot reprocessing plant Wiederaufarbeitungsanlage Karlsruhe and consisted of cemented  $\text{NaNO}_3$  solutions bearing fission products, actinides, as well as process chemicals. With respect to the long-term behavior of these wastes, the licensing authorities requested leaching experiments with full scale samples in relevant salt solutions which were performed between 1979 and 2013. These long-term experiments aimed on demonstration of the transferability of results obtained by laboratory samples to real waste forms and on the investigation of the effects of the industrial cementation process on the properties of the waste forms. The full-scale experiments at Asse II salt mine were performed at a temperature of  $28 \pm 1^\circ\text{C}$  defined by the ambient conditions depth of 490 m below ground. At the nuclear research centre Karlsruhe (KfK, today KIT), leaching and corrosion of simulated and of real full-scale cemented wastes were investigated using similar leachates at a temperature of  $40^\circ\text{C}$ .

In all experiments with initially  $\text{MgCl}_2$ -rich leachants, the Ca-Mg exchange was considered as measure of the corrosion progress. Fig. 1 shows the temporal evolution of the  $\text{Ca}^{2+}$  and  $\text{Mg}^{2+}$  concentrations in the leachates of the full-scale blocks leached at  $40^\circ\text{C}$  (KfK #5 and KfK #6, both W/C ratio 0.44 l/kg) and at  $28^\circ\text{C}$  (#29, WC = 0.43 l/kg and #34, W/C = 0.5 l/kg). Samples #5 and #6 were leached over a period of 8.5 years. The decrease of the  $\text{Mg}^{2+}$  concentration and the corresponding increase of  $\text{Ca}^{2+}$  is clearly shown. After about 7.5 years, the concentrations (mol/l) intercepted. The  $\text{Ca}^{2+}$  and  $\text{Mg}^{2+}$  concen-

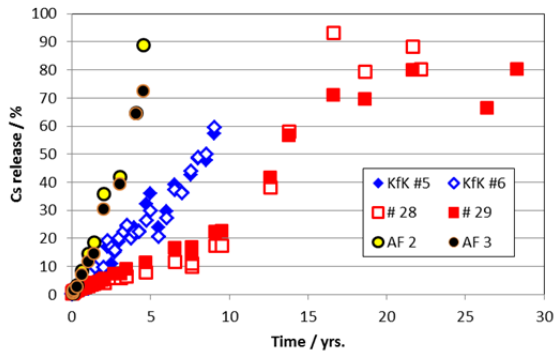
trations in the leachates of the full-scale blocks #29 and #34 were not measured in the beginning of the experiments; measurements started after 7.6 years. These data show some scatter until 28 years, but the same tendency is obvious as in the case of the experiments KfK #5 and #6. At  $28^\circ\text{C}$  and  $40^\circ\text{C}$ , the Mg concentration is very low after about 10 years which means that the Ca-Mg exchange reaction was almost complete. For blocks #29 and #34, the sulfate concentrations were measured after ~16 and 11 years, respectively, the  $\text{SO}_4^{2-}$  concentrations were below 0.01 mol/l. Unfortunately, the evolution of the pH of the leachates of blocks KfK #5 and #6 is not available, anymore.

Fig. 1 shows clearly that the Ca-Mg exchange processes were not affected by the temperatures in the range from  $28^\circ\text{C}$  and  $40^\circ\text{C}$ . A different observation was obtained for the diffusive cesium release. Fig. 2 shows the Cs mobilization as function of time for three types of full-scale cemented waste forms exposed to  $\text{MgCl}_2$  solution: #28 and #29 the full-scale simulates leached at  $28^\circ\text{C}$ , KfK #5 and #6 full-scale simulates leached at  $40^\circ\text{C}$  and AF2 and AF3 real waste forms leached at  $40^\circ\text{C}$ . The real cemented waste forms AF2 and AF3 were prepared with a W/C ratio of 0.65 l/kg.

Fig. 2 shows the release of cesium as function of time from the 3 types of full-scale cemented blocks exposed to  $\text{MgCl}_2$  solution. The Cs mobilization from simulated blocks stored at  $40^\circ\text{C}$  was faster in comparison to the release under  $28^\circ\text{C}$ . After 9 years, 60 % of the initial Cs content was released at  $40^\circ\text{C}$ , a level reached only after ~14 years at  $28^\circ\text{C}$ . In the case of the radioactive waste forms this level of release was achieved already after 4 years and after 4.5 years, about 90% of the Cs inventory was found in the leachate. This high level of Cs mobilization was reached only after 15 years for the blocks #28 and #29. The real waste forms, however, had a distinctly



**Fig. 1:** Comparison of the Ca and Mg concentrations as function of time in experiments #29 and #34 at the Asse II salt mine ( $28 \pm 1^\circ\text{C}$ ) and in experiments at KIT / KfK #5 and KfK #6 ( $40^\circ\text{C}$ ). The initial Mg concentrations of the leachates were identical.



**Fig. 2:** Cs mobilization as function of time from simulated and real full-scale cemented waste forms exposed to  $MgCl_2$  solution. Red squares: Full-scale blocks #28 and #29 at  $28^\circ C$ , W/C ratio 0.43 l/kg; blue diamonds: Inactive blocks KfK #5 and #6 at  $40^\circ C$ , W/C ratio 0.44 l/kg; black circles: Real radioactive cemented waste forms AF2 and AF3 at  $40^\circ C$ , W/C ratio 0.63 l/kg.

higher W/C ratio which gave rise to the accelerated exchange processes.

Fig. 2 also shows that after 5 years in the case of the blocks KfK #5 and #6 and after 10 years for #28 and #29 the slope of the release curves change. This change which cannot be seen for AF2 and 3 indicate the formation of cracks and a correlated increase of exposed surfaces.

An important conclusion from the long-term experiments is that the durability of cemented waste forms depends on the porosity (W/C ratio) and on the type of the attacking solution.  $MgCl_2$  solution is significantly more corrosive than NaCl solution. In  $MgCl_2$ -rich solution, cement products with W/C ratios ( $> 0.4$  l/kg) typical for real waste forms corrode within about 15 years. In this time, a geochemical equilibrium is established between the attacking solutions and the solids (corrosion products). Depending on the (volume) ratio of cement to the solution, the Ca-Mg exchange occurs, the pH increases, magnesium precipitates and results in a calcium-dominated solution. In the case of the contact to NaCl solutions, the ongoing reactions of the cement products are scarcely affected by their porosity. The pH of the NaCl solution rises within months to a constant value (portlandite buffering) and does not change in the long-term.

### Characterization of solids, groundwater and gas phase of rock formation overlaying the Asse II salt mine

To perform sorption studies with the overburden rocks of the Asse II salt mine, the application of a natural groundwater was requested by Federal Office of Radiation Protection (BfS). The groundwater should be typical for the highly relevant rock layers of the Lower Triassic Röt formation. To obtain the water, groundwater sampling was performed at the monitoring well GW-023. The concept of sampling was developed and implemented by Asse GmbH. KIT-INE received water from a depth of about 200 m below ground. Two types of sampling techniques

were applied: Sampling by pumping and sampling by sinking autoclaves to a depth of 200 m. Both types of samples were analyzed with respect to the composition and properties of the groundwater. The groundwater contained Ca (13 mmol), Mg (8 mmol)  $SO_4$  (20 mmol), and NaCl (10 mmol). pH was 7.07 and Eh = 261.1 mV SHE. Particular attention was given to the  $CO_2$  content of the groundwater sampled in the autoclaves.

The autoclaves were filled at the level of 200 m below ground. It was assumed that the dissolved gas was in equilibrium with the prevailing hydrostatic pressure at this depth. In the laboratory, the autoclaves were connected to evacuated gas sampling containers and the valves were opened and the gas phase expanded. However, the release of dissolved gas was kinetically controlled. For this reason, the gas sampling was extended for several days. Gas mass spectrometry was applied for the analyses.  $CO_2$  concentrations in the gas phase between 5 and 22 % were found. Under consideration of the sample volumes and the system pressures the concentrations were converted to the mass of dissolved  $CO_2$ , amounting to 4.5 mmol/l groundwater. This value corresponds well with measured TIC values.

By means of model calculations, the speciation of the carbonate and the  $CO_2$  partial pressure was determined. Solid calcite was assumed to be present. The  $Ca^{2+}$  concentration in the groundwater is controlled by calcium sulfate at a concentration of 15 mmol/l.

$[Ca^{2+}]$  was by a factor of 4 above the equilibrium concentration in the presence of calcite. Fig. 3 shows that  $[Ca^{2+}]$  remains constant independently on the pH. The same is true for  $[CO_3^{2-}]$  which remains also constant for  $pH > 6.3$ . This result is of high importance for the planned sorption experiments: The concentration of carbonate which could form complexes especially with the actinides is independent on the pH and on the actual  $CO_2$  fugacity in the systems consisting of the overlaying rocks and the groundwater.

As it was not clear from the beginning of these investigations, whether natural groundwater could be sampled at the monitoring well GW-023, a backup procedure was considered. Pure water was equilibrated with the relevant rock materials. The following

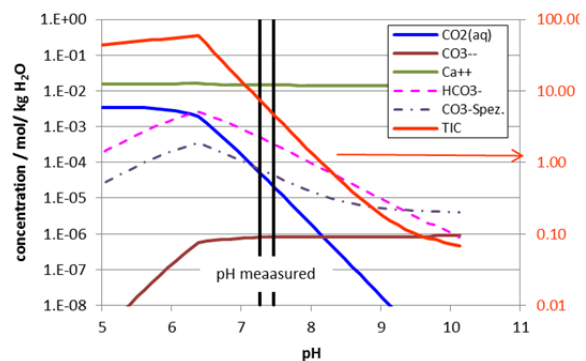


**Fig. 3:** Calculated carbonate species distributions (and  $Ca^{2+}$ ) in groundwater GW-023 as function of the pH. Calculated total inorganic carbon (TIC) is also shown (right axis).

**Tab. 1:** Comparison between natural groundwater GW-23 and the equilibrated solid-water systems at comparable depths.

	equilibrium		Natural water	
Layer	Röt 4 006_KIT	Röt 3 007_KIT	GW-023	units
Depth	173.8	225.5	230.0	m
Ca <sup>2+</sup>	525.4	590	500.4	mg/kg
Mg <sup>2+</sup>	60	99.7	201	mg/kg
Na <sup>+</sup>	376.8	194.3	307.5	mg/kg
K <sup>+</sup>	106	166.6	21.06	mg/kg
Fe <sup>3+</sup>	0.1	0.1	0.3	mg/kg
Al <sup>3+</sup>	< NGW	< NGW	0.002	mg/kg
SO <sub>4</sub> <sup>2-</sup>	2383	2182	1946.1	mg/kg
Cl <sup>-</sup>	142.9	280	324.5	mg/kg
F <sup>-</sup>	2.8	2.2	1.8	mg/kg
NO <sub>3</sub> <sup>-</sup>	1.5	1.3	< NGW	mg/kg

table (Tab. I) compares the cation and anion concentrations of the natural groundwater GW-23 with the equilibrated rock-water system 006\_KIT and 007\_KIT. These rocks originated from a similar depth as the groundwater GW-23. The concentrations of the matrix elements agree reasonably. One may conclude that such an equilibrated solution could sufficiently well mimic the natural groundwater.

### Retention of trivalent actinides by stable and metastable solid phases in the system Mg<sup>2+</sup>-Na<sup>+</sup>-Cl<sup>-</sup>-OH<sup>-</sup>(±CO<sub>2</sub>)-H<sub>2</sub>O

Intrusion of aqueous solutions into a repository for nuclear waste cannot be excluded in the long-term, although geological and geotechnical barrier systems may prevent ground water from contacting the waste. In a disposal system in a rock salt formation, solutions are characterized by high ionic strengths, mostly dominated by high [Na<sup>+</sup>], [Mg<sup>2+</sup>] and [Cl<sup>-</sup>] concentrations. Suitable geotechnical barrier materials like Mg<sup>2+</sup>/OH<sup>-</sup>-bearing solids are considered, providing for buffering the pH and limiting the aqueous carbonate concentration. Anoxic container corrosion leads to strongly reducing conditions in deep geological repositories, thereby actinides are expected to prevail in tri- / tetravalent redox states, e.g. Am(III), Cm(III), Pu(III/IV), Np(IV), U(IV).

For the Asse II salt mine (Lower Saxony, Germany) and the repository for radioactive waste Morsleben (ERAM, Saxony-Anhalt, Germany) brucite Mg(OH)<sub>2</sub>(cr) (Brc) or magnesium oxychloride (MOC) cement Mg<sub>2</sub>(OH)<sub>3</sub>Cl·4H<sub>2</sub>O(cr) frequently called Sorel cement is considered. In the Waste Isolation Pilot Plant (WIPP, New Mexico, USA), where low / intermediate level radioactive waste products are emplaced, periclase MgO(cr) is used as geochemical buffer material [1]. This material will be transformed in Mg(OH)<sub>2</sub>(cr) [2]. In NaCl or MgCl<sub>2</sub> dominated brines, Mg(OH)<sub>2</sub>-based materials buffer at  $pH_m$  of about 9 and scavenges carbonate, potentially produced by microbial degradation of organic waste constituents [3].

In case of contact of MgCl<sub>2</sub>-rich solutions with CO<sub>2</sub> / CO<sub>3</sub><sup>2-</sup>, long-term metastable hydroxo(chloro) carbona-

to (hydromagnesite Mg<sub>5</sub>(OH)<sub>2</sub>(CO<sub>3</sub>)<sub>4</sub>·4H<sub>2</sub>O (H-Mgs) and chlorartinite Mg<sub>2</sub>(OH)CO<sub>3</sub>Cl·3H<sub>2</sub>O) phases (Cl-Art) will be formed (Fig. 1). These phases provide also for retention of Am(III) and Cm(III) in MgCl<sub>2</sub> and NaCl containing solutions (± Na<sub>2</sub>CO<sub>3</sub>) ( $I = 0.15 - 15$  molal), at room temperature. In presence of brucite and Mg-oxychloride, the specific  $pH_m$  values are buffered in a range of  $8.8 \leq pH_m \leq 9.3$ . For H-Mgs and Cl-Art the  $pH_m$  values decrease with the precipitation of the solid phase to  $8.4 \pm 0.1$ .

For the sorption experiments the MgCl<sub>2</sub> / NaCl solutions equilibrated with the solids under investigation were doped with [<sup>241/243</sup>Am] ≤ 6.7·10<sup>-7</sup> mol·L<sup>-1</sup> or with 1·10<sup>-7</sup> mol·L<sup>-1</sup> curium. The latter element allowed the investigation of Cm(III) speciation by Time-Resolved Laser Fluorescence Spectroscopy (TRLFS). The method could be applied to the doped sorption / co-precipitation samples consisting of Brc, MOC, H-Mgs and Cl-Art. The investigation of samples formed by co-precipitation or by recrystallization processes and the combination of spectroscopic analyses with sorption studies revealed a better understanding of the retention mechanism of actinides onto these solids.

Brucite was purchased from Fluka, MOC, H-Mgs and Cl-Art were synthesized and characterized by Raman spectroscopy, SEM-EDX, TGA-DSC and XRD. The molar  $H^+$  concentration of the suspensions was determined with combination pH electrodes (Orion Ross, Thermo Scientific). To convert the operational measured  $pH_{exp}$  values, the approach of Altmaier et al. [4] was applied. [<sup>241/243</sup>Am] and [Cm] were determined by LSC (Quantulus) and by  $\gamma$ -counting. Cm(III) fluorescence spectra were collected using a Nd:YAG laser (Continuum Surelite II 10 Hz) pumping a dye laser (Narrowscan Dye Laser, Radiant Dyes).

A strong retention of americium was observed in brucite / MgCl<sub>2</sub> ± NaCl batch experiments ( $0.15 \leq I \leq 5.2$  molal) within 2 days. A log K<sub>D</sub>(Am) of  $5.4 \pm 0.3$  L·kg<sup>-1</sup> (> 99 % uptake) was determined. Only a weak ionic strength effect on the retention ( $0.1 - 0.2$  log K<sub>D</sub> values) was observed. The retention of curium on Mg(OH)<sub>2</sub>-based materials was measured applying sorption and co-precipitation experiments. For all

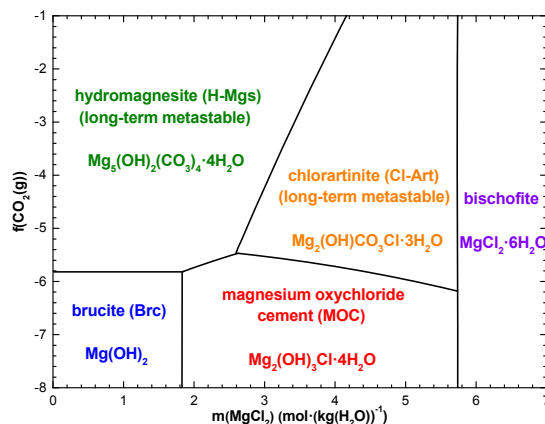


**Fig. 4:** Stability field of stable and metastable solids in the system Mg<sup>2+</sup>-Na<sup>+</sup>-Cl<sup>-</sup>-OH<sup>-</sup>(±CO<sub>2</sub>)-H<sub>2</sub>O ( $0 \leq I \leq 15$  molal).

solid phases a significant retention of  $\log K_D(\text{Cm}) = 3.1 - 5.4 \pm 0.5 \text{ L} \cdot \text{kg}^{-1}$  was determined. The retention decreased in following order:  $\text{Brc}_{\text{cop}} \approx \text{Brc}_{\text{sorp}} \gg \text{H-Mgs} \approx \text{Cl-Art} > \text{MOC}$  (from  $> 99\%$  to  $\leq 40\%$  uptake).

Long-term sorption / co-precipitation experiments with Cm onto Brc, MOC, H-Mgs and Cl-Art in the  $\text{MgCl}_2$ -rich solutions were monitored by TRLFS at periods between 30 minutes up to 318 d, respectively (exemplary spectra are shown Figure 2). The emission spectra of all systems show significant red shift towards the Cm aqua ion indicating a serious change of the first coordination sphere of curium. The emission spectra for Cm sorption onto brucite showed a decreasing red-shifted peak (from 609.2 nm to 606.2 nm with a shoulder at 609.7 nm) within 318 and 278 d, respectively. For co-precipitation experiments with brucite the same phenomena were observed (decreased peak from 611.3 nm to 609.0 nm). Due to the strong sorption, dissolved Cm species were not found. In the case of MOC sorption experiments a red-shifted peak to 603.8 nm was found as well as dissolved Cm (chloro and hydroxo) species.

With increasing ionic strength, a stronger red-shift was observed (increase from 601.4 nm to 603.7 nm). Samples with H-Mgs and Cl-Art showed various red-shifted peak up to 614.1 nm within 60 d. A (carbonato) solution species was identified. With increasing ionic strength, the peak positions hardly change. For Brc, H-Mgs and Cl-Art incorporation species were identified by long fluorescence lifetimes ( $\gg 210 \mu\text{s}$ ). These long lifetimes indicate a low  $\text{H}_2\text{O}$  content in the first coordination sphere of curium (1.2 to 2.8  $\text{H}_2\text{O}$  molecules) which is typical for an inner-sphere sorption surface complex. Thermodynamically stable (Brc, MOC) and long-term metastable (H-Mgs, Cl-art) solids showed significant retention of trivalent actinides in saline systems.

## References

- [1] Brush, L.H. et al., Denver Annual Meeting, Geological Society of America, 36, 296 (2004).

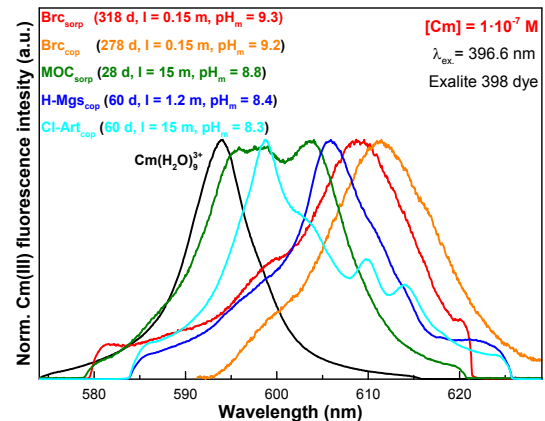


**Fig. 5:** Cm(III)-TRLFS emission spectra of  $\text{Mg}(\text{OH})_2$ -based materials in  $\text{MgCl}_2$ -rich solutions ( $0.15 \leq I \leq 15$  molal) at different interaction times.

- [2] Schüssler, W. et al., *Geochim. Cosmochim. Acta suppl.*, Goldschmidt Conference Abstracts, Davos, Switzerland, A690 (2002).
- [3] Monastra, V., Grandstaff, D.E., *Mat. Res. Soc. Symp. Proc.* **556**, 625-632 (1999).
- [4] Metz, V. et al., *Radiochim. Acta.* **92**, 819-825 (2004).
- [5] Altmaier, M. et al., *Geochim. Cosmochim. Acta* **67**, 3595-3601 (2003).

## Acknowledgements

Studies on long-term interactions of full-scale cemented waste simulates in salt brines project were funded by the Federal Ministry of Education and Research (Bundesministerium für Bildung und Forschung) under contract 02ALVF2012. Characterization of solids, groundwater and gas phase of rock formation overlaying the Asse II salt mine was funded by the Federal Office of Radiation Protection (BfS).

## 5.3 Colloid impact on radionuclide migration

M. Bouby, G. K. Darbha, L. Delavernhe, F. Friedrich, M. Fuß, H. Geckeis, F. Geyer, R. Götz, S. Heck, S. Hilpp, F. Huber, F. Rinderknecht, T. Schäfer, M. Stoll, C. Walschburger

In co-operation with:

I. Blechschmidt<sup>a</sup>, K. Emmerich<sup>b,c</sup>, B. Lanyon<sup>d</sup>, A. Martin<sup>a</sup>, K. K. Norrfors<sup>e</sup>

<sup>a</sup>NAGRA, Wettingen, Switzerland, <sup>b</sup>Competence Center for Material Moisture (CMM), <sup>c</sup>Institute of Functional Interfaces (IFG), Karlsruhe Institute of Technology, Hermann-von-Helmholtz-Platz 1, D-76344 Eggenstein-Leopoldshafen, Germany, <sup>d</sup>Fracture Systems Ltd., St. Ives, UK, <sup>e</sup>KTH Royal Institute of Technology, Stockholm, Sweden

Long term safety is the pre-requisite to any deep geological nuclear waste repository (DGR). Performance assessment (PA) has to consider which parameters to take into account for reliable predictions.

Aquatic colloids (particles having at least in one direction a dimension between 1 and 1000 nm) are ubiquitous (up to  $10^6$  part./mL in surface fresh waters) and continuously generated by multiple physico-chemical processes (*inter alia* erosion, nucleation/ precipitation ...) [1]. To be considered as a relevant safety issue concerning radionuclide (RN) transport, these colloids have to be stable, mobile and to interact irreversibly with the RNs potentially released. Besides acting as a transport vehicle for contaminants colloid release/ bentonite buffer erosion is also an issue with respect to the long-term integrity of the geo-engineered barrier. Our aim is to identify if colloids have to be considered in PA and defining the boundary conditions for the colloid relevance. Our activities concentrate on two main colloid sources: the bentonite backfill material and the naturally organic matter (OM) present in clay formations as the Boom Clay.

The intrinsic properties of colloids released from the bentonite buffer have to be studied in comparison to the fundamental properties of clay colloid suspension, which have been characterized in numerous peer-reviewed publications in the literature. The idea behind this approach is to what extend the intrinsic properties of montmorillonite colloids (fundamental particles) might govern those of the bulk material. Stability of organic and inorganic

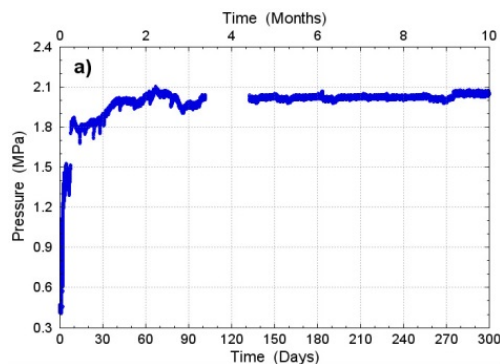


**Fig. 1:** Time-dependent swelling pressure measured in a compacted bentonite ring (Nanocor product) emplaced at a dry density of  $1400 \text{ kg/m}^3$ .

colloids are studied in details as a function of the pH, ionic strength and water chemistry composition, over short and long time periods, especially in the frame of the *Kolorado-e* and *BELBaR* (<http://www.skb.se/belbar>) projects. RNs sorption and reversibility studies are on-going, under realistic conditions, i.e. by contacting the RNs to the clay colloids under clay pore water conditions prior to any desorption test (PhD work of F. Rinderknecht), and by examining the potential effect of the multimodal clay colloid size distribution on their own stability [2, 3] and their RNs (de)sorption properties [4, 5]. Migration processes are investigated in the laboratory by looking at the deposition of colloids onto mineral surfaces or *in-situ* at the Grimsel Test Site (GTS, [www.grimsel.com](http://www.grimsel.com)) by following the release of colloidal material and radionuclides of a compacted bentonite source in the so-called Long-term In-situ Test (LIT) of the Colloid Formation and Migration (CFM) project or investigating radio-tracer migration tests in presence of clay colloids, under real conditions.

### Bentonite erosion experiments

**Benchmark Test.** Bentonite erosion experiments have been an important component within the *Kolorado-e* and *BELBaR* projects. In the framework of the *BELBaR* project *inter alia* an artificial fracture benchmark erosion test was conducted by several partners using a commercial sodium montmorillonite product (Nanocor, PGN grade) emplaced at a dry density of  $1400 \text{ kg/m}^3$  using the set-ups favored by the different partners. Although different in

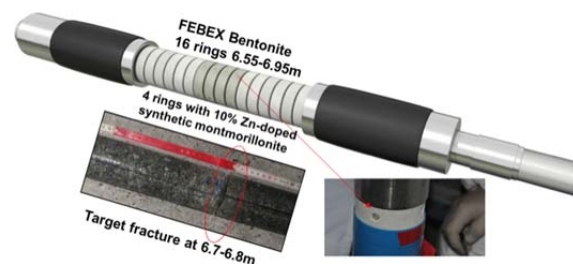


**Fig. 2:** Schematic overview of the LIT packer system emplaced in the MI shear zone showing the compacted bentonite ring set-up and the glass vials emplaced with the radionuclide/Amino-G doped slurry.

geometry a fixed fracture aperture of 0.1 mm was used in all laboratories. Experiments were carried out in three subsequent phases: I) stagnant conditions (no flow), II) low-flow conditions ( $\sim 10^{-6}$  m/s) and III) high-flow conditions ( $\sim 10^{-4}$  m/s) using 1 mM NaCl solution. The cell at INE was equipped with a pressure sensor, measuring the swelling pressure on top of the bentonite ring. The swelling pressure rapidly increased to 1.85 MPa within the first ten days (Fig. 1) and levelled off to a plateau value of 2.05 MPa after 65 days remaining constant over the entire experimental duration. This swelling pressure is slightly above the approx. 1 MPa (10 bar) expected for bentonites, but still within the uncertainty limits, based on the regression fit found in Agus & Schanz [Fig. 5 in 6].

*Grimsel Test Site activities.* In the course of the LIT experiment within the CFM project at the GTS, a bentonite source was emplaced in a water conducting feature. The bentonite plug consists in total of 16 compacted bentonite rings. 12 rings are composed of pure Febex bentonite and 4 rings in contact with the shear zone produced with a 10% admixture of synthetic Zn-labeled montmorillonite [7]. In all four Zn-/Febex bentonite rings glass vials were emplaced with a Ni- montmorillonite [8] slurry doped with a cocktail of radionuclides ( $^{45}\text{Ca}$ ,  $^{75}\text{Se}$ ,  $^{99}\text{Tc}$ ,  $^{137}\text{Cs}$ ,  $^{233}\text{U}$ ,  $^{237}\text{Np}$ ,  $^{241}\text{Am}$ ,  $^{242}\text{Pu}$ ) and a conservative tracer (Amino G). The packer system was emplaced in the shear zone in May 2014.

This experiment allows the determination of bentonite erosion rates under glacial melt water conditions in a real fracture and hydraulic conditions comparable to the repository post closure phase. Another aspect is the mobilization of bentonite colloids and radionuclides being initially a part of the compacted bentonite over a considerable time frame. This experiment combines for the first time in-situ colloid generation with radionuclide interaction and migration in an advection dominated natural shear zone under well-controlled low flow groundwater conditions over a length of  $\sim 6\text{m}$ .

Geochemical and hydro-mechanical parameters are monitored continuously on-site with the digital acquisition system (DAS) as volumetric flow velocity, pH,  $E_h$ , specific conductivity, fluorescence signal of the effluent (conservative tracer) and swelling pressure of the bentonite source at different locations within the packer system. Samples are taken from the surface packer at the tunnel wall (Pinkel) and from an observation borehole close to the bentonite source (distance:  $\sim 10\text{ cm}$ ). The later samples are taken at a flow rate of  $50\mu\text{L}/\text{min}$  with a fraction collector in head-space vials emplaced inside an Argon glovebox to keep Eh/pH conditions constant. All samples taken are transferred to KIT/INE and analyzed off-site to monitor in addition to the DAS data potential changes in pH, conductivity and fluorescence signal during transfer. The main objective of the sample analysis was however the measurements concerning the mean

colloid size and concentration via LIBD (laser induced breakdown detection) and colloid size distribution (s-curve LIBD) and the water chemistry analysis (ICP-MS, IC) and radionuclide analysis (ICP-MS, SF-ICP-MS, AMS, LSC and  $\gamma$ -spectroscopy).

After 100 days, the conservative tracer (Amino G) was detectable by fluorescence measurements and its concentration steadily increased (see Fig. 3) while pH was considerably lower in the near-field with pH 9.1 compared to the Grimsel groundwater usually showing pH  $\sim 9.6$ . Both parameters are very comparable to the in-line on-site DAS- measurements. The total mass of conservative tracer released currently corresponds to approx. 0.4% of the total source term mass.

Radiochemical investigations only found  $^{99}\text{Tc}$  in the effluent samples. Technetium was introduced as Tc(VII) in the source and shows a release very comparable to the conservative tracer AGA indicating the absence of Tc(IV) in line with the Eh values measured in the near-field (around -100 to 100 mV). Assuming that the Zn and Al concentrations above the background level are directly originating from bentonite colloids, colloid concentrations range between 1-2 mg/L colloids (acc. to the Al signal) and 1.5-3 mg/L colloids (acc. to the Zn signal) in the effluent samples and an increase with time as also validated by LIBD. The mean colloid size is around 60 nm and steadily increasing. Dis-

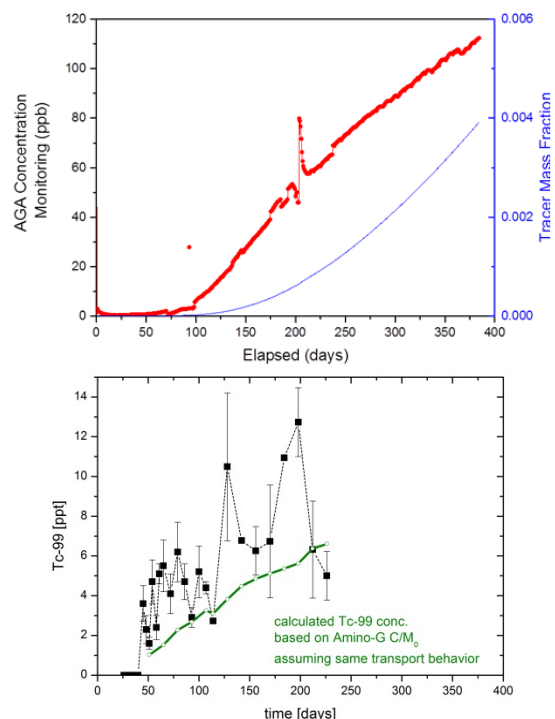


**Fig. 3:** (upper graph) Time dependent conservative tracer Amino-G (AGA) concentration evolution and total mass released from source. (lower graph) Tc-99 concentration measured in the LIT samples taken from borehole CFM- 11.002.i02 and for comparison estimated Tc-99 concentration based on conservative tracer release (green line).

proportionately high Mg concentrations and reversed Mg/Al-ratios in the effluent samples compared to the background level along with decreasing Ca concentrations suggests cation exchange reactions taking place. Constant and elevated sulphate release of ~15 mg/L over the last 350 days indicates that sulphate reducing bacteria (SRB) have not been active so far. Monitoring is still on-going and samples are analyzed by AMS for trace actinide concentrations.

### Influence of mineralogical and morphological properties on the cation exchange behaviour of dioctahedral smectite < 0.2 $\mu$ m

A fundamental understanding of the dioctahedral smectite properties is the prerequisite for assessing the bentonite behavior. Intrinsic properties of smectite, combined with the process parameters, determine the resulting behavior. The aim of this study was to investigate how the structure and morphology govern the smectites' properties (Fig. 4) [9].

Na-saturated dioctahedral smectites <0.2  $\mu$ m separated from bentonites of different origin were characterized in detail with respect to their structure (layer charge, octahedral cation distribution, iron content, and layer charge distribution within tetrahedral and octahedral sheets). Furthermore, reduced charge materials (RCM) obtained after heating Li-saturated subsamples at 300  $^{\circ}$ C were studied. Particle dimension was estimated from argon adsorption, calculation of specific surface area and direct observation of single layers by atomic force microscopy (AFM), which also revealed morphology and particle size distribution of single layers. The cation exchange capacity (CEC) was measured both for Na-saturated samples and RCM using the Curi method over a pH range of 4 to 9.

The studied smectites belong to the montmorillonite-beidellite series [10]. The smectite from Wyoming (MX-80) with a mean layer diameter of 277 nm and a low layer charge of 0.26 eq/f.u. (equivalent per formula unit) differed strongly from the other smectites with a mean layer diameter of about 100 nm and layer charges between 0.30 and 0.37 eq/f.u.. Furthermore, the layer stacking was much higher for the smectite from Wyoming with about 15 layers against 7 layers for the other smectites.

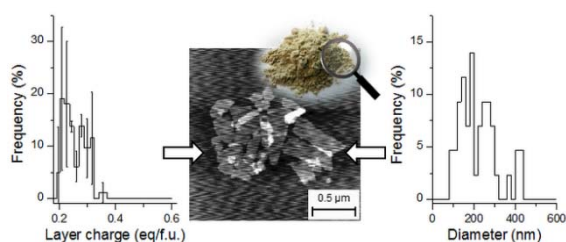


**Fig. 4:** Mineralogical (here layer charge) and geometrical properties (diameter) of smectite governing their material properties.

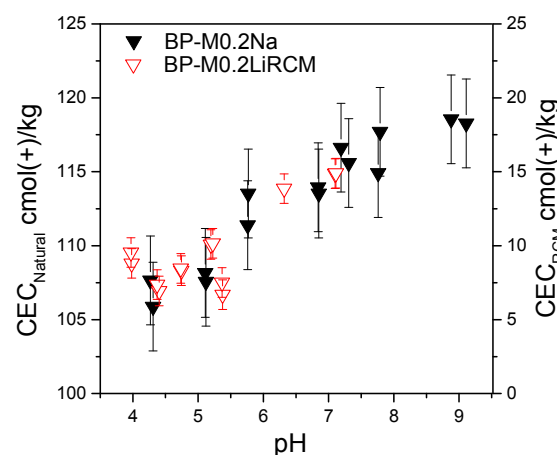


**Fig. 5:** CEC of natural clay material and reduced charge material (RCM) as a function of pH.

The edge surfaces ( $a_{s,edge}$ ), that play a key role for the reactivity and colloidal behavior of the smectite, represented only 1-3% of the total surface area. However, the variable charges contributed up to 10% of the total cation exchange capacity measured between 90 and 120 cmol(+)/kg. Concerning the RCM, their CEC were reduced up to 92% due to collapsed interlayers leading to inaccessible interlayers for cations exchange. The CEC dependency in function of the pH above their  $pH_{pZC,edge}$  was equal for the Na-saturated dioctahedral smectites and the RCM (Fig. 5).

Based on calculation of edge site density and CEC measurements, we showed that the RCM can be suitable materials to study the edge site reactivity of the montmorillonites. The widespread use of the bentonites from Wyoming known as MX-80 or SWy-1(2) as reference material could lead to some uncertainties, if their structure and dimension are used as generalized input parameters for assessment behavior of other bentonites. Thus, comprehensive characterization of any bentonite under consideration is recommended.

The materials characterized in this study will be used in sorption and diffusion experiments to investigate the influence of smectite diversity (i.e. isomorphic substitutions and particle morphology).

### Predicting the deposition of colloids onto granite surface

Understanding the deposition of bentonite colloids onto granite surface has been very complex as the surface inhomogeneity and chemical heterogeneity arises mainly from its mineral constituents such as K-feldspar, quartz, biotite and plagioclase. Thus the current study is aimed to evaluate colloid filtration theory (CFT) and the degree of predictability of colloid retention onto granite and its mineral constituents. Colloid deposition experiments with Eu(III) at ( $10^{-7}$  M,  $5 \times 10^{-7}$  M,  $10^{-6}$  M) or without were performed using 1  $\mu$ m carboxylated latex spheres at pH 5 and 1 mM NaCl. Interferometry is applied to quantify the particle deposition on the mineral substrates. AFM colloid probe technique is

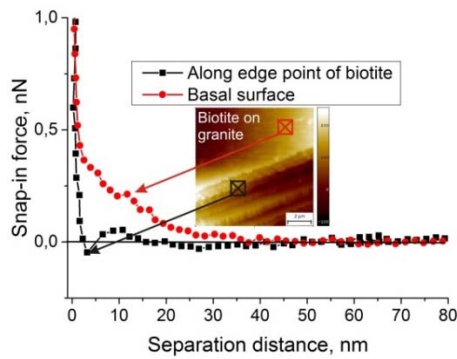


**Fig. 6:** Approach force curves between 1  $\mu\text{m}$  polystyrene (carboxylate functionality) colloid and biotite surface identified on Grimsel granodiorite surface at pH 5. The inset picture shows the topography of the biotite surface (basal and edge points) where the force curves are obtained.

applied to obtain the forces between carboxylated polystyrene particle and mineral surfaces. Further, the force curves are analyzed to estimate the mineral specific surface potentials using DLVO theory [11]. The surface potentials are included into CFT to calculate the colloid deposition efficiency [12].

Deposition experiments show that in absence of Eu the colloid deposition follows the order: K-feldspar > plagioclase > biotite > quartz. At  $[\text{Eu}] = 10^{-6}$  M, the colloid deposition follows plagioclase > biotite > quartz > K-feldspar. It was observed that, CFT and experimental results agree when no Eu is present. At  $10^{-6}$  M Eu, according to CFT the colloid deposition is ranked as plagioclase > K-feldspar > biotite  $\approx$  quartz. In the presence of Eu, biotite is observed to retain more colloids but CFT predicts a higher deposition in favor of K-feldspar.

The reason could be that CFT does not include surface topography of the substrate. AFM force measurements (colloid probe technique) also predicted a lower potential along the mica-edges than the basal plane and explain the observed discrepancy on colloid deposition (Fig. 6) [13]. These findings are on a par with the colloid deposition results where an increase in colloid deposition efficiency ( $Sh$ ) with the roughness ( $Rq$ ) of granite substrate was observed (Fig. 6).

The effect of roughness is rather considerable at low colloid concentration. The observed increase in roughness is due to the contribution from the enhanced mica content where the number concentration of exposed biotite edges is dominant [14]. Interestingly, during the flow through experiments

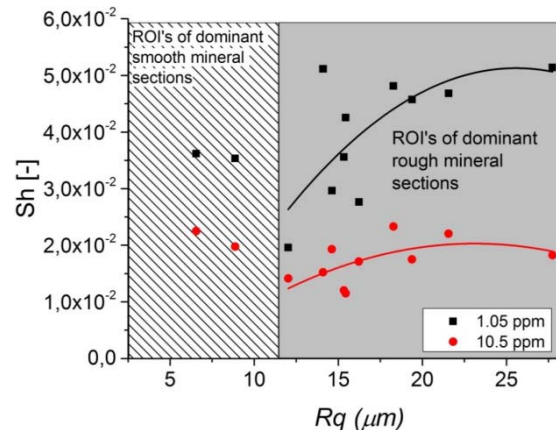


**Fig. 7:** Colloid deposition efficiency ( $Sh$ ) vs. roughness of the granite surface ( $Rq$ ) measured at selected sections on the granite surface.

using granite fracture, the prior deposited particles at pH 5 showed re-entrainment with a change in pH to 9. Hence the next studies will be focused to systematically investigate the re-entrainment of colloids under pH transient conditions.

## References

- [1] Stumm, W. et al., Aquatic Chemistry: chemical equilibria and rates in natural waters, 3rd. Ed., John Wiley & Sons, USA, 1996.
- [2] Norrfor, K.K. et al., App. Clay Sci. **114**:179 (2015)
- [3] Henry, C. et al., Adsorption, DOI 10.1007/s10450-015-9714-4
- [4] Norrfor, K.K. et al., App. Clay Sci. DOI 10.1016/j.clay.2016.01.017
- [5] Norrfor, K.K. et al., App. Clay Sci. (2016), in prep.
- [6] Agus, S.S. & Schanz, T., Acta Geotechnica **3**: 125 (2008)
- [7] Reinholdt, M. et al., Eur. J. Inorg. Chem. **11**: 2831 (2001).
- [8] Reinholdt, M. et al., Nanomaterials **3**: 48 (2013).
- [9] Delavernhe, L. et al., Coll. Surf. A: Physicochem. Eng. Aspects, **481**:591(2015)
- [10] Emmerich, K. et al., Clays and Clay Minerals, **57**:104 (2009)
- [11] Assemi, S. et al., Coll. Surf. A: Physicochem. Eng. Aspects, **286**:70 (2006).
- [12] Shen, C.Y. et al., Wat. Res. Research, **46**:1(2010).
- [13] Zhao, H.Y. et al., Langmuir, **24**: 12899 (2008).
- [14] Darbha, G.K. et al., ES&T **46**: 9378 (2012).

## 5.4 Reactive transport modelling

*F. Huber, V. Metz, V. Montoya, T. Schäfer*

In co-operation with:

*S. Dubey*<sup>a</sup>

<sup>a</sup> L'Ecole des Mines de Nantes, France

### Introduction

Advanced mathematical and numerical methods are needed to quantitatively assess and predict radionuclide migration and geochemical evolution of different systems of interest for nuclear waste disposal by reactive transport modelling approaches. Quantitative calculations of radionuclide release and migration are necessary to evaluate the safety of the different engineered barriers and geometry included in a geological disposal system.

The understanding of the evolution of a disposal system over geological time scales requires a detailed knowledge of a series of highly complex coupled processes. By using small-scale laboratory experiments, under well-defined boundary conditions, numerical modelling can provide information to help in the repository design and predict future radionuclide migration in case of water access to the waste emplacement rooms.

Research activities on reactive transport modelling during 2015 have been focused on coupled advective or diffusive transport processes with different chemical reactions (sorption, precipitation, aqueous speciation, kinetics). As a site for disposal of heat generating waste has not yet been selected in Germany, research in the reactive transport field deal with all relevant host rock types (rock salt, clay / claystone and crystalline rock) in close cooperation and interaction with strong national and international academic partners as well as waste management organizations.

At this moment there are different systems under study in a laboratory scale where reactive transport modelling is applied:

- Diffusion and sorption of radionuclides in illite and montmorillonite.
- Diffusion in the interface clay / low pH cement system (European Union Horizon2020 project CEBAMA) and study of the change in the pore structure.
- Diffusion and precipitation in sea sand and clay.
- Migration of redox sensitive radionuclides in fractured crystalline rock.

Other systems where transport processes are modelled also includes:

- Modelling the effect of fracture geometry on the bentonite erosion.
- Simulation of colloid transport in artificial and real gap geometries.

This kind of calculations in the laboratory scale can provide the scientific basis for the performance as-

essment of various repository design options. Additionally, reactive transport modelling tools have also been used to predict radionuclides release from different generic repository scenarios in clay and rock salt (ENTRIA project, funded by the Federal Ministry of Education and Research, BMBF).

The reactive transport simulations described previously, have been conducted with different codes depending on the system: PHREEQC v. 3 [1] and COMSOL Multiphysics® 5.0 [2]. Additionally, the interface iCP [3] has been used and tested taking advantage that KIT-INE is part of the consortium where this tool has been developed. One of the advantages of using these codes is that all of them are in continuous development. iCP [3] is an interface developed in Java® that couples two simulator programs: COMSOL Multiphysics® [2] and the geochemical code PHREEQC [1]. One of the characteristics of iCP is that the program is not in charge of the numerical calculations, and it is only used as an interface to couple and maximize the synergies between COMSOL and PHREEQC. This interface provides a numerical platform that can efficiently simulate a wide number of multiphysics problems coupled to geochemistry (i.e. liquid flow, solute and heat transport, elastic and plastic mechanical deformations and geochemical reactions). In this sense, iCP is an extraordinary tool to be used in reactive transport modeling which can account *inter alia* for multiphase flow, pore-scale simulations, and fractured rocks hydrogeology coupled with mineral dissolution/ precipitation, porosity changes and cation exchange.

### Modelling of coupled transport processes in the near field of a generic spent nuclear fuel repository in a deep clay formation

The objective of this work is to develop a reactive transport model accounting for (geo-)chemical and physical processes taking place in the near-field of a generic spent nuclear fuel (SNF) repository in a deep clay rock formation. The modelling approach considers coupled processes which potentially occur in the engineered and geological barriers around the nuclear waste during a period of thousand years.

The studied multi-barrier system is composed of the waste form (spent nuclear fuel), the steel canister, the bentonite buffer, the cement liner and cement sealing as well as the clay host rock in the vicinity of the repository (see Fig 1).

Simulation calculations with respect to reactive transport processes in a fully saturated isothermal system (298 K) of a mobile anion (e.g.  $^{129}\text{I}^-$ ), a relatively mobile cation (e.g.  $^{137}\text{Cs}^+$ ) and a less mobile safety relevant radionuclide (e.g.  $\text{Am}^{3+}$ ) have been carried out.

The system studied has been implemented in the iCP interface [1] which couples two different codes: The Finite Element code COMSOL Multiphysics V.5 [2] and the geochemical simulator PHREEQC v.3.1.7. [3].

Geometrical and transport parameters including the discretization of the system have been implemented in two dimensions (2D) in COMSOL Multiphysics (see Fig 1). The mesh size was selected to ensure a satisfactory compromise between computation time and sufficient spatial resolution of the expected geochemical and transport processes, especially at the interface between the different barriers. Details of the spatial discretization are given on Fig. 2. Considering the very low permeability of the different barriers of the system, mass transport is dominated by diffusion, following Fick's law (eq. 1)

$$J = -D \frac{\partial C}{\partial x} \quad (\text{eq. 1})$$

where  $J$  is the substance flux [ $\text{kg}/\text{m}^2 \cdot \text{s}$ ];  $\frac{\partial C}{\partial x}$  is the concentration gradient [ $\text{kg}/\text{m}^4$ ]; and  $D$  is the diffusion coefficient [ $\text{m}^2/\text{s}$ ] that in porous media depends on the properties of the diffusing chemical species, the pore fluid and the porous medium. In this study, it is considered the same diffusion coefficient for all the chemical species and only dependency with the porous medium is applied. Porosity changes due to mineral precipitation/dissolution and feedback on transport is also taken into account.

The (geo-) chemical conceptual model has been implemented in the geochemical code PHREEQC v.3.1.7. For the initial boundary conditions, it is as-

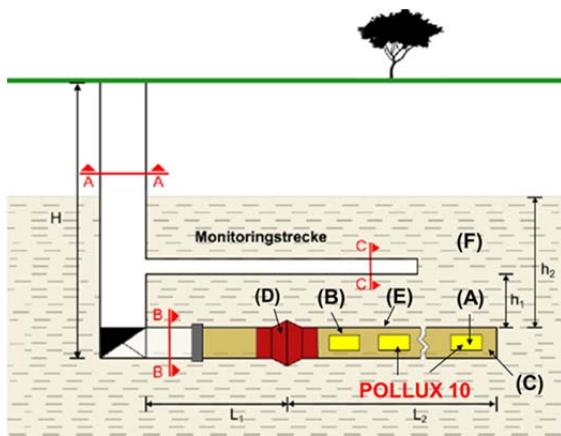


**Fig. 1:** Schematic representation of the studied system, representing A) the SNF, B) the steel container, C) bentonite, D) cement plug, E) cement liner, F) Surrounding clay rock. Figure of generic repository adapted from Stahlmann et al. [4]

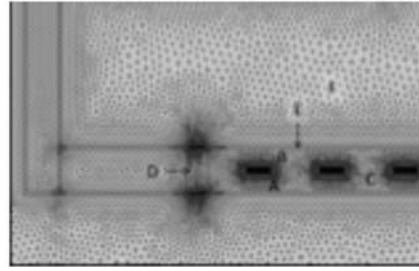


**Fig. 2:** 2D -Geometry and computational mesh of the studied system implemented in COMSOL Multiphysics.

sumed that the pore water from the host rock penetrates into damaged SNF packages and dissolves some of the radionuclides that later can be released. It is assumed that time zero of the simulations is the time at which radionuclide will release from the SNF domain and start diffusing in the engineering barriers. Chemical reactions (precipitation/dissolution) of major components and radionuclides at equilibrium have been simulated using the thermodynamic database ThermoChimie v.9. [5], available in PHREEQC format. Although, ThermoChimie v.9 includes the Specific Ion Interaction Theory (SIT) parameters for the activity correction, at present status, the Davies equation, valid for the ionic strength of the studied system ( $<0.5 \text{ M}$ ) has been preferred to save computational time.

The chemical composition of the pore solution and the solid phases present in the different barriers have been defined in PHREEQC. The mineralogical and pore water composition of the cement considered in the cement liner and the cement plug is representative of a Portland cement (pH  $\sim 12.5$ ) consisting mainly on portlandite as a solid phase.

The mineralogy and pore-water composition of the clay rocks are representative of the Opalinus clay for the surrounding clay rock and the MX-80 bentonite in the backfill material. Considering that the main component of bentonite is montmorillonite. The model includes ion exchange and surface complexation on montmorillonite and competition effects with the major background dissolved elements (e.g. Ca, Mg, Fe, K and Sr) are also considered.

A kinetic model with a constant rate for corrosion of steel canister under anoxic condition has been considered assuming that corrosion will generate magnetite and hydrogen.

The simulation output includes the concentration profiles the major elements (Si, Al, Ca, Na, Mg, K,  $\text{SO}_4$ ,  $\text{HCO}_3$  and Fe) and radionuclides (Am, I, and Cs) as well as pH changes across the different barriers. A mechanistic specific migration model is defined separately for each radioactive element in each barrier. As example, an initial concentration of  $\sim 10^{-5} \text{ M}$  for I and  $\text{Cs}^+$  in the nuclear waste is assumed.  $^{129}\text{I}^-$  presents the higher mobility, diffusing from the waste to the bentonite barrier resulting in concentration up to  $3 \times 10^{-7} \text{ M}$  in 100 years (see Figure 3).

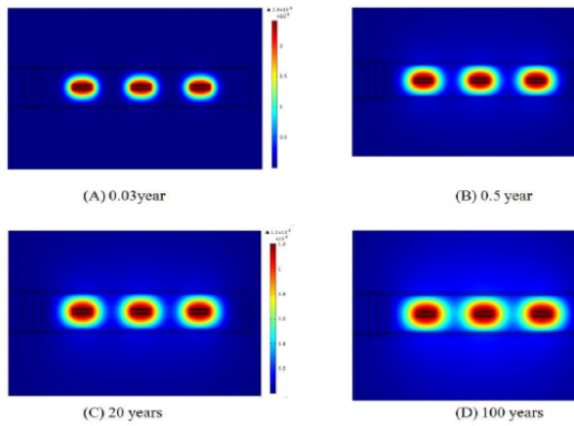


**Fig. 3:**  $^{129}\text{I}$ -diffusion in the SNF repository with respect to time (years) (A) 0.03 (B) 0.5 (C) & (D) 100

$\text{Cs}^+$  can diffuse and sorb in the different barriers. In contrast to these fast release elements iodine and cesium, the release of  $\text{Am}^{3+}$  from the waste is modelled by solubility of hydroxo-carbonate phases. Sorption and precipitation in the different barriers is taken into account. The computed results show that diffusion of  $\text{Am}^{3+}$  is significantly retarded in comparison to  $\text{I}^-$  and  $\text{Cs}^+$ . Am is sorbed in a small region of the bentonite barrier.

## References

- [1] Nardi A., et al. (2014) *Computers & Geosciences*, **69**, 10-21.
- [2] COMSOL (2014) COMSOL-Multiphysics. Version 5.0, [www.comsol.com](http://www.comsol.com)
- [3] Parkhurst and Appelo (2013) C. A. J. U.S. Geological Survey Techniques and Methods, 2013, book 6, chap. A43, 497 p.
- [4] Stahlmann J. et al., *Generische Tiefenlagermodelle mit Option zur Rückholung der radioaktiven Reststoffe*, TU-Braunschweig, Institut für Grundbau und Bodenmechanik (2014).
- [5] Giffaut, E., et al. (2014). *Applied Geochem.*, **49**, 225-236.

## Acknowledgement

Parts of this study was financially supported by the German Federal Ministry of Education and Research (BMBF) in the context of the ENTRIA project (grant number 02S9082A). We acknowledge a grant to Sanjay Dubey for his stay at KIT-INE, provided by the GENTLE project (European Union's Seventh Framework Program for research, technological development and demonstration, subprogram Fission-2012-5.1.1).



## 6 Separation of long-lived minor actinides

Transuranium elements (TRU), most notably plutonium and americium, govern the long-term heat load and radiotoxicity of used nuclear fuel. Potential benefits of their recycling as reactor fuel rather than their disposal are a matter of debate [1, 2, 3]. A suitable technique for the required separation of TRU from uranium and fission products is solvent extraction. In the framework of the EURTATOM FP7 projects, SACSESS and ASGAR we study such solvent extraction systems and processes and related aspects. A more fundamental approach is followed in the project, *f*-Kom, funded by the Federal Ministry of Education and Research (BMBF). Here, we look at the origin of nitrogen donor ligands' higher affinity for actinide ions compared to lanthanide ions.

Furthermore, we have recently started working in the field of rare earth elements (REE) separation, joining the ERA-MIN project, ENVIREE. This way we contribute our experience in actinides solvent extraction to the field of REE recycling.

Select examples of work performed in the framework of SACSESS, TALISMAN, ASGAR and ENVIREE are given below. Financial support by the European Commission (SACSESS, ASGAR, TALISMAN) and by BMBF (*f*-Kom, 02NUK020) is acknowledged.

### 6.1 Water soluble complexing agents for actinides(III)

*C. Wagner, U. Müllich, A. Geist, P. J. Panak*

In co-operation with:

*I. Herdzyk-Koniecko, J. Narbutt*

Institute of Nuclear Chemistry and Technology (IChTJ), Warsaw, Poland

#### Introduction

In recent years we have developed and studied water soluble nitrogen donor ligands to be used as selective complexing agents for actinides(III). SO<sub>3</sub>-Ph-BTP [4, 5] and SO<sub>3</sub>-Ph-BTBP [6, 7] (Fig. 1) selectively strip An(III) from an organic phase loaded with An(III) and Ln(III) [8, 9]. More recently, SO<sub>3</sub>-Ph-BTPhen (Fig. 1, bottom) has been developed at Reading University, UK [10, 11].

Equations (1) and (2) describe the process of co-extracting actinide(III) and lanthanide(III) nitrates by

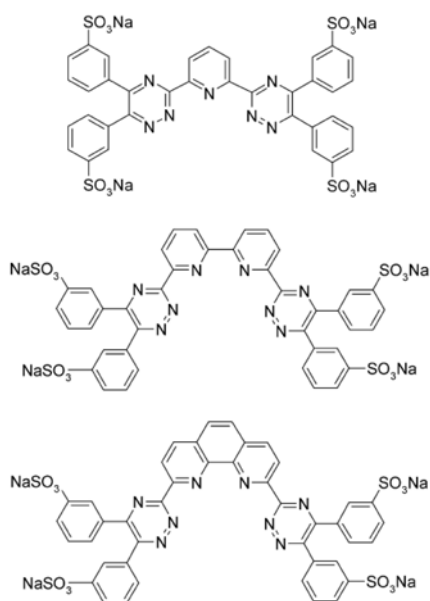
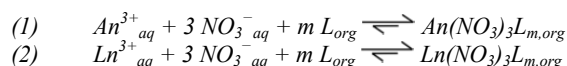
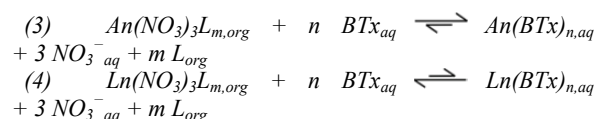


**Fig. 1:** top to bottom, SO<sub>3</sub>-Ph-BTP, SO<sub>3</sub>-Ph-BTBP and SO<sub>3</sub>-Ph-BTPhen.

a solvating extracting agent, L,



Equations (3) and (4) describe the process of selective stripping from the loaded organic phase using a water soluble stripping agent, BTx (such as SO<sub>3</sub>-Ph-BTP, SO<sub>3</sub>-Ph-BTBP or SO<sub>3</sub>-Ph-BTPhen),



Due to the stronger affinity of BTx for An(III) compared to Ln(III), equilibrium (3) shifts to the right while (4) shifts to the left. Thus An(III) are stripped into the aqueous phase, Ln(III) remain in the organic phase.

Slope analysis of solvent extraction data implies the formation of 1:2 complexes for SO<sub>3</sub>-Ph-BTP [4] (i.e. n = 2) and 1:1 complexes for SO<sub>3</sub>-Ph-BTBP [7] and SO<sub>3</sub>-Ph-BTPhen [11] (i.e. n = 1). This disagrees with the reported formation of BTP 1:3 and BTBP/BTPhen 1:2 complexes in solution [12, 13].

To understand this contradiction, aqueous and organic phases from solvent extraction experiments were investigated by TRLFS. In this context, a possible formation of heteroleptic complexes was investigated within a TALISMAN project applied for by IChTJ.

#### Investigating post-extraction phases

A significant fraction of BTx complexes of lower stoichiometry in the aqueous phase might explain the

lower-than-expected slopes. In search of such complexes, Cm(III) was extracted from aqueous phases containing SO<sub>3</sub>-Ph-BTP, SO<sub>3</sub>-Ph-BTBP or SO<sub>3</sub>-Ph-BTPPhen in HNO<sub>3</sub> into an organic phase (0.2 mol/L TODGA (N,N,N',N'-tetra-n-octyl diglycolamide) + 5% 1-octanol in kerosene). Aqueous phase samples (still containing a sufficient fraction of the initial Cm(III) concentration) were investigated by TRLFS.

The aqueous phase Cm(III) fluorescence spectra show the exclusive formation of a 1:3 complex, [Cm(III)(SO<sub>3</sub>-Ph-BTP)<sub>3</sub>] [5] and of 1:2 complexes, [Cm(III)(SO<sub>3</sub>-Ph-BTBP)<sub>2</sub>] [6, 7] and [Cm(III)(SO<sub>3</sub>-Ph-BTPPhen)<sub>2</sub>] [11]. Complexes of lower stoichiometry were not identified. These findings are evidence for the low slopes found in solvent extraction experiments not being caused by the formation of complexes of lower stoichiometry.

### In search of heteroleptic complexes

Another hypothesis is the formation of heteroleptic complexes in the organic phase, containing both the extracting agent, TODGA, and the complexing agent, BTx. Their presence would also result in lower slopes in solvent extraction slope analysis. To check this hypothesis, organic phase samples from the above solvent extraction experiments were studied by TRLFS, recording Cm(III) fluorescence spectra.

Whatever complexing agent BTx present in the aqueous phase, the fluorescence spectra obtained from the organic phase samples [7, 11] are identical to those of the [Cm(III)(TODGA)<sub>3</sub>]<sup>3+</sup> complex reported earlier [14]. No indication of additional complexes explaining the solvent extraction behavior was encountered.

Addressing the question whether heteroleptic complexes containing TODGA and SO<sub>3</sub>-Ph-BTP are able to form at all, a monophasic TRLFS titration study was performed. For solubility reasons, TEDGA (a water soluble TODGA analogue with the n-octyl moieties replaced by ethyl) was used. An aqueous solution containing SO<sub>3</sub>-Ph-BTP and Cm(III) in 1 mmol/L HClO<sub>4</sub> was titrated with TEDGA.

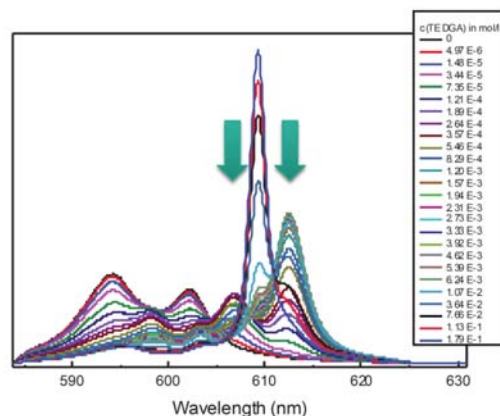


**Fig. 2:** Addition of TEDGA to a solution initially containing 10<sup>-7</sup> mol/L Cm(III) + 10<sup>-6</sup> mol/L SO<sub>3</sub>-Ph-BTP in 1 mmol/L HClO<sub>4</sub>. Normalised Cm(III) fluorescence spectra as a function of TEDGA concentration.

The following complexes were identified by their distinct emission spectra (Fig. 2): Cm(III)(SO<sub>3</sub>-Ph-BTP) and Cm(III)(TEDGA)<sub>1-3</sub>. Moreover, two further emission bands (607 nm and 613 nm) were observed which cannot be ascribed to Cm(III)-TODGA or Cm(III)-SO<sub>3</sub>-Ph-BTP complexes. The corresponding species were identified by slope analysis as heteroleptic complexes, Cm(III)(TEDGA)(SO<sub>3</sub>-Ph-BTP) and Cm(III)(TEDGA)<sub>2</sub>(SO<sub>3</sub>-Ph-BTP).

### Conclusions

The heteroleptic complex, Cm(III)(TEDGA)<sub>2</sub>(SO<sub>3</sub>-Ph-BTP) is expected to be soluble in the organic phase if TEDGA is replaced by TODGA (as is the case in solvent extraction experiments). Its presence may explain the low slopes found in extraction experiments reported in the literature.

Further work aimed at identifying heteroleptic complexes in organic phase samples from solvent extraction experiments is underway. Furthermore, equilibrium models are developed to support the experimental program.

## 6.2 Dissolution of PuO<sub>2</sub>-Mo CerMet pellets

U. Müllich, A. Geist

In co-operation with:

E. De Visser-Týnová,<sup>a</sup> E. Ebert,<sup>b</sup> G. Modolo<sup>b</sup>

<sup>a</sup>NRG, Petten, the Netherlands <sup>b</sup>Forschungszentrum Jülich, IEK-6, Jülich, Germany

### Introduction

CerMet (ceramic and metallic) materials such as actinide oxides dispersed in a molybdenum matrix are candidate materials for inert matrix transmutation fuels (IMF). Reprocessing such targets after irradiation requires the separation of molybdenum for two reasons: First, molybdenum of a tailored isotopic composition is used, which must be recycled for its economic value. Second, disposing of molybdenum as high level waste due to contamination by e.g. fission products would result in a dramatic increase of high level waste volumes [15].

A two-step dissolution process, first dissolving the molybdenum matrix followed by dissolution of the actinide oxides (including fission products) facilitates molybdenum recycling. The first step was studied using un-irradiated PuO<sub>2</sub>-Mo pellets.

### Pellets fabrication and dissolution

PuO<sub>2</sub>-Mo pellets containing 5%–40% wt. PuO<sub>2</sub> were fabricated and characterized at NRG Petten. This was done by mixing molybdenum powder, zinc stearate and PuO<sub>2</sub> powder, pressing at 600 MPa and sintering (up to 1700°C) in an argon atmosphere [16]. The pellets had a diameter of 5 mm, height of 4 mm and a density of approx. 90% of the theoretical density.

To find suitable conditions, the dissolution of molybdenum powder and molybdenum pellets was studied. Finally, it was decided to dissolve PuO<sub>2</sub>-Mo pellets containing 5%, 25% and 40% wt. PuO<sub>2</sub> in three different solutions, 3 mol/L HNO<sub>3</sub>, 1 mol/L HNO<sub>3</sub> or (0.2 mol/L Fe(NO<sub>3</sub>)<sub>3</sub> in 1 mol/L HNO<sub>3</sub>). The dissolution campaigns were performed at ambient temperature. At intervals, samples were withdrawn and analyzed for Mo and Pu content.

The molybdenum matrix was completely dissolved after approx. 20 days, except for the dissolution in 1 mol/L HNO<sub>3</sub>. In this case, the pellets were not fully dissolved after 20 days. In any case, PuO<sub>2</sub> remained as a black precipitate. The pellet composition had no significant effect on dissolution rates.

Comparing the different dissolution campaigns, Fig. 3: Clearly, the best results were achieved using a solution of 0.2 mol/L Fe(NO<sub>3</sub>)<sub>3</sub> in 1 mol/L HNO<sub>3</sub>. In this case, molybdenum dissolved fastest while the fraction of plutonium dissolved was lowest (0.1% vs. 3% in 3 mol/L or 1 mol/L HNO<sub>3</sub>).

### Conclusions

The molybdenum matrix of PuO<sub>2</sub>-Mo pellets is preferentially dissolved in a solution containing 0.2 mol/L Fe(NO<sub>3</sub>)<sub>3</sub> in 1 mol/L HNO<sub>3</sub> at ambient temperature. A small fraction of PuO<sub>2</sub> is co-dissolved. Dissolving irradiated molybdenum based IMF would thus lead to a partial co-dissolution of the actinide oxides and fission products, requiring further purification of the molybdenum. Such a purification seems viable by solvent extraction, using CYANEX® 600 [17].

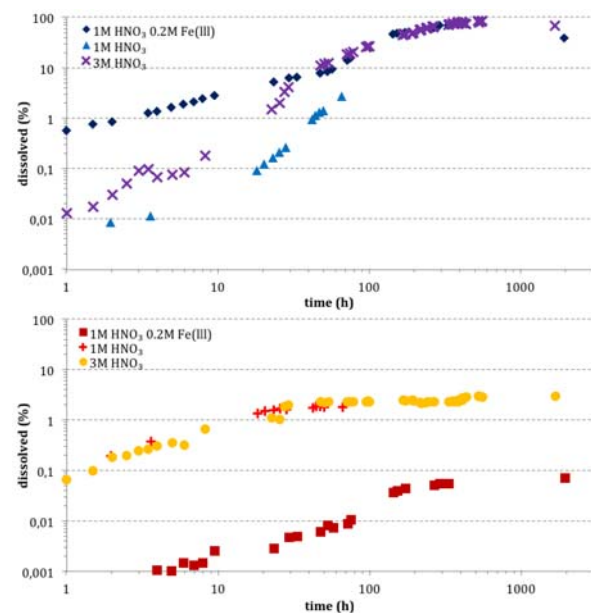


**Fig. 3:** Dissolution of PuO<sub>2</sub>-Mo pellets (25% PuO<sub>2</sub>) in 100 mL of different solutions. Fraction of molybdenum (top) and plutonium (bottom) dissolved as a function of time.

## 6.3 REE separation

C. Stauch, U. Müllich, A. Geist

### Introduction

Some of the rare earth elements (REE) are considered critical raw materials due to their importance for “green energy” applications, combined with a high supply risk [18]. The separation of REE from secondary sources such as mine tailings is studied in the ERA-MIN project ENVIREE (environmentally friendly and efficient methods for extracting rare earth elements from secondary sources). Eleven partners from eight countries contribute to ENVIREE.

Samples from different mine tailings are assessed for REE content. The most promising materials are selected, based on several criteria. These will be leached and the REE will be separated and purified by solvent extraction. Life cycle assessment and economic feasibility studies will be performed on selected processes.

### First results

As a basis for further studies with genuine leaching solutions, we determined distribution data for the extraction of REE and other metal ions from synthetic chloride, nitrate and sulphate solutions. Two extracting agents commonly used in REE separations were used, D2EHPA (di(2-ethylhexyl)phosphoric acid) and TOPO (tri-n-octyl phosphine oxide).

An example showing how selectivity is achieved by selecting a suitable leaching solution is shown in Fig. 4. Bi(III) is extracted from nitrate and sulphate solutions with distribution ratios similar to those for Tb(III). The extraction of Bi(III) is suppressed when extracting from chloride solutions of sufficient concentration (such as 1 mol/L in the example shown). This effect is caused by a more pronounced tendency of chloride complex formation with Bi(III) compared to REE(III).

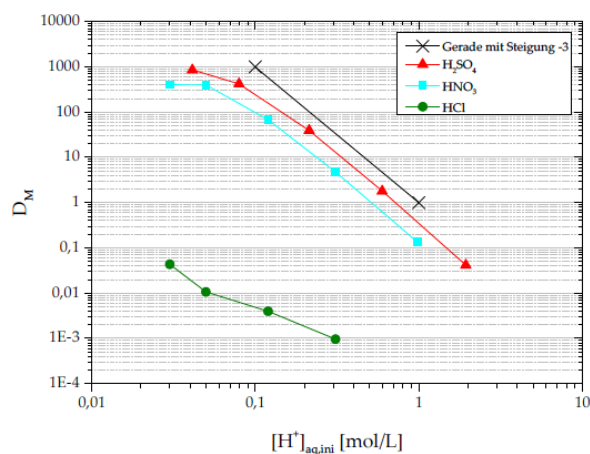


**Fig. 4:** Extraction of Bi(III) into D2EHPA, distribution ratios as a function of proton concentration. Organic phase, 0.1 mol/L D2EHPA in kerosene. Aqueous phase, 10 mg/L Bi(III) in (H, NH<sub>4</sub>)X (X = 1 mol/L NO<sub>3</sub>, Cl or SO<sub>4</sub>).

### Outlook

As soon as available, solvent extraction data will be collected using genuine leaching solutions from mine tailings. Using this data, process flow-sheets will be developed and separation process tests will be performed in collaboration with the ENVIREE consortium.

### References

- [1] *Potential Benefits and Impacts of Advanced Nuclear Fuel Cycles with Actinide Partitioning and Transmutation*; NEA No. 6894, OECD-NEA, Paris: 2011.
- [2] Renn, Ortwin (Hrsg.): *Partitionierung und Transmutation. Forschung – Entwicklung – Gesellschaftliche Implikationen (acatech STUDIE)*, Herbert Utz Verlag, München: 2014.
- [3] Poinssot, C.; Bourg, S.; Ouvrier, N.; Comber-noux, N.; Rostaing, C.; Vargas-Gonzalez, M.; Bruno, J., *Energy* **2014**, *69*, 199–211.
- [4] Geist, A.; Müllich, U.; Magnusson, D.; Kaden, P.; Modolo, G.; Wilden, A.; Zevaco, T., *Solvent Extr. Ion Exch.* **2012**, *30*, 433–444.
- [5] Ruff, C. M.; Müllich, U.; Geist, A.; Panak, P. J., *Dalton Trans.* **2012**, *41*, 14594–14602.
- [6] Wagner, C.; Müllich, U.; Geist, A.; Panak, P. J., *Dalton Trans.* **2015**, *44*, 17143–17151
- [7] Wagner, C.; Müllich, U.; Geist, A.; Panak, P. J., *Solvent Extr. Ion Exch.* **2015**, DOI: 10.1080/07366299.2015.1129192
- [8] Wilden, A.; Modolo, G.; Kaufholz, P.; Sadowski, F.; Lange, S.; Sypula, M.; Magnusson, D.; Müllich, U.; Geist, A.; Bosbach, D., *Solvent Extr. Ion Exch.* **2015**, *33*, 91–108.
- [9] Carrott, M.; Bell, K.; Brown, J.; Geist, A.; Gregson, C.; Hérès, X.; Maher, C.; Malmbeck, R.; Mason, C.; Modolo, G.; Müllich, U.; Sarsfield, M.; Wilden, A.; Taylor, R., *Solvent Extr. Ion Exch.* **2014**, *32*, 447–467.
- [10] Lewis, F. W.; Harwood, L. M.; Hudson, M. J.; Geist, A.; Kozhevnikov, V. N.; Distler, P.; John, J., *Chem. Sci.* **2015**, *6*, 4812–4821.
- [11] Kaufholz, P.; Modolo, G.; Wilden, A.; Sadowski, F.; Bosbach, D.; Wagner, C.; Geist, A.; Panak, P. J.; Lewis, F. W.; Harwood, L. M., *Solvent Extr. Ion Exch.* **2015**, DOI: 10.1080/07366299.2016.1151308.
- [12] Panak, P. J.; Geist, A., *Chem. Rev.* **2013**, *113*, 1199–1236.
- [13] Bremer, A.; Whittaker, D. M.; Sharrad, C. A.; Geist, A.; Panak, P. J., *Dalton Trans.* **2014**, *43*, 2684–2694.
- [14] Wilden, A.; Modolo, G.; Lange, S.; Sadowski, F.; Beele, B. B.; Skerencak-Frech, A.; Panak, P. J.; Iqbal, M.; Verboom, W.; Geist, A.; Bosbach, D., *Solvent Extr. Ion Exch.* **2014**, *32*, 119–137.

- [15]Ouvrier, N.; Boussier, H., *Proc. Chem.* **2012**, *7*, 322–327
- [16]De Visser-Týnová, E.; Ménard, G.; Ebert, E. L.; Modolo, G.; Cheng, M.; Steppert, M.; Walther, C.; Geist, A.; Mareš, K. V.; John, J. In *Proceedings of Top Fuel*, Zürich (CH), 13–17 September, 2015; Vol. 2, pp 497–506.
- [17]Bremer, A.; Stauch, C.; Geist, A. In *Proc. Internat. Conf. GLOBAL 2015*, Paris, France, 20–24 September, 2015; pp 1544–1546.
- [18]Critical raw materials for the European Union. European Commission, 2010.



## 7 Decommissioning of nuclear facilities

The decommissioning department at INE has formally been established in the beginning of 2015, expanding the existing activities at the Institute of Technology and Management in Construction (TMB) of the KIT. This adds a very important topic to the portfolio of the current program oriented funding (POF III) “Nuclear Waste Management and Safety as well as Radiation Research” (NUSAFE) of the Helmholtz Association, covering the final step in the product life circle of a nuclear power plant prior to safe disposal of the remaining nuclear material. In the following report, some major activities of this specific research group in 2015 will be covered.

*M. Brandauer, E. Celebic, S. Gentes<sup>a</sup>*

<sup>a a</sup> Department of Deconstruction and Decommissioning of Conventional and Nuclear Buildings, Institute for Technology and Management in Construction (TMB), Karlsruhe Institute of Technology (KIT)

### Introduction

Within the Karlsruhe Institute of Technology (KIT), the Institute of Technology and Management in Construction (TMB) has been carrying out research on the decommissioning of nuclear facilities since 2008 by its Department of Deconstruction and Decommissioning of Conventional and Nuclear Buildings. Since 2015, these activities have been included into the current program-orientated funding (POF III) of the Helmholtz Association by assigning three new positions to the Institute for Nuclear Waste Disposal (INE). This includes the professorship of Prof. Dr.-Ing. Sascha Gentes, transforming from a junior professorship into a full one. This one of a kind professorship in Germany guarantees the very important education and training at University level. A significant development of these efforts is the continuously increasing number of students attending the offered decommissioning lectures.

In addition to continuing the already established activities at the existing department, the new positions at INE are targeted to create a better understanding of the complete decommissioning process in Germany as well as on a global level. Therefore, a database of decommissioning knowledge is currently being developed with the aim to assist the enormous challenge of numerous decommissioning projects to be coped with in the coming decades simultaneously. The database will provide a basis for the standardization of dismantling procedures of nuclear facilities. Furthermore, it will reflect the current state of the art in the decommissioning of nuclear facilities and thus allow identification and definition of critical issues for future projects and research areas. This specific topic will be addressed in more detail below.

In February 2015, the “Competence Centre of Decommissioning” has been established at KIT to properly address the challenging task of the decommissioning of nuclear facilities. In this center, all existing activities related to this subject within KIT are joined to improve communication, bundle common interests and to better address future challenges. Another major activity of the research group in 2015 was the prolongation of a present research project dealing with the separation of secondary waste of the

water abrasive suspension cutting technique. Within the process of decommissioning nuclear facilities, this project aims to significantly reduce radioactive waste by applying physical separation, thus reducing final storage volume. For this reason, a separation process has been developed, a prototype system built and experimental and initial numerical investigations have been performed. This specific topic will also be further addressed in more detail below. Within this scope, Ms. B.Sc. Emilia von Fritsch was awarded the “Women in Nuclear Germany price 2015” for her bachelor thesis of numerical investigations of the fluid flow in the applied filter in the separation process.

Furthermore, great efforts were undertaken to extend the current network with different research institutions. An ongoing communication has been established with Japanese colleagues of the University of Fukui, who sent a research associate to visit our institute in a three months’ exchange initiative. Another very important aim is networking at a European level. Currently, there are plans for the establishment of a non-commercial Europe-wide training program for professionals in the decommissioning sector, promoted by the European Commission. The aim is to achieve improved international information exchange and thus generating a harmonized and professional dismantling of nuclear installations within the European market. The present group played an important role here and will continue to do so in 2016. In the following, the two main research activities concerning the database and the separation system for radioactive waste will be further discussed.

### Set up of a knowledge database

The target of creating a knowledge database with information on the decommissioning of nuclear facilities is to gather relevant characteristic values for nuclear decommissioning procedures and to illustrate the state of the art within R&D areas as well as the practical use of technologies and methods in the nuclear field. The scientific motivation is to build a knowledge base for future R&D projects, so a fast introduction to the topic of decommissioning and access to all relevant data is available. The database

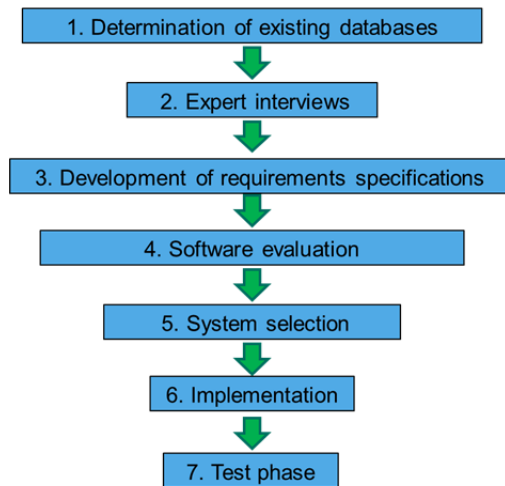


**Fig. 1:** Selection of a suitable software solution for the database

includes also a decommissioning library which is able to store and link related bibliography.

The first step towards this was the selection of a suitable software solution that fulfils the defined requirements for a decommissioning database, while being user-friendly and easy to maintain.

The selection process included the determination of existing databases and interviews with international experts within the fields of decommissioning and IT. As a result of the evaluation of possible software solutions, a commercial enterprise-wiki has been chosen and implemented. The workflow for the selection of a suitable software product is shown in the following **Fig. 1**.

In a second step, the software has been tested and modified in order to fulfil the previously defined requirements for a suitable decommissioning database. This also included structuring the database along the six following main topics:

- decommissioning in Germany,
- nuclear reactor types,
- decommissioning processes and technologies,
- decommissioning strategies,
- approval process, and
- further topics, e.g. management methods, social and political affects, further national and international research facilities in decommissioning and their present work, etc.

The current work includes the data assembly and linking of relevant information and documentation on a national basis as well as the coverage of foreign decommissioning topics.

### Treatment of secondary waste from the water abrasive cutting technique

For the reduction or even elimination of secondary waste produced by the water abrasive cutting technique, two research approaches have been followed in previous years. On the one hand, research has been undertaken to treat the secondary waste by a novel physical separation method of the radioactive particles

contained in the mixture. The second approach analyzed the possibility of admixing the secondary waste into the concrete which is used to fill-up the so-called KONRAD containers.

The combination of both approaches has the aim of significantly reducing the amount of waste in the first step and to completely eliminating it through the second approach, while only the first one has been further addressed by the present research group. For these investigations, two samples of non-radioactive mixtures have been used allowing the handling of the materials and therefore enabling actual tests. These samples have been generated by AREVA GmbH in a mock-up using the original cutting technique. Both samples differ in their material properties of the cut metal (a ferritic and an austenitic stainless steel), chosen to best resemble the properties of the usual reactor pressure vessel and its internals. These two samples have then been analyzed in detail at KIT [1]. These analyses show that both kinds of steel lead to similar characteristics in the resulting mixture after the cut. The main characteristics which could be used for the physical separation besides the density are the considerable difference in particle size of the steel chips and the remaining abrasive particles. Even though both kinds of steel have twice the density of the abrasive, due to the substantially smaller particle size of the chip fraction, the resulting sedimentation velocity is significantly slower. The second useful characteristic is the magnetic property. By applying very strong magnetic fields in primary tests, even the stainless steel particles could be successfully separated from the remaining abrasive particles.

In order to develop a separation module which can later be tested with activated waste, a big effort has been made to develop a test rig, which is as insusceptible as possible. Furthermore, since it has to be applied within the containment, the size was limited to fit into a 20" container. In order to allow the transportability between future decommissioning sites, the mobility had to be taken into account as well as the necessity to decontaminate the entire system. Considering all this, a very simple test rig has been carried

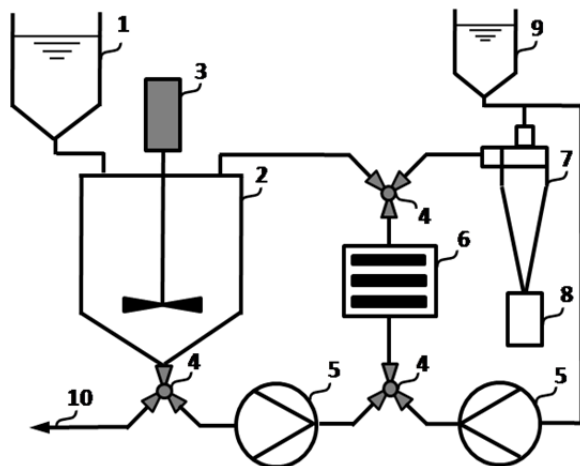


**Fig. 2:** Applied process chain of the preliminary test rig.

out. The process chain of this test rig is shown in the following Fig. 2.

In order to take advantage of the shielding effect of water against radiation and also to track possible leakage in the system, the abrasive and steel mixture is brought into suspension by adding water within a slurry feed tank (2). To avoid the abrasion by the abrasive particles caused in typical pump designs, membrane pumps (5) have been used without deterioration problems. The slurry suspension is in sequence pumped through a magnetic filter (6) in a closed loop. This loop is operated until repletion of the filter is reached and then flushed by a second loop, where the separated activated particles are drained out of the system by a hydro cyclone (7) into a depository container (8).

The remaining equipment for the separation system is a prior feed tank (1), the drivetrain and corresponding agitator (3) of the slurry feed tank, a fresh water supply (9) and 2/3-way valves (10) to operate both closed loops sequentially.

After separating the contained activated chips as thoroughly as possible from the primary mixture, the remaining mixture leaves the apparatus through the 2/3-way valve beneath the slurry feed tank. The material is then released to either further processing or discharged as decontaminated waste, depending on the remaining radiological aspect.

The functionality of the preliminary test rig has been tested by taking three portions of the sample generated by cutting stainless steel. The stainless steel was chosen first due to the lesser magnetic properties of the stainless steel particles. The tests have been performed by taking 1.000g of the mixture containing stainless steel chips and mixing in a mass proportion of 1:100 with water in the slurry feed tank (2). In order to account for the amount of material which is effectively separated by the system, an additional tank has been used to allow the entire initial batch to pass through the magnetic filter. By pumping the suspension between these two tanks in three series with 10 passes each, preliminary feasibility results have been obtained [2].

In order to allow an interpretation of these results, the same test series have been carried out with fresh unspoiled abrasive. The initial material characterization has already shown that due to the chemical composition of this natural product the abrasive also contains particles with magnetic properties amounting to approximately 2 Mass-% [1]. Maintaining the same set-up and parameters, the experiment was repeated with the fresh abrasive and compared with the results obtained with the mixture of steel chips and abrasive after the cutting. These results are shown in the following Fig. 3.

The comparison of the two curves leads to the conclusion that they reach the same asymptote after about 4 to 7 passes. In this manner, the curve containing the steel chips of the cutting process converges to the curve of the abrasive. This can be understood as the separation process of the contained steel chips. By summing up the difference between the two curves, a

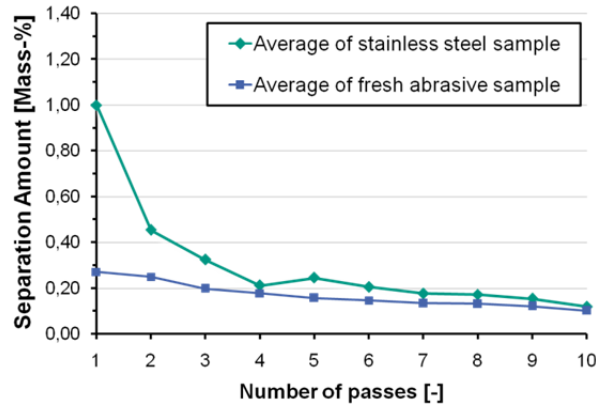


Fig. 3: Average results of carried out test series of both samples (containing stainless steel chips and the fresh abrasive)

total average mass difference of 15 mass-% is yielded. Optical analyses of the separated fraction in the filter and the “cleaned” mixture in the slurry feed tank show that a significant separation of steel particles can be achieved with this preliminary set up.

However, since these are only assumptions based on rough estimations, further analyses and tests are now necessary in order to actually quantify the separation quality and the effectiveness of the current system. This will involve optimizing the present system, realizing tests with activated and therefore radioactive material and achieving a better understanding of the separation process by numerical investigations within the applied rod magnet filter. For this reason, a follow-up project has been applied for in the previous year, which was granted to the institutes INE and TMB by the end of 2015. It provides three additional fully financed positions to the cooperating institutes, one at INE and two at TMB.

This research will actually significantly improve the treatment and disposal of the secondary waste generated by the water abrasive suspension cutting technique. By the development of the separation module shortly described in this report, the feasibility of waste reduction through physical separation has already been shown and will now be further improved. The coupling with the additional disposal technique of admixing to concrete in KONRAD-containers makes the elimination of this major drawback of this cutting technique possible and allows the water abrasive suspension cutting technology to become a very suitable tool for the upcoming decommissioning projects of nuclear facilities in Germany and worldwide.

These results have been achieved within the framework of the Project 02S8871 funded by the German Federal Ministry of Education and Research.

## References

- [1] M. BRANDAUER, M. HAIST, et al., “Separation von Sekundärabfall aus der Wasser-Abrasive-Suspension-Schneidtechnik”, *11th International Symposium on „Conditioning of Radioactive Operational & Decommissioning Wastes“ including 11th Status Report of the German Federal Minis-*

try of Education and Research (BMBF) “Decommissioning and Dismantling of Nuclear Facilities”, *KONTEC 2013*, **80**, 545, Dresden, Germany (2013).

- [2] M. BRANDAUER, J. STARFLINGER, S. GENTES, “Physical Separation And Disposal Of Was

Secondary Waste From The Decommissioning Of Nuclear Facilities”, *International Conference & Exhibition for Filtration and Separation Technology, FILTECH 2015*, 24.-26. February, Köln, Germany (2015).

## 8 Development of radionuclide speciation methods

Maintaining the state-of-the-art portfolio of advanced surface science and spectroscopy methods at INE is an important R&D activity, as these methods are crucial tools for understanding and advancing actinide and radionuclide (geo)chemistry. Radionuclide speciation methods available at INE controlled area laboratories and the KIT synchrotron radiation source ANKA are continuously adapted to serve the requirements of the INE in house R&D program. In addition, access to these facilities is provided to the radiochemistry and nuclear science community through direct cooperation with KIT-INE, thus serving as important crystallization seeds for national and international cooperation. The INE-Beamline for radionuclide science at ANKA is operated by INE since 2005 as a flexible experimental station for X-ray based radionuclide speciation investigations. Ten years later, in 2015 the commissioning of the new hard X-ray beamline ‘CAT-ACT’ for CATalysis and ACTinide research at ANKA has been successfully completed. CAT-ACT will be jointly operated by the two KIT institutes having essential expertise in these two application fields – ITCP/IKFT for in operando catalysis research and INE for radionuclide science, respectively. The portfolio of laser based speciation techniques at INE comprises different optical and non-optical methods: LIBD, TRLFS, LIBS, and LA-ICP-MS (the latter in collaboration with JRC-ITU). Currently, an ambitious program to upgrade all existing systems and to improve the performance of laser-based techniques is realized - with a focus on new instrumentation for TRLFS and LIBD investigations. Processes determining radionuclide retention or release from waste matrices or iron oxide based container corrosion products are largely governed by surface properties of these materials. Combining high efficiency EDX spectroscopy and atomic resolution HAADF-STEM, direct visualization of single Lu atoms incorporated on Fe lattice positions near the rim of goethite crystal needles has been shown to be possible, thus improving our atomic scale understanding of actinide/radionuclide retention by secondary phases. Nuclear magnetic resonance spectroscopy (NMR) is a spectroscopic method that is highly sensitive to the electron density surrounding the observed nucleus. Since the density is influenced strongly by “sharing” electrons in a covalent bond, NMR is the ideal tool to give insight into metal-ligand bonds - extensively used in 2015 at INE for the investigation of BTP-type ligands developed to separate trivalent actinides from their lanthanide counterparts. A method more recently established at INE is accelerator mass spectrometry (AMS). AMS is presently one of the most sensitive analytical techniques with an overall sensitivity of  $\sim 10^4$  atoms in a sample. A novel analytical protocol for the simultaneous ultra-trace determination of  $^{237}\text{Np}$  and  $^{243}\text{Am}$  concentrations has been developed based on the application of non-isotopic tracers. Additionally, initial results were obtained in the ultra-trace determination of the radioactive fission product  $^{99}\text{Tc}$ . Many of the in house research activities at INE benefit from strong support by quantum chemical calculations, providing molecular structures or thermodynamic data. The systems under investigation vary from small complexes in solution to crystals or interfaces. New algorithms and the constantly improving hardware allow getting closer to a detailed description of radionuclide systems at the level of electronic structure, thus complementing spectroscopic results.

### 8.1 R&D projects conducted at the INE and CAT-ACT beamline at ANKA and at external SR sources

*S. Bahl, E. Bohnert, K. Dardenne, A. Gensch, I. Pidchenko, T. Prüßmann, J. Rothe, Th. Schäfer, M. Vespa, T. Vitova*

In co-operation with:

*J.-D. Grunwaldt<sup>a</sup>, H. Lichtenberg<sup>a</sup>, A. Zimind<sup>a</sup>*

<sup>a</sup>KIT-ITCP/IKFT

#### Introduction

Synchrotron radiation (SR) based speciation techniques have become key methods in basic and applied radionuclide research. This development is primarily driven by the need to secure molecular-scale understanding for (geo-)chemical processes determining the mobility of long-lived radionuclides possibly released from a projected disposal site for highly active, heat producing nuclear waste (HAW). Presently, final disposal in deep bedrock repositories is deemed as the preferred option for the management of spent nuclear fuel (SNF) and high level waste (HLW) glass used to

immobilize highly radioactive residues from nuclear fuel reprocessing. The release of actinides, fission and activation products following corrosive HAW degradation depends mainly on the oxidation state and bonding characteristics of the radionuclides in the individual waste matrices. Solving the nuclear disposal safety case requires the assessment of an envisaged disposal site on geological time scales, where speciation techniques like XAS (X-ray Absorption Spectroscopy) provide necessary input parameters for modelling geochemical reaction and transport paths for radionuclides. The INE-Beamline for radionuclide

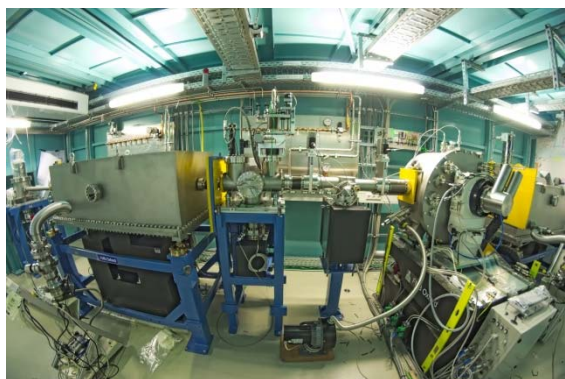


**Fig. 1:** CAT-ACT beamline optics consisting of vertically collimating mirror, DCM ( $Si\langle 111 \rangle / \langle 311 \rangle$ ), toroidal focusing mirrors and beam diagnostic devices.

science [1] at the KIT synchrotron facility ANKA [2] is operated by INE since 2005 as a flexible experimental station for X-ray based radionuclide speciation investigations. Ten years later, the commissioning of the new hard X-ray beamline ‘CAT-ACT’ for CATALysis and ACTinide research at ANKA has been successfully completed [3]. CAT-ACT will be jointly operated by the two KIT institutes having essential expertise in these two application fields – ITCP/IKFT and INE, respectively. The INE-Beamline and the ACT station are the only facilities of their kind in Europe offering direct access to radiochemistry laboratories operating a shielded box-line in close proximity to the synchrotron light source on the same research campus.

### INE-Beamline user operation in 2015

The year 2015 was marked by the abrupt halt of ANKA user operation with the end of beam time call No. 25 (October 2014 - March 2015), following the decision of the KIT executive board to transform ANKA from a LK II (HGF nomenclature for a user facility) to a LK I (KIT *in house* research) facility. Due to unsecure ANKA funding and a fire destroying a major storage ring power supply unit, in 2015 a user operation (UO) shift reduction by more than 50% (62 days compared to 126 days in 2014) had to be dealt with. Remaining UO days were mostly spent for granted TALISMAN Joint Research Projects requesting INE-Beamline access and beam time projects related to INE PhD thesis work. Nevertheless, a total of 20 *in house* and external projects were hosted at the INE-Beamline in 2015. The time available for INE internal research amounted to ~52% of all available shifts (32 days). Three days were spent for maintenance and development. A total of 27 days was given to external projects with (23 days) and without (4 days) ANKA or TALISMAN peer review (i.e., through direct cooperation with INE - for now the only possibility to get access to beam time at INE-BL and ACT stations for non-HGF users). As in previous years, INE *in house* projects in 2015 covered a broad range of systems containing actinides, fission products, their chemical homologues or materials relevant

for radionuclide retention. These were, e.g., Tc sorbed on natural granitic rocks and magnetite, Pu(III) and Pu(IV) solid phases in the presence of reducing or complexing agents, Am(III) in the presence of natural dissolved organic carbon, Np(V) complexed by chloride, Eu(III) in contact with  $Mg(OH)_2$  and  $Mg_2(OH)_3Cl \cdot 4H_2O$  phases or iron rich illite and glauconite minerals investigated at the Fe K-edge. Some of these studies are presented in more detail elsewhere in this annual report. Examples for studies applying advanced high resolution (HR) XANES techniques for measuring actinide  $M_{4,5}$  absorption edges now available at the beamline are highlighted in a separate section below.

HGF external scientists from the German and international research institutions listed below conducted experiments at the INE-Beamline in 2015:

- Trinity College Dublin, Ireland
- CEA Cadarache, France
- Manchester University, Dalton Nuclear Institute, United Kingdom
- Niederrhein University of Applied Sciences, Krefeld, Germany

Four projects in 2015 received beam time and were funded through the EU project TALISMAN as Joint Research Projects (JRP).

### Commissioning of the CAT-ACT beamline at ANKA

In the first half of 2015 all optics and control system components of the new beamline for CATALysis- and ACTinide/radionuclide science ‘CAT-ACT’ at ANKA were installed and mechanically pre-aligned (Fig. 1). The ACT (Exp1) and CAT (Exp2) experimental hutches downstream from the optics section were equipped with basic infrastructure (experimental table, media and data line connections) and later on with temporary detection systems for X-ray beam alignment and diagnostics (Fig. 2).

All steps of the ‘hot’ beamline commissioning required to meet conditions for the final component site acceptance test were successfully accomplished before the 2015/16 ANKA winter shutdown. This pro-



**Fig. 2:** The multi analyzer crystal HRXES spectrometer was transferred from the INE-Beamline and is now installed inside the ACT experimental hutch (Exp1).

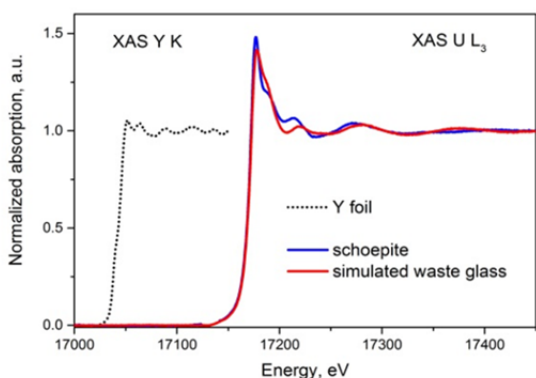


**Fig. 3:** First uranium XAFS spectra measured at CAT-ACT in December 2015: U L<sub>3</sub>-edge XANES of U(VI) 'uranyl' species in the mineral meta-schoepite (UO<sub>3</sub> · nH<sub>2</sub>O) and a simulated U-borosilicate nuclear waste glass (4.7 wt.% UO<sub>2</sub> loading). An Y metal foil was measured at the Y K-edge as energy calibration standard.

cedure included the characterization of the wiggler source inside the storage ring, alignment and tests of frontend slits and beamline diagnostic devices (beam position, profile and intensity monitors, fluorescence screens), alignment of the first upward deflecting collimating mirror, the LN<sub>2</sub>-cooled double crystal monochromator (DCM) equipped with pairs of Si<111> and Si<311> crystals for nominal low and high energies, respectively, and the downward deflecting and focusing toroidal mirrors guiding the monochromatic X-ray beam to the sample positions inside Exp1 and Exp2, where a beam spot size below 1 mm × 1 mm was achieved. In the future, the two experimental stations will be operated alternately with a share of 50% of all available UO shifts for each user community. Finishing the initial commissioning stage, the first X-ray absorption spectra were successfully acquired from materials related to both research areas (Fig. 3). Regular operation of the CAT-ACT beamline is planned to commence in the second half of 2016 once the requested license for handling radioactive materials – following the safety concept enacted for the INE-Beamline – has been approved. The new beamline will augment the X-ray spectroscopy capabilities at ANKA – which have been always under very high demand – by new high flux / high energy spectroscopy options. The wiggler source gives access to K absorption edges of heavy elements like Tc, Rh, Pd and Ag and 4f/5f-element edges until now unavailable at the INE-Beamline (actinide L<sub>1</sub>-edges and lanthanide K-edges up to Gd). The low energy limit of the beamline still allows investigations at the K-edges of transition metals and actinide M<sub>4,5</sub>-edges. Compared to ANKA bending magnet radiation, the photon flux at 20 keV has been already shown to be about two orders of magnitude higher, which is especially beneficial with respect to the spectroscopic sensitivity for dilute sample systems, e.g., for studying catalyst promoters or poisons or trace concentrations in environmental radionuclide studies.

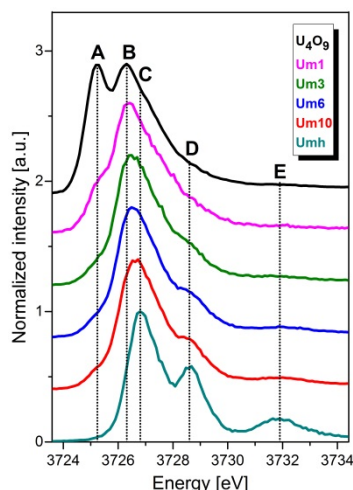


**Fig. 4:** U M<sub>4</sub> edge HR-XANES of the Um1-Um10 samples and the U<sub>4</sub>O<sub>9</sub> and Umh references.

### Redox states of U co-precipitated with magnetite nanoparticles

Uranium is a main constituent of radioactive wastes (e.g., spent nuclear fuel) but it is also present in high quantities in contaminated sites after U ore processing and technogenic accidents. Significant interest lies in the investigation of the heterogeneous reduction of U(VI) by ferrous iron (Fe(II)). Such interactions are believed to be key processes influencing mobilization / immobilization of U in the near and far field of a nuclear waste repository and generally in the environment. Due to kinetic effects during interaction with Fe(II)/Fe(III) species, U is often found as a mixture of its redox states. U has two environmentally relevant redox states, U(IV) and U(VI) and an intermediate U(V) state with poorly understood chemical behavior and interaction with the environment. U(V) is rarely considered due to the lack of reliable detection methods. A project in the frame of the PhD thesis work of I. Pidchenko concentrated on the redox speciation of U in the final product formed by co-precipitation of U(VI) with magnetite. The U redox states in magnetite nanoparticles with varying (1000, 3000, 6000 and 10000 ppm) U loadings (denoted as samples Um1-Um10) were investigated by U M<sub>4</sub> edge high energy resolution XANES (HR-XANES) at the ESRF ID26

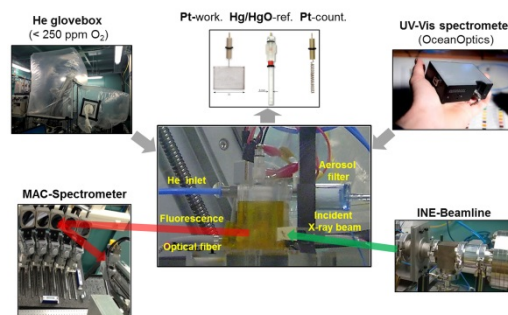


**Fig. 5:** The in situ spectroelectrochemical cell during U M<sub>4</sub> edge HR-XANES/3d4f RIXS experiments at the INE-Beamline.

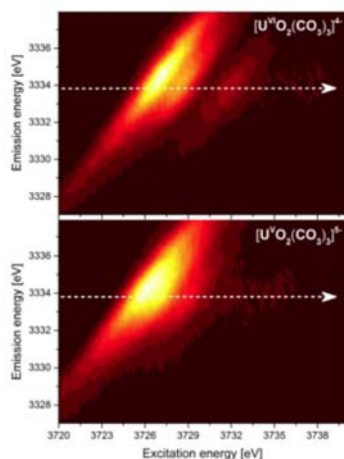


**Fig. 6:**  $3d4f$  RIXS of  $[U^{VI}O_2(CO_3)_3]^{4+}$  (top) and  $[U^VO_2(CO_3)_3]^{5+}$  (bottom).

beamline 10 days after sample preparation. The main aim of this study was to verify the presence of U(V) in this system.

Figure 4 depicts the U  $M_4$  edge HR-XANES spectra of the Um1-Um10 samples and  $U_4O_9$  as well as maghemite with 3000 ppm adsorbed U (Umh) reference materials (additional U  $M_4$  edge HR-XANES measurements of the Um1 sample aged for 289 days not shown here were performed at the INE-Beamline, publication in preparation). The U  $M_4$  absorption spectra typically shift by  $>0.5$  eV to higher energies when increasing the formal U redox state by one unit. This is induced by the reduced screening of the  $3d_{3/2}$  core-hole by the lower electronic charge density on the U atoms. Small energy shifts of about 0.2 eV for the same U redox state can be caused by variations of the electronegativity of the bonding partner, changes in symmetry, short and long range atomic order etc. as found from U  $M_4$  edge HR-XANES studies of U(V) organic and inorganic compounds. It was demonstrated that  $U_4O_9$  contains equal amounts of U(IV) and U(V) described by the two peaks A [U(IV)] and B [U(V)] separated apart by about 1 eV [4]. Maghemite has the same inverse spinel crystal structure as magnetite with the specificity that Fe(II) is oxidized to Fe(III). The main absorption peak C of the Umh spectrum is shifted by  $\sim 0.4$  eV to higher energies as compared to peak B. Hence we can deduce that U(VI) is the main redox state of U in the Umh sample. Spectral features D and E are typical for U(VI) and U(V) species forming short axial trans-dioxo bonds with lengths of about  $<1.8$  Å and  $<1.9$  Å (uranyl, U-yl), respectively [5]. The energies of the two main absorption resonances of the Um1 spectrum are very similar to the energy positions of the main peaks of the  $U_4O_9$  reference spectrum. Based on this strong experimental evidence we conclude that after 10 days interaction time U(V) is formed in Um1 coexisting with minor amount of U(IV) visible as a shoulder on the low energy side of the main absorption peak. Features D and E are absent in the Um1 spectrum. This con-

firms that U(VI) is not present in the Um1 sample and that U(V) does not form uranyl type of bonding.

It is evident that by going from the Um1 to the Um10 spectrum the intensity of feature A decreases, the energy position of feature B shifts to higher energies and features D and E gain intensities. These spectral changes strongly suggest that the relative contributions of U(IV) decreases, whereas the U(VI) content rises continuously going from 1000 ppm U (Um1) to 10000 ppm U (Um10) in the samples.

This study demonstrates that the U  $M_4$  edge HR-XANES technique is clearly capable of detecting the three different redox states, i.e., U(IV), U(V) and U(VI), simultaneously present in the same sample. A quantitative analysis is currently under development. The presented results are definitely a breakthrough in the long and intensive discussion on the reduction mechanisms of U(VI) in contact with magnetite.

### Development of an in-situ spectro-electrochemical cell

New insights into the electronic structure of actinide (An) compounds can be obtained by directly probing An valence states using advanced HR-XANES and resonant inelastic X-ray scattering (RIXS) methods. These techniques are also very valuable for detailed speciation analyses of An in different oxidation states present in one material (cf. the previous section). The potential of the HR-XANES and RIXS techniques has not yet been completely exploited as up to date only a very few electronic structure and speciation investigations of An systems are reported in the literature (e.g. [4-6]). Studies of An in intermediate oxidation states are especially challenging as they are often unstable under ambient conditions. One solution is the application of *in situ* cells working under controlled conditions, e.g., the absence of  $O_2$  or a defined redox potential.

In 2015 we designed, manufactured and tested an *in situ* spectroelectrochemical cell (Fig. 5). U  $M_4$  edge HR-XANES and  $3d4f$  RIXS investigations of  $[U^{VI}O_2(CO_3)_3]^{4+}$  and  $[U^VO_2(CO_3)_3]^{5+}$  were performed at the INE-Beamline, applying the multi-analyzer crystal spectrometer (cf. INE annual report 2014). One of the main advantages of the cell compared to those previously reported is the coupling of UV-Vis spectroscopy with electrochemistry and XAS. In addition, this cell is equipped for XAS/RIXS experiments at low photon energies  $>3000$  eV. Two Kapton win-

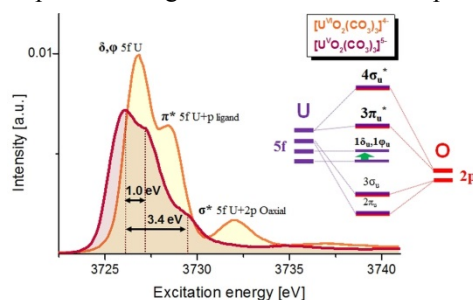


**Fig. 7:** U  $M_4$  edge HR-XANES of  $[U^{VI}O_2(CO_3)_3]^{4+}$  and  $[U^VO_2(CO_3)_3]^{5+}$ . The additional electron in the  $5f_{\delta}$  orbital is shown in the MO scheme of U(V)-yl.

dows with 10 and 13  $\mu\text{m}$  thickness absorbing only a few percent of the photon intensity ( $\sim 15\%$  at 3727 eV) but providing long-term mechanical and chemical stability are implemented. The compact size of the cell ( $15 \times 10$  cm) facilitates its transfer into a glovebox. The compulsory double containment of the cell is accomplished by an inner and an outer parts made from borosilicate glass and Plexiglas, respectively. A Pt-mesh (80  $\mu\text{m}$ ,  $25 \times 35$  mm) was used as a working electrode, a Pt-spiral (0.5 mm  $\varnothing$ , 23 cm length) as a counter electrode and Hg/HgO as a reference electrode (ALS Co., Ltd). The negative potential of -775 mV determined from cyclic voltammetry measurements was applied to reduce U(VI) to U(V). UV-Vis spectra were continuously recorded during the electrochemical reaction. The intensity of the U(VI)-yl UV-Vis spectra (cf. section 9.2) diminished 210 minutes after the beginning of the reaction. In addition, the color of the solution changed from yellow to colorless. These were clear evidences for complete reduction of U(VI) to U(V).

The  $3d4f$  RIXS maps and the U  $M_4$  edge HR-XANES spectra of  $[\text{U}^{\text{VI}}\text{O}_2(\text{CO}_3)_3]^{4-}$  and  $[\text{U}^{\text{V}}\text{O}_2(\text{CO}_3)_3]^{5-}$  depicted in Figures 6 and 7, respectively, were recorded before the beginning of the electrochemical reaction and after the reduction was completed. The HR-XANES spectra correspond to cuts through the  $3d4f$  RIXS planes parallel to the  $x$ -axes and centered at the maxima of the U  $M_\beta$  normal emission lines (cf. arrows in Fig. 6). The U  $M_4$  edge HR-XANES spectrum of U(VI) exhibits an intense main peak (A) at 3726.9 eV and two well resolved higher energy features at 3728.5 eV (B) and 3732.0 eV (C) characteristic for the U(VI)-yl type of bonding. These peaks have been assigned to transitions of  $3d_{3/2}$  electrons to  $5f\delta/5f\phi$  (A),  $5f\pi$  (B) and  $5f\sigma$  (C) unoccupied valence orbitals of U(VI) in the U(VI)-yl entity, respectively [5]. This assignment is valid also for the U(V) compound due the very similar U(V)-yl type of bonding [7]. In the U(V) spectrum the main peak A exhibits a reduced intensity and is shifted by  $\sim 0.8$  eV to lower energies compared to that of U(VI). This energy shift is due to the better screening of the core-hole by the additional electron in the U(V) atom. The decrease in absorption intensity is a consequence of the less available unoccupied  $5f$  states in U(V) ( $5f^1$ ) compared to the empty  $5f$  shell in U(VI) ( $5f^0$ ). The energy positions of the peaks B and C significantly shift to lower energies and are positioned closer to the

main peak A (U(VI): A-B = 1.6 eV, A-C = 5.1 eV; U(V): A-B = 1.0 eV, A-C = 3.4 eV).

We demonstrated that the U  $M_4$  edge HR-XANES method measures the change in the energy gaps between the  $5f$  based orbitals as a function of the electronic density variations in the vicinity of the U atoms. DFT calculations previously suggested that the additional electron is transferred to the  $5f\delta$  orbital of U(V) [4]. This result is in agreement with our experimental results as we observe a pronounced reduction of the area of peak A. The  $5f\delta$  and the  $5f\phi$  orbitals are non-bonding orbitals therefore the area of the peak A should not be influenced by changes of mixing of metal  $5f$  with ligand  $p$  orbitals. This is however likely for probed  $5f\pi$  and  $5f\sigma$  molecular orbitals. Since the study is performed *in situ*, experimental artefacts influencing positions, shapes and intensities of the spectral features can be neglected. Hence it can be postulated that one additional electron leads to about 20 % decrease of the area of the U  $M_4$  edge HR-XANES spectrum of  $[\text{U}^{\text{V}}\text{O}_2(\text{CO}_3)_3]^{5-}$  compared to the spectrum of  $[\text{U}^{\text{VI}}\text{O}_2(\text{CO}_3)_3]^{4-}$ . Currently carried out quantum chemical calculations will complement the experimental results.

### Acknowledgements

Many thanks to H. Blank (Bonn University), J. Thomas, A. Bauer and Ch. Marquardt (all KIT-INE), T. Hoffmann and G. Christill (both KIT-SUM) for invaluable technical and logistic support. T. Vitova, T. Průbmann, I. Pidchenko, S. Bahl acknowledge the Helmholtz Association of German Research Centres and KIT for the Helmholtz Young Investigators Group grant (VH-NG-734).

### References

- [1] J. Rothe et al., *Rev. Sci. Instrum.* **83**, 043105 (2012)
- [2] [www.anka.kit.edu](http://www.anka.kit.edu)
- [3] A. Zimina et al., *Journal of Physics: Conference Series* **712** (2016)
- [4] K. O. Kvashnina et al., *Phys. Rev. Letters* **111** (2013)
- [5] T. Vitova et al., *Inorganic Chemistry* **52**, 174-182 (2015)
- [6] T. Vitova et al., *Phys. Rev. B* **82** (2010)
- [7] A. Ikeda et al., *Inorganic Chemistry* **46**, 4212-4219 (2007)

## 8.2 Laser spectroscopy

C. Garcia, R. Götz, F. Heberling, T. Hippel, P. Linqvist-Reis, I. Pidchenko, F. Rinderknecht, J. Rothe, T. Schäfer, M. Trumm, T. Vitova

In co-operation with:

N. Bogachev

Institute of Chemistry, Saint Petersburg State University, Saint Petersburg, Russia

### Introduction

For over 50 years after it was conceived, the laser has been involved in many aspects of analytical chemistry, especially in the field of atomic and molecular spectroscopy. Laser based spectroscopy methods are not only very sensitive, allowing very low limits of detection, they can also provide very accurate speciation information. Those advantages are very important when investigating the speciation of different lanthanide (Ln) and actinide (An) compounds and their interaction with the environment. Nowadays, there are different optical and non-optical laser spectroscopy methods available at INE: LIBD, TRLFS, LIBS, and LA-ICP-MS (the latter in collaboration with JRC-ITU). Different upgrades have been accomplished in the above mentioned instrumentation along the last year in order to improve the performance of the techniques in our fields of interest. In the case of the TRLFS setups, further developments have been carried out in 2015, e.g., allowing for direct Eu(III) and Cm(III) excitation luminescence spectroscopy. Regarding the LIBD instrumentation, an update on all available instrumentation and setups developed at INE has been finished considering the information compiled in previous years. Besides the development in laser spectroscopy, in a collaboration with the YIG of T. Vitova an electrochemical cell for in-situ XAFS measurements has been modified for simultaneous XAFS and UV-Vis absorption measurements (cf. section 9.1).

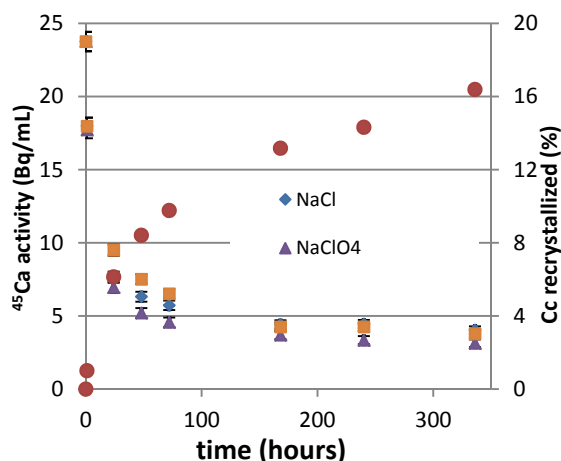


**Fig. 1:** Decrease of <sup>45</sup>Ca activity (left ordinate) and corresponding average progression of Cc recrystallization (right ordinate).

### Low temperature (<6K) Eu<sup>3+</sup> direct excitation TRLFS

Eu<sup>3+</sup> direct excitation TRLFS in an excitation wavelength range from 575 nm to 582 nm can now be performed on a Radiant Dyes Narrow Scan dye-laser system, using Pyromethene 597 as a lasing dye, pumped by a Nd-YAG laser at 532 nm. To improve spectral resolution, the sample is contained in a He-cryostat. The temperature is monitored by two thermoelements at the cold finger and directly at the sample position and is confirmed to remain  $\leq 6$ K throughout the run of the experiment at  $< 10^{-6}$  mbar. Luminescence emission is recorded on an Andor multi-channel analyzer equipped with a 1200 lines/mm polychromator and a diode array detector.

As one of the first series of samples investigated using this new laser setup, we measured samples of ground calcite (Cc), recrystallized in Cc saturated solutions containing 10 mmol/L background salt (NaCl, NaClO<sub>4</sub>, NaNO<sub>3</sub>) for about two weeks. Initial Eu<sup>3+</sup> concentration in the experiments was 1  $\mu$ mol/L. In parallel experiments, using <sup>45</sup>Ca as a radio tracer, we quantified the amount of recrystallized Cc based on the homogeneous recrystallization model by Curti et al. [1]. Radiotracer experiments indicate that 16% of the Cc recrystallize within the timeframe of the experiments (Fig. 1). Differences between the background electrolytes are minor. If any, it is indicated

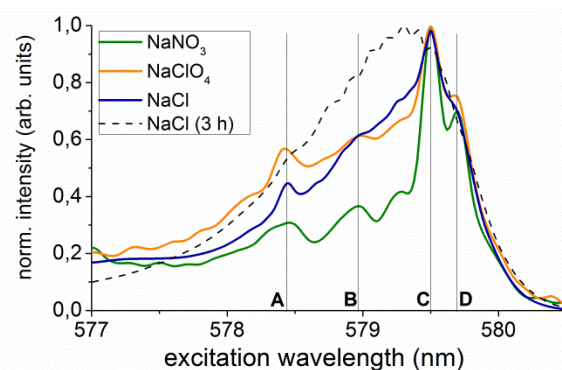


**Fig. 2:** Excitation spectra, integrating over the  $5D_0 \rightarrow 7F_2$  fluorescence emission, obtained on Eu-doped Cc samples recrystallized for two weeks in Cc saturated solution containing 10 mmol/L of three different background electrolyte salts: NaNO<sub>3</sub>, NaClO<sub>4</sub>, and NaCl. Straight lines indicate the positions of four main species A-D. The dashed line depicts a spectrum from a Eu-doped Cc recrystallized in an NaCl medium for about 3h.

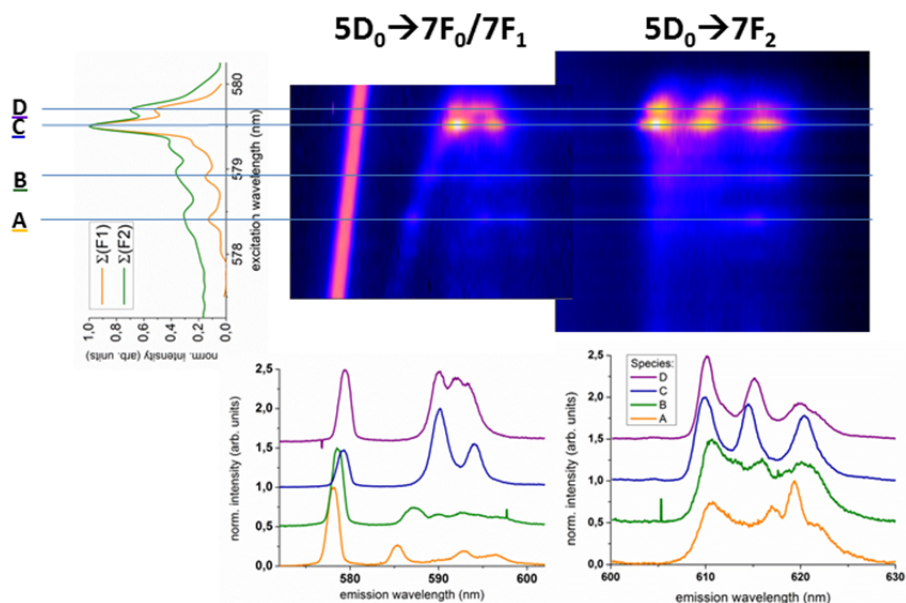


**Fig. 3:** 2D plots (upper right) display data obtained during measurements of two excitation spectra on Eu-doped Cc recrystallized in the presence of NaNO<sub>3</sub>. One plot is obtained recording emission from 572 nm to 603 nm, i.e. the Eu<sup>3+</sup> 5D<sub>0</sub> → 7F<sub>0</sub>/7F<sub>1</sub> transitions, and the other one recording emission from 600 nm to 630 nm, i.e. the 5D<sub>0</sub> → 7F<sub>2</sub> transition. Integrated excitation spectra are displayed in the left panel. Emission spectra of the four main species A-D are displayed in the lower panels. Note that emission spectra are offset for clarity.

that recrystallization is faster in the NaClO<sub>4</sub> medium.

The comparison of excitation spectra (Fig. 2) shows that all samples exhibit at least four species which we label A-D. Species A and C at 578.4 nm and 579.5 nm, respectively, show clear peaks in all spectra. Species B and D at 578.95 nm and 579.75, respectively, are less well pronounced and are merely a shoulder on a broad feature for the NaCl sample. One might even infer a fifth species at 579.3 nm, where all spectra exhibit a shoulder, which coincides with the maximum of the spectrum obtained after 3 h recrystallization (dashed line in Fig. 2).

A more detailed representation of the data measured on the sample which recrystallized in the presence of NaNO<sub>3</sub> is given in Fig. 3. Excitation spectra obtained by integrating over the F1 band and the F2 band, respectively, exhibit the same spectral features (left panel in Fig. 3). The peak observed at the position of the F0 band is constant in intensity at all excitation wavelength, indicating that it is likely a remainder of the laser signal rather than a fluorescence peak.

If we compare our results with spectra from previous studies [2-4], it is clear that our main species C, found on all samples at 579.5 nm after two weeks' recrystallization upon excitation, is identical with the well-ordered incorporation species identified in all previous studies [2-4] (labelled site C in previous papers), but not upon incorporation in the presence of NaNO<sub>3</sub> [4]. Species C exhibits a twofold splitting of the F1-band and a threefold splitting of the F2-band in line with Eu<sup>3+</sup> being incorporated onto an octahedral Ca-site in the Cc structure. Our species A, excited at 578.4 nm, appears very similar with the disordered incorporation species labelled site B in the previous studies [2-4]. A very characteristic feature of this species is the sharp

peak around 618 nm in the F2 emission band (cf. Fig 1b in [4] or Fig. 2a in [3]). The spectral features of species B are not well pronounced. Species D is not clearly separate from species C. The three main peaks in the F2 band are still visible. The F1-band, however, shows a distinct threefold splitting, indicating lower symmetry. Fluorescence lifetimes of all species A-D (data not shown) contain long-lived (> 3 ms) and relatively short lived (< 1 ms) contributions, indicating that all species are incorporated into the Cc structure, either into the bulk or into the surface mono-layer, where they still have contact to ~1 water molecule.

We interpret the results in a way that upon contact with Cc a large amount of Eu<sup>3+</sup> (96%) is rapidly incorporated into a near surface region on the Cc minerals. After 3 h 1.4% of ground Cc recrystallized, an amount which is equivalent to 5 Cc mono-layers. The broad feature in the corresponding excitation spectrum (dashed line Fig. 2) is likely a distribution species with no well-defined chemical environment. Upon further recrystallization Eu-species in Cc develop more well defined coordination environments, resulting in the development of pronounced peaks in the excitation spectra. The energetically most favorable coordination environment seems to be that of the well-ordered octahedral species C. The degree to which this development takes place does not correlate with the overall progress of the recrystallization reaction (Fig. 1). Instead it is indicated that the kinetics of this development are influenced by the background electrolyte, and are fastest in the NaNO<sub>3</sub> medium, followed by NaClO<sub>4</sub> and NaCl. This observation matches with the faster interfacial reaction reported by Ruiz Agudo et al. [5] for Cc growth in the presence of NaNO<sub>3</sub> compared to NaCl.

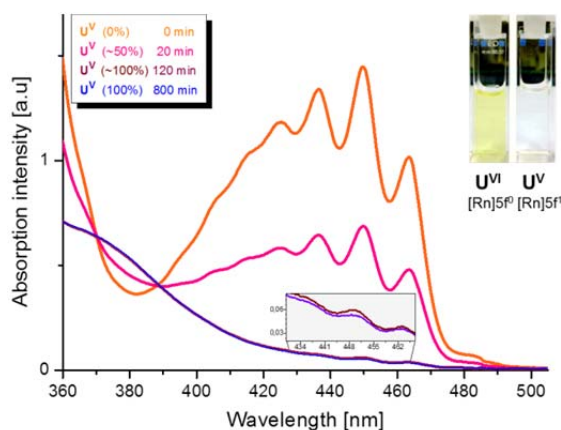


**Fig. 4:** In-situ measured UV-Vis spectra: U(VI) (orange), 50 % reduced U(VI) (magenta), 100% reduced U(VI) to U(V) (brown and violet). The time passed after the beginning of the electrochemical reaction is indicated. Photographs of the U(VI) and U(V) tricarbonate complexes in aqueous carbonate media as prepared under laboratory conditions (top-right).

#### Development of an in-situ spectroelectrochemical cell for combining electrochemistry with UV-Vis and HR-XANES/RIXS measurements

In 2015 a spectroelectrochemical cell developed for HR-XANES and RIXS investigations of aqueous actinide species (e.g.,  $[\text{U}^{\text{VI}}\text{O}_2(\text{CO}_3)_3]^{4-}$  and  $[\text{U}^{\text{V}}\text{O}_2(\text{CO}_3)_3]^{5-}$ ) at the INE-Beamline has been implemented with an UV-Vis absorption line for simultaneous UV-Vis, electrochemistry and XAFS measurements. The UV-Vis spectroscopic technique can be used for molecular speciation of U [6]. The advanced setup has been used to follow in situ the electrochemical reduction of a U(VI) carbonate complex applying both absorption techniques simultaneously.

The cell, designed to fit into the transfer chambers of the gloveboxes at the INE laboratories and the INE-Beamline, was modified adding the windows for the two UV-Vis fibers attached to the outer part of the cell. UV-Vis spectra were continuously recorded in the range 360-520 nm in transmission mode during the in-situ electrochemical process using a compact USB4000 UV-Vis spectrometer, a D-2000 Deuterium lamp as a UV light source both attached to the cell by using two UV-Vis optical fibers with a cord diameter of 400  $\mu\text{m}$  (all from OceanOptics GmbH). A negative potential of -775 mV determined from cyclic voltammetry measurements was applied to reduce U(VI) to U(V). To obtain the individual spectra shown in Fig. 4, 100 spectra with 100 nm acquisition time were recorded and averaged by using SpectraSuit Software (OceanOptics GmbH) for the acquisition.

The clearly resolved eight bands of the U(VI)-yl fine structure are measured for the U(VI) tricarbonate complex before starting the reaction and agree well

with results from previous studies. [7-8] The orange curve in Figure 4 represents the UV-Vis absorption spectrum of the U(VI) ion in 1.5 M  $\text{Na}_2\text{CO}_3$ . The absorption spectrum is characterized by a very weak and broad absorption in the visible range between 380 nm and 490 nm with a characteristic fine structure as well as an intense absorption in the UV range that extends nearly continuous to lower wavelengths. The intense absorption in the UV range (not shown) has no structure and does not offer characteristic features for spectroscopic speciation. [6] The fine structure of the low-energy absorption band is due to coupling of electronic transitions with the symmetric stretching vibration of the U(VI)-yl entity. [9-11] During the U(VI) reduction to U(V) the intensity of the absorption bands decreases (Figure 4, magenta curve). The intensity of the U(VI)-yl UV-Vis spectra diminished 210 minutes after the beginning of the reaction. In addition, the color of the solution changed from yellow to colorless. These were clear evidences for complete reduction of U(VI) to U(V). The broad band characteristic for U(V) is in the Vis-NIR region, which is not measured in this study due to the limited spectral range of the spectrometer. U(V) was then stable for more than 12 hours while the redox potential was kept constant (Figure 4, brown and violet curves).

#### References

- [1] E. Curti et al., *Geochim. Cosmochim. Acta*, **69**, 1721-1737 (2005).
- [2] M. Marques-Fernandes et al. *JCIS*, **321**, 323-331 (2008).
- [3] M. Schmidt et al. *Angew. Chem. Int. Ed.*, **47**, 5846-5850 (2008).
- [4] S. Hofmann et al. *Geochim. Cosmochim. Acta*, **125**, 528-538 (2014).
- [5] E. Ruiz-Agudo et al. *Geochim. Cosmochim. Acta*, **75**, 3803-3814 (2011).
- [6] G. Meinrath, Uranium(VI) speciation by spectroscopy, *J Radioanal Nucl Ch*, 224 (1997) 119-126.
- [7] K. Mizuguchi, Y.Y. Park, H. Tomiyasu, Y. Ikeda, Electrochemical and Spectroelectrochemical Studies on Uranyl Carbonato and Aqua Complexes, *J Nucl Sci Technol*, 30 (1993) 542-548.
- [8] A. Ikeda, C. Hennig, S. Tsushima, K. Takao, Y. Ikeda, A.C. Scheinost, G. Bernhard, Comparative study of uranyl(VI) and -(V) carbonato complexes in an aqueous solution, *Inorg Chem*, 46 (2007) 4212-4219.
- [9] E. Rabinowitch, R.L. Belford, Spectroscopy and photochemistry of uranyl compounds, Macmillan, 1964.
- [10] R.G. Denning, Electronic-Structure and Bonding in Actinyl Ions, *Struct Bond*, 79 (1992) 215-276.
- [11] L.S. Natrajan, Developments in the photophysics and photochemistry of actinide ions and their coordination compounds, *Coordin Chem Rev*, 256 (2012) 1583-1603.

## 8.3 Microscopy and surface analytics

T. Yokosawa, R. Polly, N. Finck, M. Bouby-Laliron, K. Dardenne, A. Geist, W. Grünewald, W. Tobie, A. Salimi, S. Weisenburger, E. Soballa, D. Schild, H. Geckeis

In co-operation with:

E. Prestat<sup>a</sup>, T. Kerry<sup>b</sup>, C. Sharrad<sup>b</sup>, S.J. Haigh<sup>a</sup>, M. A. Denecke<sup>c</sup>

<sup>a</sup>School of Materials, <sup>b</sup>School of Chemical Engineering and Analytical Science, <sup>c</sup>Dalton Nuclear Institute, The University of Manchester, Manchester M13 9PL, United Kingdom

### Introduction

Iron (hydr)oxides are widespread in nature and can play an important role in the bioavailability and migration of pollutants, such as heavy metal ions or radionuclides (RNs). Ferrihydrite and its transformation products (hematite and goethite) are commonly found in nature. In nuclear waste disposal sites, iron (hydr)oxides are also expected to form upon steel canister corrosion. Such neo formed corrosion phases can thus serve as sinks for RNs, either by surface adsorption and/or by structural incorporation, investigated by scanning transmission electron microscopy (STEM).

Materials in nuclear decommissioning activities are decontaminated by individually tailored procedures. Stainless steel surfaces were exposed to the acidic conditions of a nuclear reprocessing facility and analyzed by autoradiography, SEM-EDX, and XPS.

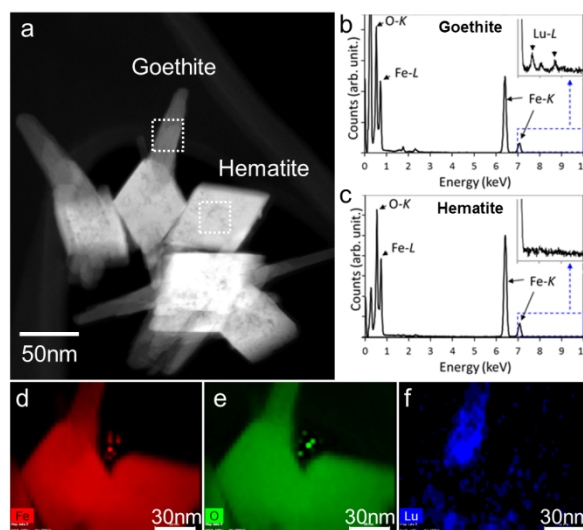
Liquid fed ceramic-lined waste glass melters are used for the vitrification of highly radioactive residues from reprocessing. Interaction of ceramic furnace lining with the glass melt is studied by SEM-EDX elemental phase mapping.

### STEM detection of Lu incorporated in a transformation product of 2-line ferrihydrite

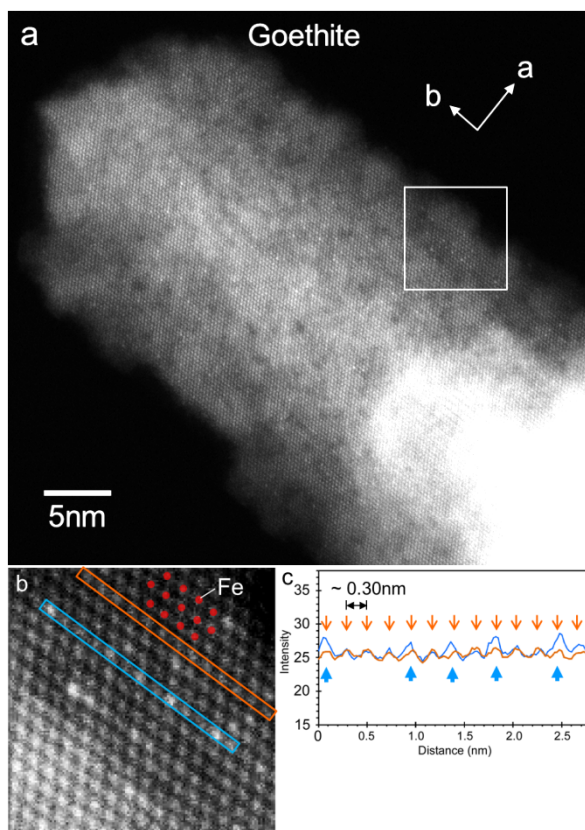
In this study, 2-line ferrihydrite was synthesized in the presence of Lu(III) used as homologue for trivalent actinides and the suspension was aged for 12 years. Here, we applied high efficiency energy dispersive X-ray spectroscopy (EDX) [1] and probe-side aberration corrected high-angle annular dark field STEM (HAADF-STEM) [2] on the individual hematite nanoparticles and the goethite needles growing on them by using a FEI Titan G2 80-200 S/TEM “ChemiSTEM™” instrument at 200 kV installed at the University of Manchester.

Figure 1a shows an HAADF-STEM image of rhombic and needle shaped particles, which correspond to hematite ( $\alpha$ -Fe<sub>2</sub>O<sub>3</sub>) and goethite ( $\alpha$ -FeOOH) crystals, respectively. It is unclear whether the higher intensities are attributed to Lu atoms or not. This is because intensities in HAADF-STEM images depend on sample thickness as well as the atomic number. Conventional (not high efficiency) STEM-EDX was performed on goethite particles. However, the sample was severely damaged since much larger amount of electrons were needed to irradiate on the sample in order to obtain the X-ray signal of Lu. Therefore, we performed high efficiency EDX analysis in order to

obtain more reliable elemental information of the sample. Figures 1b,c show high efficiency EDX spectra obtained for the hematite particle and for the goethite particle, indicated by squares with dotted lines in Figure 1a, respectively. The corresponding characteristic X-rays from O and Fe atoms are indicated in Figures 1b,c. The insets in Figures 1b,c depict a zoom into the high efficiency EDX spectra between 7 and 10 keV (Lu-L <sub>$\alpha$</sub> : 7.65 keV, Lu-L <sub>$\beta$</sub> : 8.75 keV). The Lu-L lines are recognized only in the case of goethite as indicated by arrowheads (Figure 1b). Thus, it is suggested that Lu atoms are associated mainly with the goethite particle. Figures 1d-f show high efficiency EDX spectrum images obtained from an area around the center of Figure 1a. Fe and O distribute homogeneously in hematite and goethite, indicating that iron oxides are uniformly formed. On the other hand, the high efficiency EDX spectrum image shows clearly that the Lu atoms segregate predominantly at goethite (Figure 2). The Lu atoms are, therefore, considered to incorporate in and/or adsorb on the goethite particle. The Lu content in the goethite particle is approximately 0.3 at.% which is around the detection limit of typical EDX systems in TEM. Thus, it is obvious that a higher electron beam intensity and/or longer exposure time is necessary in order to detect the signal with



**Fig. 1:** a) HAADF-STEM image taken from hematite and goethite. b,c) high efficiency EDX spectra obtained from goethite and hematite indicated by the squares in a), respectively, d-f) EDX spectrum images of goethite and hematite. The images are taken from a central area in a).



**Fig. 2:** a) Atomic resolution HAADF-STEM image of goethite with the [001] incidence, b) broader view of area indicated by a square in a), c) intensity distribution obtained from the orange and blue stripe regions shown in b).

such amount of Lu.

In order to know where Lu atoms are located at a goethite nanoparticle, atomic resolution HAADF-STEM with a probe-side aberration corrector was performed. Figure 2a shows a HAADF-STEM image taken from goethite along the [001] direction. Figure 2b shows a zoom of the area indicated by a square in Figure 2a. The bright dots represent the Fe atomic columns in this projection image. Some of the Fe positions are marked by red dots. Relative intensities of the bright dots in the area can be evaluated since the area has relatively homogeneous thickness. An intensity distribution obtained from the region marked by an orange rectangle in Figure 2b is shown in Figure 2c. The intensity distribution has the periodicity of about 0.30 nm as indicated by red arrows, consistent with the interatomic distance between two Fe atoms along the [010] direction of goethite. Some of the bright dots in the area show higher intensities compared to the other dots (Figure 2b). An intensity distribution obtained from the area (blue marked region) is shown in Figure 2c as well. Intensity changes can be recognized in the distribution as indicated by blue arrows, indicating the presence of heavier elements.

Based on the EDX result for the goethite sample, it is considered that the heavier atoms correspond to Lu atoms. Importantly, the brighter dots are located at the same crystallographic sites as the Fe atomic columns in the image. This implies that Lu atoms are partially

occupying Fe sites in goethite. Thus, it is revealed by atomic resolution HAADF-STEM that the Lu atoms are incorporated in the goethite crystal lattice.

It was shown that high efficiency EDX is more suitable than conventional EDX for detecting low amounts of Lu associated with the goethite nanoparticle. This method can be applied for other combinations between iron oxides and lanthanides/actinides. It is considered from the result by high resolution HAADF-STEM that direct observation of trace level lanthanides/actinides associated with iron based phases is effective especially 1) when there are several phases in one sample, 2) when there is a peak overlap problem between signals of Fe and of some lanthanides in case of EDX and other spectroscopic methods such as EXAFS. The methods applied in this study are promising for an atomic level study of trace level lanthanides/actinides associating with iron based phases, thus providing new insight for studies of long-term performance assessment of nuclear repositories.

### Interaction of transuranic elements with stainless steel at high nitric acid concentration

Dissolution of spent nuclear fuel in the PUREX process in a reprocessing plant is performed by concentrated nitric acid. Prior to dismantling a decommissioned reprocessing plant, all vessels and tubes have to be decontaminated. Information about levels of radioactive contamination and of corrosive attack helps to optimize decontamination procedures. To simulate operating conditions, stainless steel (304L) coupons with different surface pre-treatments were immersed into 4 M or 10.5 M HNO<sub>3</sub> solutions containing either no actinides (blank sample), Np, Pu or Am during 30 days at 50 °C. Afterwards, the coupons were analyzed by autoradiography, SEM-EDX, and XPS.

Autoradiography was performed by placing the coupons (1×1 cm<sup>2</sup>) on a storage phosphor screen together with drops of radionuclide standard solutions with known volume and concentration for calibration purpose (Figure 3). In case of Am, concentration is about independent on surface pre-treatment, whereas Np and Pu showed enhanced uptake on polished surfaces. K<sub>d</sub>

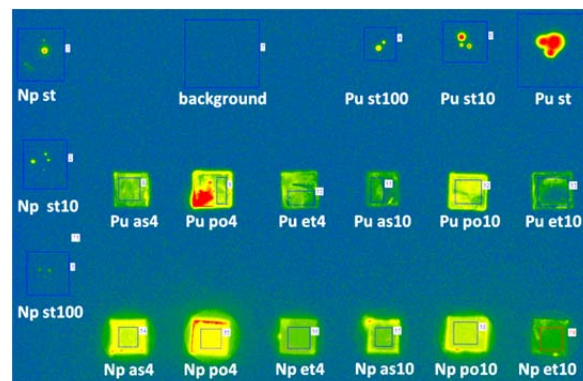


**Fig. 3:** Autoradiography of 304L stainless steel coupons immersed in nitric acid containing Pu or Np with different surfaces. Abbreviations: as received (as), polished (po), etched (et), 4M HNO<sub>3</sub> (4), 10.5M HNO<sub>3</sub> (10), and standard solutions (st, dilution) as references. Areas of analysis are indicated.

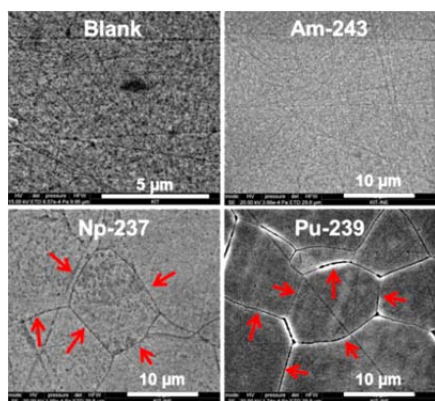


**Fig. 4:** SEM images of the surface of polished 304L stainless steel coupons after immersion in 10.5 M HNO<sub>3</sub>: blank, Am (931 ppm), Np (471 ppm), Pu (97 ppm). Intergranular corrosion indicated by red arrows.

value in case of polished samples (10.5 M HNO<sub>3</sub>) for Np is of the order of 0.2, Pu 0.006, and Am 0.06 L/m<sup>2</sup>. SEM images (Figure 4) show uniform dissolution in case of the blank sample and Am(III) solution, scratches from polishing still visible. Intergranular corrosion is detected if oxidizing elements like Np(VI) or Pu(VI) were present in solution [3]. SEM-EDX and XPS however could not detect the actinides due to their low concentrations at the stainless steel surfaces.

### Interaction of furnace lining ceramics with the glass melt by SEM-EDX phase maps

Furnace linings of electrode glass furnaces for vitrification of highly radioactive liquid waste consist of refractory ceramics made from aluminum and chromium oxide as main components and smaller amounts of ZrO<sub>2</sub>. The ceramic is in permanent contact to the glass melt and serves as thermal isolation for the vessel. Fused cast ceramic, like Monofrax K3, is to be replaced on the long-term due to environmental regulation issues concerning manufacturing. Sintered ceramic is a candidate but exhibits higher porosity. Durability of the sintered ceramics and Monofrax K3 was compared by immersion into a glass melt (1200 °C, 144 h). Subsequently, cross sections were prepared for analysis of the ceramic-glass interface by SEM, an example is depicted in Figure 5. Elemental maps by SEM-EDX were recorded from the rim of the ceramic body exhibiting a corrosion layer. Discrimination

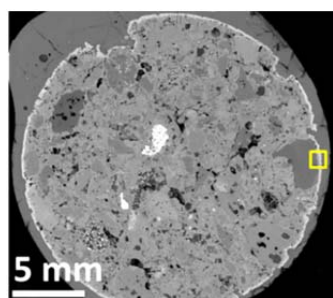


**Fig. 5:** Cross-section of a sintered ceramic cylinder after glass melt immersion by backscattered electron imaging. The bright grains are composed of ZrO<sub>2</sub>. The bright rim denotes the corrosion layer, analyzed at the area indicated.

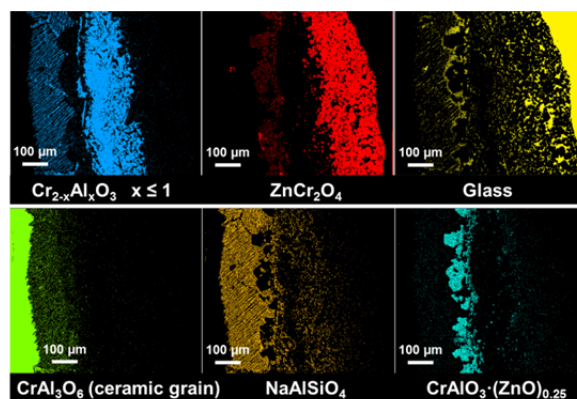


**Fig. 6:** Individual elemental phases by multivariate analysis of SEM-EDX elemental maps of the corrosion layer, area of analysis indicated in Figure 5.

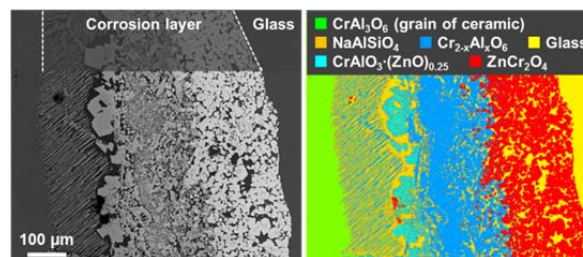


**Fig. 7:** Backscattered electron image of glass corrosion layer (left image), SEM-EDX elemental phase map of same area (right image).

between corrosion products containing elements from the ceramic and from the glass is challenging since the glass is composed of 28 elements but can be solved by multivariate analysis of the EDX spectra stored at every point of the elemental map (Thermo Scientific NORAN System7 software, ver. 3.3). Individual phases are defined if a certain amount of similar spectra are present in the data set. The elemental phases differ in their compositions and are not necessarily crystalline. The spatial distribution of phases of the corrosion layer is depicted in Figure 6. Glass intrusion into the porous corrosion layer thus can be detected. The corrosion of the ceramic is predominantly caused by the reaction of Al of the ceramic grains with Na and Si from the glass melt while Cr is enriched in the corrosion layer. Small Cr<sub>2</sub>O<sub>3</sub> needles are observed occasionally. The glass in this case contains 3.1 wt% ZnO, and 0.04 wt% Cr<sub>2</sub>O<sub>3</sub>. Zn reacts with the Cr rich corrosion layer, i.e. (Cr,Al)<sub>2</sub>O<sub>3</sub> solid solution, to form ZnCr<sub>2</sub>O<sub>4</sub>. In Figure 7, the backscattered electron image of the corrosion layer and a composite map of the individual phases (Figure 6) are depicted. Similar corrosion processes are observed also in case of Monofrax K3 fused cast ceramic. SEM-EDX phase maps enable the visualization of compositional phases and thus facilitate analysis of complex samples.

### References

- [1] Schlossmacher, P. et al., *Microscopy and Analysis* **24(7)**: S5-S8 (EU) (2010).
- [2] Varela, M. *Annu. Rev. Mater. Res.* **B37**: 539 (2005).
- [3] Fauvet, P. et al., *J. Nucl. Mat.* **375**: 52-64 (2008).

## 8.4 Investigations into structure and bonding by NMR spectroscopy

Ch. Adam, V. Rohde, P. Kaden, P. J. Panak

### Introduction

Since their discovery as potential extraction ligands for Partitioning and Transmutation (P&T) strategies, soft N-donor ligands in general and BTP-type ligands (Fig. 1) in particular, have been thoroughly studied using numerous techniques [1-3]. Despite all the efforts, the molecular reason for their selective complexation of actinide ions in the presence of lanthanide ions is still not entirely clear.

Early on, a larger degree of covalence in the metal-ligand bonding was brought forward as an explanation. As the actinides' 5f orbitals are more diffuse and have a greater radial extension compared to the more localized 4f orbitals of lanthanide ions, it was assumed that 5f orbitals participate in covalent bonding. While covalence (as a shared electron density between two atoms in spatially overlapping atomic orbitals) is a useful and well-established concept for the description of chemical bonding, it is not directly observable [4]. The degree of covalence in bonding can only be determined by effects that arise of covalent contributions to the metal-ligand bond. Among others, optical spectroscopy, electron paramagnetic resonance spectroscopy (EPR), Mößbauer spectroscopy, photoelectron spectroscopy and X-ray absorption spectroscopy (XAS) are sensitive to effects that are based on covalence.

Nuclear magnetic resonance spectroscopy (NMR) is a spectroscopic method that is highly sensitive to the electron density surrounding the observed nucleus. Since the density is influenced strongly by "sharing" electrons in a covalent bond, NMR is the ideal tool to give insight into metal-ligand bonds. In the case of paramagnetic complexes, further contributions to the observed chemical shift from dipolar electrostatic coupling and covalently transferred electron spin density arise, thus complicating the evaluation of NMR spectra [5-9]. In principle, these contributions can be separated by several approaches and offer a valuable way to gauge covalence in the coordination compound. Currently, research within the INE NMR working group aims at transferring strategies for the mathematical treatment of paramagnetic lanthanide complexes to actinide complexes.

#### Effects of BTP substituents

A change of the aliphatic side chains of the lateral rings in BTP-type ligands influences the solubility in organic solvents. Since the side chains also "fine-tune" the electronic properties of the triazine moieties by their inductive effects, this also modifies the extraction properties and the selectivity of the ligands. These effects are strong if the side-chains are exchanged *e.g.* for aromatic rings or functional groups bearing heteroatoms, whereas the differences between the isomeric *n*-propyl- and *iso*-propyl substituted BTPs (Fig. 1) are expected to be small.

However, the differences between the two related ligands were found to be larger than expected. Compared to *n*PrBTP, *i*PrBTP has a higher distribution ratio in Am(III) extraction experiments, yet shows very odd extraction kinetics: Am(III) is extracted very quickly, whereas Eu(III) extraction happens much slower. As a consequence, the selectivity depends on the contact time between aqueous and organic phase. Under equilibrium conditions, the selectivity for Am(III) over Eu(III) of *i*PrBTP is lower than for *n*PrBTP. These findings suggest that the complex formation mechanisms for the two ligands are different.

Additionally, complex stability constants for *i*PrBTP with Cm(III) and Eu(III) were determined at INE using time-resolved laser fluorescence spectroscopy (TRLFS). The stability constant for  $[\text{Cm}(\text{iPrBTP})_3]^{3+}$  ( $\log\beta'_3 = 16.3$ ) is almost two logarithmic units higher than for  $[\text{Cm}(\text{nPrBTP})_3]^{3+}$  ( $\log\beta'_3 = 14.4$ ) in the same solvent mixture. A similar trend is observed for the analogous Eu(III) complexes. The stability constant for  $[\text{Eu}(\text{iPr-BTP})_3]^{3+}$  ( $\log\beta'_3 = 14.9$ ) is even three logarithmic units higher than the analogous *n*Pr-BTP complex ( $\log\beta'_3 = 11.9$ ) [10], resulting in a lower selectivity for Am(III) over Ln(III). This shows nevertheless that *i*PrBTP is a distinctively stronger ligand towards trivalent lanthanides and actinides compared to *n*PrBTP. These results are due either to a different complex formation mechanism or differences in chemical bonding, or even a superposition of both effects. These results prompted us to investigate the bonding situation in *i*PrBTP complexes with NMR spectroscopy.

### Synthesis and NMR

Changes in the bonding between metal and ligand have the strongest effect on the coordinating nitrogen atoms. Unfortunately, the more abundant natural occurring isotope  $^{14}\text{N}$  has very poor NMR properties that lead to severe line broadening and often render signals unobservable. The other naturally occurring

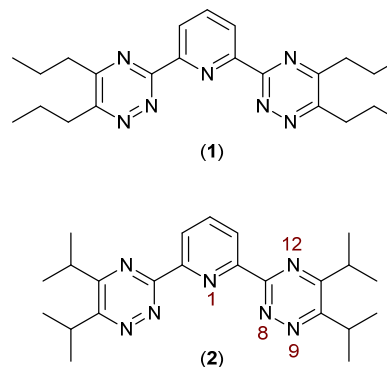
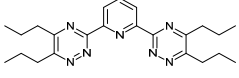
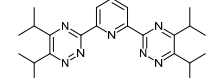


Fig. 1: Structures of the ligands (1) *n*PrBTP and (2) *i*PrBTP. The numbering scheme for the nitrogen atoms is displayed for *i*PrBTP.

**Table 1:** Comparison of the chemical shifts for the nitrogen atoms of *nPrBTP* and *iPrBTP* complexes. All values are given in ppm relative to  $\square(\text{NH}_4\text{Cl}) = 0$  ppm.

								
	N <sub>1</sub>	N <sub>8</sub>	N <sub>9</sub>	N <sub>12</sub>	N <sub>1</sub>	N <sub>8</sub>	N <sub>9</sub>	N <sub>12</sub>
free ligand	303	353	403	288	303	353	402	288
Y(III)	268	307	386	293	267	310	390	290
Lu(III)	269	308	387	293	270	312	390	293
Sm(III)	226	261	383	293	226	263	387	292
Am(III)	-25	-18	419	289	-31	-16	421	289

isotope,  $^{15}\text{N}$ , has a half-integer nuclear spin and more benevolent NMR properties, but a very low natural abundance of only 0.364%. This low natural abundance often impedes the effective acquisition of direct excitation  $^{15}\text{N}$ -NMR spectra, so we synthesized a  $^{15}\text{N}$  labelled *iPrBTP* ligand (positions 8 and 9). Isotope labelling was achieved by using 10%  $^{15}\text{N}_2\text{H}_4$ , while in all other respects following the original synthesis protocol [11-13].

Having obtained the labelled ligand in good yield, we conducted a systematic NMR study of the complexes with the diamagnetic lanthanide ions (Lu(III) and Y(III), which is frequently used as a lanthanide analogue), and the weakly paramagnetic Sm(III). As a representative of the actinide ions, we also synthesized the  $^{243}\text{Am}$ (III) complex. Although the exact nature of the magnetic behavior of this ion is still a matter of debate, it is clear that it has a non-zero magnetic moment, yet only has a very weak paramagnetism, i.e. a magnetic moment lower than  $1 \mu\text{B}$  [14-22]. As the same set of complexes has been investigated previously with the *nPrBTP* ligand, a direct comparison of the two complex series is possible [23-24]. Any differences in bonding should reflect in differing shifts for the coordinating nitrogen atoms  $\text{N}_1$  and  $\text{N}_8$ . The results for all nitrogen atoms of the two ligands in different complexes are shown in table 1.

The chemical shifts for the free ligands are almost identical for both molecules. This confirms that their electronic structure is almost identical, thus proving the assumption that the electronic structure should remain largely unperturbed upon exchange of the aliphatic substituents.

Upon coordination to the lanthanide ions or Y(III) the observed trends are the same for both ligand systems: Except for  $\text{N}_{12}$  all resonance signals are shifted upfield (i.e. towards smaller shift values), while  $\text{N}_{12}$  is almost unperturbed or shows only minute downfield shifts. In general, the nitrogen atoms show a slightly stronger shift in the *nPrBTP* ligand, however, the differences are negligible.

The situation is different for Am(III), where the coordinating nitrogen atoms  $\text{N}_1$  and  $\text{N}_8$  show remarkable upfield shifts, while the  $\text{N}_9$  resonance signals are shifted noticeably downfield. Once more, the differences between *nPrBTP* and *iPrBTP* are very small (below 6 ppm), indicating a closely resembling electronic

structure. The huge shift difference between actinide and lanthanide complexes shows that the bonding situation is drastically different in complexes of the two element groups, and can be interpreted in terms of an increased covalence in the actinide compounds [23-25].

The very small shift differences between the two complex series with *nPrBTP* and *iPrBTP* indicate that the metal-ligand bonding situation is nearly identical. This in turn confirms that the observed differences in the complex stability constants are not caused by structural differences in the complexes, but by differences in the complex formation mechanism.

These results are in good agreement with quantum chemical calculations performed at INE [10]. Molecular dynamics simulations of the complex formations show that in the Cm(III) complexes of *iPrBTP* a significantly lower number of water molecules reside in the inter-ligand space compared to the *nPrBTP* complex. This is due to a sterically shielding effect of the bulkier iso-propyl sidechains. Furthermore, during the complex formation the bulkier side chains effectively block escape pathways for the water molecules which are dislodged by the organic ligand, thus explaining the slower extraction kinetics of *iPrBTP*.

## Summary and Conclusion

Through comparison of two sets of closely related complexes of BTP-type N-donor ligands with trivalent lanthanide and Am(III) ions by NMR spectroscopy important results were obtained. Firstly, our results clearly show differences in the bonding situation between the lanthanide and actinide complexes which are interpreted as the result of an increased covalence in the Am(III) complex. Secondly, as no significant differences between the *iPrBTP* and *nPrBTP* complexes with identical metal ions are observed, we exclude differences in the structure and bonding of the complexes as the reason for the observed difference in extraction behavior and complex stability constants. These results point to different mechanisms of complex formation, which is also confirmed by quantum chemical investigations.

## References

- [1] Z. Kolarik, U. Müllich, F. Gassner, *Solvent Extr. Ion Exch.* 1999, 17, 23 - 32.
- [2] Z. Kolarik, U. Müllich, F. Gassner, *Solvent Extr. Ion Exch.* 1999, 17, 1155-1170.
- [3] P. J. Panak, A. Geist, *Chem. Rev.* 2013, 113, 1199-1236.
- [4] M. L. Neidig, D. L. Clark, R. L. Martin, *Coord. Chem. Rev.* 2013, 257, 394-406.
- [5] I. Bertini, C. Luchinat, G. Parigi, *Solution NMR of paramagnetic molecules: applications to metallo-biomolecules and models*, 1. ed., Elsevier, Amsterdam, 2001.
- [6] S. Di Pietro, S. L. Piano, L. Di Bari, *Coord. Chem. Rev.* 2011, 255, 2810-2820.
- [7] H. J. Keller, K. E. Schwarzhans, *Angew. Chem.* 1970, 82, 227-236.

- [8] K. E. Schwarzhan, *Angew. Chem.* 1970, 82, 975-982.
- [9] C. Piguet, C. F. G. C. Geraldes, in *Handbook on the Physics and Chemistry of Rare Earths*, Vol. Volume 33 (Eds.: J. K.A. Gschneidner, J. C. G. Bünzli, V. K. Pecharsky), Elsevier, 2003, pp. 353-463.
- [10] B. B. Beele et al., manuscript in preparation.
- [11] J. H. Snell, *Organic Syntheses* 1933, 13, 24.
- [12] F. H. Case, *J. Heterocycl. Chem.* 1971, 8, 1043-1046.
- [13] V. Rohde, Diploma thesis, Karlsruher Institut für Technologie (Karlsruhe), 2014.
- [14] P. Hessler Jan, T. Carnall W, in *Lanthanide and Actinide Chemistry and Spectroscopy*, Vol. 131, American Chemical Society, 1980, pp. 349-368.
- [15] L. Soderholm, *J. Less-Common Met.* 1987, 133, 77-85.
- [16] L. Soderholm, N. Edelstein, L. R. Morss, G. V. Shalimoff, *J. Magn. Magn. Mater.* 1986, 54-7, 597-598.
- [17] G. Gaigalas, E. Gaidamauskas, Z. Rudzikas, N. Magnani, R. Caciuffo, *Phys. Rev. A* 2009, 79, 022511.
- [18] C. Apostolidis, B. Schimmelpfennig, N. Magnani, P. Lindqvist-Reis, O. Walter, R. Sykora, A. Morgenstern, E. Colineau, R. Caciuffo, R. Klenze, R. G. Haire, J. Rebizant, F. Bruchertseifer, T. Fanghänel, *Angew. Chem. Int. Ed.* 2010, 49, 6343-6347.
- [19] P. G. Huray, S. E. Nave, R. G. Haire, *J. Less-Common Met.* 1983, 93, 293-300.
- [20] S. E. Nave, R. G. Haire, P. G. Huray, *Phys. Rev. B* 1983, 28, 2317-2327.
- [21] T. F. Wall, S. Jan, M. Autillo, K. L. Nash, L. Guerin, C. L. Naour, P. Moisy, C. Berthon, *Inorg. Chem.* 2014, 2450-2459.
- [22] M. Autillo, P. Kaden, A. Geist, L. Guerin, P. Moisy, C. Berthon, *PCCP* 2014, 8608 - 8614.
- [23] C. Adam, Ph. D. thesis, Ruprecht-Karls-Universität Heidelberg (Heidelberg), 2016.
- [24] C. Adam, P. Kaden, B. B. Beele, U. Müllich, S. Trumm, A. Geist, P. J. Panak, M. A. Denecke, *Dalton Trans.* 2013, 42, 14068-14074.
- [25] C. Adam, B. B. Beele, A. Geist, U. Müllich, P. Kaden, P. J. Panak, *Chemical Science* 2015, 6, 1548-1561.

## 8.5 Accelerator mass spectrometry

F. Quinto, S. Heck, M. Lagos, M. Plaschke, T. Schäfer, and H. Geckeis

In co-operation with:

P. Steier

VERA Laboratory, Faculty of Physics, University of Vienna, Währinger Straße 17, A-1090 Vienna, Austria

Th. Faestermann, J. M. Gómez Guzmán, K. Hain, G. Korschinek and P. Ludwig

Physik Department, Technische Universität München, James-Frank-Straße 1, D-85748 Garching, Germany

### Introduction

With accelerator mass spectrometry (AMS) a wide range of nuclide masses spanning from  $^{10}\text{Be}$  up to the actinides can be detected without interferences from molecular isobars and tailing from neighboring abundant masses. In this way, all the actinide nuclides can be unambiguously detected with an overall sensitivity of  $10^4$  atoms in a sample. We have developed a novel analytical method consisting in the simultaneous determination of several actinide nuclides without previous chemical separation from each other with the use of non-isotopic tracers for the ultra-trace determination of  $^{237}\text{Np}$  and  $^{243}\text{Am}$ . Such multi-actinide analysis with AMS has proven to be a valuable tool for the investigation of actinides inherent both to global fallout in natural water samples and to *in situ* radionuclide tracers tests, e.g., run 12-02 of the CFM project [1]. In the actual report we present the recent findings from the application of the multi-actinide analysis with AMS to the successive *in situ* experiment, run 13-05. We discuss the complementary roles of AMS and SF-ICP-MS as well as a direct comparison between the two analytical methods on a chosen group of samples.

First results were furthermore achieved in the ultra-trace determination of  $^{99}\text{Tc}$  ( $t_{1/2} = 2.1 \times 10^5$  years), a fission product of concern for the long term radiotoxicity of spent nuclear fuel. Similar as for the actinides, the analytical capability of investigating  $^{99}\text{Tc}$  in natural samples at concentrations lower than ppq levels can be exploited in the study of its environmental behavior, both in the frame of *in situ* tracers tests and diffusion experiments and in the determination of ultra-trace contamination of the environment from global fallout and nuclear reprocessing.

### Multi-actinide analysis applied to the CFM project run 13-05

At the Grimsel Test Site (GTS), the *in situ* tracer test run 13-05 consisted in the injection of  $^{233}\text{U}$ ,  $^{237}\text{Np}$ ,  $^{242}\text{Pu}$  and  $^{243}\text{Am}$  in a dipole of a water conducting granodiorite shear-zone fracture in the presence of bentonite colloids and under near natural flow conditions. Similarly like for the previous experiment, run 12-02 [1], the concentrations of  $^{233}\text{U}$ ,  $^{237}\text{Np}$ ,  $^{242}\text{Pu}$  and  $^{243}\text{Am}$  were investigated with SF-ICP-MS, obtaining a dense group of data describing the peak of the breakthrough curve and limited to ca. 25 days from the

injection of the actinide tracers (not reported here). In order to investigate the behavior of the actinides in the tailing of the breakthrough curve below the detection limits (DL) of SF-ICP-MS equal to ca. 10 ppq, the multi-actinide analysis with AMS (VERA laboratory, Vienna) has been employed in the actual experiment. Furthermore, 10 samples belonging to the peak of the breakthrough curve were analyzed with AMS in order to allow a direct comparison between the two employed analytical methods. For the AMS analysis,  $^{233}\text{U}$ ,  $^{237}\text{Np}$  and  $^{242}\text{Pu}$  were determined by using  $^{239}\text{Pu}$  as yield tracer, while  $^{243}\text{Am}$  by using  $^{248}\text{Cm}$ . In order to normalize the measured concentrations relative to the corresponding yield tracer, the chemical and the ionization yields (CIY) of the five actinides in the Cs negative ion sputtering source of AMS have been determined according to the procedure described in [1].

The groundwater samples of run 13-05 were sized according to the expected concentration of the actinides from 0.1 g to 250 g. In this way, the detection of the injected actinides with AMS was possible over six orders of magnitude, in particular from 10 ppt down to 0.1 ppq, as depicted in Figure 1. On the horizontal axis, the sampling time from the injection of the actinide tracers is expressed in days and with a logarithmic scale. As it can be seen in Figure 1, the determination of the actinide tracers was successful until the last sampling time at 8 months after the starting of the experiment. The first four sample depicted in Figure 1 are believed to carry the signal of previous *in situ* tracer tests performed at the GTS. This hypothesis is supported by the detection in the four samples of masses 241 and 244 ascribable to the use of  $^{241}\text{Am}$  and  $^{244}\text{Pu}$  as tracers in such previous tests.

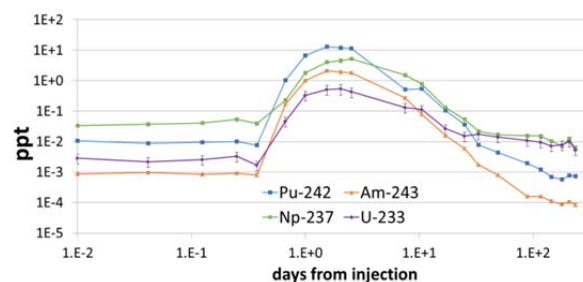
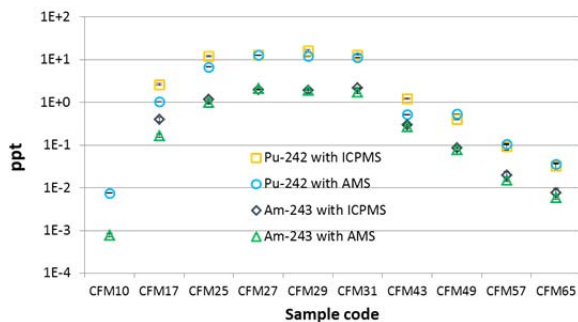


Fig. 1: Determination of the actinide tracers in run 13-05 over 8 months with AMS.



**Fig. 2:** Comparison between the concentrations of  $^{242}\text{Pu}$  and  $^{243}\text{Am}$  measured with AMS and SF-ICP-MS in ten samples belonging to the peak of the breakthrough curve of run 13-05.

The relative uncertainties change substantially according to the nuclide.

While the concentrations of  $^{242}\text{Pu}$  have a relative error between 1% and 5% due mainly to counting statistics, the other nuclides have higher uncertainties due to the use of non-isotopic tracers. The variability of the ionization yield of Np relative to Pu and Am relative to Cm has been lower than in the previous experiment (run 12-02), resulting in uncertainties of ca. 10% and 12%, respectively. On the other hand, the variability of the ionization yield of U relative to Pu has been higher, so that for the concentrations of  $^{233}\text{U}$  a relative uncertainty of up to 35% is obtained. However, even considering such high relative uncertainty, the multi-actinide analysis with AMS enables long-term field studies of multiple actinide tracers at unrivalled low concentration levels. In the ten samples belonging to the peak of the breakthrough curve chosen for the direct comparison between the two employed analytical methods, the concentrations of the actinides measured with the multi-actinide method and AMS mirror the behavior of those measured with SF-ICP-MS, as it can be seen in Fig. 2 for  $^{242}\text{Pu}$  and  $^{243}\text{Am}$ . However, the AMS values are in almost all the cases lower than the corresponding ones measured with SF-ICP-MS. Since such behavior is observed also for  $^{242}\text{Pu}$ , we conclude that it does not depend on the use of non-isotopic tracers.

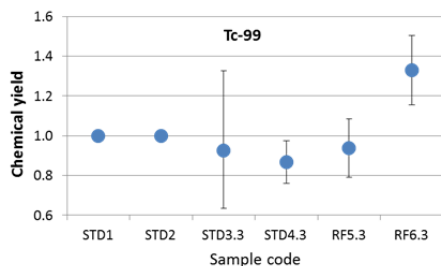


**Fig. 3:** Chemical yield of  $^{99}\text{Tc}$  chromatographic extraction from standard solutions (STD3.3 and STD4.3) and from two aliquots of RM IAEA-443 (RF5.3 and RF6.3) relative to the standard samples (STD1 and STD2).

## $^{99}\text{Tc}$

The radiometric determination of the long lived pure  $\beta^-$  emitter  $^{99}\text{Tc}$  with LSC or gas ionization detection presents DL of  $10^{-10} - 10^{-12}$  g. Comparable DL are achieved with NAA, while significantly higher sensitivity is associated to the mass spectrometric determination of  $^{99}\text{Tc}$ . ICP-MS offers DL of ca.  $10^{-12}$  g that can be lowered down to ca.  $10^{-14}$  g with the use of an electrothermal vaporization device (ETV-ICP-MS). The highest sensitivity is achieved with TIMS, RIMS and AMS with DL of ca.  $10^{-15}$  g [2]. The main limitation to the sensitivity of the mass spectrometric analysis of  $^{99}\text{Tc}$  is the background of the stable isobar  $^{99}\text{Ru}$ , which must be reduced both with a chemical separation of technetium from ruthenium and with additional filtering devices in the mass spectrometer. We present in this report first results in the determination of  $^{99}\text{Tc}$  in standard solutions and in the reference material (RM) IAEA-443 (radionuclides in Irish Seawater).

We have tested a chemical procedure for the separation of technetium from matrix elements and from ruthenium, employing TEVA resin [2]. Four samples bearing each ca.  $1.7 \times 10^9$  atoms equivalent to ca.  $3 \times 10^{-13}$  g of  $^{99}\text{Tc}$  were prepared from a  $^{99}\text{Tc}$  standard solution (GE Healthcare Limited Product code: TCZ44). Two of such samples, named STD3.3 and STD4.3, were submitted to the extraction chromatography together with two aliquots of the RM IAEA-443 bearing ca.  $2 \times 10^9$  and  $2 \times 10^{10}$  atoms of  $^{99}\text{Tc}$  and named RF5.3 and RF6.3, respectively. The remaining two standard samples, STD1 and STD2, did not undergo chromatographic separation. The six samples were measured at the 13 MV Tandem AMS facility of TUM (Garching). A Gas-Filled Analyzing Magnet System (GAMS) placed before the ionization chamber detector was used in order to further suppress the interference from the isobar  $^{99}\text{Ru}$ . With this setup the suppression of the  $^{99}\text{Ru}$  signal has been achieved up to 4 orders of magnitude, allowing an accurate measurement of  $^{99}\text{Tc}$ . The sensitivity of the measurement procedure is presently at the levels of  $10^7$  atoms in a sample, corresponding to ca.  $10^{-15}$  g. In Figure 3 the yield of the employed chemical procedure is represented taking samples STD1 and STD2 as reference. The chemical yield for the four samples that underwent chemical separation is higher than 80%. We plan to increase the overall sensitivity of the method by increasing the ionization yield of  $^{99}\text{Tc}$  and testing different sputtering matrices for the samples.

## References

- [1] Quinto F, Golser R, Lagos M, Plaschke M, Schaffer T, Steier P, et al. Accelerator Mass Spectrometry of Actinides in Ground- and Seawater: An Innovative Method Allowing for the Simultaneous Analysis of U, Np, Pu, Am, and Cm Isotopes below ppq Levels. *Anal Chem.* 2015;87(11):5766-73.
- [2] Shi K, Hou X, Roos P, Wu W. Determination of technetium-99 in environmental samples: A review. *Analytica Chimica Acta.* 2012;709:1-20.

## 8.6 Computational chemistry

*B. Schimmelpfennig, R. Polly, M. Trumm, M. Altmaier*

In co-operation with:

*P. Lindqvist-Reis, N. Lal Banik, A. Baumann, E. Yalcintas, X. Gaona, N. Finck, T. Yokosawa, M. Bouby, K. Dardenne, T. Schäfer, H. Geckeis*

### Introduction

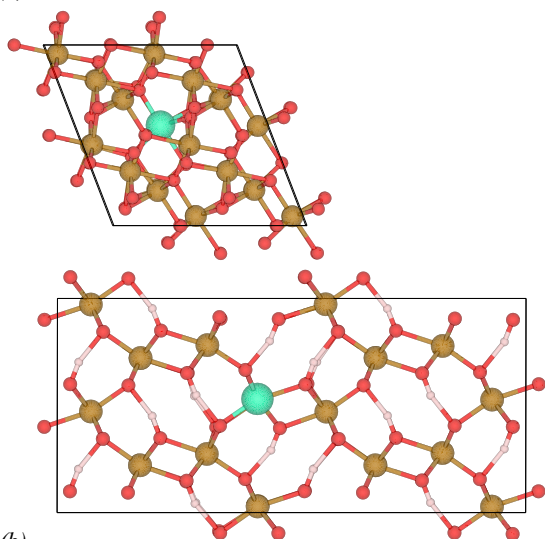
Computational Chemistry at KIT-INE is a well-established and very valuable theoretical tool assisting and complementing experimental investigations in the field of nuclear waste disposal. There is a wide range of applications for Computational Chemistry at KIT-INE: from providing structures of complex chemical systems including actinides in solution or solid phase, thermodynamic data or reproducing the actual experimental spectra for EXAFS or XANES, to performing simulations and visualization of complex chemical reactions. The systems under investigation thus vary from small complexes in solution to crystal phases or mineral/liquid interfaces. New algorithms and the constantly improving hardware allow a steady improvement of the detailed description of actinide systems at the level of electronic structure. This lead to the possibility to use quantum chemistry as a predictive tool and to suggest further experimental studies.

### Quantum chemical investigation of incorporation of lanthanides and actinides into iron oxides

In this study we tackle several different systems: (1) the incorporation of  $\text{Lu}^{3+}$  into hematite and goethite, (2) the incorporation of  $\text{U}^{6+}$  into hematite and (3) the incorporation of  $\text{U}^{5+}$  into magnetite.

The theoretically sound consideration of iron oxides is a great challenge due to the occupation of the 3d orbitals of Fe.  $\text{Fe}^{3+}$  is a high spin open shell case with

(a)



(b)

**Fig. 1:** (a) Incorporation of  $\text{Lu}^{3+}$  into (a) hematite and (b) goethite.

a  $3d^5$  occupation. The workhorse of solid state theoretical chemistry is density functional theory (DFT) with periodic boundary conditions as implemented in VASP. However, DFT has severe problems in describing such highly correlated open shell systems. Conventional DFT provides very unreliable results for these systems, therefore we have to employ DFT+U in our investigations.

$\text{Fe}^{2+}$ , as present in magnetite, is even more of a challenge. The occupation of the 3d orbitals in  $\text{Fe}^{2+}$  is  $3d^6$ . Additional to the strong interaction of the 3d electrons multi reference effects occur. DFT is not able to deal with such systems, but is restricted to single reference systems. Hence a careful consideration of the systematic error introduced by the inadequate theoretical treatment has to be included and the theoretical results have to be validated case by case with multi reference methods such as the complete active space self-consistent field (CASSCF) method. Such theoretical investigations are routinely done in our laboratory.

### Incorporation of $\text{Lu}^{3+}$ into hematite and goethite

This study is motivated by different experiments at KIT-INE describing the incorporation of  $\text{Lu}^{3+}$  into hematite and goethite. But, depending on the pre-treatment of the sample, either preferable incorporation into hematite or goethite is found. Hence we carried out DFT calculations to help answer this question. And provided structural data as well as information about the reaction energies [1].

The structural data presented in Table 1 shows the excellent agreement of experimental EXAFS data with our calculated DFT results. This emphasizes the high

**Table 1:** Comparison of experimental and theoretical bond lengths in hematite and goethite with and without incorporation of  $\text{Lu}^{3+}$  (all distances in [pm]).

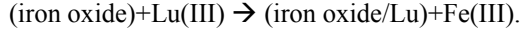
Hematite [1]					
$\text{Lu}^{3+}$ incorporated			pure hematite		
r	EXAFS	DFT+U	r	EXAFS	DFT+U
Lu-O	219	220	Fe-O	205	202
Lu-Fe	309	305	Fe-Fe	292	295
Lu-Fe	342	342			
Lu-Fe	389	378			
Goethite [2]					
$\text{Lu}^{3+}$ incorporated			pure goethite		
r	EXAFS	DFT+U	r	EXAFS	DFT+U
Lu-O	220	217	Fe-O	194	196
Lu-Fe	308	302	Fe-Fe	301	302
Lu-O	332	316	Fe-Fe	321	328
Lu-Fe	347	350			

**Table 2:** Comparison of experimental and theoretical bond lengths in hematite with  $U^{6+}$  incorporated (all distances in [pm]).

r	EXAFS [3]	DFT+U
U-O	228	208
U-Fe	319	315

quality of the DFT results.

In a second step we determined the reaction energies of the incorporation of  $Lu^{3+}$  into hematite and goethite using the following reaction



Here (iron oxide) could be either hematite or goethite and (iron oxide/Lu) denotes the replacement of one Fe(III) by Lu(III) in either hematite or goethite. Since the energies of the two ions (Fe(III) and Lu(III)) are identical for both incorporation reactions we focused on the energy differences  $E(\text{iron oxide}/Lu) - E(\text{iron oxide}/Fe)$  in order to judge where Lu(III) is incorporated more likely. For hematite we obtained  $E_{\text{hem}} = E_{\text{hematite}/Lu} - E_{\text{hematite}} = -2.87$  eV and for goethite  $E_{\text{goe}} = E_{\text{goethite}/Lu} - E_{\text{goethite}} = -2.75$  eV. Since the energy difference between hematite and goethite is so small, the DFT calculations show that the incorporation of Lu(III) should be equally likely for hematite and goethite. This leads to the conclusion that from an energetic point of view the incorporation of  $Lu^{3+}$  into hematite and goethite is equally likely and the pre-treatment of the sample is the deciding factor, whether it is incorporated into either of the two iron oxide minerals.

### Incorporation of $U^{6+}$ into hematite

Duff et al. [3] showed that uranium is incorporated as the  $U^{6+}$  ion into hematite and not as an uranyl ion. We considered this system with our calculations and found very good agreement between the experimental values [3] and our calculations.

Therefore, our calculations confirm the experimental findings and the assignment that the  $U^{6+}$  ion is incorporated into hematite.

### Incorporation of $U^{5+}$ into magnetite

The theoretical consideration of the incorporation of  $U^{5+}$  into magnetite poses several challenges for the calculations since we have to deal with a variety of open shell systems ( $Fe^{3+}$ :  $3d^5$ ,  $Fe^{2+}$ :  $3d^6$ ,  $U^{6+}$ :  $5f^1$ ) simultaneously.

The corresponding experiments are currently carried

**Table 3:** Comparison of experimental and theoretical bond lengths in magnetite with  $U^{5+}$  incorporated (all distances in [pm]).

r	EXAFS [4]	DFT+U
U-O	217	215
U-Fe	318	319
U-Fe	355	355

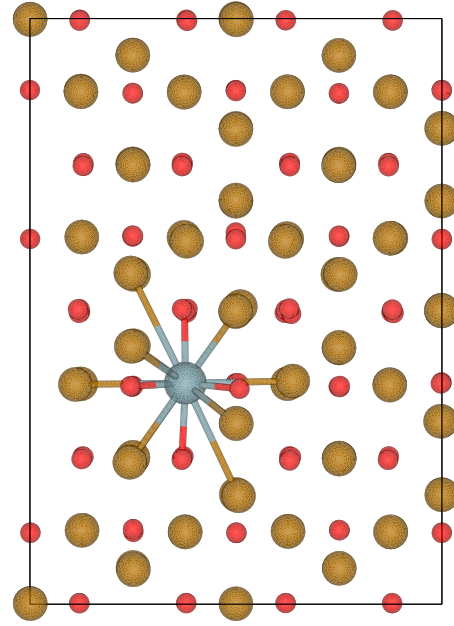


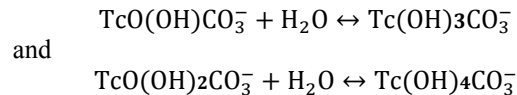
**Fig. 2:** Incorporation of  $U^{5+}$  into magnetite.

out at KIT-INE in the framework of the PhD thesis of I. Pidchenko [4] and provide a direct comparison with the results obtained with DFT.

In all three cases, (1) the incorporation of  $Lu^{3+}$  into hematite and goethite, (2) the incorporation of  $U^{6+}$  into hematite and (3) the incorporation of  $U^{5+}$  into magnetite we find excellent agreement between the experimental EXAFS results and our calculations. Hence, by means of these calculations we were able to proof that DFT is an adequate theoretical tool for the description of lanthanides and actinides into iron oxides.

### Quantum chemistry of ternary Tc(IV)-OH-CO<sub>3</sub> complexes

We investigated the  $TcO(OH)_kCO_3$  ( $k=1,2$ ) and  $Tc(OH)_lCO_3$  ( $l=3,4$ ) species with multi reference ab initio (CASSCF) and first principle methods (DFT). The initiating question was whether the  $TcO(OH)_kCO_3$  ( $k=1,2$ ) or the  $Tc(OH)_lCO_3$  ( $l=3,4$ ) species are more stable in different pH ranges. We answered this question investigating the reaction energies of



with DFT. We studied these reactions (1) in the gas phase, (2) using the conductor-like screening model (COSMO) as a continuum solvation model and (3) explicitly adding a large number of solvent molecules (100  $H_2O$  molecules in our case) to these calculations (see Fig. 3).

As a result, we found that the  $Tc(OH)_lCO_3$  ( $l=3,4$ ) are significantly more stable compared to the  $TcO(OH)_kCO_3$  ( $k=1,2$ ) species.

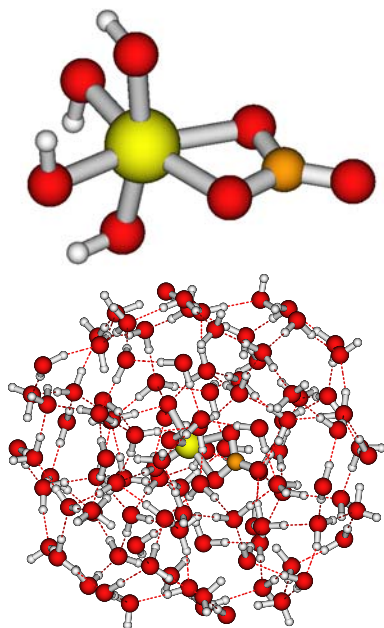


**Fig. 3:**  $Tc(OH)_4CO_3$  in the gas phase and with 100 water molecules.

### Fundamental understanding of An(III)/Ln(III) separation with N-donor ligands

With the development of soft nitrogen based extracting ligands An(III) and Ln(III) can be separated efficiently, reaching separation factors over 100. The origin of this separation as well as the failure of structurally similar ligands to accomplish separation is still a matter of controversy. Hence we performed a theoretical investigation of the ligands and their An(III)/Ln(III) complexes to shed further light on this origin. The Hirshfeld method is a well-established atoms-in-molecules approach allowing the computation of atomic charges and polarizabilities of the extracting agents. Whereas the nitrogen-charges are very close among structurally similar ligands, the polarizabilities change significantly depending on the ring-structure and the side-chain positions. We were able to connect these changes to the ligands' separation factors by computation of the binding energies (BEs) of the corresponding Cm(III) and Gd(III) using state-of-the-art ab initio calculations on the MP2/aug-cc-pVTZ level. [5] Using short gas-phase molecular dynamics (MD) simulations we proposed the existence of an optimal separation zone (Fig. 4), a ratio of polarizabilities of the coordinating nitrogen atoms that results in an optimum separation. This approach explains the superiority of the bis-triazine-pyridine (BTP) ligands of the structurally similar bis-diazine-pyridine (BDP) and bis-tetrazine-pyridine (BQP) ligands in perfect agreement with the experimental study of these ligands by Beele et al. [6] Based on these results a variety of new extracting ligands have been proposed and are currently being synthesized. They will allow a methodical comparison of the polarizabilities to meas-

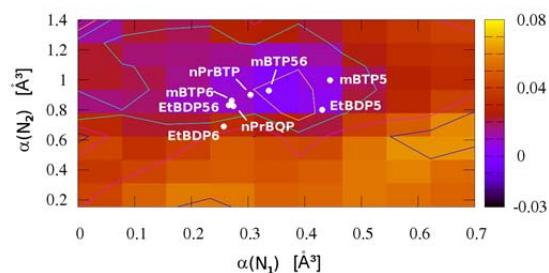


**Fig. 4:** An(III)/Gd(III) separation as a function of the coordinating nitrogen atoms' polarizabilities  $\alpha$  obtained by MD simulations.

ured NMR-shieldings which could identify higher covalence in the actinide-bonds.

To pursue the investigation further we used the computed atomic properties as well as BEs to adjust force field parameters for some of the aforementioned ligands. With the help of these parameters MD simulations of *i*Pr-BTP and CyMe4-BTP, two relevant extracting ligands, have been performed in a simulation box consisting of 1000 water molecules. Snapshots taken from these simulations were used as input to excitation-energy calculations on the DFT level. The resulting energies give rise to UV/vis spectra in solution which are in perfect agreement with the experimental spectra (Fig. 5). [7]

In further studies we plan to investigate the dependence of the spectra on the concentration of the organic solvent. In recent years water soluble versions of the BTP and BTBP ligands have been developed. [8,9] Whereas there have been studies reporting the intrusion of nitrate in the first coordination shell of An(III)-BTBP complexes under certain conditions, the intrusion of water molecules has not yet been observed. To clarify the coordination form for the water soluble  $SO_3$ -Ph-BTBP ligand we combined the computation of vibrational frequencies with TRLFS and VSB measurements. TRLFS life-times of the  $[Cm(SO_3\text{-Ph-BTBP})_2]^{5-}$  complex in both  $H_2O$  and  $D_2O$  show an increase from 173  $\mu s$  to 394  $\mu s$  suggesting the coordination of water molecules in the first hydration shell increasing the quenching.

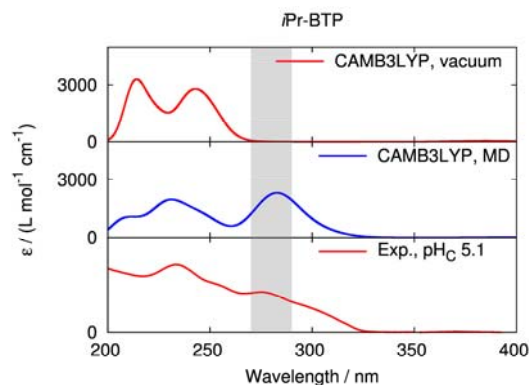


**Fig. 5:** Computed *i*Pr-BTP absorption spectra in gas-phase (top) and solution (middle) in comparison with the experimental spectrum (bottom).

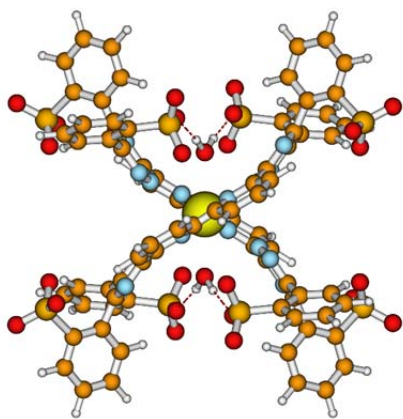


**Fig. 6:** Optimized complex structure of  $[Cm(SO_3\text{-Ph-BTBP})_2(H_2O)_2]^{5+}$ .

Also vibronic side-bands recorded for the system in  $D_2O$  show the characteristic DO-vibration from  $2100\text{-}2480\text{ cm}^{-1}$  which is in good agreement with the theoretical prediction of  $2100\text{-}2290\text{ cm}^{-1}$ . Computed binding energies on the MP2/def-TZVP level suggest the coordination of two water molecules in the first coordination shell leading to a  $D_2$  symmetrical complex (Fig. 6).

### Vibrational spectra of $Cm(III)_{aq}$

Within the ongoing studies on differences between trivalent actinides and lanthanides many different techniques have been used to highlight various properties of the ions. Vibronic side bands of the non-hydrated  $M(III)$  ion in  $[M(H_2O)_9](CF_3SO_3)_3$  ( $M = La, Y$ ) and  $[Y(H_2O)_9](C_2H_5SO_3)_3$  salts have been reported by Lindqvist-Reis et al. [10] Recently we recorded vibronic spectra of the  $Cm(III)$  aquo ion in the temperature range  $20 - 100^\circ C$ . With increasing temperature, a red-shift of the HO vibrations is observed that we attribute to an increasing 8-fold coordinated species (Fig. 7).

This is as well confirmed by ab initio molecular dynamics (AIMD) simulations. Here we first optimized a structure of a nona-coordinated  $[Cm(H_2O)_{63}]^{3+}$  complex as a starting structure for the simulation. Within the time-frame of circa 10 ps a decrease of the

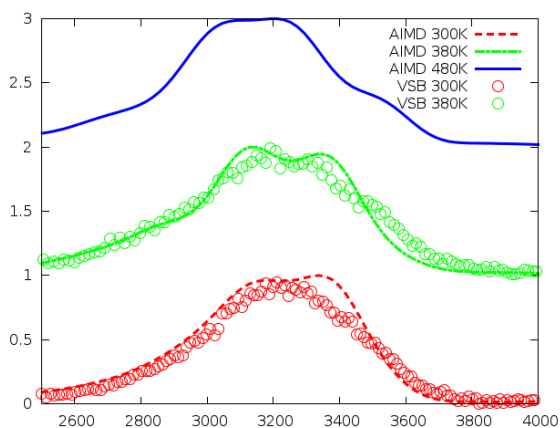


**Fig. 7:** Measured VSBS (circles) and simulated (lines) vibrational spectra of  $Cm(III)_{aq}$  from  $20 - 200^\circ C$ .

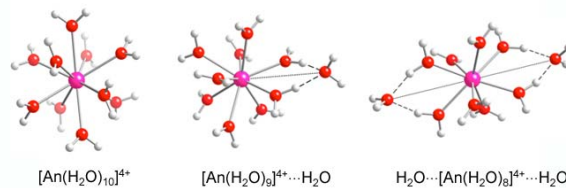


**Fig. 8:** (U)-MP2 gas-phase optimized isomeric structures

coordination number from 9.0 to 8.4 upon increasing the temperatures from  $20^\circ C$  to  $200^\circ C$  was observed. Corresponding vibrational spectra were determined by Fourier-transformation of the velocity auto-correlation function in very good agreement with the measurements. The length of the AIMD time-frame, however, is not sufficient to provide sophisticated data concerning coordination numbers as average exchange rates between the hydration shells are larger than 100 ps. To overcome these limitations classical force-field calculations on the ns time scale have been performed. The force-field parameters have been adjusted to state-of-the-art ab initio calculations. [11] A similar trend was observed for the coordination number along a 10 ns trajectory of a  $Cm(III)$  ion solvated in a cubic box of 1000 water molecules (Fig. 7). A decrease from 8.9 water molecules with a mean bond distance of  $2.50\text{ \AA}$  at  $20^\circ C$  to 8.7 at  $200^\circ C$  was determined by analysis of the radial distribution functions. The same setup was used for the  $Gd(III)$  aquo-ion. In this case, however, the VSB spectra suggest a blue-shift of the OH vibrational manifold. The corresponding AIMD simulations are currently being performed and will be analyzed to

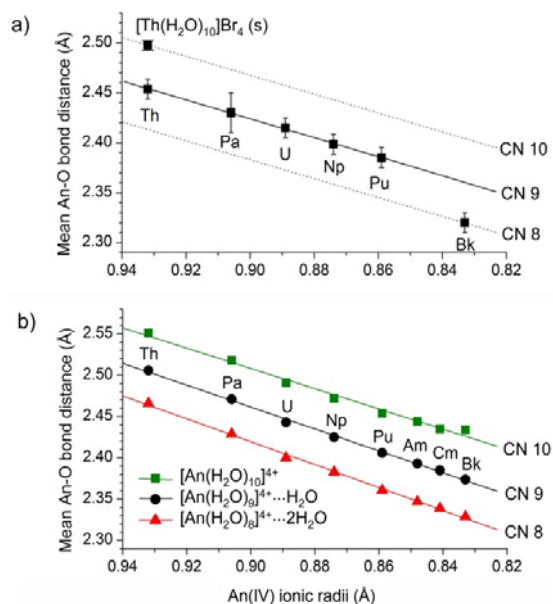


**Fig. 9:** Mean An-O bond distance vs.  $An(IV)$  ionic radii for 8, 9, and 10-coordinated  $An^{4+}$  aqua ions from a) EXAFS data of  $An^{4+}$  ions in aqueous solutions, single crystal XRD data of  $[Th(H_2O)_{10}]Br_4$ , and b) quantum chemical data of  $[An(H_2O)_{10}]^{4+}$ ,  $[An(H_2O)_9]^{4+}\cdot H_2O$ , and  $[An(H_2O)_8]^{4+}\cdot (H_2O)_2$  clusters. The lines represent mean An-O bond distances of hydrated  $An^{4+}$  ions in 8, 9, and 10-coordination.

explain this surprising difference in the temperature dependence of both ions. Classical MD simulations suggest a smaller coordination number of 8.6 with a mean distance 2.44 Å at ambient conditions in accordance with earlier studies on lanthanide hydration.

### **Tetravalent An(IV) in aqueous solution**

A combined theoretical and experimental approach was used to investigate tetravalent actinides in aqueous solution with 8-, 9- and 10-fold coordination as shown in Fig. 8.

The computed bond distances show some systematic shift compared to the experiment but follow the trend along the series compared to the ionic radii (Fig. 9). A careful analysis of the data confirmed Pa(IV) to be nine-fold coordinated, Bk(IV) to be eight-fold coordinated and a Curium break just as for the trivalent actinides [12].

### **References**

- [1] T. Yokosawa, in preparation
- [2] N. Finck, M. Bouby and K. Dardenne, in preparation
- [3] C. Duff et al., *Geochimica et Cosmochimica Acta*, 2001, **66**, 3533
- [4] I. Pidchenko, PhD thesis, KIT-INE (2016)
- [5] M. Trumm and B. Schimmelpfennig, *Mol. Phys.*, 2016, **114**, 876
- [6] B. Beele et al, *Procedia Chem.*, 2012, **7**, 146
- [7] S. Höfener et al., *PCCP*, 2016, **18**, 7728
- [8] C. Wagner et al., *Dalton Trans.*, 2015, **44**, 143
- [9] C. Wagner et al., *Solvent Extraction and Ion Exchange*, 2015, accepted
- [10] P. Lindqvist-Reis et al., *J. Phys. Chem. C*, 2009, **113**, 449
- [11] F. Réal et al., *J. Comput. Chem.*, 2015, **34**, 707
- [12] N. L. Banik et al., *Dalton Trans.*, 2016, **45**, 453



## 9 (Radio-)chemical analysis

At INE a pool of advanced analytical techniques, well-developed procedures and competences in radio-analytical sample preparation, handling and technical skills are available. These capabilities are not only needed for the R&D projects of the institute but also requested by external clients, e.g., in the fields of decommissioning of nuclear installations, nuclear waste declaration, quality control of radio-analytical separation materials and of radiopharmaceuticals. A special focus is in mass spectrometry techniques that are adapted and improved for trace element analysis and speciation studies of actinides and fission products. The use of hyphenated techniques, like Sector Field (SF)-ICP-MS or Collision Cell Quadrupole CC-Q-ICP-MS coupled to species sensitive methods, e.g., to capillary electrophoresis (CE) or ion chromatography (IC), enables speciation of actinide, of fission product and iron redox states. Supersensitive determination of actinides and  $^{99}\text{Tc}$  below ppq levels in ground-, surface and seawater is achieved by accelerator mass spectrometry (AMS); see chapter 9.5 for further details. New separation methods are developed for the simultaneous investigation of actinides, i.e., Np and Pu, in environmental samples, e.g., clay deposits. Additionally, the analytical group supports the INE infrastructure, is involved in various teaching activities and is responsible for education of chemical laboratory assistants.

*M. Plaschke, A. Bauer, N. Banik, K. Bender, M. Böttle, L. Böringer, M. Fuss, F.W. Geyer, C.-H. Graser, S. Heck, S. Hilpp, A. Kaufmann, T. Kisely, M. Lagos, C.M. Marquardt, S. Moisei-Rabung, F. Quinto, T. Renz, E. Rolgejzer, J. A. Schäfer, A. Seither, C. Walschburger, and H. Geckeis*

### (Radio-)chemical analysis for the INE R&D projects

Advanced analytical techniques, well-developed procedures, competence in the fields of radio-analytical sample preparation and separation techniques, elemental and isotope analysis, chromatographic methods and nuclear spectroscopic techniques are the core competences of the INE analytical group. Our personnel is trained in handling of nuclear samples and in the operation and maintenance of instruments adapted to glove boxes. Several analytical techniques listed in Table 1 are available both in inactive and active labs. In the reporting period over twenty thousand samples are routinely analyzed providing the data mainly for the INE R&D projects but also for external clients (see next paragraph).

Our routine instrumentation is continuously improved and modernized, e.g., in 2015 a new carbon analyzer was installed. For element and isotope analysis sensitive ICP optical emission and different types of mass spectrometers are available. For the higher concentration range two ICP-OES (a Perkin Elmer Optima 4300 adapted to a glove box, and an Optima 8300) are available. For the lower concentration range, our ICP-MS equipment includes two quadrupole instruments (a Perkin Elmer Elan 6100 adapted to a glove-box, and a Thermo X-Series2 equipped with reaction/collision cell technology) and a sector field SF-ICP-MS (a Thermo Element XR/2 adapted to a glove box). SF-ICP-MS provides detection limits for transuranium elements as low as  $\sim 10^{-14}$  mol/L (lower ppq range) and elevated mass resolution (up to 10.000) which is beneficial for accurate determination of elements suffering from interfering species, e.g., Fe or Se (see below). Even lower detection limits, down to  $10^4$  actinide atoms per sample, can be obtained by Acceleration Mass Spectrometry (AMS). For such ultra-trace determination of actinides [1] and  $^{99}\text{Tc}$ , we maintain close co-operations with the AMS communi-

ty at national and international facilities (cf chapter 9.5).

### Commercial Analytical Services

Commercial analytical service is offered to various clients on the basis of formal contract agreements. Data are recorded, documented and quality controlled according to the requirements of the clients.

#### *Quality Control of Radiopharmaceuticals*

A  $^{223}\text{Ra}$  containing alpha-radiopharmaceutical is regularly analyzed with regard to toxic heavy metal trace impurities.  $^{223}\text{Ra}$  acts as a calcium mimic and is indicated for patients suffering from bone metastases. Due to the short penetration of the alpha emitter, a highly-localized tumor cell killing is achieved with minimal damage to surrounding healthy tissue. The radiopharmaceutical is successfully introduced in the market and the number of samples measured at INE is markedly increasing in 2015.

#### *Nuclear Waste Treatment and Decommissioning of Nuclear Facilities (WAK-HDB)*

Samples from the WAK-HDB (Wiederaufarbeitungsanlage Karlsruhe GmbH, Hauptabteilung Dekontaminationsbetriebe) are classified according to their origin in samples from the HDB incineration (ashes) or LAW evaporation plants (liquid concentrates), annually averaged samples, samples from decommissioning of nuclear facilities and others. Samples are processed by radio-analytical separation methods and analyzed using elemental, isotope and nuclear spectroscopic techniques in order to obtain isotope concentrations and vectors. The nuclides routinely determined include (but are not limited to):  $^{55}\text{Fe}$ ,  $^{63}\text{Ni}$ ,  $^{90}\text{Sr}$ ,  $^{233,234,235,236,238}\text{U}$ ,  $^{238,239,240,241,242}\text{Pu}$ ,  $^{241}\text{Am}$  and  $^{242,243+244}\text{Cm}$ . Starting fall 2015  $^{90}\text{Sr}$  is furthermore determined in all routine samples.

**Table 1:** Analytical techniques available at INE

#### **Elemental and Isotope Analysis**

Quadrupole Inductively Coupled Mass Spectrometry (Q-ICP-MS)  
Collision Cell Q-ICP-MS (CC-Q-ICP-MS)  
Sector Field ICP-MS (SF-ICP-MS)  
Inductively Coupled Optical Emission Spectrometry (ICP-OES)  
Atomic Absorption Spectrometry (AAS)  
Flame Atomic Emission Spectrometry (F-AES)  
X-Ray Fluorescence Spectrometry (XRF)

#### **Nuclear Spectroscopic Methods**

Alphaspectrometry  
Liquid Scintillation Counting (LSC, conventional/high sensitivity)  
Gammascpectrometry (with auto-sampler)

#### **Other Methods**

Ion Chromatography (IC) for cations and anions  
Gas Chromatography (GC)  
Carbon Analysis (TOC, DOC, TIC, NPOC)  
Specific Surface Area Analysis (BET)  
Differential Thermal Analysis (DTA)  
Dilatometry  
Fusion and Microwave Digestions  
Gravimetry and Titrations

#### *Quality Control of Separation Resins*

INE is the quality control lab of the TRISKEM Sr separation resin. Our analytical service comprises the determination of the capacity of the Sr resin, column tests, determination of possible interferences and carbon analysis of eluted organic material. On average, one sample batch of Sr resin is analyzed each month.

#### **Development of a method for the simultaneous determination of Np and Pu in clay samples using mass spectrometry**

Depending on the redox state, neptunium (Np) and plutonium (Pu) can form highly mobile species under various environmental conditions. This makes them two of the most relevant radioelements of concern for the long-term disposal of nuclear waste. Clay formations are under consideration as a potential host rock for disposal of high-level nuclear waste. In the framework of experiments studying the diffusion behavior and retention potential of actinides in clay, an analytical procedure for the determination of Np and Pu at femto- to atto-gram levels in clay(rock) samples is required. Np lacks a long-lived isotope which can be obtained isotopically pure enough to serve as isotopic yield-tracer for the analysis of  $^{237}\text{Np}$ . A method is developed where a Pu isotope is used as non-isotopic yield tracer for the determination of  $^{237}\text{Np}$  in clay samples with mass spectrometric techniques. Fields of application are the investigation of the diffusion behavior of actinides in compacted clay liners used as technical barriers in nuclear waste repositories and of global fallout actinides in environmental clay-rich samples, considered as natural analogues.

Clay samples are spiked with characterized in-house solutions of  $^{242}\text{Pu}$  and  $^{237}\text{Np}$ . The presented analytical method, includes a) leaching of the spiked clay sam-

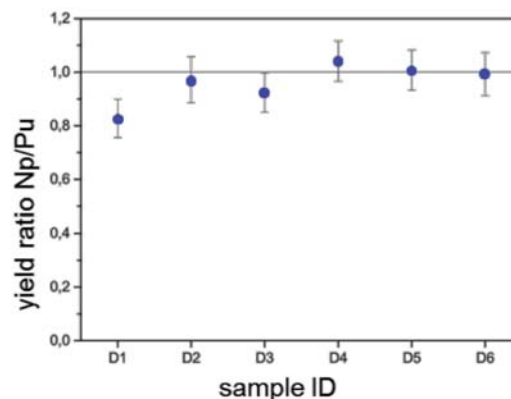


**Fig. 1:** Ratio of the chemical yields of Np/Pu in the eluate: D1 and D2 (100 mg SWy-2), D3 and D4 (100 mg Illite du Puy), D5 and D6 (1g SWy-2);  $[\text{Pu}]_{\text{added}} = 0,86 \text{ ng}$ ,  $[\text{Np}]_{\text{added}} = 1,08 \text{ ng}$ , error bars 1 SD.

ples, b) redox adjustments and pre-concentration of Np and Pu using iron-hydroxide co-precipitation, c) chromatographic separation of Pu and Np from the sample matrix and d) measurement of the actinides with Sector Field (SF)ICP-MS and Quadrupole (Q)ICP-MS. After leaching with aqua regia and subsequent co-precipitation, Np and Pu are stabilized as tetravalent nitrate-complexes, which is a prerequisite for the subsequent chromatographic co-extraction using TEVA<sup>®</sup> resin.

Our experimental results show that accurate pH adjustment during the reductive co-precipitation and short processing times are vital steps in order to obtain yield ratios close to 1, as well as high chemical yields. The analytical procedure is successfully applied to montmorillonite (SWy-2) and illite (Illite du Puy) clay up to 1 g sample size allowing for high chemical yields between 80 and 90 % (not shown). Values of chemical yield ratios of the two investigated nuclides ( $\text{yield}_{\text{Np}}/\text{yield}_{\text{Pu}}$ ) close to 1 prove the suitability of Pu as non-isotopic yield tracer for determination of  $^{237}\text{Np}$  in clay samples (Fig. 1).

The method aims at future applications using acceleration mass spectrometry (AMS) and meets the specific requirements of this method. It is planned to apply the method to the ultra-trace analysis of actinides in natural near-surface clay stones for the study of sorption and migration phenomena of global fallout actinides and for the determination of actinide background concentrations.

#### **Redox speciation of Selenium by CE-SF-ICP-MS**

Both the geochemical conditions, in particular host rock and groundwater composition, and the layout and components of a nuclear waste repository determine the evolution of redox potentials. At the same time, the solubility, sorption and migration behavior of redox-sensitive radioelements, like the long-lived fission products (e.g., Tc, Se) and actinides (e.g., U, Np, Pu), are controlled by their redox states.

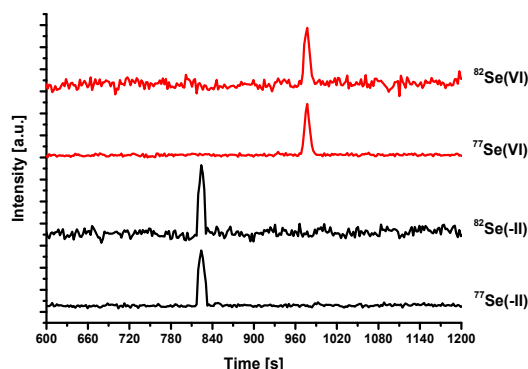


**Fig. 2:** Determination of a Se(-II) and a Se(VI) standard solution by CE-SF-ICP-MS;  $c_{\text{Se}} = 1 \cdot 10^{-5}$  M;  $\text{pH}=10$ ; see text.

It is, therefore, of great importance to predict the behavior of such redox sensitive radionuclides during the evolution of a nuclear waste repository. In the case of  $^{79}\text{Se}$  ( $t_{1/2} = 4.8 \cdot 10^5$  a), the redox chemistry of Selenium, which is characterized by four oxidation states, Se(-II), Se(0), Se(IV) and Se(VI), needs to be understood with respect to the geochemical conditions present in a waste repository site.

By hyphenating a capillary electrophoresis (CE) to a high resolution SF-ICP-MS it is possible to derive redox species distribution data in different matrices at trace concentration levels [2]. In order to determine the redox speciation of Selenium, a CE device (Beckman Coulter P/ACE) was hyphenated to a SF-ICP-MS (Thermo Element XR). The carrier electrolyte was prepared from 1,2,4,5-benzenetetracarboxylic acid (pyromellitic acid, Merck, Darmstadt) with a concentration of 3.8 mM. Hexamethonium chloride with a concentration of 1.3 mM was used as an electroosmotic flow modifier. The pH was adjusted to 10 with triethanolamine (1.6 mM) and sodium hydroxide (1.0 mM) [3]. Selenium stock solutions were prepared from iron(II)selenide (99.9% metals basis, AlfaAesar) and from sodium selenite (99.9% metals basis, Alfa Aesar). All solutions were handled under argon atmosphere. The CE separation voltage was adjusted to -25 kV in reverse polarity mode. The neutral species added to the sample in order to determine the electroosmotic flow was 1M 2-bromoethanol solution in 2% nitric acid (ultrapure; named eof marker). The mass spectrometer was set to medium resolution mode ( $R = 4000$ ), allowing for the suppression of spectral interferences. The analyzed selenium isotopes were  $^{82}\text{Se}$  and  $^{77}\text{Se}$ .

With this setup it was possible to separate two Selenium species, Se(-II) and Se(VI), within a 20 minutes' measurement time (Figure 2). The calculation of the experimental electrophoretic mobility  $\mu(\text{exp.})$  was done by inserting the migration times of the analytes and the eof marker in equation (1):

$$\mu(\text{exp.}) = \frac{l^2}{U} \cdot \left( \frac{1}{t_{\text{species}}} - \frac{1}{t_{\text{marker}}} \right) \quad (1)$$

where  $l$  = capillary length [cm];  $U$  = separation voltage [V];  $t_{\text{species}}$  = migration time of the analyte [s];  $t_{\text{marker}}$  = migration time of the eof marker [s].

The calculated experimental electrophoretic mobilities for Se(-II) and Se(VI) are:

$$\begin{aligned} \mu(\text{exp.})_{\text{Se(-II)}} &= 1.57 \cdot 10^{-5} \text{ cm}^2 \text{V}^{-1} \text{s}^{-1} \\ \mu(\text{exp.})_{\text{Se(VI)}} &= 4.28 \cdot 10^{-5} \text{ cm}^2 \text{V}^{-1} \text{s}^{-1} \end{aligned}$$

The detection limit (DL) is calculated based on the  $3 \cdot \sigma$  criterion. For  $^{77}\text{Se}$  and  $^{82}\text{Se}$ , with natural abundances of 7.6 and 9.4%, DL are determined to  $1 \cdot 10^{-7}$  and  $5 \cdot 10^{-7}$  M, respectively.

The present results demonstrate that capillary electrophoresis hyphenated to a high resolution sector field mass spectrometer is capable to conduct redox speciation analysis of Selenium. Future developments aim at lowering the detection limits to trace concentration levels, e.g., by the application of the hydride generation technique.

## References

- [1] Quinto, F.; Golser, R.; Lagos, M.; Plaschke, M.; Schäfer, T.; Steier, P.; Geckeis, H. Accelerator mass spectrometry of actinides in ground- and seawater: An innovative method allowing for the simultaneous analysis of U, Np, Pu, Am, and Cm isotopes below ppq levels. *Analytical Chemistry* 2015, **87**, 5766.
- [2] Graser, C.H.; Banik, N.I.; Bender, K.A.; Lagos, M.; Marquardt, C.M.; Marsac, R.; Montoya, V.; Geckeis, H. Sensitive redox speciation of iron, neptunium, and plutonium by capillary electrophoresis hyphenated to inductively coupled plasma sector field mass spectrometry. *Analytical Chemistry* 2015, **87**, 9786.
- [3] Pobozy, E.; Jarczynska, M.; Trojanowicz, M.; Speciation of sulfur-containing anions by use of capillary electrophoresis. *Chromatographia* 2002, **56**, 723.



## 10 Radiation protection research

Radiation Protection Research at KIT-INE deals with the assessment of radiation exposures by estimation of doses from external radiation fields or from intakes of radionuclides. The techniques applied for assessing radiation exposures are direct measurements and numerical simulation of radiation fields, as well as numerical simulation of individual dosimetry for working scenarios in the vicinity of various radiation fields. During 2015, research activities have been focused on the development of techniques and models for an individualized dosimetry taking into account not only the radiation fields but also the individual itself, considering anatomical properties and body movements. Investigations presented in this chapter deal with individual dosimetry of personnel in a generic deep geological repository for heat-generating waste, development of a novel radiation detector to assess radioactive surface contamination and numerical simulations with respect to nano- and microdosimetry. Close collaborations are established with national and international partners in networks such as “Strahlung und Umwelt” in Competence Alliance Radiation Research KVSF and the European Radiation Dosimetry Group (EURADOS).

### 10.1 Modeling of individual dosimetry for working scenarios with respect to emplacement of spent nuclear fuel canister in a rock salt repository

*F. Becker; V. Metz; B. Pang; H. Sauri Suárez*

#### Introduction

A responsible and safe management of radioactive residues, especially heat-generating waste from commercial nuclear power plants, is a complex subject of social controversies, unresolved conflicts and uncertainties. The interdisciplinary research platform “ENTRIA” has been established to develop evaluation principles for comparison of different options for the management of heat-generating waste. Three generic disposal and storage concepts are studied in the research platform, i.e. emplacement in deep geological formations with monitoring and retrievability measures, deep disposal without retrievability measures, and prolonged surface storage. Certain working scenarios in the storage / disposal facilities might lead to an enhanced level of radiation exposure for workers. Hence, a realistic estimation of the personal dose during individual working scenarios is desired. In this sub-chapter, we describe our modelling of individual dosimetry of personnel involved in emplacement of canisters with spent nuclear fuel (SNF) in a generic repository.

#### Modelling of a canister with SNF elements

The POLLUX-10 cask is designed as a technical barrier to prevent the release of the radioactive nuclides contained in the nuclear waste as well as to facilitate a proper protection of the workers from radiation [1]. Some simplifications were assumed to model the canister with MCNP6 [2] as shown in Figure 1. The nuclear waste stored inside the internal cask was assumed as a homogeneous mixture, which is modelled as an isotropic volumetric source in MCNP6. The fuel zone was divided in two parts: An active one, which represents the fuel pellets and the structural materials, and an inactive one, which represents the top and bottom of the fuel assemblies.

According to the composition of spent nuclear fuel of German light water reactors to be disposed of (given in [3]), the studied representative fuel is a mixture of 89% DWR-UO<sub>2</sub> and 11% DWR-MOX spent nuclear fuel assemblies. The time between unloading from reactor and final disposal was assumed to be 50 years. At the time of final disposal <sup>244</sup>Cm is the main contributor to radiation exposure due to the neutrons coming from its spontaneous fission.

The horizontal emplacement drift is located in a generic rock salt repository. The geometry and properties of the emplacement drift was adapted from [4] and implemented in a MCNP6 model (see Figure 2).

#### Modelling of a human phantom

A worker inside the gallery is represented with a simplified anthropomorphic phantom. The phantom is a

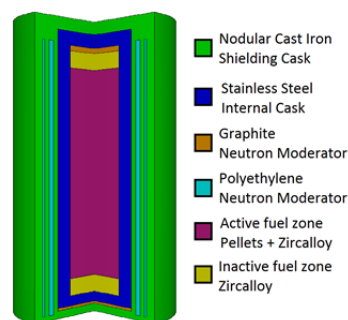


**Fig. 1:** Simplified MCNP6 model of a POLLUX-10 cask loaded with spent nuclear fuel elements.

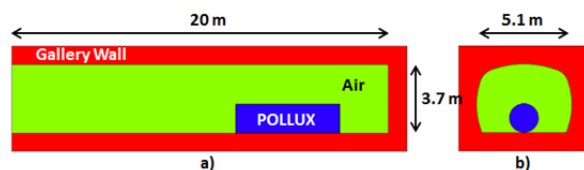


**Fig. 2:** Simplified MCNP6 model of a POLLUX-10 cask in an emplacement drift of a rock salt repository.

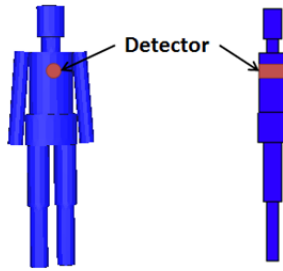


Fig. 3: Representation of the BOMAB phantom in the MCNP6 model.

virtual representation of the BOMAB (BOTTle MAnnikin ABSorber) phantom [5] which represents the head, neck chest, abdomen, thighs, calves, and arms with cylinders or elliptical cylinders. Figure 3 shows a representation of the phantom in MCNP6.

To obtain the depth-dose curve, a four centimeters radius cylindrical detector is modelled in the center of the chest. The detector crosses the chest and allows to register the dose rate every 0.1 mm of the 20 centimeters thick chest (see red cylinder in Figure 3).

Depth-dose curves are calculated for the phantom placed at 1, 5 and 10 meters' distance from the POLLUX. For the 5 meters' position, simulations were also performed with the phantom at angles of 0°, 45°, and 90° with respect to the POLLUX symmetrical axis as shown in Figure 4.

#### Influence of the distance between source and phantom on the depth-dose curve

Figure 5 shows the variation of the dose rate with the tissue depth (depth-dose curve) for different distances of the phantom from the POLLUX. A decrease of the dose rate is observed until 170 mm. An increase when approaching to 200 millimeters is attributed to the backscattered radiation from the salt rock layer that has an impact on the radiation exposure from the back side of the phantom. The highest dose rates occur at the first two millimeters.

#### Influence of the angle between the phantom and the POLLUX-10 on the depth-dose curve

When rotating the phantom, the depth-dose curve changes significantly as shown in Figure 6. The dose rate at the front of the phantom decreases with increasing angles, while the dose rate at the back increases. The backscattered radiation plays a more significant role in the received dose when the angle increases. This effect can be explained by the decrease-

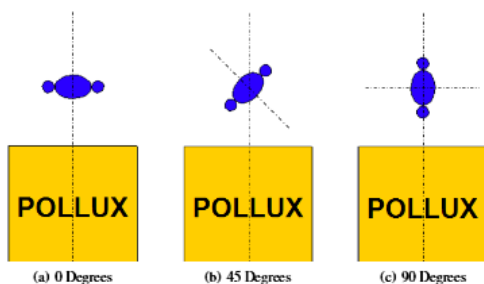


Fig. 4: Different angles of the BOMAB phantom with respect to the POLLUX-10 cask.

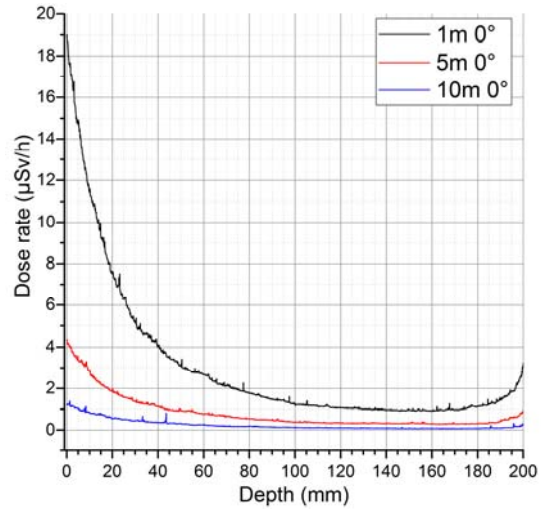


Fig. 5: Influence of the distance of the phantom from the POLLUX-10 cask on the depth-dose curve.

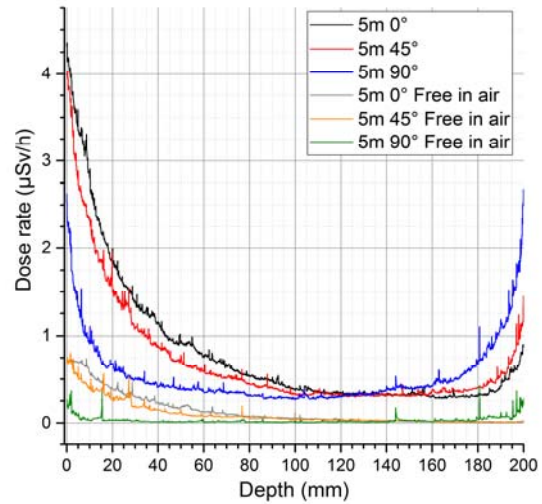


Fig. 6: Influence of the angle between the phantom and the POLLUX-10 cask on the depth-dose curve.

ing of the relative distance of the detector to the salt rock layer and the increased shielding of the direct radiation from the POLLUX by shoulder and arm. In Figure 6 the results for the POLLUX free in air, i.e. without backscattering radiation, are also presented. The strong influence of the backscattering from the walls is confirmed while effects of shielding by shoulder and arm play a minor role.

If a worker wears only one dosimeter on the front of the torso, the personal exposure might be underestimated when the worker is not facing the POLLUX. Wearing two dosimeters, one on the front and the other one on the back of the torso, can reduce the angular dependence of the individual dose estimation.

#### References

- [1] Janberg K. et al., *Nuclear Technology*, **121**, 136-147 (1998).
- [2] Pelowitz, D. B. et al. (2013): MCNP6 User Manual. LA-CP-13-00634, Rev. 0.
- [3] Peiffer, F., McStocker, A., *Abfallspezifikation und Mengengerüst, Basis Ausstieg aus der Kern-*

*energienutzung*. Bericht zum Arbeitspaket 3 Vorläufige Sicherheitsanalyse für den Standort Gorleben, GRS-278 (2011).

- [4] Stahlmann J. et al., *Generische Tiefenlagermodelle mit Option zur Rückholung der radioaktiven Reststoffe*, TU-Braunschweig, Institut für Grundbau und Bodenmechanik (2014).
- [5] U.S. Department of Energy, *Bottle Manikin Absorption (BOMAB) Phantoms*. (2015)

<http://www.id.energy.gov/resl/phantom/bomab.html>

#### **Acknowledgement**

This study was financially supported by the German Federal Ministry of Education and Research (BMBF) in the context of the ENTRIA project (grant number 02S9082A).

## 10.2 A novel radiation detector for deconstruction and decommissioning of nuclear buildings

F. Becker; S. Gentes; P. Kern

### Introduction

In the framework of the research project Manipulator Operated Release Measurement of Surfaces (MAFRO – Manipulatorgesteuertes Freimessen von Oberflächen), located at the KIT Department of Deconstruction and Decommissioning of Conventional and Nuclear Buildings, a novel radiation detector to assess radioactive surface contamination was investigated. Such a detector is destined as an equipment component of a climbing robot for locomotion on walls.

The major challenge in the construction of the detector was to ensure a distinction between alpha and beta radiation and to allow for measurements in corners. As a result, a rectangular shaped detector was constructed [1] consisting of five sensitive scintillation areas (see Fig. 1).

### Methodology

The radiation-sensitive five sides of the detector (front surface  $10 \times 10 \text{ cm}^2$ , and four side surfaces, each with  $10 \times 5 \text{ cm}^2$ ) are coated with silver-activated zinc sulfide followed by a 0.5 mm thick scintillator layer of polystyrene. The scintillator layers are coupled to a block of Plexiglas, which acts as light guide to the photomultiplier. To avoid damages of the five radiation-sensitive sides of the detector, they are enclosed with a protective grid (see photo in Fig. 1).  $\alpha$ -particles are stopped and registered in the thin ZnS-layer while  $\beta$ -particles deposit their energy mainly in the polystyrene. A choice of a thin  $\beta$ -sensitive layer ensures the reduction of events stemming from  $\gamma$ -rays. Pulse height discrimination allows for a distinction between  $\alpha$ - and  $\beta$ -radiation, since  $\alpha$ -particles cause signals stronger than  $\beta$ -particles. Two signal channels with different adjustable pulse height levels are provided by the detector. Hence, one channel provides  $\alpha$ - and the other  $\beta$ -counting.

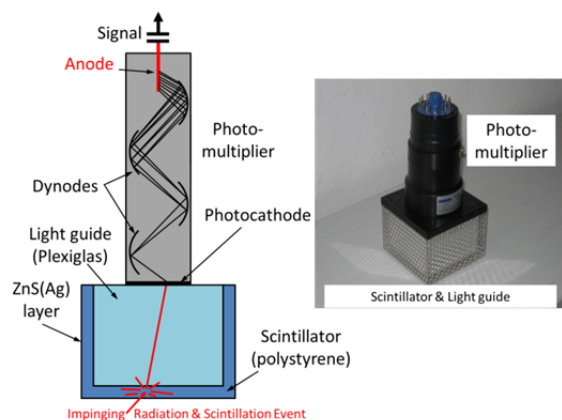


Fig. 1: Schematic diagram (left) and photo (right) of the rectangular shaped scintillation detector.

### Results and discussion

Different sources, emitting  $\alpha$ -,  $\beta$ -, and/or  $\gamma$ -particles were employed to study the detector response. Exemplary experimental results obtained with two point sources are presented in the following. Po-210 was employed as an alpha emitter and Sr-90/Y-90 as a beta emitting source. The pulse height levels of the detector were adjusted to 0 - 2500 mV and 2700 - 5000 mV, for the  $\beta$ - and  $\alpha$ -counting, respectively. In this way, after subtracting the background, 83 % of the total events are registered in the  $\alpha$ -channel in case of Po-210, while employing the Sr-90/Y-90 source yields 97 % of the events in the  $\beta$ -channel. As a result, with the chosen pulse height discriminator settings, in case of  $\alpha$ -counting an efficient  $\alpha$ - $\beta$ -discrimination with only 3% spill-over of  $\beta$ -pulses into the  $\alpha$ -channel was obtained.

The operation of the detector on a climbing robot requires measurements to be performed at variable distances from the wall surface. The knowledge of the detection efficiency at a given distance to the wall surface is essential in particular for the measurement of alpha contamination. Therefore, experiments were performed varying the distance between the source and detector. For this purpose, an apparatus was constructed to position the detector in a vertical or horizontal position, i.e. the front surface or one of the side surfaces facing the source, respectively.

Results for the alpha emitter Po-210 and the beta

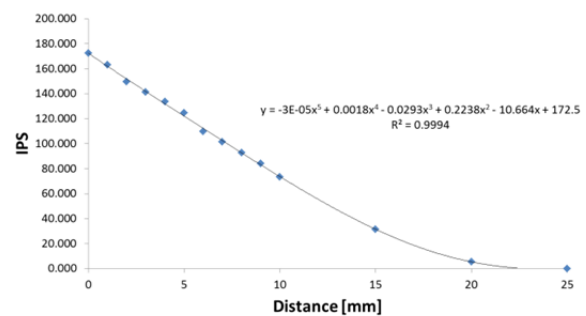


Fig. 2: Measured IPS vs. the distance of the alpha emitter Po-210 to the detector's protective grid

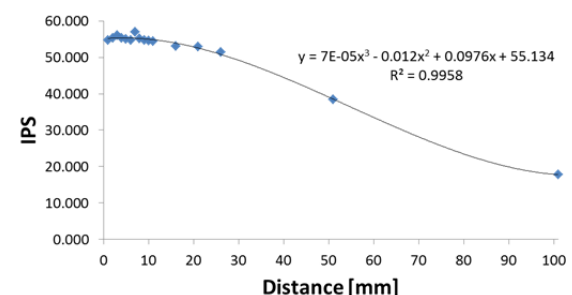


Fig. 3: Measured IPS vs. the distance of the beta source Sr-90/Y-90 to the detector's protective grid

emitter Sr-90/Y-90 are shown in figure 2 and 3, respectively. The measured counts per second (IPS) are background corrected and plotted against the distance of the source to the detector's protective grid. The known fact that  $\alpha$ -particles range only up to a few centimeters in air, whereas  $\beta$ -particles could pass several hundred centimeters in air, is clearly visible. A polynomial fit through the data points yields a function proving distance dependent correction factors. Using e.g. a laser to monitor the distance of the detector to the wall surface allows together with the distance correction function to obtain the extrapolated information of the IPS on the surface.

The ratio of the detected IPS to the activity of the source in Bq defines the counting efficiency  $\eta$ . For the  $\alpha$ -source placed on the protective grid in front of the detector  $\eta$  amounted to 14 %, while 13 % for the  $\beta$ -source could be achieved. Irradiation of different sides of the detector showed that  $\eta$  of a side surface compared to the front surface has no difference within the measurement uncertainty (sources placed on the

center of the surface). Hence efficient detection in corners is ensured.

A calibrated detector would give in turn the information on the surface's activity for the two channels beta and alpha. These activities can be evaluated with respect to release limits of the Radiation Protection Ordinance to decide for further measures.

Concluding, the novel radiation detector for deconstruction and decommissioning of nuclear buildings proved its suitability with respect to fundamental source measurements. Further investigations, e.g. its application on a climbing robot system together with a computer-assisted evaluation of contamination levels, are in progress within in the framework of MAFRO.

### References

- [1] Freiburger Sensortechnik Hegewald & Kandler GbR

### Acknowledgements

Federal Ministry of Education and Research (BMBF)  
BMBF-Förderkennzeichen:02S8881

## 10.3 Stochastic chemistry for human-cell equivalent systems

B. Heide, V. Metz

The biological effect of ionizing radiation is mainly caused by radiolytic / radiation induced damages of the DNA in cells [1]. Ionizing radiation interacts to some extent directly with DNA chains. However, the radiation reacts mostly with the intercellular fluid, resulting in radicals and molecular radiolysis products. In particular for radiation with a low linear-energy-transfer (LET), the production of hydroxyl radicals ( $\cdot\text{OH}$ ) due to radiolysis of  $\text{H}_2\text{O}$ , the main constituent of the intercellular fluid, is of importance. Hydroxyl radicals may diffuse over distances of several nm to react with DNA or proteins [1]. Since the hydroxyl radical is considered as the most aggressive product of water radiolysis with respect to the indirect effect of ionizing radiations on DNA, the indirect action exceeds the direct action of radiation, especially for low LET radiation.

Using the Geant4-DNA software package [2,3], both actions of radiation are taken into account to assess the hazard of radiation to human cells. The present radiolysis module of Geant4-DNA refers to interactions of radiation with pure water, only. The intercellular fluid, however, also contains chloride

in considerable concentrations. For instance, the human blood serum contains 0.098 to 0.109 mol/L chloride. Chloride reacts with hydroxyl radical to produce the oxidative anion  $\text{ClOH}^-$ . G-values of primary radiolysis products in chloride bearing solutions were studied in concentrated solutions [4,5,6]. However, there is a lack of radiolysis data for aqueous solutions with physiological relevant chloride concentrations.

In the present study we investigate the effect of chloride on the radiolytic yield in human-cell equivalent systems. In order to implement the radiolysis induced reaction  $\text{Cl}^- + \cdot\text{OH} \rightarrow \text{ClOH}^-$  into the radiolysis module of Geant4-DNA, we developed a code to calculate G-values of the various radiolysis products. For radiolysis of pure water, results of our calculations were compared to published simulations with Geant4-DNA. The validation was done by comparing our G values with those of [2] with respect to protons impinging on a cube of water; cf. figures 1 and 2.

The agreement between our G values and the ones of Karamitros et al. [2] seems to be sufficient for intermediate time intervals. Some differences are observed for G-values of hydroxyl radicals for the initial time interval of less than 10 ps and time intervals longer than 104 ps (Fig. 2). These differences may be caused by different parameters of one or more of the default Geant4-DNA model classes. A careful investigation of this matter is being done. Nevertheless, the good agreement of the main temporal evolution of the G-values may indicate that no principal error is present in our simulations.

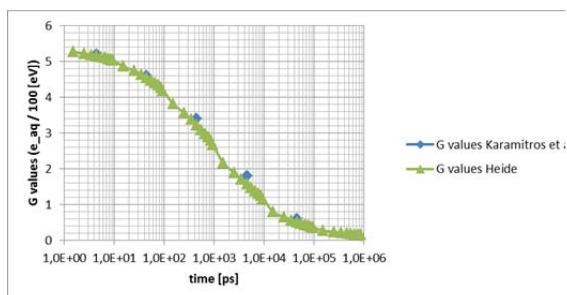


**Fig. 1:** Time-dependent yield of solvated electrons for 500 keV protons impinging on a cube (edge length 5  $\mu\text{m}$ ) of water.

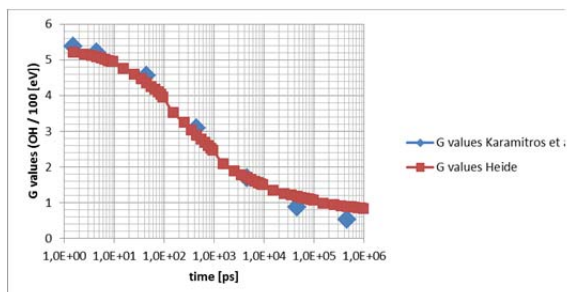


**Fig. 2:** Time-dependent hydroxyl radical yield for 500 keV protons impinging on a cube (edge length 5  $\mu\text{m}$ ) of water.

### References

- [1] Han, W. and Yu, K. N. *Ionizing Radiation, DNA Double Strand Break and Mutation*. Advances in Genetics Research. Vol. 4 (2010).
- [2] M. Karamitros et al., *Journal of Computational Physics* **274**, 841–882 (2014).
- [3] S. Incerti, A. et al., *Med. Phys.* **37**, 4692– 4708 (2010).
- [4] Draganic, Z.D., Draganic, I.G., *Journal of Physical Chemistry* **77**, 765-772 (1973).
- [5] Pucheault, J. et al., *Journal of Physical Chemistry* **83**, 330-336 (1979).
- [6] Kelm, M., Bohnert, E., *Nuclear Technology* **129**, 119-122 (2000).

## 11 Geoenergy

The focus of geoenergy research at INE concerns mainly geothermal energy research in fractured reservoir systems with special focus on Enhanced Geothermal Systems (EGS). The technical feasibility of EGS has first been demonstrated in fractured crystalline basement at the Soultz-sous Forêts project (France). Different hydraulic experiments were performed in four wells at three different reservoir levels located between 2 and 5 km depth. These measures enhanced significantly the hydraulic yield of these reservoirs, in some instances by about two orders of magnitude. We identify cyclic injection in combination with circulation between wells reaching exceptional high hydraulic yield at comparatively low injected volume. The Soultz data provide also indication on how to maximize injection and minimize induced seismicity [1]. Such findings have been further investigated on medium-scale in the Äspö Hard Rock Laboratory (Äspö HRL, Sweden) [2]. In this respect, new monitoring approaches have been successfully tested. Here, pressure-dependent variation of electromagnetic emission signals is indicated at the frequency range acoustic emissions. This applies to both, continuous pressure increase during injection and pressure drop due to failure of the rock. To meet the evolving needs to carry out more EGS-specific experiments in underground research laboratories, a preliminary study on the condition of the southern Black Forest-Odenwald complex for a Geothermal Laboratory in Crystalline Basement (GeoLaB) has been carried out [3]. This site aims on closing the gap between geothermal researches on reservoir- and laboratory-scale. The latter at INE concerns mainly the influence of rough and altered surfaces on clay mineral transport. Although in simplified geometries and under low ionic and low flow rate groundwater conditions first experiments reveal the significant effect of fracture roughness and orientation on colloid deposition [4].

*Y. Abdelfettah, G.K. Darbha, F. Huber, Th. Schäfer, E. Schill, M. Stoll*

In co-operation with:

*N. Cuenot<sup>a</sup>, A. Genter<sup>b</sup>, M. Grimm<sup>c</sup>, J. C. Grimmer<sup>c</sup>, T. Kohl<sup>c</sup>, J. Meixner<sup>c</sup>, C. Meller<sup>c</sup>, I. Stober<sup>c</sup>, A. Zang<sup>d</sup>*

<sup>a</sup> GEIE "Exploitation Minière de la Chaleur", Kutzenhausen, France, <sup>b</sup> ÉS Géothermie, Strasbourg, France, <sup>c</sup> AGW, Karlsruhe Institute of Technology, Germany, <sup>d</sup> Helmholtz-Zentrum Potsdam – Deutsches GeoForschungsZentrum, Potsdam, Germany

### Introduction

In Europe, major geothermal resources outside of the volcanic or metamorphic complexes in Iceland and Italy are contained within deep fractured crystalline rock at high differential stresses. Economic viable projects require about 50L/s of flow at temperature >130°C. There are a number of scientific challenges that limit environmentally friendly development of deep geothermal energy in these geothermal fields, today. Key issues relate mainly to sensible seismicity during enhancement of the reservoir performance and operation, as well as radioactive scaling.

The geothermal research at INE is embedded into Helmholtz Portfolio project *Environmentally friendly provision of local energy from georesources – Geoenergy* and the Helmholtz program *Renewable Energies*. Its scientific program addresses the issues of economically viable condition and low environmental impact by advanced exploration and monitoring methods. In this respect, fundamental research is needed in particular on the relations between fluid circulation, hydro-mechanics, alteration and geophysical properties such as electric resistivity. At present, the majority of the phenomena are investigated at reservoir level. This concerns the investigation of hydraulic condition in natural geothermal systems and based on this, the understanding of reservoir engineering techniques for the crystalline basement. Furthermore, new monitoring techniques are developed in order to study of processes related to reservoir engineering. First labor-

atory experiments have been started to study specific issues under controlled condition. This activity will be intensified at KIT–INE in the coming years.

INE is strongly involved in the preparation of the large-scale research infrastructure application GeoLaB. GeoLaB is planned as large-scale underground research facility for controlled high flow-rate (CHFE) experiments in fractured, crystalline basement. With the aim to investigate hydraulic, hydro-mechanic and heat transfer processes, and existing mine is envisaged to be equipped for such experiments. In this respect, exploration methods for the crystalline basement are validated and extended to larger frequency bands. This includes comparable to acoustic emission adding up to seismic monitoring, high-frequency electromagnetic measurements. These ongoing developments will be completed in the following years.

### Hydraulic performance history at the Soultz EGS reservoirs from stimulation and long-term circulation tests

In the framework of developing new environmentally friendly stimulation and circulation concepts, the geoenergy group at INE has evaluated the efficiency of different stimulation and long-term circulation measures taking into consideration the initial hydraulic conditions of the three reservoirs. Compiling a total of 61 tests and circulation experiments, the improvement of reservoir condition under stimulation and long-term circulation has been demonstrated to

provide general conclusions for EGS reservoir engineering [1]. As example, the evolution of the hydraulic yield in the 5km reservoir (R5) of GPK2 is provided in Fig. 1.

The review illustrates the first order engineering learning curve achieved in Soultz. The shallow 2km reservoir having highest hydraulic performance was developed with only little injection rates. At the 3.5km reservoir flow rate was drastically increased. Finally, it being developed as a triplet EGS operation started under crucial observation of induced seismicity. The analyses of the hydraulic data indicated clear trends for effective stimulation experiments carried out at this worldwide unique EGS reference site and reveal that

- 1) With the exception of GPK3 in R5, the initial hydraulic conditions from single-well injection tests are comparable to each other in the three reservoirs. Thus, this allows for a comparison of the effectiveness of different stimulation measures.
- 2) Even if productivity and injectivity values in the same openhole sections are initially of same order of magnitude, they can develop differently during stimulation procedure.
- 3) During stimulation, hydraulic yield appears to be enhanced most effectively using cyclic injection schemes in combination with circulation (Fig. 2).
- 4) Cumulative test volume and cumulative total volume appears to be key driving factors for enhancing hydraulic conditions of Soultz.

In the last years, the production in Soultz was optimized for reducing induced seismicity during operation. It was achieved by reducing the injection well-head pressure leading to reduction in production flow rates by almost 50%. It is evident for the further development of EGS to economic levels that this learning curve needs to be continued by applying controlled high flowrate injection.

This compilation presents a starting basis for future research in fractured rock that should target more extensive conceptual models of this most intensive

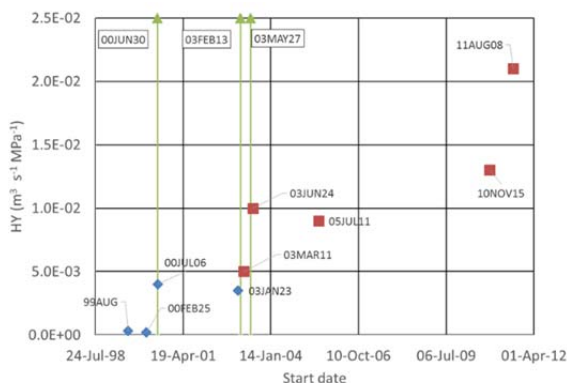


**Fig. 1:** Evolution of GPK2 hydraulic yield (HY), injectivity until 03MAR11 and productivity starting from 03JUN24, in the deep reservoir measured during single well injection tests (blue) and circulation production tests (red). Hydraulic stimulation is indicated in green [1].

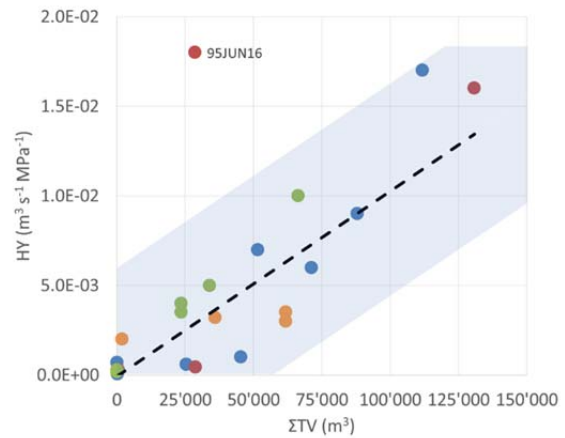


**Fig. 2:** Hydraulic yields, HY, obtained from stimulation and test experiments in the wells GPK1 (blue), GPK2 (red) in R3 and GPK2 (green) and GPK3 (orange) in R5 versus the cumulative total volume  $\Sigma TV$  at the Soultz EGS site [1]. Data include experiments and test of 93MAY27 to 95AUG01 (GPK1, II), 95FEB10 to 95JUN16 and 96OCT13 (GPK2, II), 99OCT13 to 03JUN24 (GPK2, III), 03MAR11 to 04AUG17 (GPK3, III).  $HY = 10^{-7} m^3 s^{-1} MPa^{-1} \cdot \Sigma TV$  ( $R^2 = 0.77$ ). Similar behaviour can be deduced from R2 (not shown).

and documented site. This first assemblage of the hydraulic performance in Soultz provides key aspects to design and engineer the EGS performance at other locations.

### GeoLaB

Cyclic injection along with production from a second well has been found to be most effective for reservoir development at Soultz [1]. Yet, controlled high flowrate injection is a crucial issue for large-industrial development and economic viability of EGS. Although experimental progress has been made, fundamental constitutive laws of flow and thermo-hydraulic-mechanical-chemical (THMC) coupling during reservoir engineering and plant operation in fractured environments are at present insufficiently demonstrated.

Underground research laboratories (URLs) are best suited to monitor and quantify the interrelated processes and should address key issues for safe and economic use of geothermal energy. Following related geo-disciplines like nuclear waste disposal research, a specific URL for geothermal purpose is proposed, located in a typical EGS environment to conduct fundamental 4D controlled high flow rate experiments (CHFE, Fig. 3).

Four criteria have been established and investigated for URLs worldwide and mines along the Upper Rhine valley in crystalline basement [3]:

- 1) Rather homogenous crystalline matrix with a high density of connected and highly permeable natural fractures (fracture densities of 2-10 m<sup>-1</sup> with major fault lengths of < 400-500 m and fracture transmissivities > 10<sup>-4</sup> m<sup>2</sup> s<sup>-1</sup>).
- 2) Controllable hydraulic boundary conditions.

- 3) Hydrothermal alteration products in the illite to smectite range.
- 4) Fractures that are favorably oriented for reactivation in the ambient stress field and uniform stress field across the tunnel with variation in magnitude of the maximum stress orientation  $< 1$  MPa.

Although, the Äspö HRL (Sweden) approximates the requirements for a new generic GeoLaB and may be used for complementary experimentation, none of the existing URLs matches all four criteria.

Due to the vicinity to geothermal production and favorable geological, hydraulic and stress conditions, site assessments have been carried out in the southern Black Forest-Odenwald complex (Germany). Tectonic and (hydro-)geological conditions in both regions match so far the established criteria for CHFEs in a geothermal URL. A preliminary exploration concept localization of fracture zones has been tested successfully. For final decision on the suitability of a site exploration wells are envisaged. The analyses have provided key steps for developing a generic URL in a favorable geological environment for geothermal production.

### Electromagnetic emission monitoring during injection experiments

Changes in fluid pathways induced achieved by geothermal reservoir engineering are typically inferred from micro-seismic monitoring. Electromagnetic methods are of comparably lower resolution since they base on the diffusion equation. On the other hand, they are sensitive to electric conductivity contrasts that are an indicator of fracture connectivity. The relation between electromagnetic emissions and deformation processes, i.e. electro-kinetics, during stimulation processes is indicated in self-potential measurements [5].

In order to improve the understanding of electro-kinetic effects during reservoir engineering and its effect on electromagnetic monitoring, a field test has been carried out during May and June 2015 in crystalline rock at -410 m in the Äspö HRL. The test was

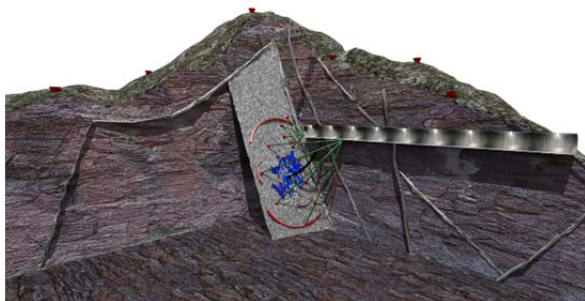


**Fig. 3:** Possible layout of the planned geothermal URL, GeoLaB, with an access tunnel to a fracture zone and observation wells from the tunnel into the fracture zone [3]. In addition to the monitoring stations (red cones), the main injection well for controlled high-flow experiments (CHFE) could be achieved from surface boreholes targeting the fracture zones next to experimental caverns.

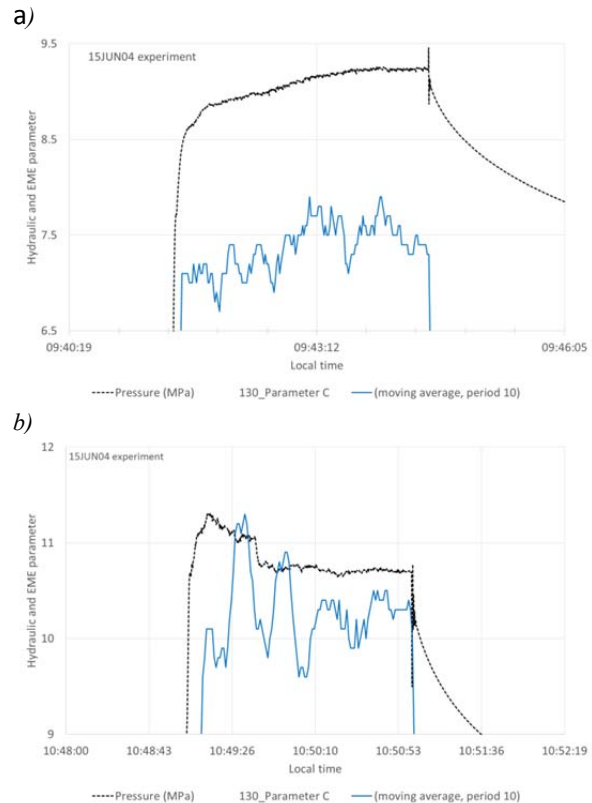


**Fig. 4:** Emitted electromagnetic energy (EME, 35-50 kHz) acquired sub-parallel to the fracture plane (N130E) generated during the injection experiment compared to injection pressure for two individual injection steps.

connected to injection experiments partly based on injection schemes by [6] and monitored simultaneously with acoustic emission, micro-seismic, broad-band seismic and electromagnetic/self-potential sensors in a joint project coordinated by Helmholtz-Zentrum Potsdam – Deutsches GeoForschungsZentrum.

The electromagnetic/self-potential monitoring network was operated at frequencies between 1 Hz and 50 kHz. High frequency signals were measured using a beam antenna/ferrite aerial.

High variation of EM noise caused mainly by pumping during injection periods prevents from comparable observations of EM for the pumping and non-pumping periods of the experiment. The observation of pressure-dependent EME signal in the frequency range between 37 kHz and 50 kHz is a major outcome of the hybrid monitoring setup. The emitted electromagnetic energy (EME parameter in Fig. 4) generally follows the pressure build-up during injection (Fig. 4a). Larger pressure drops are accompanied by increased EME activity (Fig. 4b). EME of similar frequency ranges are observed also in low and medium velocity impact experiments on gabbro and granite blocks using about  $100 \text{ m s}^{-1}$  and  $1500 \text{ m s}^{-1}$ , respectively. EME at this frequency range correlate with failure of rock [7]

## Particle retention on granite using a synthetic fracture flow cell

Clay coating of fracture zones modifies strongly the hydraulic and mechanical properties. On the one hand, clay may completely clog a fracture and on the other hand, it may reduce the shear strength of rock and thus, lead to more favorable condition for hydraulic stimulation [8].

In order to understand the accumulation and mobilization of clay particles in hydraulically active fractures, flow cell experiments have been carried out in the laboratory of INE [4]. The interaction of monodispers fluorescent carboxylated polystyrene colloids (25 nm and 1000 nm diameter) with a cut granodiorite surface (Grimsel granodiorite; Switzerland) and with acrylic glass is investigated both experimentally and numerically. Colloid transport experiments are conducted in a cylindrical parallel plate type fracture flow cell with an aperture of 0.75 mm at pH 5 under low ionic strength (1 mM NaCl) conditions. The study focuses on the effect of residence time, colloid size, collector material, and fracture orientation on colloid retention. Long colloid residence times are achieved by stop-flow experiments. Using atomic force microscopy and, more specifically, the colloid probe technique surface roughness and force distance information of the collector material (granodiorite or acrylic glass) as a function of probe size (cantilever) are obtained. The experiments are quantitatively modelled using COMSOL Multiphysics® 2-D numerical simulations.

The experimental and the modelled results lead to the conclusion that large colloids (1000 nm diameter) undergo sedimentation and deposition on the surface during stop-flow. Collector interaction is not affected by the surface roughness variation. Contrariwise, for the investigated 25 nm colloids sedimentation does not play a role under the experimental conditions and collector interaction is triggered by surface inhomogeneities such as surface roughness. In addition to the colloids, a conservative solute tracer (Amino-G) is added to the system to characterize the flow and

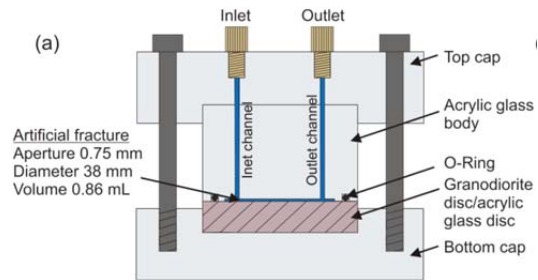


**Fig. 5:** Sketch of the synthetic fracture flow cell with a internal diameter of 38 mm and aperture of the synthetic fracture of 0.75 mm. The distance between in- and outflow is 29.8 mm. The upper part is made of acrylic glass and the lower part of the cell is exchangeable.

transport conditions. Results show earlier first arrivals and more pronounced tailings in the measured breakthrough curves for the colloids compared to the conservative tracer.

These results will be compared to experiments using natural polydisperse clay particles mainly consisting of illite. These particles are obtained from hydrothermal altered natural fractured granite drill cores from Soultz-sous-Forêts (France) and also of an illite deposit near Le-Puy-en-velay (France) which is already purified and fully Na-exchanged.

## References

- [1] Schill, E., et al., *Geothermics* (subm.).
- [2] Zang, A., et al., *Geophysical Journal International* (subm.).
- [3] Schill, E., et al., *Geothermal Energy Journal* (subm.).
- [4] Stoll, M., et al., *Journal of Colloid and Interface Science* (subm.).
- [5] Darnet, M., et al., *Geophysical Research Letters*, **31**, 19 (2004).
- [6] Klee, G. and Rummel, F., *International Progress Report, IPR-02-02* (2004).
- [7] Freund, F., *Journal of Geophysical Research: Solid Earth*, **105**, B5 (2000)
- [8] Evans, K. F., et al., *Geophys. J. Int.* **160**, 1 (2005)

## 12 Publications

### ISI/SCOPUS

- [1] Abdelmonem, A.; Luetzenkirchen, J.; Leisner, T., *Probing ice-nucleation processes on the molecular level using second harmonic generation spectroscopy*, *Atmos Meas Tech* **2015**, 8, 3519-3526.
- [2] Adam, C.; Beele, B. B.; Geist, A.; Muellich, U.; Kaden, P.; Panak, P. J., *NMR and TRLFS studies of Ln(III) and An(III) C5-BPP complexes*, *Chem Sci* **2015**, 6, 1548-1561.
- [3] Afsar, A.; Harwood, L. M.; Hudson, M. J.; Westwood, J.; Geist, A., *Effective separation of the actinides Am(III) and Cm(III) by electronic modulation of bis-(1,2,4-triazin-3-yl)phenanthrolines*, *Chem Commun* **2015**, 51, 5860-5863.
- [4] Altwegg, P.; Schill, E.; Abdelfettah, Y.; Radogna, P. V.; Mauri, G., *Toward fracture porosity assessment by gravity forward modeling for geothermal exploration (Sankt Gallen, Switzerland)*, *Geothermics* **2015**, 57, 26-38.
- [5] Amayri, S.; Fröhlich, D. R.; Kaplan, U.; Trautmann, N.; Reich, T., *Distribution coefficients for the sorption of Th, U, Np, Pu, and Am on Opalinus Clay*, *Radiochim Acta* **2015**, 104, 33-40.
- [6] Arnold, U.; Altesleben, C.; Behrens, S.; Essig, S.; Lautenschütz, L.; Schild, D.; Sauer, J., *Ionic liquid-initiated polymerization of epoxides: A useful strategy for the preparation of Pd-doped polyether catalysts*, *Catal Today* **2015**, 246, 116-124.
- [7] Banik, N. L.; Vallet, V.; Real, F.; Belmecheri, R. M.; Schimmelpfennig, B.; Rothe, J.; Marsac, R.; Lindqvist-Reis, P.; Walther, C.; Denecke, M. A.; Marquardt, C. M., *First structural characterization of Pa(IV) in aqueous solution and quantum chemical investigations of the tetravalent actinides up to Bk(IV): the evidence of a curium break*, *Dalton T* **2015**, 45, 453-457.
- [8] Bauer, N.; Panak, P. J., *Influence of carbonate on the complexation of Cm(III) with human serum transferrin studied by time-resolved laser fluorescence spectroscopy (TRLFS)*, *New J Chem* **2015**, 39, 1375-1381.
- [9] Bauer, N.; Smith, V. C.; MacGillivray, R. T. A.; Panak, P. J., *Complexation of Cm(III) with the recombinant N-lobe of human serum transferrin studied by time-resolved laser fluorescence spectroscopy (TRLFS)*, *Dalton T* **2015**, 44, 1850-1857.
- [10] Beattie, J. K.; Djerdjev, A. M.; Kallay, N.; Preocanin, T.; Lutzenkirchen, J., *Response to comment on "James K. Beattie, Alex M. Djerdjev, Angus Gray-Weale, Nikola Kallay, Johannes Lutzenkirchen, Tajana Preocanin, Atida Selmani, pH and the surface tension of water" J. Colloid Interface Sci. 422 (1) (2014), 54-58*, *Journal of colloid and interface science* **2015**, 448, 594-595.
- [11] Becker, F.; Kienzler, B., *Simulation of alpha dose for predicting radiolytic species at the surface of spent nuclear fuel pellets*, *Open Chem* **2015**, 13, 586-590.
- [12] Bouby, M.; Finck, N.; Geckeis, H., *Synthetic smectite colloids: Characterization of nanoparticles after coprecipitation in the presence of lanthanides and tetravalent elements (Zr, Th)*, *Chromatography* **2015**, 2, 545-566.
- [13] Bourg, S.; Geist, A.; Narbutt, J., *SACSESS – the EURATOM FP7 project on actinide separation from spent nuclear fuels*, *Nukleonika* **2015**, 60, 809-814.
- [14] Bremer, A.; Muellich, U.; Geist, A.; Panak, P. J., *Influence of the solvent on the complexation of Cm(III) and Eu(III) with nPr-BTP studied by time-resolved laser fluorescence spectroscopy*, *New J Chem* **2015**, 39, 1330-1338.
- [15] Brookshaw, D. R.; Patrick, R. A. D.; Bots, P.; Law, G. T. W.; Lloyd, J. R.; Mosselmans, J. F. W.; Vaughan, D. J.; Dardenne, K.; Morrie, K., *Redox Interactions of Tc(VII), U(VI), and Np(V) with Microbially Reduced Biotite and Chlorite*, *Environ Sci Technol* **2015**, 49, 13139-13148.
- [16] Caisso, M.; Picart, S.; Belin, R. C.; Lebreton, F.; Martin, P. M.; Dardenne, K.; Rothe, J.; Neuville, D. R.; Delahaye, T.; Ayrat, A., *In situ characterization of uranium and americium oxide solid solution formation for CRMP process: first combination of in situ XRD and XANES measurements*, *Dalton T* **2015**, 44, 6391-6399.

- [17] Carrott, M.; Geist, A.; Heres, X.; Lange, S.; Malmbeck, R.; Miguirditchian, M.; Modolo, G.; Wilden, A.; Taylor, R., *Distribution of plutonium, americium and interfering fission products between nitric acid and a mixed organic phase of TODGA and DMDOHEMA in kerosene, and implications for the design of the "EURO-GANEX" process, Hydrometallurgy* **2015**, *152*, 139-148.
- [18] Chagneau, A.; Claret, F.; Enzmann, F.; Kersten, M.; Heck, S.; Made, B.; Schafer, T., *Mineral precipitation-induced porosity reduction and its effect on transport parameters in diffusion-controlled porous media, Geochem T* **2015**, *16*.
- [19] Chagneau, A.; Tournassat, C.; Steefel, C. I.; Bourg, I. C.; Gaboreau, S.; Esteve, I.; Kupcik, T.; Claret, F.; Schäfer, T., *Complete Restriction of Cl-36(-) Diffusion by Celestite Precipitation in Densely Compacted Illite, Environ Sci Tech Let* **2015**, *2*, 139-143.
- [20] Dardenne, K.; Gonzalez-Robles, E.; Rothe, J.; Mueller, N.; Christill, G.; Lemmer, D.; Praetorius, R.; Kienzler, B.; Metz, V.; Roth, G.; Geckeis, H., *XAS and XRF investigation of an actual HAWC glass fragment obtained from the Karlsruhe vitrification plant (VEK), J Nucl Mater* **2015**, *460*, 209-215.
- [21] Delavernhe, L.; Steudel, A.; Darbha, G. K.; Schäfer, T.; Schuhmann, R.; Wöll, C.; Geckeis, H.; Emmerich, K., *Influence of mineralogical and morphological properties on the cation exchange behavior of dioctahedral smectites, Colloids and Surfaces A: Physicochemical and Engineering Aspects* **2015**, *481*, 591-599.
- [22] Ekberg, C.; Lofstrom-Engdahl, E.; Aneheim, E.; Foreman, M. R. S. J.; Geist, A.; Lundberg, D.; Denecke, M.; Persson, I., *The structures of CyMe<sub>4</sub>-BTBP complexes of americium(III) and europium(III) in solvents used in solvent extraction, explaining their separation properties, Dalton T* **2015**, *44*, 18395-18402.
- [23] Finck, N.; Dardenne, K.; Geckeis, H., *Am(III) coprecipitation with and adsorption on the smectite hectorite, Chemical Geology* **2015**, *409*, 12-19.
- [24] Finck, N.; Schlegel, M. L.; Bauer, A., *Structural iron in dioctahedral and trioctahedral smectites: a polarized XAS study, Phys Chem Miner* **2015**, *42*, 847-859.
- [25] Frankel, G.; Thornton, G.; Street, S.; Rayment, T.; Williams, D.; Cook, A.; Davenport, A.; Gibbon, S.; Engelberg, D.; Ornek, C.; Mol, A.; Marcus, P.; Shoesmith, D.; Wren, C.; Yliniemi, K.; Williams, G.; Lyon, S.; Lindsay, R.; Hughes, T.; Lutzenkirchen, J.; Cheng, S. T.; Scully, J.; Lee, S. F.; Newman, R.; Taylor, C.; Springell, R.; Mauzeroll, J.; Virtanen, S.; Heurtault, S.; Sullivan, J., *Localised corrosion: general discussion, Faraday Discuss* **2015**, *180*, 381-414.
- [26] Froehlich, D. R.; Skerencak-Frech, A.; Bauer, N.; Rossberg, A.; Panak, P. J., *The pH dependence of Am(III) complexation with acetate: an EXAFS study, J Synchrotron Radiat* **2015**, *22*, 99-104.
- [27] Frohlich, D. R.; Skerencak-Frech, A.; Kaplan, U.; Koke, C.; Rossberg, A.; Panak, P. J., *An EXAFS spectroscopic study of Am(III) complexation with lactate, J Synchrotron Radiat* **2015**, *22*, 1469-1474.
- [28] Frohlich, D. R.; Skerencak-Frech, A.; Panak, P. J., *Complex formation of Cm(III) with formate studied by time-resolved laser fluorescence spectroscopy, Appl Geochem* **2015**, *61*, 312-317.
- [29] Geckeis, H., *Transmutation cannot replace permanent repository [Transmutation kann Endlager nicht ersetzen], Nachrichten aus der Chemie* **2015**, *63*, 127.
- [30] Geckeis, H.; Filby, A.; Plaschke, M., *Response to J.J. Weimer, L.A.W. Sanderson, "Corrections to the born repulsion term for energy and force in a sphere-plate colloidal system", Colloid Surface A* **2015**, *472*, 126-126.
- [31] Gonzalez-Robles, E.; Fuss, M.; Bohnert, E.; Müller, N.; Herm, M.; Metz, V.; Kienzler, B., *Study of the release of the fission gases (Xe and Kr) and the fission products (Cs and I) under anoxic conditions in bicarbonate water, Materials Research Society Symposium Proceedings* **2015**, *1744*, 283-289.
- [32] González-Robles, E.; Serrano-Purroy, D.; Sureda, R.; Casas, I.; De Pablo, J., *Dissolution experiments of commercial PWR (52 MWd/kgU) and BWR (53 MWd/kgU) spent nuclear fuel cladded segments in bicarbonate water under oxidizing conditions. Experimental determination of matrix and instant release fraction., J Nucl Mater* **2015**, *465*, 63-70.
- [33] Grangeon, S.; Vinsot, A.; Tournassat, C.; Lerouge, C.; Giffaut, E.; Heck, S.; Groschopf, N.; Denecke, M. A.; Wechner, S.; Schaefer, T., *The influence of natural trace element distribution on the mobility of radionuclides. The exemple of nickel in a clay-rock, Appl Geochem* **2015**, *52*, 155-173.
- [34] Graser, C. H.; Banik, N. L.; Bender, K. A.; Lagos, M.; Marquardt, C. M.; Marsac, R.; Montoya, V.; Geckeis, H., *Sensitive Redox Speciation of Iron, Neptunium, and Plutonium by Capillary*

- Electrophoresis Hyphenated to Inductively Coupled Plasma Sector Field Mass Spectrometry, Anal Chem* **2015**, *87*, 9786-9794.
- [35] Henry, C.; Norrfors, K. K.; Olejnik, M.; Bouby, M.; Luetzenkirchen, J.; Wold, S.; Minier, J.-P., *A refined algorithm to simulate latex colloid agglomeration at high ionic strength, Adsorption* **2015**, 1-13.
- [36] Herm, M.; Gaona, X.; Rabung, T.; Fellhauer, D.; Crepin, C.; Dardenne, K.; Altmaier, M.; Geckeis, H., *Solubility and spectroscopic study of An(III)/Ln(III) in dilute to concentrated Na-Mg-Ca-Cl-NO<sub>3</sub> solutions, Pure Appl Chem* **2015**, *87*, 487-502.
- [37] Hinz, K.; Altmaier, M.; Gaona, X.; Rabung, T.; Schild, D.; Richmann, M.; Reed, D.; Geckeis, H., *Complexation of Ln(III) and An(III) with borate in dilute to concentrated alkaline NaCl, MgCl<sub>2</sub> and CaCl<sub>2</sub> solutions: solubility and TRLFS studies, New J Chem* **2015**, 39.
- [38] Hinz, K.; Altmaier, M.; Gaona, X.; Rabung, T.; Schild, D.; Richmann, M.; Reed, D. T.; Alekseev, E. V.; Geckeis, H., *Interaction of Nd(III) and Cm(III) with borate in dilute to concentrated alkaline NaCl, MgCl<sub>2</sub> and CaCl<sub>2</sub> solutions: solubility and TRLFS studies, New J Chem* **2015**, *39*, 849-859.
- [39] Huber, F. M.; Heck, S.; Truche, L.; Bouby, M.; Brendle, J.; Hoess, P.; Schafer, T., *Radionuclide desorption kinetics on synthetic Zn/Ni-labeled montmorillonite nanoparticles, Geochim Cosmochim Acta* **2015**, *148*, 426-441.
- [40] Ibrahimkuty, S.; Seiler, A.; Pruessmann, T.; Vitova, T.; Pradip, R.; Bauder, O.; Wochner, P.; Plech, A.; Baumbach, T.; Stankov, S., *A portable ultrahigh-vacuum system for advanced synchrotron radiation studies of thin films and nanostructures: EuSi<sub>2</sub> nano-islands, J Synchrotron Radiat* **2015**, *22*, 91-98.
- [41] Jain, R.; Jordan, N.; Schild, D.; van Hullebusch, E. D.; Weiss, S.; Franzen, C.; Farges, F.; Hubner, R.; Lens, P. N. L., *Adsorption of zinc by biogenic elemental selenium nanoparticles, Chem Eng J* **2015**, *260*, 855-863.
- [42] Kallay, N.; Preocanin, T.; Selmani, A.; Kovacevic, D.; Luetzenkirchen, J.; Nakahara, H.; Shibata, O., *Thermodynamic Model of Charging the Gas/Water Interface, Journal of Physical Chemistry C* **2015**, *119*, 997-1007.
- [43] Kiefer, C.; Wagner, A. T.; Beele, B. B.; Geist, A.; Panak, P. J.; Roesky, P. W., *A Complexation Study of 2,6-Bis(1-(p-tolyl)-1H-1,2,3-triazol-4-yl)pyridine Using Single-Crystal X-ray Diffraction and TRLFS, Inorg Chem* **2015**, *54*, 7301-7308.
- [44] Kovacs, A.; Apostolidis, C.; Walter, O.; Lindqvist-Reis, P., *'Lanthanide contraction' in [Ln(BTP)(3)](CF<sub>3</sub>SO<sub>3</sub>)(3) complexes, Struct Chem* **2015**, *26*, 1287-1295.
- [45] Kulik, D. A.; Hummel, W.; Luetzenkirchen, J.; Lefevre, G., *Preface: SI: Geochemical speciation codes and databases, Appl Geochem* **2015**, *55*, 1-2.
- [46] Kupcik, T.; Rabung, T.; Lützenkirchen, J.; Finck, N.; Geckeis, H.; Fanghänel, T., *Macroscopic and spectroscopic investigations on Eu(III) and Cm(III) sorption onto bayerite (β-Al(OH)<sub>3</sub>) and corundum (α-Al<sub>2</sub>O<sub>3</sub>), Journal of Colloids and Interface Science* **2015**, *461*, 215-224
- [47] Léon, A.; Finck, N.; Rothe, J.; Felderhoff, M.; Fichtner, M., *Fluorescence X-ray Absorption Study of ScCl<sub>3</sub>-Doped Sodium Alanate, J. Phys. Chem. C* **2015**, *119*, 15810-15815.
- [48] Lewis, F. W.; Harwood, L. M.; Hudson, M. J.; Geist, A.; Kozhevnikov, V. N.; Distler, P.; John, J., *Hydrophilic sulfonated bis-1,2,4-triazine ligands are highly effective reagents for separating actinides(III) from lanthanides(III) via selective formation of aqueous actinide complexes, Chem. Sci.* **2015**, *6*, 4812-4821.
- [49] Lewis, F. W.; Harwood, L. M.; Hudson, M. J.; Mullich, U.; Geist, A., *Efficient masking of corrosion and fission products such as Ni(II) and Pd(II) in the presence of the minor actinide Am(III) using hydrophilic anionic or cationic bis-triazines, Chem Commun* **2015**, *51*, 9189-9192.
- [50] Luetzenkirchen, J.; Marsac, R.; Casey, W. H.; Furrer, G.; Kupcik, T.; Lindqvist-Reis, P., *The Effect of Monovalent Electrolytes on the Deprotonation of MA112 Keggin Ions, Aquatic Geochemistry* **2015**, *21*, 81-97.
- [51] Luetzenkirchen, J.; Marsac, R.; Kulik, D. A.; Payne, T. E.; Xue, Z.; Orsetti, S.; Haderlein, S. B., *Treatment of multi-dentate surface complexes and diffuse layer implementation in various speciation codes, Appl Geochem* **2015**, *55*, 128-137.
- [52] Lutzenkirchen, J.; Heberling, F.; Supljika, F.; Preocanin, T.; Kallay, N.; Johann, F.; Weisser, L.; Eng, P. J., *Structure-charge relationship - the case of hematite (001), Faraday Discuss* **2015**, *180*, 55-79.

- [53] Marsac, R.; Banik, N. L.; Luetzenkirchen, J.; Buda, R. A.; Kratz, J. V.; Marquardt, C. M., *Modeling plutonium sorption to kaolinite: Accounting for redox equilibria and the stability of surface species*, *Chemical Geology* **2015**, *400*, 1-10.
- [54] Marsac, R.; Banik, N. L.; Lutzenkirchen, J.; Marquardt, C. M.; Dardenne, K.; Schild, D.; Rothe, J.; Diacorn, A.; Kupcik, T.; Schafer, T.; Geckeis, H., *Neptunium redox speciation at the illite surface*, *Geochim Cosmochim Acta* **2015**, *152*, 39-51.
- [55] Marzocchi, O.; Leone, D., *Iterative optimisation of Monte Carlo detector models using measurements and simulations*, *Nucl Instrum Meth A* **2015**, *779*, 47-51.
- [56] Mauzeroll, J.; Thornton, G.; Rayment, T.; Maurice, V.; Williams, D.; Heberling, F.; Marcus, P.; Wren, C.; Yliniemi, K.; Lindsay, R.; Lyth, S.; Majchrowski, T.; Hussain, H.; Hunt, G.; Renner, F.; Williams, G.; Newman, R.; Frankel, G.; Lutzenkirchen, J.; Bluhm, H., *Solid/fluid interface: general discussion*, *Faraday Discuss* **2015**, *180*, 81-96.
- [57] Moog, H. C.; Bok, F.; Marquardt, C. M.; Brendler, V., *Disposal of nuclear waste in host rock formations featuring high-saline solutions - Implementation of a thermodynamic reference database (THEREDA)*, *Appl Geochem* **2015**, *55*, 72-84.
- [58] Nazmov, V.; Völker, A.; Fischböck, T.; Rothe, J.; Huttel, E., *Mass loss by SU-8 polymer under X-ray irradiation*, *Bulletin of the Russian Academy of Sciences: Physics* **2015**, *79*, 5-9.
- [59] Nogueira, P.; Ruhm, W.; Lopez, M. A.; Vrba, T.; Buchholz, V. V.; Fojtik, P.; Etherington, G.; Broggio, D.; Huikari, J.; Marzocchi, Lynch, T.; Lebacqz, A. L.; Li, C.; Osko, J.; Malatova, I.; Franck, D.; Breustedt, B.; Leone, D.; Scott, J.; Shutt, A.; Hauck, B.; Capello, K.; Perez-Lopez, B.; Navarro-Amaro, J. F.; Pliszczyrski, T.; Fantinova, K.; Tolmachev, S. Y., *EURADOS Am-241 skull measurement intercomparison*, *Radiat Meas* **2015**, *82*, 64-73.
- [60] Norrfors, K. K.; Bouby, M.; Heck, S.; Finck, N.; Marsac, R.; Schafer, T.; Geckeis, H.; Wold, S., *Montmorillonite colloids: I. Characterization and stability of dispersions with different size fractions*, *Applied Clay Science* **2015**, *114*, 179-189.
- [61] Quinto, F.; Golser, R.; Lagos, M.; Plaschke, M.; Schafer, T.; Steier, P.; Geckeis, H., *Accelerator Mass Spectrometry of Actinides in Ground- and Seawater: An Innovative Method Allowing for the Simultaneous Analysis of U, Np, Pu, Am, and Cm Isotopes below ppq Levels*, *Anal Chem* **2015**, *87*, 5766-5773.
- [62] Rolker, J.; Schill, E.; Schneider, J.; Stober, I.; Neumann, T.; Kohl, T., *Hydrochemical characterization of a major central European heat flux anomaly: The Bürchau Geothermal Spring system, Southern Black Forest, Germany*, *Geothermal Energy Journal* **2015**, *3*.
- [63] Schnurr, A.; Marsac, R.; Rabung, T.; Lutzenkirchen, J.; Geckeis, H., *Sorption of Cm(III) and Eu(III) onto clay minerals under saline conditions: Batch adsorption, laser-fluorescence spectroscopy and modeling*, *Geochim Cosmochim Acta* **2015**, *151*, 192-202.
- [64] Selmani, A.; Spadina, M.; Plodinec, M.; Marion, I. D.; Willinger, M. G.; Lutzenkirchen, J.; Gafney, H. D.; Redel, E., *An Experimental and Theoretical Approach to Understanding the Surface Properties of One-Dimensional TiO<sub>2</sub> Nanomaterials*, *Journal of Physical Chemistry C* **2015**, *119*, 19729-19742.
- [65] Skerencak-Frech, A.; Maiwald, M.; Trumm, M.; Froehlich, D. R.; Panak, P. J., *The Complexation of Cm(III) with Oxalate in Aqueous Solution at T=20-90 degrees C: A Combined TRLFS and Quantum Chemical Study*, *Inorg Chem* **2015**, *54*, 1860-1868.
- [66] Spichak, V.; Geiermann, J.; Zakharova, O.; Calcagno, P.; Genter, A.; Schill, E., *Estimating deep temperatures in the Soultz-sous-Forets geothermal area (France) from magnetotelluric data*, *Near Surf Geophys* **2015**, *13*, 397-408.
- [67] Thorpe, C. L.; Morris, K.; Lloyd, J. R.; Denecke, M. A.; Law, K. A.; Dardenne, K.; Boothman, C.; Bots, P.; Law, G. T. W., *Neptunium and manganese biocycling in nuclear legacy sediment systems*, *Appl Geochem* **2015**, *63*, 303-309.
- [68] Trumm, M.; Schimmelpfennig, B.; Geist, A., *Structure and separation quality of various N- and O-donor ligands from quantum-chemical calculations*, *Nukleonika* **2015**, *60*, 847-851.
- [69] Vasiliev, A. N.; Banik, N. L.; Marsac, R.; Froehlich, D. R.; Rothe, J.; Kalmykov, S. N.; Marquardt, C. M., *Np(V) complexation with propionate in 0.5-4 M NaCl solutions at 20-85 degrees C*, *Dalton T* **2015**, *44*, 3837-3844.

- [70] Vespa, M.; Wieland, E.; Dahn, R.; Lothenbach, B., *Identification of the Thermodynamically Stable Fe-Containing Phase in Aged Cement Pastes*, *Journal of the American Ceramic Society* **2015**, *98*, 2286-2294.
- [71] Vitova, T.; Green, J. C.; Denning, R. G.; Loeble, M.; Kvashnina, K.; Kas, J. J.; Jorissen, K.; Rehr, J. J.; Malcherek, T.; Denecke, M. A., *Polarization Dependent High Energy Resolution X-ray Absorption Study of Dicesium Uranyl Tetrachloride*, *Inorg Chem* **2015**, *54*, 174-182.
- [72] Vrba, T.; Broggio, D.; Caldeira, M.; Capello, K.; Fantinova, K.; Franck, D.; Gomez-Ros, J. M.; Hunt, J.; Kinase, S.; Leone, D.; Lombardo, P. A.; Manohari, M.; Marzocchi, O.; Moraleda, M.; Nogueira, P.; Osko, J.; Arron, S.; Suhl, S.; Takahashi, M.; Teles, P.; Tremblay, M.; Tyminska, K.; Lopez, M. A.; Tanner, R., *EURADOS intercomparison exercise on MC modelling for the in-vivo monitoring of AM-241 in skull phantoms (Part II and III)*, *Radiat Phys Chem* **2015**, *113*, 59-71.
- [73] Wagner, C.; Müllich, U.; Geist, A.; Panak, P. J., *TRLFS study on the complexation of Cm(III) and Eu(III) with SO<sub>3</sub>-Ph-BTBP*, *Dalton T* **2015**, *44*, 17143-17151.
- [74] Wallner, A.; Faestermann, T.; Feige, J.; Feldstein, C.; Knie, K.; Korschinek, G.; Kutschera, W.; Ofan, A.; Paul, M.; Quinto, F.; Rugel, G.; Steier, P., *Abundance of live Pu-244 in deep-sea reservoirs on Earth points to rarity of actinide nucleosynthesis*, *Nat Commun* **2015**, *6*.
- [75] Wilden, A.; Modolo, G.; Kaufholz, P.; Sadowski, F.; Lange, S.; Munzel, D.; Geist, A., *Process development and laboratory-scale demonstration of a regular-SANEX process using C5-BPP*, *Separ. Sci. Technol.* **2015**, *50*, 2467-2475.
- [76] Wilden, A.; Modolo, G.; Kaufholz, P.; Sadowski, F.; Lange, S.; Sypula, M.; Magnusson, D.; Mullich, U.; Geist, A.; Bosbach, D., *Laboratory-Scale Counter-Current Centrifugal Contactor Demonstration of an Innovative-SANEX Process Using a Water Soluble BTP*, *Solvent Extr Ion Exc* **2015**, *33*, 91-108.
- [77] Wilhelm, E.; Deshpande, K.; Kotz, F.; Schild, D.; Keller, N.; Heissler, S.; Sachsenheimer, K.; Lange, K.; Neumann, C.; Rapp, B. E., *Polysiloxane layers created by sol-gel and photochemistry: ideal surfaces for rapid, low-cost and high-strength bonding of epoxy components to polydimethylsiloxane*, *Lab Chip* **2015**, *15*, 1772-1782.
- [78] Woodall, S. D.; Swinburne, A. N.; Banik, N. L.; Kerridge, A.; Di Pietro, P.; Adam, C.; Kaden, P.; Natrajan, L. S., *Neptunyl(VI) centred visible LMCT emission directly observable in the presence of uranyl(VI)*, *Chem Commun* **2015**, *51*, 5402-5405.
- [79] Yalcintas, E.; Gaona, X.; Scheinost, A. C.; Kobayashi, T.; Altmaier, M.; Geckeis, H., *Redox chemistry of Tc(VII)/Tc(IV) in dilute to concentrated NaCl and MgCl<sub>2</sub> solutions*, *Radiochim Acta* **2015**, *103*, 57-72.

### Other referred publications

- [80] Altmaier, M., *Solubility Phenomena and Related Equilibrium Processes*, *Chemistry International* **2015**, *37*, 30-31.
- [81] Altmaier, M.; Gaona, X.; Geckeis, H., *Actinidenchemie in wässrigen Lösungen*, *GDCh-Broschüre „HighChem hautnah – Aktuelles aus der Wasserchemie“*, **2015**, pp. 76-77.
- [82] Altmanns, S.; Aertens, M.; Appelo, T.; Bruggeman, C.; Gaboreau, S.; Glaus, M.; Jacquier, P.; Kupcik, T.; Maes, N.; Montoya, V.; Rabung, T.; Robinet, J.-C.; Savoye, S.; Schaefer, T.; Tournassat, C.; Van Laer, L.; Van Loon, L., *Processes of cation migration in clayrocks: Final Scientific Report of the CatClay EuropeanProject*, *CEA-R-6410* **2015**.
- [83] Bahl, S., *Advanced spectroscopic and microscopic investigations of Pu-doped borosilicate glass*, *TALISMAN – Report JRP TALI-C03-01*, **2015**.
- [84] Bahl, S., *Advanced spectroscopic and microscopic investigations of Pu-doped borosilicate glass*, *TALISMAN – Report JRP TALI-C03-01*, **2015**.
- [85] Bahl, S.; Koldeisz, V.; Bohnert, E.; González-Robles, E.; Schild, D.; Kienzler, B.; Kvashnina, K.; Rothe, J.; Dardenne, K.; Boshoven, J.; Martel, L.; Pidchenko, I.; Prübmann, T.; Roth, G.; Geckeis, H.; Vitova, T., *Comparative U, Np and Pu M edge high energy resolution X-ray absorption spectroscopy (HR-XANES) investigations of model and genuine active waste glass*, *GDCh Wissenschaftsforum Chemie 2015*, Dresden, Germany **2015**

- [86] Bauer, N.; Fröhlich, D. R.; Dardenne, K.; Rothe, J.; Panak, P. J., *EXAFS investigation on actinide and lanthanide transferrin complexes*, *ANKA User Reports 2012/2013*, **2015**, pp. 12-13.
- [87] Borkel, C.; Kienzler, B.; Schlieker, M.; Metz, V.; Schild, D.; Soballa, E.; Lagos, M.; Walschburger, C.; Heck, S.; Moisei-Rabung, S.; Seither, A., *Experimentelles Programm zur Untersuchung von simulierten, zementierten 1:1 Gebinden aus dem Auslaugversuchsfeld Nr. 1 der Schachanlage Asse. Teil III: Ergebnisse der Festkörperanalysen, KIT-INE 001/15, Technischer Bericht* **2015**.
- [88] Buckau, G.; Carbol, P.; Geckeis, H.; Glatz, J. P.; Gouder, T.; Malmbeck, R.; Metz, V.; Peugeot, S.; Rondinella, V.; Serrano-Purroy, D.; Souček, P.; van Kalleveen, A.; Wegen, D.; Wiss, T.; Fazio, C., *Training course Introduction to the back-end of the nuclear fuel cycle, European Nuclear Safety and Security School. Joint Research Centre of the European Commission, JRC Technical Report*, **2015**.
- [89] Deutsche; Arbeitsgemeinschaft; Endlagerforschung, *Key topics in deep geological disposal: Conference report, KIT Scientific Reports, Vol. KIT-SR 7696, Cologne*, **2015**.
- [90] Gaona, X.; Tasi, A.; Fellhauer, D.; Böttle, M.; Rothe, J.; Schild, D.; Altmaier, M.; Geckeis, H., *Redox behaviour, solubility and sorption of Pu(III/IV) in the absence and presence of ISA and cement SKB-Pu-ISA, WPI. Final report, October 2014 – July 2015*, **2015**.
- [91] González-Robles, E.; Loida, A.; Müller, N.; Bohnert, E.; Herm, M.; Montoya, V.; Kienzler, B.; Metz, V., *Investigation of the Corrosion Behaviour of Spent Nuclear Fuel Fragments in High pH Solutions under H<sub>2</sub> Overpressure, Final Report, Working Period 2012-2013, Contract No 20120014495 with ONDRAF/NIRAS (B)*, **2015**.
- [92] Herm, M.; González-Robles, E.; Böttle, M.; Müller, N.; Papaioannou, D.; Wegen, D. H.; Dagan, R.; Kienzler, B.; Metz, V., *Description of Zircaloy-4 dissolution experiment in a shielded box, Carbon-14 Source Term – CAST, Deliverable D3.8.*, **2015**.
- [93] Kaplan, U.; Fröhlich, D. R.; Finck, F.; Maiwald, M. M.; Schäfer, T., *Speciation of americium(III) by illite under Boom Clay conditions: Influence of dissolved organic carbon, ERSF Report*, **2015**.
- [94] Marzocchi, O.; Romanello, V., *Analysis of a Radioactive Lens and of the Correlated UV Light Bleaching Properties, Strahlenschutz Praxis Vol. 2/2015*, **2015**.
- [95] Modolo, G.; Geist, A.; Miguirditchian, M., *Minor actinide separations in the reprocessing of spent nuclear fuels: recent advances in Europe*, Woodhead Publishing, **2015**.
- [96] Prieur, D.; Martin, P.; Bes, R.; Pruessman, T.; Vitova, T.; Lebreton, F.; Strach, M.; Caisso, M.; Delahaye, T.; Belin, R.; Somers, J., *HR-XANES study of the electronic structures of (U,Am)O<sub>2</sub> and of associated binary systems UO<sub>2+x</sub> and AmO<sub>2-x</sub>, TALISMAN – Report JRP TALI-C02-08*, **2015**.
- [97] Prieur, D.; Martin, P.; Bes, R.; Prüssman, T.; Vitova, T.; Lebreton, F.; Strach, M.; Caisso, M.; Delahaye, T.; Belin, R.; Somers, J., *HR-XANES study of the electronic structures of (U,Am)O<sub>2</sub> and of associated binary systems UO<sub>2+x</sub> and AmO<sub>2-x</sub>, TALISMAN – Report JRP TALI-C02-08, 2015*, **2015**.
- [98] Ragoussi, M. E.; Altmaier, M.; Reed, D. T., *Assessing high ionic strength solutions: A new activity of the TDB Project, NEA News Vol. 31.3, Nuclear Energy Agency (NEA), Paris, France*, **2015**.
- [99] Schäfer, T.; Dohrmann, R.; Greenwell, C.; Jensen, M., *Filling the Gaps–From Microscopic Pore Structures to Transport Properties in Shales, Fourth International Conference on Fault and Top Seals*, **2015**
- [100] Vitova, T., *Status report of the Helmholtz Young Investigators Group (HYIG VH-NG-734) “Advanced synchrotron-based systematic investigations of actinide (An) and lanthanide (Ln) systems to understand and predict their reactivity”, March 2015 (Report)*, **2015**.
- [101] Waghorne, E.; Altmaier, M., *16th International Symposium on Solubility Phenomena and Related Equilibrium Processes (ISSP-16), Pure Appl. Chem.* **2015**, 87, 443.

#### Invited talks

- [102] Altmaier, M., *Aquatic radionuclide chemistry and thermodynamics at KIT-INE, Kyoto University, Kyoto, Japan*, **2015**
- [103] Altmaier, M., *Aqueous chemistry and thermodynamics of actinides, lanthanides and long-lived fission products, GENTLE Intersemester Course, Karlsruhe, Germany*, **2015**

- [104] Altmaier, M.; Bourbon, X.; Claret, F.; Grambow, B.; Holt, E.; Idiart, A.; Mäder, U.; Perrone, J., *The CEBAAMA Project, 6th IGD-TP Exchange Forum*, London, UK, **2015**
- [105] Altmaier, M.; Kienzler, B.; Rothe, J.; Schäfer, T.; Geckeis, H., *Geochemical Research for Nuclear Waste Disposal Safety, Energy, Science and Technology Conference & Exhibition EST 2015*, Karlsruhe, Germany, **2015**
- [106] Geckeis, H., *Safety of nuclear waste disposal – Radio/geochemical research still needed?*, Washington State University, Pullman, USA,
- [107] Geckeis, H., *Das umstrittene Problem der nuklearen Entsorgung - aus der Sicht des Chemikers*, GDCH Vortragsreihe, Jungchemikerforum, Uni Saarbrücken, Germany, **2015**
- [108] Geckeis, H., *Molecular scale investigations towards actinide retention at mineral surfaces*, Glenn T. Seaborg Award Symposium, ACS spring meeting, Denver, USA, **2015**
- [109] Geckeis, H., *Nuclear waste disposal in Germany: Present situation-Nuclear waste disposal options*, International Workshop on Actinide-Brine-Chemistry (ABC-Salt IV), **2015**
- [110] Geckeis, H., *Kontroverse: nukleare „Entsorgung“*, GDCH Kolloquium, Jungchemikerforum, Uni Kiel, Germany, **2015**
- [111] Geckeis, H., *Disposal of high level nuclear waste - Facts and perspectives*, 8<sup>th</sup> Summer School on Actinide Science and Applications, Karlsruhe, Germany, **2015**
- [112] Geckeis, H., *Kann Transmutation die Lösung sein?*, Karlsruher Atomtage, Karlsruhe, Germany, **2015**
- [113] Geckeis, H., *Einladung zur öffentlichen Anhörung*, Deutscher Bundestag Umweltausschuss: Pfade für die Endlagerung radioaktiver Abfälle, Berlin, Germany, **2015**
- [114] Geckeis, H.; Bouby, M., *Actinide environmental behavior-role of nanoparticle formation*, 3rd FFF-MS Workshop, University of Vienna, Austria, **2015**
- [115] Heberling, F.; Paulig, L., *Recrystallization kinetics of calcite, morphology controls, and the influence of Eu<sup>3+</sup> and SeO<sub>3</sub><sup>2-</sup>*, Goldschmidt Conference 2015, Prague, Czeck Republic, **2015**
- [116] Kienzler, B., *Investigations on high level waste materials (spent fuel, glass, steel, cladding) at KIT-INE*, U.S. Nuclear Regulatory Commission (NRC), Rockville, USA, **2015**
- [117] Kienzler, B., *Outcome and added value of FIRST-Nuclides*, Center of Nuclear Waste Regulatory Analyses (CNWRA), Southwest Research Institute, San Antonio, USA, **2015**
- [118] Kienzler, B., *Conceptual ideas about the radio-geochemical monitoring during the operational phase*, Int. Expert Workshop “Endlagerung in tiefen Bohrlöchern”, Berlin, Germany, **2015**
- [119] Kienzler, B., *Implementing Geological Disposal for Radioactive Waste - Technology platform (IGD-TP)*, IGD-TP Exchange Forum n°6, London, UK, **2015**
- [120] Kienzler, B., *Results of long-term leaching experiments of low level waste forms in salt brines*, American Nuclear Society, Carlsbad Chapter Lecture Series, New Mexico State University, Carlsbad, USA, **2015**
- [121] Kienzler, B., *Fast Radionuclide Release from the Waste Form “Used Nuclear Fuel”*, Migration 2015, Santa Fe, USA, **2015**
- [122] Kienzler, B., *Outcome and added value of FIRST-Nuclides*, Center of Nuclear Waste Regulatory Analyses (CNWRA), Southwest Research Institute, San Antonio, TX, USA, **2015**
- [123] Lützenkirchen, J., *Charging of small Keggin-ions and adsorption of Europium*, “Quo Vadis” Coordination Chemistry?, Debrecen, Hungary, **2015**
- [124] Lützenkirchen, J., *Some experimental observations on and modelling of the 001 plane of sapphire and a comparison to hematite*, Goldschmidt Conference, Prague, CZ, **2015**
- [125] Lützenkirchen, J., *Nikola Kallay - a personal note*, Department of Chemistry, Faculty of Science, University of Zagreb, Zagreb, Croatia, **2015**
- [126] Lützenkirchen, J., *Nikola Kallay and his (scientific) achievements*, ISSHAC-9, Wroclaw, Poland, **2015**
- [127] Panak, P. J., *Spectroscopic Characterization of actinides*, 8<sup>th</sup> Summer School on Actinide Science & Applications 2015, Karlsruhe, Germany **2015**

- [128] Rabung, T., *Sorption processes on clays*, 6th DTTG International Workshop “Clays and clay minerals”, Karlsruhe, Germany, **2015**
- [129] Schäfer, T., *Can a macroscopic modeling approach properly describe transport in porous media during mineral precipitation induced clogging?*, Geoscience Colloquium TU Munich, Munich, Germany, **2015**
- [130] Schäfer, T., *The fate of radionuclides in the multi-barrier system of a deep-geological repository*, Materials Science & Technology conference, Columbus, Ohio, USA, **2015**
- [131] Schäfer, T.; Geckeis, H., *Naturally Occurring Radioactive Materials (NORM): A Comparison Between Geothermal Energy, Fracking and Uranium Mining Overburden*, 46<sup>th</sup> Annual Meeting on Nuclear Technology, Berlin, Germany, **2015**
- [132] Schill, E., *Geothermal energy from the crystalline basement: exploration and monitoring from reservoir scale to laboratory and rock laboratory*, Kolloquium Geowissenschaften, University of Göttingen, Germany, **2015**
- [133] Schill, E.; Kohl, T.; Geiermann, J.; Baujard, C.; Koch, S.; Deckert, H.; Munoz, G.; Abdelfettah, Y.; Wellmann, J. F., *Alternative exploration methods for risk mitigation in the crystalline basement*, IGC, Offenburg, Germany, **2015**
- [134] Steier, P.; Eigl, R.; Lachner, J.; Priller, A.; Quinto, F.; Sakaguchi, A.; Winkler, S.; Golser, R., *AMS detection of actinides at high mass separation*, DPG-Frühjahrstagung 2015, Heidelberg, Germany, **2015**
- [135] Steier, P.; Fröhlich, M.; Lachner, J.; Martschini, M.; Pitters, J.; Quinto, F.; Sakaguchi, A.; Winkler, S.; Golser, R., *New frontiers for accelerator mass spectrometry – new isotopes and new applications*, ENVIRA2015, International Conference on Environmental Radioactivity: New Challenges with New Technologies, Thessaloniki, Greece, **2015**
- [136] Vitova, T., *Structural properties of actinide materials revealed by high energy resolution X-ray absorption spectroscopy*, National Conference on Environmental Radiochemistry, Chengdu, China, **2015**
- [137] Vitova, T., *Structural properties of nanomaterials studied by high energy resolution X-ray emission and absorption spectroscopy techniques*, International Joint School on Smart Nanomaterials and X-ray Optics 2015. Modeling, Synthesis and Diagnostics, Rostov-on-Don, Russia, **2015**
- [138] Vitova, T., *High Resolution X-ray Absorption Spectroscopy as an Advanced Tool for Structural Investigations of Actinides*, AVS 62nd International Symposium & Exhibition, San Jose, USA, **2015**
- [139] Vitova, T., *High energy resolution X-ray absorption spectroscopy: a tool for structural studies of actinide materials*, 4rd ITU – INE Research Fellow Day, Karlsruhe, Germany, **2015**
- [140] Vitova, T., *Workshop lectures*, ASEAN Workshop on XANES Simulations and In-situ XAS Experiments (AWXIXE2015), Synchrotron Light Research Institute (SLRI), Thailand, **2015**
- [141] Vitova, T., *High energy resolution XANES as a tool for electronic structure and oxidation states investigations of actinide materials*, ThUL School in Actinide Chemistry, Karlsruhe, Germany, **2015**

## Proceedings

- [142] Abdelfettah, Y.; Schill, E., *Use of gravity post-processing and accurate 3D forward modeling to identify and characterize geothermal target*, Proceedings, World Geothermal Congress 2015, Melbourne, Australia, **2015**
- [143] Bouby, M.; Heyrich, Y.; Heck, S.; Hilpp, S.; Schäfer, T., *Influence of organic matter (fulvic acids) on the long term stability of clay colloids prepared under different chemical conditions*, 3rd BELBAR Project Annual Workshop, Madrid, Spain, **2015**
- [144] Bouby, M.; Kaplan, U.; Bruggeman, C.; Durce, D.; Maes, N.; Brassinnes, S.; Schäfer, T., *Characterization of Dissolved Organic Matter (DOM) derived from Boom Clay, I: Size distribution and element association*, 6th International Clay Conference, Brussels, Belgium, **2015**
- [145] Bremer, A.; Stauch, C.; Geist, A., *Extraction of molybdenum from CERMET target dissolution solutions using CYANEX® 600*, Proc. Internat. Conf. GLOBAL 2015 (Nuclear Fuel Cycle for a Low-carbon Future), Paris, France, **2015**

- [146] DeVisser-Týnová, E.; Ménard, G.; Ebert, E. L.; Modolo, G.; Cheng, M.; Steppert, M.; Walther, C.; Geist, A.; Mareš, K. V.; John, J., *Dissolution behaviour of inert matrix fuels, Proceedings of Top Fuel, Zürich, Switzerland, 2015*
- [147] Hampel, A.; Günther, R. M.; Salzer, K.; Minkley, W.; Pudewills, A.; Yildirim, S.; Rokahr, R.; Gährken, A.; Missal, C.; Stahlmann, J.; Herchen, K.; Lux, K. H., *Joint Project III on the comparison of constitutive models for the thermo-mechanical behavior of rock salt: I. Overview and results from model calculations of healing of rock salt. Mechanical Behavior of Salt VIII, Proc. of intern. Conf., Rapid City, Rapid City, SD, USA, 2015*
- [148] Hampel, A.; Günther, R.-M.; Salzer, K.; Minkley, W.; Pudewills, A.; Yildirim, S.; Rokahr, R.; Gährken, A.; C., M.; Stahlmann, J.; Herchen, K.; Lux, K.-H., *Joint Project III on the comparison of constitutive models for the thermo-mechanical behavior of rock salt: I. Overview and results from model calculations of healing of rock salt, Proc. of intern. Conf. Mechanical Behavior of Salt VIII, Rapid City, SD, USA, 2015*
- [149] Held, S.; Schill, E.; Sanchez, P.; Neumann, T.; Emmerich, K.; Morata, D.; Kohl, T., *Geological and Tectonic Settings Preventing High-Temperature Geothermal Reservoir Development at Mt. Villarrica (Southern Volcanic Zone): Clay Mineralogy and Sulfate-Isotope Geothermometry, Proceedings, World Geothermal Congress 2015, Melbourne, Australia, 2015*
- [150] Huber, F.; Totskiy, Y.; Montoya, V.; Enzmann, F.; Trumm, M.; Wenka, A.; Geckeis, H.; Schäfer, T., *Modelling of Tc migration in a non-oxidized fractured drill core from Äspö, Sweden., AGU Fall Meeting, San Francisco, CA, USA, 2015*
- [151] Jahn, M.; Breunig, M.; Butwilowski, E.; Kuper, P. V.; Thomsen, A.; Al-Doori, M.; Schill, E., *Temporal and spatial database support for geothermal subsurface applications, PROCEEDINGS, 3D Geoinfo 2015, Joint International Geoinformation Conference, Kuala Lumpur, Malaysia, 2015*
- [152] Kaplan, U.; Bouby, M.; Kupcik, T.; Schild, D.; Kaden, P.; Bruggeman, C.; Durce, D.; Maes, N.; Brassinnes, S.; Schäfer, T., *Characterization of Dissolved Organic Matter (DOM) derived from Boom Clay, II: Organic Functionality, 6th International Clay Conference, Brussels, Belgium, 2015*
- [153] Kienzler, B.; Metz, V.; Schlieker, M.; Bohnert, E., *Evolution of cement based materials in a repository for radioactive waste and their chemical barrier function, Proceedings of the International conference on "Key topics in deep geological disposal", Cologne, Germany, 2015*
- [154] Merk, B.; Geist, A.; Modolo, G.; Knebel, J., *The German P&T study: results and conclusions in the view of the contributing Helmholtz Research Centres, Actinide and Fission Product Partitioning and Transmutation, 13th Information Exchange Meeting, Seoul, Republic of Korea, 2015*
- [155] Merk, B.; Knebel, J.; Geist, A.; Modolo, G., *Results and conclusions from the German P&T study — a view of the contributing Helmholtz research centres, 46. Jahrestagung Kerntechnik, Berlin, Germany, 2015*
- [156] Metz, V.; González-Robles, E.; Dardenne, K.; Rothe, J.; Altmaier, M.; Kienzler, B.; Geckeis, H., *Current state of knowledge on long term behavior of highly active waste forms, Proceedings of the International conference on "Key topics in deep geological disposal", Cologne, Germany, 2015*
- [157] Metz, V.; González-Robles, E.; Dardenne, K.; Rothe, J.; Altmaier, M.; Kienzler, B.; Geckeis, H., *Current state of knowledge on long term behavior of spent nuclear fuel under conditions of deep geological, Proceedings of the International conference on "Key topics in deep geological disposal", Cologne, Germany, 2015*
- [158] Pudewills, A., *Numerical Analysis of a Drift Intersection in a Waste Repository in Rock, Proc. of intern. Conf. Mechanical Behavior of Salt VIII, Rapid City, SD, USA, 2015*
- [159] Rinderknecht, F.; Bouby, M.; Friedrich, F.; Heck, S.; Götz, R.; Huber, F.; Schäfer, T., *Bentonite Erosion Experiments, 3rd BELBAR Project Annual Workshop, Madrid, Spain, 2015*
- [160] Schill, E.; Cuenot, N.; Genter, A.; Kohl, T., *Review of the Hydraulic Development in the Multi-Reservoir / Multi-Well EGS Project of Soultz-sous-Forêts, Proceedings, World Geothermal Congress 2015, Melbourne, Australia, 2015*
- [161] Wilden, A.; Modolo, G.; Lange, S.; Sadowski, F.; Kardhashi, D.; Li, Y.; Kowalski, P.; Beele, B. B.; Skerencak-Frech, A.; Panak, P. J.; Geist, A.; Rothe, J.; Dardenne, K.; Schäfer, S.; Wagner, A. T.; Roesky, P. W.; Verboom, W., *Complex structure of An and Ln complexes with modified diglycolamides in solution and solid state using different speciation techniques, Proc. Internat. Conf. GLOBAL 2015 (Nuclear Fuel Cycle for a Low-carbon Future), Paris, France, 2015*

## Oral and poster presentations

- [162] Adam, C.; Kaden, P.; Beele, B. B.; Müllich, U.; Geist, A.; Panak, P. J., *Comparison of Model-free Methods for Paramagnetic Chemical Shifts in Lanthanide and Americium(III) Complexes, Second Joint Workshop on f-element Chemistry*, Karlsruhe, Germany, **2015**
- [163] Adam, N.; Smith, V. C.; MacGillivray, R. T. A.; Panak, P. J., *Investigation of the interaction of Cm(III) with human serum transferrin and hTf/2N, INE/ITU Research Fellow Day*, Karlsruhe, Germany **2015**
- [164] Altmaier, M.; Brush, L.; Costa, D.; Felmy, A.; Moog, H. C.; Ragoussi, M.; Reed, D. T.; Runde, W.; Voigt, W., *High ionic-strength solutions: state of the art report within NEA-TDB to assess modeling and experimental approaches, Migration 2015*, Santa Fe, USA, **2015**
- [165] Altmaier, M.; Duro, L.; Montoya, M.; Kienzler, B.; Perrone, J.; Holt, E.; Claret, F.; Mäder, U.; Grambow, B.; Idiart, A., *CEBAMA – a collaborative project on cement-based materials, properties, evolution, barrier functions within the European Commission / Horizon 2020 frame, Migration 2015*, Santa Fe, USA, **2015**
- [166] Altmaier, M.; Gaona, X.; Endrizzi, F.; Brendler, V.; Steudtner, R.; Franzen, C.; Tsushima, S.; Panak, P. J.; Skerencak-Frech, A.; Hagemann, S.; Brandt, F.; Krüger, S.; Colàs, E.; Grivé, M.; Thoenen, T.; Kulik, D. A., *ThermAc – a joint project on aquatic actinide chemistry and thermodynamics at elevated temperature conditions, Migration 2015*, Santa Fe, USA, **2015**
- [167] Altmaier, M.; Kienzler, B.; Rothe, J.; Schäfer, T.; Geckeis, H., *Geochemical Research for Nuclear Waste Disposal Safety, Energy, Science and Technology Conference & Exhibition (EST 2015)*, Karlsruhe, Germany, **2015**
- [168] Altmaier, M.; Metz, V.; Reed, D. T., *Report on Pitzer State-of-Art-Report and OECD NEA Thermochem. Database Project and International Workshop on Actinide-Brine-Chemistry, ABC-Salt (IV), 6th US/German Workshop on Salt Repository Research, Design, and Operation*, Dresden, Germany, **2015**
- [169] Altmaier, M.; Reed, D., *Update on activities: (i) Pitzer State of Art Report (NEA-TDB), (ii) JIPD initiative within NEA-Salt Club, International Workshop on Actinide Brine Chemistry in a Salt-Based Repository (ABC-Salt IV)*, Heidelberg, Germany, **2015**
- [170] Arnold, P. L.; Zegke, M.; Jones, G.; Pecharman, A.; Lord, R.; Hollis, E.; Dutkiewicz, M.; Love, J.; Caciuffo, R.; Magnani, N.; Apostolidis, C.; Walter, O.; Zhang, X.; Schreckenbach, G.; Pidchenko, I.; Vitova, T., *From hydrogen to neptunium: Uranyl oxo-functionalisation by as much of the periodic table as possible, International Chemical Congress of Pacific Basin Societies (PACIFICHEM 2015)* Honolulu, Hawaii, USA, **2015**
- [171] Bahl, S.; Koldeisz, V.; Bohnert, E.; González-Robles, E.; Schild, D.; Kienzler, B.; Kvashnina, K.; Rothe, J.; Dardenne, K.; Boshoven, J.; Martel, L.; Pidchenko, I.; Prüßmann, T.; Roth, G.; Geckeis, H.; Vitova, T., *Comparative U, Np and Pu M edge high energy resolution X ray absorption spectroscopy (HR-XANES) investigations of model and genuine active waste glass, 16th International Conference on X-ray Absorption Fine Structure (XAFS16)*, Karlsruhe, Germany, **2015**
- [172] Bahl, S.; Koldeisz, V.; Bohnert, E.; González-Robles, E.; Schild, D.; Kienzler, B.; Kvashnina, K. O.; Pidchenko, I.; Prüßmann, T.; Günther, R.; Geckeis, H.; Vitova, T., *Comparative U and Pu M edge high energy resolution X-ray absorption spectroscopy (HR-XANES) investigations of model and genuine active waste glass, EUFEN4*, Lisbon, Portugal, **2015**
- [173] Bahl, S.; Koldeisz, V.; Bohnert, E.; González-Robles, E.; Schild, D.; Metz, V.; Kienzler, B.; Kvashnina, K.; Pidchenko, I.; Prüßmann, T.; Roth, G.; Geckeis, H.; Vitova, T., *Comparative U and Pu M edge high energy resolution X-ray absorption spectroscopy (HR-XANES) investigations of model and genuine active waste glass, Energy, Science & Technology Conference 2015 (EST)*, Karlsruhe, Germany **2015**
- [174] Bahl, S. P.; Koldeisz, V.; Bohnert, E.; Gonzalez-Robles, E.; Schild, D.; Kienzler, B.; Kvashnina, K. O.; Pidchenko, I.; Prüßmann, T.; Roth, G.; Geckeis, H.; Vitova, T., *Comparative U and Pu M edge high energy resolution X-ray absorption spectroscopy (HR-XANES) investigations of model and genuine active waste glass, 2nd Joint Student Workshop on f-Element Chemistry*, Karlsruhe, Germany, **2015**
- [175] Baker, R. J.; Walshe, A.; Keyes, T. E.; Forster, R. J.; Prüßman, T.; Pidchenko, I.; Vitova, T., *Uranyl Minerals as Models for the Long Term Storage of Spent Nuclear Fuels Catalysis and Sensing for our Environment Symposium*, Dublin, Ireland, **2015**

- [176] Baumann, A.; Yalcintas, E.; Gaona, X.; Altmaier, M.; Geckeis, H., *Chemistry of technetium under repository-relevant conditions: solubility and hydrolysis of Tc(IV) in KCl solutions*, *International Workshop on Actinide Brine Chemistry in a Salt-Based Repository (ABC-Salt IV)*, Heidelberg, Germany, **2015**
- [177] Baumann, A.; Yalcintas, E.; Gaona, X.; Altmaier, M.; Geckeis, H., *Chemistry of technetium under repository-relevant conditions: solubility and hydrolysis of Tc(IV) in KCl solutions*, *INE-ITU Research Fellows Day 2015*, Karlsruhe, Germany, **2015**
- [178] Baumann, A.; Yalcintas, E.; Gaona, X.; Altmaier, M.; Geckeis, H., *Chemistry of technetium under repository-relevant conditions: solubility and hydrolysis of Tc(IV) in KCl solutions*, *GDCh-Wissenschaftsforum Chemie 2015*, Dresden, Germany, **2015**
- [179] Becker, F., *Grundlagen Low Dose Regime (Grundlagen Freigabe), 4. ENTRIA-Bearbeiter-Treffen*, Berlin, Germany, **2015**
- [180] Becker, F., *H\*(10) aus einen einfachen Perspektive, 83. Sitzung des Arbeitskreises Dosimetrie*, Forschungszentrum Jülich, Germany **2015**
- [181] Bennett, K.; Graser, C.-H.; Marquardt, C. M.; Clark, S. B., *Estimation of complexation constants between actinides and simple carboxylic acids in solvent media composed of water and methanol*, *MIGRATION 2015*, Santa Fe NM, USA, **2015**
- [182] Borkel, C.; Grivé, M.; Bruno, J., *Modeling Degradation of Cement at Different pCO<sub>2</sub> in Flow-Through Conditions*, *Goldschmidt Conference*, Prague, CZ, **2015**
- [183] Bouby, M., *A short introduction to the FFFF principles and uses*, *Training course student*, *BELBAR Project Workshop*, Karlsruhe, Germany, **2015**
- [184] Bouby, M.; Heyrich, Y.; Heck, S.; Hilpp, S.; Schäfer, T., *Influence of organic matter (fulvic acids) on the long term stability of clay colloids prepared under different chemical conditions*, *3d BELBAR Project Annual Workshop*, Madrid, Spain, **2015**
- [185] Bouby, M.; Heyrich, Y.; Heck, S.; Hilpp, S.; Schäfer, T., *Influence of organic matter (fulvic acids) on the long term stability of clay colloids prepared under different chemical conditions*, *4th BELBAR Project Workshop*, Karlsruhe, Germany, **2015**
- [186] Bouby, M.; Kaplan, U.; Bruggeman, C.; Durce, D.; Maes, N.; Brassinnes, S.; Schäfer, S., *Characterization of Dissolved Organic Matter (DOM) derived from Boom Clay, I: Size distribution and element association*, *6th International Clay Conference*, Brussels, Belgium **2015**
- [187] Delavernhe, L.; Steudel, A.; Darbha, G. K.; Schäfer, T.; Schuhmann, R.; Wöll, C.; Geckeis, H.; Emmerich, K., *Size and structure - the key to different ratios of edge to face charge for smectite*, *6th International Conference on Clays in Natural and Engineered Barriers for Radioactive Waste Confinement*, Bruxelles, Belgium, **2015**
- [188] Dubey, S.; Montoya, V.; Huber, F.; Metz, V.; Kienzler, B., *Reactive transport model accounting for (geo-)chemical and physical processes taking place in the near-field of a generic spent nuclear fuel repository in a deep clay rock formation*, *MIGRATION 2015*, Santa Fe, USA, **2015**
- [189] Fellhauer, D.; Altmaier, M.; Reed, D. T., *Update on ABC-Salt (IV) conference and Update on Pitzer Database activity within NEA Salt Club*, *NEA Salt Club Meeting*, Paris, France, **2015**
- [190] Fellhauer, D.; Gaona, X.; Altmaier, M.; Geckeis, H., *Np(V) solubility and speciation in alkaline NaCl solutions*, *International Workshop on Actinide Brine Chemistry in a Salt-Based Repository (ABC-Salt IV)*, Heidelberg, Germany, **2015**
- [191] Fellhauer, D.; Gaona, X.; Altmaier, M.; Geckeis, H., *Neptunium(V) solubility and hydrolysis in dilute to concentrated chloride solutions relevant for nuclear waste disposal*, *34th International Conference on Solution Chemistry (ICSC 2015)*, Prague, Czech Republic, **2015**
- [192] Finck, N.; Dardenne, K., *Interaction of selenite with reduced Fe and/or S species*, *XAFS16*, Karlsruhe, Germany, **2015**
- [193] Finck, N.; Nedel, S.; Dideriksen, K.; Schlegel, M. L., *EXAFS signatures of trivalent actinides uptake by green rust and magnetite*, *XAFS16*, Karlsruhe, Germany, **2015**
- [194] Finck, N.; Nedel, S.; Dideriksen, K.; Schlegel, M. L., *Trivalent actinides retention by iron (hydr)oxides*, *MIGRATION Conference*, Santa Fe, NM, USA, **2015**

- [195] Finck, N.; Schlegel, M. L.; Bauer, A., *Polarized XAS signatures of structural Fe in dioctahedral and trioctahedral smectites, XAFS16*, Karlsruhe, Germany, **2015**
- [196] Friedrich, F.; Schild, D.; Weidler, P. G.; Schäfer, T., *Hydration of Febex-bentonite observed by environmental scanning electron microscopy (ESEM), EUROCLAY*, Edinburgh, GB, **2015**
- [197] Fröhlich, D. R.; Skerencak-Frech, A.; Rossberg, A.; Panak, P. J., *Complexation of trivalent actinides with acetate studied by TRLFS and EXAFS spectroscopy, 45èmes Journées des Actinides*, Prague-Průhonice, Czech Republic, **2015**
- [198] Galan, H.; Nunez, A.; Gonzalez, A.; Cobos, J.; Durana, A.; de Mendoza, J.; Egberink, R. J. M.; Verboom, W.; Munzel, D.; Müllich, U.; Geist, A., *Partitioning processes for minor actinides: influence of gamma radiation on extraction systems based on diglycolamides, 10th International Conference on Methods and Applications of Radioanalytical Chemistry (MARC X)*, Kailua-Kona, Hawaii, USA, **2015**
- [199] Gaona, X.; Maques Fernandes, M.; Baeyens, B.; Altmaier, M., *Solubility and hydrolysis of U(VI) at elevated temperature, HiTAC II Workshop – High Temperature Aqueous Chemistry*, Heidelberg, Germany, **2015**
- [200] Gaona, X.; Rojo, H.; Rabung, T.; Garcia-Gutierrez, M.; Missana, T.; Altmaier, M., *Thermodynamic description of An(III/IV) interaction with gluconate in NaCl and CaCl<sub>2</sub> systems, MIGRATION 2015*, Santa Fe, NM, USA, **2015**
- [201] Geist, A., *Untersuchungen zum grundlegenden Verständnis der selektiven Komplexierung von f Elementen (f-Kom), 2. Projektstatusgespräch zur BMBF-geförderten Nuklearen Sicherheitsforschung*, Dresden, Germany, **2015**
- [202] Geist, A., *Fundamental An(III)-Ln(III) separation chemistry of N-donor ligands, 10th International Conference on Methods and Applications of Radioanalytical Chemistry (MARC X)*, Kailua-Kona, Hawaii, USA, **2015**
- [203] Geist, A., *Some aspects of used nuclear fuel recycling, GENTLE Intersemester Course on "Nuclear Waste Management"*, Karlsruhe, Germany, **2015**
- [204] Geist, A.; Modolo, G., *Hydrometallurgische Abtrennung von Actiniden: Kann man daraus für die Rezyklierung von strategischen Metallen lernen?, Jahrestreffen der ProcessNet-Fachgruppen "Extraktion" und "Mischvorgänge"*, Heidelberg, Germany, **2015**
- [205] Gonzalez-Robles, E.; Herm, M.; Müller, N.; Montoya, V.; Kienzler, B.; Genzs, R.; Metz, V., *Dissolution of spent nuclear fuel fragments at high alkaline conditions under H<sub>2</sub> overpressure, Materials Research Society Symposium Proceedings Scientific Basis for Nuclear Waste Management XXXIX*, Montpellier, France, **2015**
- [206] González-Siso, M. R.; Gaona, X.; Duro, L.; Altmaier, M.; Bruno, J., *Solubility and hydrolysis of Ni(II) under alkaline to hyperalkaline conditions, International Workshop on Actinide Brine Chemistry in a Salt-Based Repository (ABC-Salt IV)*, Heidelberg, Germany, **2015**
- [207] Gonzalez-Siso, M. R.; Gaona, X.; Duro, L.; Schild, D.; Fellhauer, D.; Pidchenko, I.; Vitova, T.; Altmaier, M.; Bruno, J., *Interaction of Pu, U and Tc with iron corrosion products under hyperalkaline reducing conditions, Migration 2015*, Santa Fe, NM, USA, **2015**
- [208] Gonzalez-Siso, M. R.; Gaona, X.; Duro, L.; Schild, D.; Lagos, M.; Darbha, G.; Finck, N.; Altmaier, M.; Bruno, J., *Redox chemistry and solubility of Fe in reducing alkaline to hyperalkaline conditions: Fe(0)-Fe<sub>3</sub>O<sub>4</sub>-Fe(II)<sub>aq</sub> system., Migration 2015*, Santa Fe, NM, USA, **2015**
- [209] González-Siso, M. R.; Gaona, X.; Duro, L.; Schild, D.; Lagos, M.; Darbha, G.; Finck, N.; Altmaier, M.; Bruno, J., *Redox chemistry and solubility of Fe in reducing alkaline to hyperalkaline conditions: Fe(0)-Fe<sub>3</sub>O<sub>4</sub>-Fe(II)<sub>aq</sub> system, MIGRATION Conference*, Santa Fe, NM, USA, **2015**
- [210] Graser, C.-H.; Banik, N. L.; Lagos, M.; Marquardt, C. M.; Marsac, R.; Geckeis, H., *SENSITIVE REDOX SPECIATION OF ELEMENTS RELEVANT TO NUCLEAR WASTE DISPOSAL BY CAPILLARY ELECTROPHORESIS HYPHENATED TO INDUCTIVELY COUPLED PLASMA SECTOR FIELD MASS SPECTROMETRY, MIGRATION 2015*, Santa Fe NM, USA, **2015**
- [211] Gyekye, P. K.; Becker, F., *Optimisation of Scatter Radiation to Staff during CT Fluoroscopy: Monte Carlo studies, International Conference on Individual Monitoring of Ionising Radiation (IM 2015)*, Bruges, Belgium, **2015**
- [212] Heberling, F.; Lützenkirchen, J.; Eng, P. J., *The hematite (001) – water interface, insights from surface diffraction investigations, Faraday Discussion 2015*, London, U.K., **2015**

- [213] Heide, B., *Stochastic chemistry for human-cell equivalent systems, Eurados WG6/WG7 autumn meeting*, Paris, France, **2015**
- [214] Heide, B., *Stochastic chemistry for human-cell equivalent systems Eurados WG6/WG7 autumn meeting*, Paris, France, **2015**
- [215] Held, S.; Schill, E.; Kohl, T., *Geothermal reservoir characterization using strontium isotopes in a medium-temperature geothermal system at Villarrica volcano, southern Chile, HiTAC (II) workshop*, Heidelberg, Germany, **2015**
- [216] Herm, M.; Gaona, X.; Fellhauer, D.; Metz, V.; Altmaier, M.; Geckeis, H., *Mixed Nd(III)–OH–Cl(s) phases in concentrated NaCl, MgCl<sub>2</sub> and CaCl<sub>2</sub> brines: Formation, stability and solubility, International Workshop on Actinide and Brine Chemistry in a Salt-Based Repository (ABC-Salt IV)*, Heidelberg, Germany, **2015**
- [217] Herm, M.; Gaona, X.; Fellhauer, D.; Metz, V.; Altmaier, M.; Geckeis, H., *Formation, stability and solubility of mixed Nd–OH–Cl(s) phases in concentrated NaCl, MgCl<sub>2</sub> and CaCl<sub>2</sub> solutions, MIGRATION 2015*, Santa Fe, NM, USA, **2015**
- [218] Herm, M.; Gaona, X.; Fellhauer, D.; Metz, V.; Altmaier, M.; Geckeis, H., *Nd–OH–Cl(s) phases in concentrated Na–Mg–Ca–Cl solutions: A study on formation, stability and solubility, 4th JRC – KIT Research Fellows Day 2015*, Eggenstein-Leopoldshafen, Germany, **2015**
- [219] Herm, M.; Gaona, X.; Rabung, T.; Fellhauer, D.; Crepin, C.; Dardenne, K.; Altmaier, M.; Geckeis, H., *Effect of nitrate on An<sup>III</sup>/Ln<sup>III</sup> solubility in Na-, Mg- and Ca-brines: Thermodynamic and activity models, International Workshop on Actinide and Brine Chemistry in a Salt-Based Repository (ABC-Salt IV)*, Heidelberg, Germany, **2015**
- [220] Herm, M.; Gonzalez-Robles, E.; Böttle, M.; Müller, N.; Bohnert, E.; Dagan, R.; Papiouannou, D.; Kienzler, B.; Metz, V.; Geckeis, H., *Determination of <sup>14</sup>C and other activation/fission products in Zircaloy-4 cladding from an irradiated UO<sub>2</sub> fuel rod segment, Scientific Basis for Nuclear Waste Management XXXIX*, Montpellier, France, **2015**
- [221] Herm, M.; Gonzalez-Robles, E.; Böttle, M.; Müller, N.; Bohnert, E.; Kienzler, B.; Dagan, R.; Papiouannou, D.; Metz, V.; Geckeis, H., *Chemical form of <sup>14</sup>C released from irradiated Zircaloy-4 and inventory of <sup>14</sup>C and other activation/fission products in the studied cladding, 4th JRC – KIT Research Fellows Day 2015*, Eggenstein-Leopoldshafen, Germany, **2015**
- [222] Herm, M.; González-Robles, E.; Böttle, M.; Müller, N.; Papiouannou, D.; Wegen, D. H.; Dagan, R.; Kienzler, B.; Metz, V., *Description of Zircaloy-4 dissolution experiment in a shielded box (D3.8), CARbon-14 Source Term – CAST, Deliverable D3.8*, **2015**
- [223] Hinz, K.; Altmaier, M.; Gaona, X.; Fellhauer, D.; Schild, D.; Geckeis, H., *Interaction of Np(V) with borate in dilute to concentrated alkaline NaCl and MgCl<sub>2</sub> solutions, Migration 2015*, Santa Fe, NM, USA, **2015**
- [224] Hinz, K.; Gaona, X.; Fellhauer, D.; Schild, D.; Vespa, M.; Dardenne, K.; Altmaier, M.; Geckeis, H., *Np(V)–borate interaction in dilute to concentrated alkaline NaCl and MgCl<sub>2</sub> solutions, International Workshop on Actinide and Brine Chemistry in a Salt-Based Repository (ABC-Salt IV)*, Heidelberg, Germany, **2015**
- [225] Kaden, P., *02NUK020 – Selektive Komplexierung von f-Elementen, 2. Projektstatusgespräch zur BMBF-geförderten Nuklearen Sicherheitsforschung*, Dresden, Germany, **2015**
- [226] Kaplan, U.; Bouby, M.; Kupcik, T.; Schild, D.; Kaden, P.; Bruggemann, C.; Durce, D.; Maes, N.; Brassinnes, S.; Schäfer, T., *Characterization and interaction with radionuclides (RNs) of Natural Organic Matter (NOM) derived from different layers within the Boom clay formation, 4 th JRC – KIT Research Fellow Day*, Eggenstein-Leopoldshafen, Germany, **2015**
- [227] Kaplan, U.; Bouby, M.; Rabung, T.; Kupcik, T.; Schild, D.; Kaden, P.; Bruggeman, C.; Durce, D.; Maes, N.; Brassinnes, S.; Schäfer, T., *Characterization and interaction with Radionuclides (RNs) of natural organic matter (NOM) derived from different layers within the Boom Clay (BC) formation, 15th International Migration Conference*, Santa Fe, USA, **2015**
- [228] Kienzler, B.; Borkel, C.; Schlieker, M.; Metz, V., *Long-Term Investigations of Simulated Full-Scale Cemented Waste Forms - Results from Analyses of Solids and Solutions, ABC Salt Conference*, Heidelberg, Germany, **2015**

- [229] Kienzler, B.; Lemmens, K., *First-nuclides: results on radionuclide release from used fuel*, ANS International High-Level Radioactive Waste Management Conference (IHLRWM 2015), Charleston, USA, **2015**
- [230] Kohl, T.; Schill, E.; Bremer, J., *Experiences from the geothermal projects and necessity for a geoscientific underground laboratory*, Energy Science and Technology International Conference and Exhibition, Karlsruhe, Germany, **2015**
- [231] Koke, C.; Skerencak-Frech, A.; Panak, P. J., *Komplexierung von trivalenten Actiniden mit Chlorid in Alkali- und Erdalkalichloridlösungen im Temperaturbereich von  $T = 20 - 200$  °C*, GDCh-Wissenschaftsforum Chemie, Dresden, Germany, **2015**
- [232] Koke, C.; Skerencak-Frech, A.; Panak, P. J., *The Thermodynamics of the Complexation of Cm(III) with Chloride in Alkali and Alkali Earth Metal Solutions at Elevated Temperatures*, Migration 2015, Santa Fe, USA, **2015**
- [233] Koke, C.; Skerencak-Frech, A.; Panak, P. J., *The Thermodynamics of the Complexation of Cm(III) with Chloride in Alkali and Alkali Earth Metal Solutions at Elevated Temperatures*, 4. JRC - KIT Research Fellow Day, Karlsruhe, Germany, , **2015**
- [234] Lee, J.-Y.; Gaona, X.; Vespa, M.; Dardenne, K.; Rothe, J.; Rabung, T.; Altmaier, M.; Yun, J.-I., *Formation and structural analysis of ternary  $UO_2-CO_3$  complexes using TRLS and EXAFS*, Migration 2015, Santa Fe, USA, **2015**
- [235] Leon, A.; Rothe, J.; Finck, N.; Felderhoff, M.; Fichtner, M., *How X-ray absorption spectroscopy highlighted some relevant aspects of a hydrogen storage material*, XAFS16, Karlsruhe, Germany, **2015**
- [236] Lindqvist-Reis, P.; Trumm, M.; Schimmelpfennig, B., *Influence of temperature and the ionic strength on the structure and the vibrational spectra of Ln(III) and An(III) ions in aqueous perchlorate solution "Quo Vadis" Coordination Chemistry?*, Debrecen Hungary, **2015**
- [237] Metz, V., *Untersuchungen von Zircaloy-Hüllrohr und Edelstahl eines bestrahlten PWR-Brennstoffsegments*, 90. Sitzung des AK HAW-Produkte, Berlin, Germany, **2015**
- [238] Metz, V., *The back-end of the nuclear fuel cycle. Graduate and Executive Nuclear Training and Lifelong Education (GENTLE), Intersemester Course on "Nuclear Waste Management"*, Karlsruhe, Germany, **2015**
- [239] Metz, V.; González-Robles, E.; Loida, A.; Müller, N.; Kienzler, B., *Research at KIT-INE on spent nuclear fuel behavior under conditions of a generic salt based repository*, International Workshop on Actinide and Brine Chemistry in a Salt-Based Repository (ABC-Salt IV), Heidelberg, Germany, **2015**
- [240] Montoya, V.; Kupcik, T.; Van Laer, L.; Bruggeman, C.; Glaus, M. A.; Baeyens, B.; Maes, N.; Schäfer, T.; Geckeis, H., *Zn and Co sorption onto Na-illite – batch sorption study and modelling*, 6th Conference on Clays in Natural and Engineered barriers for radioactive waste confinement, Brussels, Belgium, **2015**
- [241] Natrajan, L. S.; Woodall, S. D.; Swinburn, A. N.; Randall, S.; Banik, N.; Adam, C.; Di Pietro, P.; Kaden, P.; Kerridge, A., *Monitoring Redox Behaviour of Actinide Ions by a Combination of Emission and NMR Spectroscopy*, Second Joint Workshop on f-element Chemistry, Karlsruhe, Germany, **2015**
- [242] Pang, B.; Sauri Suarez, H.; Becker, F., *Individual dosimetry in final disposal repository of heat-generating nuclear waste*, International Conference on Individual Monitoring of Ionising Radiation (IM 2015), Bruges, Belgium, **2015**
- [243] Pang, B.; Sauri Suárez, H.; Becker, F., *Individual dosimetry in final disposal repository of heat-generating nuclear waste*, International Conference on Individual Monitoring of Ionising Radiation (IM 2015), Bruges, Belgium, **2015**
- [244] Pidchenko, I.; Fellhauer, D.; Prüssmann, T.; Dardenne, K.; Rothe, J.; Vitova, T., *Plutonium oxidation state speciation in aqueous solution studied by high-energy resolution  $L_3$  and  $M_5$  edge XANES*, 4rd ITU – INE Research Fellow Day, Karlsruhe, Germany, **2015**
- [245] Pidchenko, I.; Kvashnina, K. O.; Yokosawa, T.; Finck, N.; Schild, S.; Schäfer, T.; Rothe, J.; Geckeis, H.; Vitova, T., *U redox state and speciation of U in contact with magnetite nanoparticles: High resolution XANES, EXAFS, XPS and TEM study*, XAFS16, Karlsruhe, Germany, **2015**
- [246] Pidchenko, I.; Kvashnina, K. O.; Yokosawa, T.; Finck, N.; Schild, S.; Schäfer, T.; Rothe, J.; Geckeis, H.; Vitova, T., *U redox state and speciation of U coprecipitated with magnetite nanoparticles: High resolution XANES, EXAFS, XPS and TEM study*, MIGRATION Conference, Santa Fe, NM, USA, **2015**

- [247] Podkovyrina, Y.; Pidchenko, I.; Pruessman, T.; Bahl, S.; Soldatov, A.; T., V., *U M4 HR-XANES and ab-initio investigations of  $UO_3$  polymorphic forms*, 16th International Conference on X-ray Absorption Fine Structure (XAFS16), Karlsruhe, Germany, **2015**
- [248] Podkovyrina, Y.; Pidchenko, I.; Soldatov, A.; Polly, R.; Vitova, T., *Study of  $Fe_3O_4$  nanoparticles with U using HR-XANES and DFT calculations*, International Joint School on Smart Nanomaterials and X-ray Optics 2015. Modeling, Synthesis and Diagnostics, Rostov-on-Don, Russia, **2015**
- [249] Polly, R.; Schimmelpfennig, B.; Heberling, F.; Geckeis, H., *Calcite: sorption and incorporation of radionuclides*, INT, KIT, **2015**
- [250] Polly, R.; Schimmelpfennig, B.; Lindqvist-Reis, P., *Violation of Badger's rule in the series of  $AnO_2^{(2+)}$  Iones ( $An = U, Np, Pu$ ): A quantum chemical study*, Migration 2015, Santa Fe, New Mexico, USA, **2015**
- [251] Polly, R.; Schimmelpfennig, B.; Yalcintas, E.; Gaona, X.; Altmaier, M., *Tc(IV) hydrolysis species and ternary Na/Ca-Tc<sup>IV</sup>-OH complexes in alkaline  $CaCl_2$  and NaCl solutions: a quantum chemical study*, Migration 2015, Santa Fe, New Mexico, USA, **2015**
- [252] Prieur, D.; Martin, P.; Bes, R.; Lebreton, F.; Caisso, M.; Delahaye, T.; Strach, M.; Belin, R.; Martel, L.; Vigier, J.-F.; Pruessmann, T.; Vitova, T.; Solari, P.; Kvashnina, K.; Scheinost, A. C.; Somers, J., *Electronic and structural changes induced by the incorporation of aliovalent cation in  $UO_2$* , 16th International Conference on X-ray Absorption Fine Structure (XAFS16), Karlsruhe, Germany, **2015**
- [253] Prüßmann, T.; Geist, A.; Rothe, J.; Lindqvist-Reis, P.; Schimmelpfennig, B.; Kvashnina, K.; Fryer-Kanssen, I.; Kerridge, A.; Vitova, T., *High energy resolution XANES studies of lanthanide partitioning complexes*, 16th International Conference on X-ray Absorption Fine Structure (XAFS16), Karlsruhe, Germany **2015**
- [254] Pudewills, A., *Simulation of thermo-mechanical behavior of WIPP-salt and preliminary simulation of Room D and B in the WIPP site (Carlsbad, NM, USA) with ADINA code*, US-German Workshop, Rapid City, USA **2015**
- [255] Quinto, F.; Golser, R.; Lagos, M.; Plaschke, M.; Steier, P.; Schäfer, T.; Geckeis, H., *Analysis of Uranium, Neptunium, Plutonium, Americium and Curium isotopes below ppq levels in groundwater samples from an underground research facility in Switzerland*, MIGRATION 2015, Santa Fe NM, USA, **2015**
- [256] Quinto, F.; Lagos, M.; Plaschke, M.; Schäfer, T.; Steier, P.; Golser, R.; Geckeis, H., *AMS of actinides in ground- and seawater: a new procedure for simultaneous analysis of U, Np, Pu, Am and Cm isotopes below ppq levels*, DPG-Frühjahrstagung 2015, Heidelberg, Germany, **2015**
- [257] Reed, D. T.; Altmaier, M., *Actinide solubility and speciation in a salt repository: current status*, Migration 2015, Santa Fe, USA, **2015**
- [258] Renz, T.; Plaschke, M.; Quinto, F.; Lagos, M.; Bauer, A.; Taubald, H., *Development of a sample preparation procedure for the simultaneous determination of neptunium and plutonium in clay samples using mass spectrometry techniques*, Vortrag Universität Tübingen, Tübingen, Germany, **2015**
- [259] Renz, T.; Quinto, F.; Lagos, M.; Plaschke, M.; Bauer, A.; Geckeis, H.; Taubald, H., *Development of a sample preparation procedure for the simultaneous determination of Np and Pu in clay samples*, DPG-Frühjahrstagung 2015, Heidelberg, Germany, **2015**
- [260] Rinderknecht, F.; Bouby, M.; Friedrich, F.; Heck, S.; Götz, R.; Huber, F.; Schäfer, S., *Bentonite Erosion Experiments, 3d BELBAR Project Annual Workshop*, Madrid, Spain, **2015**
- [261] Rinderknecht, F.; Bouby, M.; Friedrich, F.; Heck, S.; Götz, R.; Huber, F.; Schäfer, T., *Bentonite Erosion Experiments, 4th BELBAR Project Workshop*, Karlsruhe, Germany, **2015**
- [262] Saurí Suárez, H.; Pang, B.; Becker, F., *Monte-Carlo Calculations of the radiation field in a rock salt horizontal emplacement gallery of an underground nuclear waste disposal facility*, Annual Meeting Nuclear Technology, Berlin, Germany **2015**
- [263] Schäfer, T.; Huber, F. M.; Lagos, M.; Quinto, F.; Heck, S.; Martin, A.; Blechschmidt, I., *Effect of desorption and redox kinetics on radionuclide transport in crystalline formations*, MARC X conference, 10th International Conference on Methods and Applications of Radioanalytical Chemistry, Kailua-Kona, Hawaii, USA, **2015**

- [264] Schepperle, J.; Fellhauer, D.; Gaona, X.; Altmaier, M.; Geckeis, H., *Solubility, hydrolysis and carbonate complexation of NpO<sub>2</sub>(am) and PuO<sub>2</sub>(am) in dilute to concentrated NaCl brines, International Workshop on Actinide and Brine Chemistry in a Salt-Based Repository (ABC-Salt IV)*, Heidelberg, Germany, **2015**
- [265] Schepperle, J.; Fellhauer, D.; Gaona, X.; Altmaier, M.; Geckeis, H., *Investigation of the solubility and hydrolysis of NpO<sub>2</sub>(am,hyd) and PuO<sub>2</sub>(am,hyd) in dilute to concentrated NaCl brines, International Workshop on Actinide Brine Chemistry in a Salt-Based Repository (ABC-Salt IV)*, Heidelberg, Germany, **2015**
- [266] Schepperle, J.; Fellhauer, D.; Gaona, X.; Altmaier, M.; Geckeis, H., *Solubility, hydrolysis and carbonate complexation of Np(IV) and Pu(IV) in dilute to concentrated NaCl brines, GDCh Wissenschaftsforum Chemie 2015*, Dresden, Germany, **2015**
- [267] Schepperle, J.; Fellhauer, D.; Gaona, X.; Altmaier, M.; Geckeis, H., *Solubility, hydrolysis and carbonate complexation of Np(IV) and Pu(IV) in dilute to concentrated NaCl brines, Migration 2015*, Santa Fe, USA, **2015**
- [268] Schepperle, J.; Fellhauer, D.; Gaona, X.; Altmaier, M.; Geckeis, H., *Solubility, hydrolysis and carbonate complexation of Np(IV) and Pu(IV) in dilute to concentrated NaCl brines, 4th JRC - KIT Research Fellows Day 2015*, Eggenstein-Leopoldshafen, Germany, **2015**
- [269] Schill, E.; Abdelfettah, Y.; Saillhac, P.; Larnier, H., *Reservoir characterization and monitoring at Soultz and Rittershoffen (France) using magnetotelluric methods, 2nd Bochum Workshop on Geothermal Reservoir Monitoring and Characterization*, Bochum, Germany, **2015**
- [270] Schnurr, A.; Marsac, R.; Marques, M.; Rabung, T.; Lützenkirchen, J.; Gaona, X.; Baeyens, B.; Geckeis, H., *Sorption of Eu(III)/Cm(III), Np(V) and U(VI) onto clay minerals under saline conditions. Experiment and modeling in NaCl, CaCl<sub>2</sub> and MgCl<sub>2</sub> media, 15th International Conference on the Chemistry and Migration Behaviour of Actinides and Fission Products in the Geosphere*, Santa Fe, NM, USA, **2015**
- [271] Schnurr, A.; Marsac, R.; Rabung, T.; Lützenkirchen, J.; Gaona, X.; Geckeis, H., *Sorption of Eu(III)/Cm(III), Np(V) and U(VI) onto clay minerals under saline conditions. Experiment and modeling. , International Workshop on Actinide and Brine Chemistry in a Salt-Based Repository (ABC-Salt IV)*, Heidelberg, Germany, **2015**
- [272] Schnurr, A.; Marsac, R.; Rabung, T.; Lützenkirchen, J.; Gaona, X.; Geckeis, H., *Sorption of Eu(III)/Cm(III), Np(V) and U(VI) onto clay minerals under saline conditions. Experiment and modeling, GDCh Wissenschaftsforum*, Dresden, Germany, **2015**
- [273] Schnurr, A.; Schäfer, T.; Marsac, R.; Rabung, T.; Lützenkirchen, J.; Geckeis, H., *Sorption studies of actinides/lanthanides onto clay minerals under saline conditions, 6th International conference on "Clays in natural and engineered barriers for radioactive waste confinement"*, Brussels, Belgium, **2015**
- [274] Skerencak-Frech, A.; Froehlich, D. R.; Maiwald, M.; Trumm, M.; Panak, P. J., *Complexation of trivalent actinides with clay-organic ligands at T = 20 – 90°C, Migration 2015*, Santa Fe, NM, USA, **2015**
- [275] Skerencak-Frech, A.; Koke, C.; Fröhlich, D. R.; Rothe, J.; Dardenne, K.; Panak, P. J., *A combined TRILFS and EXAFS study on the complexation of Cm(III) and Am(III) with chloride at T = 25 – 200°C, HiTAC (II) Workshop*, Heidelberg, Germany, **2015**
- [276] Skerencak-Frech, A.; Maiwald, M.; Trumm, M.; Froehlich, D. R.; Panak, P. J., *Komplexierung von Cm(III) mit Oxalat in wässriger Lösung bei T = 20 – 90°C, GDCh Wissenschaftsforum '15*, Dresden, Germany, **2015**
- [277] Stoll, M.; Darbha, G. K.; Huber, F.; Schill, E.; Schäfer, T., *Particle retention on granite as a function of residence time and particle size using a synthetic fracture flow cell, Goldschmidt Conference 2015*, Prague, Czech Republic, **2015**
- [278] Stoll, M.; Darbha, G. K.; Huber, F.; Schill, E.; Schäfer, T., *Particle retention on granite as a function of residence time and particle size using a synthetic fracture flow cell, 4th ITU-INE Research Fellows Day*, Karlsruhe, Germany, **2015**
- [279] Stoll, M.; Darbha, G. K.; Huber, F.; Schill, E.; Schäfer, T., *Particle retention on granite as a function of residence time and particle size using a synthetic fracture flow cell, European Geothermal Workshop 2015*, Strasbourg, France, **2015**

- [280] Stoll, M.; Huber, F.; Darbha, G. K.; Schill, E.; Schäfer, S., *Particle transport in fractured environment: Lab experiments using a synthetic fracture flow cell*, HGF-Workshop Geothermie am KIT, Karlsruhe, Germany, **2015**
- [281] Tasi, A.; Gaona, X.; Böttle, M.; Fellhauer, D.; Dardenne, K.; Grivé, M.; Bruno, J.; Altmaier, M.; Geckeis, H., *Redox chemistry and solubility of Plutonium under hyperalkaline, reducing conditions*, MIGRATION 2015, Santa Fe, NM, USA, **2015**
- [282] Tasi, A.; Gaona, X.; Böttle, M.; Fellhauer, D.; Dardenne, K.; Grivé, M.; Bruno, J.; Altmaier, M.; Geckeis, H., *Solubility and redox behaviour of Plutonium under hyperalkaline reducing conditions*, 4th JRC – KIT Research Fellows Day 2015, Eggenstein-Leopoldshafen, Germany, **2015**
- [283] Tasi, A.; Gaona, X.; Rabung, T.; Kutus, B.; Palinko, I.; Sipos, P.; Altmaier, M.; Geckeis, H., *Interaction of Gluconate with An(III)/Ln(III) in diluted to concentrated MgCl<sub>2</sub> solutions* MIGRATION 2015, Santa Fe, NM, USA, **2015**
- [284] Tasi, A.; Kutus, B.; Gaona, X.; Rabung, T.; Palinko, I.; Sipos, P.; Altmaier, M.; Geckeis, H., *Complexation of gluconate with An(III)/Ln(III) in diluted to concentrated MgCl<sub>2</sub> solutions: Mg(II)–gluconate and Mg(II)–AnIII/LnIII–gluconate systems*, International Workshop on Actinide Brine Chemistry in a Salt-Based Repository (ABC-Salt IV), Heidelberg, Germany, **2015**
- [285] Totskiy, Y.; Huber, F.; Schild, D.; Heck, S.; Geckeis, H.; Kalmykov, S.; Schäfer, T., *Effect of ferrous iron pool and magnetite stoichiometry on Tc(VII) and U(VI) retention*, MARC X conference, 10th International Conference on Methods and Applications of Radioanalytical Chemistry, Kailua-Kona, Hawaii, USA, **2015**
- [286] Trumm, M., *Molecular dynamics and quantum chemical investigation of N-donor ligands interacting with Ln(III)/An(III) ions*, SACSESS Workshop, Warsaw, Poland, **2015**
- [287] Trumm, M., *Theoretical calculation of vibrational motions in An(III)/Ln(III) complexes*, fCOM Workshop, Karlsruhe, Germany, **2015**
- [288] Vitova, T.; Altmaier, M.; Bahl, S.; Bohnert, E.; Dardenne, K.; Denning, R. G.; Denecke, M. A.; Fellhauer, D.; Geckeis, H.; Gonzalez-Robles, E.; Green, J. C.; Jorissen, K.; Rehr, J.; Kas, J. J.; Kienzler, B.; Kvashnina, K.; Pidchenko, I.; Prüßmann, T.; Rothe, J.; Schäfer, T.; Somers, J., *High energy resolution XANES as a tool for electronic and geometric structural investigations of actinide materials*, 16th International Conference on X-ray Absorption Fine Structure (XAFS16), Karlsruhe, Germany, **2015**
- [289] Vitova, T.; Green, J. C.; Denning, R. G.; Löble, M.; Kvashnina, K.; Kas, J. J.; Jorissen, K.; Rehr, J. J.; Malcherek, T.; Denecke, M. A., *Polarization Dependent High Energy Resolution X-ray Absorption Study of Dicesium Uranyl Tetrachloride*, EUFEN4, Lisbon, Portugal, **2015**
- [290] Wagner, C.; Müllich, U.; Geist, A.; Panak, P. J., *Selective Separation of Americium from PUREX Raffinate*, First SACSESS International Workshop, Warsaw, Poland, **2015**
- [291] Wagner, C.; Müllich, U.; Geist, A.; Panak, P. J., *A new process for the selective extraction of trivalent americium from PUREX raffinate (The Amsel Process)*, Second Joint Student Workshop on f-Element Chemistry 2015, Karlsruhe, Germany, **2015**
- [292] Wagner, C.; Müllich, U.; Geist, A.; Panak, P. J., *Development of a new system for the separation of Am(III) from PUREX raffinate*, 4th JRC-KIT Research Fellow Day, Karlsruhe, Germany, **2015**
- [293] Wallesch, M.; Volz, D.; Batchelor, D.; Vitova, T.; Steininger, R.; Göttlicher, J.; Bräse, S.; Heske, C.; Weinhardt, L., *Cu K XANES and EXAFS spectroscopy on Cu(I)-emitters*, 16th International Conference on X-ray Absorption Fine Structure (XAFS16), Karlsruhe, Germany, **2015**
- [294] Wallesch, M.; Volz, D.; Vitova, T.; Göttlicher, J.; Steininger, R.; Bräse, S.; Heske, C.; Weinhardt, L., *Using X-ray absorption to probe the structural integrity of photoluminescent Cu(I)-complexes upon processing*, 21st International Symposium on the Photochemistry and Photophysics of Coordination Compounds (ISPPCC 2015), Kraków, Poland, **2015**
- [295] Walshe, A.; Biswas, A.; Spain, E. D.; Keys, T. A.; Forster, R. A.; Prüßman, T.; Pidchenko, I.; Vitova, T.; Baker, R. J., *Uranyl Minerals as Models for the Long Term Storage of Spent Nuclear Fuels*, 9th International Conference on f-element chemistry, Oxford, UK, **2015**
- [296] Wiedemann, M.; Metz, V.; Finck, N.; Rabung, T.; Geckeis, H., *Retention of trivalent curium and europium by Mg(OH)<sub>2</sub>-bearing solids in the system Mg<sup>2+</sup>-Na<sup>+</sup>-Cl<sup>-</sup>-OH-H<sub>2</sub>O*, GDCh-Wissenschaftsforum Chemie 2015, Dresden, Germany, **2015**

- [297] Wiedemann, M.; Metz, V.; Rabung, T.; Finck, N.; Geckeis, H., *Retention of trivalent europium and curium by Mg(OH)<sub>2</sub>(cr) in the system Mg<sup>2+</sup>-Na<sup>+</sup>-Cl-OH-H<sub>2</sub>O*, *International Workshop on Actinide and Brine Chemistry in a Salt-Based Repository (ABC-Salt IV)*, Heidelberg, Germany, **2015**
- [298] Wiedemann, M.; Metz, V.; Rabung, T.; Finck, N.; Geckeis, H., *Rückhaltung von Radionukliden durch Brucit und Sorelphasen, Fachgespräch „Verschlussysteme – In-situ Bauwerke aus Magnesiabaustoff und dessen chemisch-mechanische Eigenschaften im Hinblick auf HAW-Endlager*, Freiburg, Germany, **2015**
- [299] Yalcintas, E.; Baumann, A.; Gaona, X.; Altmaier, M.; Geckeis, H., *Thermodynamic description of Tc(IV) in Tc<sup>4+</sup>-Na<sup>+</sup>-K<sup>+</sup>-Mg<sup>2+</sup>-Ca<sup>2+</sup>-H<sup>+</sup>-Cl-OH-H<sub>2</sub>O systems: application to repository-relevant conditions*, *Migration 2015*, Santa Fe, USA, **2015**
- [300] Yalcintas, E.; Gaona, X.; Kobayashi, T.; Altmaier, M.; Geckeis, H., *Technetium chemistry in dilute to concentrated saline systems*, *International Workshop on Actinide and Brine Chemistry in a Salt-Based Repository (ABC-Salt IV)*, Heidelberg, Germany, **2015**
- [301] Yokosawa, T.; Prestat, E.; Finck, N.; Bouby-Laliron, M.; Dardenne, K.; Polly, R.; Haigh, S.; Denecke, M. A.; Geckeis, H., *Scanning transmission electron microscopy detection of Lu incorporated in a transformation product of 2-line ferrihydrite*, *Pacificchem 2015*, Honolulu, Hawaii, USA, **2015**
- [302] Zimina, A.; Dardenne, K.; Denecke, M. A.; Grunwaldt, J. D.; Huttel, E.; Mangold, S.; Lichtenberg, H.; Rothe, J.; Steininger, R.; Pruessmann, T.; Vitova, T., *The CAT-ACT Beamline at ANKA: A new high energy X-ray spectroscopy facility for CATalysis and ACTinide research*, *16th International Conference on X-ray Absorption Fine Structure (XAFS16)*, Karlsruhe, Germany **2015**

#### Others

- [303] Pang, B., *Some current activities of radiation protection research in INE*, *IFRT-Seminar*, KIT, **2015**
- [304] Saurí Suárez, H., *Entwicklung von Verfahren für individuelle Dosimetrie für Beschäftigte in Entsorgungsanlagen. Strahlenfeld in einer Steinsalzstrecke*, *INR-Seminar*, KIT, **2014**
- [305] Borkel, C.; Kienzler, B.; Schlieker, M.; Metz, V.; Schild, D.; Soballa, E.; Lagos, M.; Walschburger, C.; Heck, S.; Hilpp, S.; Moisei-Rabung, S.; Seither, A., „*Experimentelles Programm zur Untersuchung von simulierten, zementierten 1:1 Gebinden aus dem Auslaugversuchsfeld Nr. 1 der Schachanlage Asse: Teil III: Ergebnisse der Festkörperanalysen*“, *Auftrag des Helmholtz Zentrums München (HMGU)*, Vol. *KIT-INE 001/2015*, **2015**.
- [306] Grünewald, W.; Tobie, W.; Schild, D.; Salimi, A., *Alternative ceramic refractory study (sintered-bonded)*, (Ed.: Y. Technical report for IHI, Japan, IHI-KIT Cooperation), **2015**.
- [307] Kienzler, B.; Schlieker, M.; Krepper, V.; Rabung, T., *Schachanlage Asse II, Sorptionsuntersuchungen an Gesteinsproben aus der Bohrung Remlingen 15: Teil 1: Probenahme*“, *Auftrag des Bundesamts für Strahlenforschung (BfS)*, Vol. *KIT-INE 003/2014*, **2015**.
- [308] Kienzler, B.; Schlieker, M.; Schäfer, T.; Rabung, T.; Finck, N.; Heberling, F.; Friedrich, F.; Schild, D.; Soballa, E.; Bohnert, E.; Krepper, V.; Plaschke, M.; Geyer, F.; Hilpp, S.; Moisei-Rabung, S.; Seither, A.; Walschburger, C.; Krullikowski, J.; Graser, C.-H.; Haas-Nüesch, R., „*Schachanlage Asse II, Sorptionsuntersuchungen an Gesteinsproben aus der Bohrung Remlingen 15, Teil 2: Charakterisierung der Gesteine*“ *Auftrag des Bundesamts für Strahlenforschung (BfS)*, Vol. *KIT-INE 002/2015*, **2015**.
- [309] Schäfer, T.; Kaplan, U.; Bouby, M.; Rabung, T.; Kupcik, T.; Kaden, P.; Schild, D.; Heck, S., *Characterization of Natural organic matter (NOM) derived from different layers within the Boom Clay Formation and their radionuclide interaction*, *Research Contract No.: CCHO-2012-0422/00/00*, **2015**.



